THE UNIVERSITY OF READING

Department of Meteorology

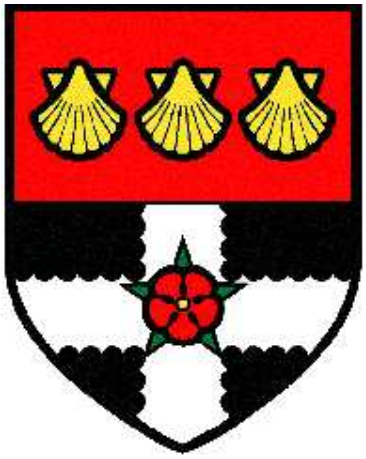

Self organisation of convection as a mechanism for memory

Laura Davies

A thesis submitted for the degree of Doctor of Philosophy

June 7, 2008

Declaration

I confirm that this is my own work and the use of all material from other sources has been properly and fully acknowledged.

Laura Davies

Abstract

Convection is a well-observed atmospheric phenomenon, which has a fundamental role in global weather and climate. The transport of heat, moisture and momentum that result from convection are significant at a range of temporal and spatial scales. Convective clouds have a wide range of non-linear interactions with other atmospheric processes which make them difficult to understand and model numerically.

Due to resolution constraints in climate models, sub-grid convection is represented by a *parameterisation*. Many parameterisation schemes are based on an assumed temporal and spatial separation between convection and its forcing. The implied *equilibrium* relates current convection directly to the large-scale forcing. The validity of the temporal scale separation is directly tested in this thesis by examining the convective response to a time-varying forcing.

An analytic model of convection with an explicit memory timescale is used to characterise the convective response dependent on the memory in the system. A definition of an equilibrium, based on the total convection in a forcing cycle, is used to characterise model response regimes. These regimes are used to interpret the response of cloud-resolving model simulations of realistic convection. It was found that for long forcing timescales ($\gtrsim 10$ *hr*) the response was in equilibrium, without memory effects. At short forcing timescale ($\lesssim 10$ *hr*) an equilibrium was not achieved and the response resembled a system with memory. The current convection was found to be dependent on the time-history of the convective system.

Further analysis of the complete lifecycle of the convective clouds showed self-organisation on scales of $5-10$ *km* during active convection. As clouds decayed thermodynamic spatial structures were found to persist on scales of $5-20$ *km*. The presence of these structures in the initial conditions pre-conditioned the atmosphere, modifying the subsequent convective response at triggering, and hence provided a mechanism for memory.

Acknowledgements

I would like to thank my supervisor, Dr Robert Plant, for his support and guidance. His unfaltering enthusiasm and optimism have been infectious.

I would like to thank NERC for financially supporting the project and the Met Office for providing the CASE award. In particular, I am grateful for the helpful discussions with my Met Office supervisor, Dr Steve Derbyshire, and the members of APP in Exeter.

I am very grateful to Giovanni Leoncini for his proof reading and meticulous attention to detail. Thank you for questioning those points that seemed obvious!

I would like to acknowledge the great help and inspiration of Alan Grant in spending hours discussing convection and quasi-equilibrium. Also Marc Stringer for being a LEM computational wizard and an understanding housemate!

Thank you to Sarah Keeley and Jolene Cook for constant encouragement during the dark days of the fourth year and to Helen Dacre for believing anything is possible.

I would finally like to thank the guys in 1U07, particularly those at the far end, for making office life so enjoyable. Special mention should go to Emma Irvine for proof reading.

We learn wisdom from failure much more than from success.
We often discover what will do, by finding out what will not do;
and probably he who never made a mistake never made a discovery.

Samuel Smiles, Scottish author, 1812-1904

Contents

CHAPTER 1

Introduction

1.1 Introduction

Convection is an important process in the global atmosphere as it is a major contributor to the vertical transport of heat, moisture and momentum. Convection is fundamentally an adjustment process where localised density gradients are removed by rising, buoyant plumes. However, convection is a complicated process and involves highly non-linear interactions with the surrounding atmosphere. Furthermore, convection acts and interacts on a wide range of temporal and spatial scales. It is this wide range of interactions which convection has with weather and climate systems that make the accurate representation of convection a fundamental requirement for reliable numerical models. However, in practice the representation is complicated by both the scales at which convection occurs and computational constraints of the numerical model.

The transport of moisture by convection often produces convective clouds. The latent heat released due to condensation of water vapour within the clouds adds additional energy to the motion and furthers complicates the processes within the convective system. Convective clouds exist on a wide range of spatial and temporal scales. Individual clouds, such as small, shallow cumulus (which are non-precipitating), have spatial scales of a couple of hundred metres and exist on timescales of minutes. Larger-scale cloud systems such as those that develop in response to (and feedback on) the Walker cell and the Madden-Julian Oscillation (MJO, Sui and Lau, 1992) exist over thousands of kilometres and can persist for several days. However, fundamentally, these larger scale convective complexes consist of a range of convective features at smaller scales that interact with each other to create the large system. Furthermore, all convective clouds are under-pinned by sub-cloud-scale processes such as turbulence, entrainment, detrainment and microphysics which act on spatial and temporal scales much smaller than the clouds themselves.

The method of representation for convection in numerical models is dependent on the scale of the model. For example, sufficiently high resolution cloud-resolving models (CRMs) are designed to

capture the processes directly responsible for cloud development, with the important sub-cloud-scale processes being represented by parameterised schemes. To be capable of this level of complexity, however, these models can not practically be integrated over a sufficient area to capture the larger-scale atmospheric systems which often provide the means of forcing convection. Therefore, CRMs must have explicitly prescribed forcing mechanisms and this, inherently, does not permit the full range of interactions between the convection and the forcing. Whilst large-scale weather and climate models can represent large-scale systems that may force convection, they have insufficient resolution to represent the details of the resulting convection directly. In these models a *parameterisation scheme* is used to represent the *the mean effect of the sub-grid scale convection on the large-scale flow*. Hence, a direct modification of the resolved scale quantities is made to represent the effect of convection which is unresolved by the model. The parameterisation scheme is developed by making assumptions about the sub-grid-scale convection which it represents in order to determine its mean effect, and the feedbacks on the large scale.

One of the fundamental assumptions made to facilitate parameterisations is the assumption of a physical *scale separation* in space and time between the scale of the clouds and the large-scale forcing which is causing convection. Investigation of this assumption in terms of the implied *spatial* scale of separation between the convective-scale processes and the large-scale forcing has been addressed, for example by Cohen (2001); Craig and Cohen (2006); Cohen and Craig (2006). The main purpose of this thesis is an investigation of the assumption in terms of the *temporal* scale of separation and an assessment of the timescales for which the assumption is valid.

1.2 Background

Convection occurs due to the action of gravity on density gradients. Localised warming reduces air density and creates positive buoyant instability. As the warm air rises and begins to cool the air loses its buoyancy, the instability decreases and vertical motion reduces. If a specified volume of air is continuously heated from below, then to compensate for the localised upward motions there must also be descent and hence circulations develop. A simple example is that of Rayleigh-Benard convection. In the early 20th century studies of the fluid flow between two fixed plates, where the lower surface was held at a temperature warmer than the upper surface, showed that circulations developed, in which the width-to-height ratio of the circulations was close to unity (Emanuel, 1994). In these simple experiments the convection was only responding to the externally-imposed forcing

and could not interact with it.

1.2.1 The characteristics of convection in the atmosphere

Convection in the global atmosphere presents many levels of complexity not seen in simple laboratory experiments of convection. Many of these additional complexities involve inter-related mechanisms and feedbacks but some key processes are summarised here:

• Convective systems exist on a range of spatial and temporal scales for which the relevant scales are comparatively 'close' together. Consider for example the MJO. This is a large convective complex over thousands of kilometres in extent, which moves from the Indian Ocean eastwards over the West Pacific over a period of 40-60 days. Within the MJO are westward moving clusters of convection lasting 1-2 days (Sui and Lau, 1992). Embedded within these storm systems are smaller scale cumulonimbus which exist over a couple of kilometres for several hours. The MJO may also spawn tropical cyclones which can last for several days, travel over a few hundred kilometres and develop further, independently from the MJO.

• The role of moisture in atmospheric convection also introduces additional complexity and potential for feedback. Latent heat release due to the condensation of water vapour within clouds provides additional energy to the cloud to fuel convective motions. Latent heat release in moist, rising air more than offsets the cooling from dry adiabat ascent providing a considerable source of energy.

• The drag of falling precipitation and the evaporation of precipitation produces negatively buoyant downdrafts. These bring cool, dry air into the lower atmosphere. At the surface these downdrafts spread into cold pools with associated gust fronts. These may initiate secondary convection.

• In atmospheric convection the compensating downward motion, in the form of large-scale subsidence, results in net warming and drying of the environment as a whole *around* the convective clouds.

• Convective clouds re-distribute moisture from the boundary layer to the rest of the atmosphere. This may alter the ability of the environment to support subsequent convection. The removal of moisture from the atmosphere by precipitation dissipates cloud. However, locally moistening the atmosphere, through the re-evaporation of water vapour, or moistening a land surface, through

precipitation, may enhance the likelihood of subsequent convection.

• Convective cloud that becomes sufficiently deep may develop cirrus ice clouds (anvils). Cirrus clouds spread into ice shields at the top of the troposphere. This restricts shortwave solar radiation reaching the surface and hence may limit the amount of warming the surface experiences. Due to the suppression of surface heating, convective instabilities may not occur that could otherwise have formed as a result of solar surface heating.

• In most situations cloud droplets are not formed spontaneously. Cloud droplet formation is enhanced when cloud condensation nuclei (CCN) are present. CCNs are often aerosols or dust particles in the atmosphere on which water vapour condenses into droplets. When these droplets fall as precipitation the CCN are removed from the atmosphere. The removal of CCN from the atmosphere may restrict the formation of further cloud droplets.

• In the atmosphere convective organisation occurs with very different characteristics from that seen in laboratory experiments. Reasons for the different organisations may be due to the different nature of the interactions between convective clouds, and between convection and the large scale.

• Localised triggering of convection can result in atmospheric instability being released over a large area. Atmospheric profiles can be unstable through significant depth and over a wide area, and can develop into large cumulonimbus when triggered at small scales, for example due to ascent over orography.

These are just some examples of processes through which convection may interact with its forcing, and through which convective clouds may interact with other convective clouds. Many of these processes are highly non-linear and the interactions occur on a range of temporal and spatial scales. It is of particular note that many of the processes imply that current convective activity influences any subsequent convection. Such processes can affect the complete lifecycle of a convective cloud and the development of convective cloud systems. Despite the presence of these complicating processes, many of which are not explicitly resolved in weather and climate models, a convective parameterisation scheme is required to make a statement of the level of convection present at any given place and time and to determine how this convection modifies the large-scale flow.

1.2.2 Convective timescales

Convective parameterisations are based on the assumption of a scale separation in time and space between the scale of the convective clouds and the large-scale forcing: i.e. the scales at which convection acts both temporally and spatially are very different from the forcing which is causing it. Assuming for the moment that such a separation exists, we can construct the schematic in Figure 1.1. As stated in Section 1.1 the focus in this thesis is on the temporal scales of convection and Figure 1.1 shows schematically the temporal scales associated with convection.

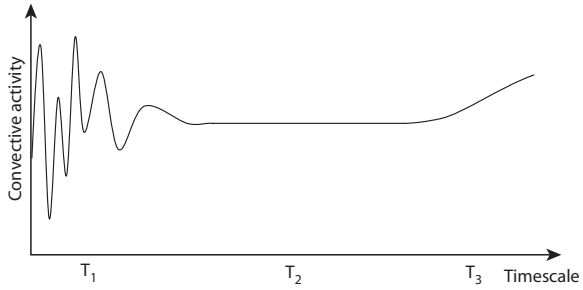

Figure 1.1: *Schematic showing the different timescales associated with convection. T_1 is the timescale at which individual clouds act, and T_3 is the timescale over which the forcing evolves. T_2 represents a timescale over which cloud-scale fluctuations are not significant but the forcing does not change significantly. The assumption that T_2 exists is the basis of the scale separation assumption used in parameterisations. See text for a full discussion.*

Figure 1.1 shows the convective activity averaged over increasing periods of time for a region that contains convection. (At this point there is no need to specify the size or nature of this region). Figure 1.1 shows that at small temporal scales individual clouds cause fluctuations in the convective activity. Averaged over sufficient time these cloud-scale fluctuations are no longer observed and the response represents some mean convective state that is established in response to the slowly evolving forcing. As the time-averaging period increases further the convection becomes subject to variations in the forcing and so the convective response is modified. According to Figure 1.1 there are timescales for which the fluctuations in the convective activity of the individual clouds are masked but where the forcing is effectively time invariant.

It is the existence of such a spectral gap which a traditional parameterisation exploits. The parameterisation does not usually seek to represent the fluctuations due to the individual clouds but rather the time-averaged response of several clouds. If there is a spectral gap then there is a timescale over which the fluctuations of the convective clouds can be averaged, but that timescale is distinctly

shorter than the timescale on which the forcing may vary. These assumptions as they apply to parameterisations will be discussed further in Section 1.3 but the investigation and validation of these assumptions will form the basis of this thesis.

1.3 The representation of convection in numerical models

Despite the complexities of convection discussed in Section 1.2.1 a method whereby convection can be represented in numerical weather and climate models is necessary. There have been various approaches to convective parameterisation in the literature and there is still much study on how existing schemes may be modified and improved or new schemes developed. A recent review of the development of convective parameterisations can be found in Arakawa (2004). In this section a brief overview of convective parameterisations will be given in order to establish how the concept of a 'spectral gap' has been implemented in parameterisation schemes, and also to introduce the key concept of quasi-equilibrium.

Two main methodologies have been proposed to parameterise convection: adjustment schemes and mass flux schemes. Although these schemes have different methods for formulating the parameterisation they both rely on the same principles. These principles were first formally discussed by Arakawa and Schubert (1974). The theoretical ideas introduced in this seminal paper (Arakawa and Schubert, 1974) will be presented first in order to provide a basis for the parameterisation schemes to be discussed.

Arakawa and Schubert (1974), subsequently AS74, presented the theory that convective parameterisation could be developed by considering the sub-grid convection as an ensemble of convective clouds. The convective ensemble contains a theoretical spectrum of convective clouds at random stages of the convective lifecycle, i.e. the development, mature and decay phases. Figure 1.2 represents a horizontal area through such an ensemble at a height between cloud base and cloud top. Convective clouds in various stages of development can be seen penetrating this layer and entraining environmental air as they grow. A cloud which has lost its buoyancy is seen as detraining cloudy air into the environment. The principles of convective parameterisations developed by AS74 are based on the assumption that such a horizontal area exists which is " large enough to contain an ensemble of cumulus clouds but small enough to cover only a fraction of the large-scale disturbance", p675. In other ways, there is a spectral gap in spatial terms.

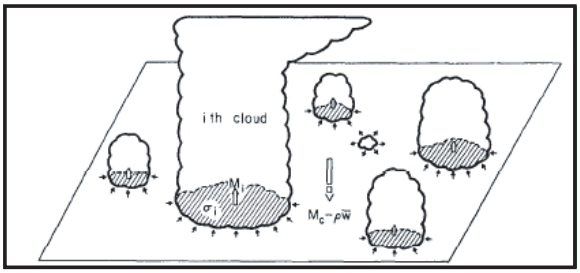

Figure 1.2: *A unit horizontal area at a level between cloud base and cloud top. Clouds are shown in various stages of development and are taken to be representative of a convective ensemble. If the area is that of a grid box then it is the ensemble of convection that a parameterisation scheme is required to represent. (After Arakawa and Schubert (1974).)*

In a numerical model, such a horizontal area is often taken to be the area of a grid box. The clouds in Figure 1.2 are representative of the clouds which are sub-grid and therefore not explicitly represented by the model. It is the effect of these clouds which a convective parameterisation must represent. AS74 introduced a mass flux convective parameterisation which determined the effect of these sub-grid scale clouds on the large-scale through a representation of the properties of these clouds.

Fundamental to all mass flux parameterisations are three components: a trigger function, which determines when a convective parameterisation is required; a cloud model, which computes the vertical extent of the convection, including how the convection would modify the environment; and, finally, a closure scheme which links the intensity of the convection to the magnitude of the large-scale forcing. The closure scheme determines the extent to which the cloud scheme alters the large scale environment. AS74 discuss in detail their proposition for what was then a new theory of mass flux parameterisation. A brief overview is given here of the cloud model and the closure theory. All parameterisations have different methodologies for the components of their schemes and the focus here will be on the theoretical background to AS74 in terms of the assumptions made.

The individual clouds (i) in Figure 1.2 contribute to the total mass flux of the convective ensemble (M_c) given by:

$$M_c = \sum_i \rho \sigma_i w_i \tag{1.1}$$

where ρ, the density, is a function of height only and σ and w_i are the fractional area and area-average vertical velocity of the *i*th cloud, respectively.

The changes in large-scale temperature and moisture due to convective processes, and the tendency terms produced by the parameterisation, may be derived with reference to M_c. Therefore, the formulation of M_c is key to a convective parameterisation.

In AS74 M_c is formed, in the cloud model, from a spectrum of individual clouds where each cloud type is characterised by a single positive parameter λ. λ may be defined differently in different convective parameterisation schemes and whilst the details are not important here, it is assumed that there is some 'plume' model available to determine vertical profiles of cloud characteristics as a function of z for given λ. In AS74 different cloud types detrain at different heights (z_D), and therefore different λ are associated with clouds of different depths. For each cloud type, the vertical profile of mass flux can be scaled by the cloud base mass flux (M_b) and therefore the vertical profile of M_c can be written as:

$$M_c(z) \propto \sum_{\lambda} M_b(\lambda) \times f(z,\lambda) \tag{1.2}$$

where f is a term that gives the vertical structure of each cloud type as a function of height. (f is a combination of several variables in AS74 but is introduced here for simplicity.) M_b is at a carefully chosen *base* of the updrafts. The task in the parameterisation then becomes to define the spectrum of cloud base mass flux.

AS74 introduce a cloud work function (A) which is a measure of the efficiency of kinetic energy generation by the convective ensemble. A convective ensemble where the forcing is time invariant will itself not be evolving in time (although individual clouds progress through lifecycles), and so A is constant in time. Convective clouds produce kinetic energy either through cloud-scale processes or the large-scale. Therefore, in response to the forcing the cloud ensemble must do work. The derivative of the cloud work function, $\frac{dA(t)}{dt}$, can be expressed as a sum of separate contributions for both the work done by the cloud scale processes and in response to the large-scale forcing. It is useful to compare these terms to determine the relative time which it takes convection to respond to a change in large-scale forcing compared to the time scale of the cloud processes.

The rate of change of cloud work function due to changes in the cloud-scale processes will occur over a timescale τ_{adj} while the timescale to respond to the large-scale forcing is given by τ_{ls}. τ_{adj} sets how long convection takes to adjust itself to changes in the convective ensemble and τ_{ls} determines the time it takes the convective ensemble to respond to changes in the large scale. It is argued in AS74 that $\tau_{adj} \ll \tau_{ls}$. This implies that there is a *temporal separation scale* between the processes within the convective ensemble and the external, large-scale forcing. It is hypothesised by AS74 that if this is the case then the cloud base mass flux (M_b) can be treated as a function of the large-scale forcing only. Thus, the spectral gap discussed in Section 1.2.2 can be exploited by a parameterisation.

If the external forcing does not vary with time then $\tau_{ls} \to \infty$, so trivially $\tau_{adj} \ll \tau_{ls}$ and AS74 define that the convective ensemble is in *equilibrium* with the large-scale forcing. However, AS74 acknowledge that the actual large-scale forcing may vary with time:

> "Usually the large-scale forcing is changing in time and, therefore, the cumulus ensemble will not reach an exact equilibrium. The properties of the cumulus ensemble will then depend on the past history of the large-scale forcing, but ... only within the timescale of the adjustment time." AS74, p691.

The authors go on to argue that if the timescale of the large-scale forcing (τ_{ls}) is sufficiently large compared to the adjustment time of the convective ensemble (τ_{adj}) then the past history of the forcing, and its associated convective response, are essentially given by the large-scale environment. The convective ensemble acted to remove instabilities due to previous forcing, and in the process modified the atmospheric temperature, moisture and stability to account for the changes in forcing.

Given that the forcing does vary in time, and assuming that $\tau_{adj} \ll \tau_{ls}$, then the convective ensemble will follow a series of equilibrium states, *quasi-equilibria*. Here the cloud base mass flux can *still* be related to the large-scale forcing alone, although that forcing is slowly time-varying. In convective parameterisations this is called the *quasi-equilibrium assumption*.

> "It is also an assumption on parameterisability...Unless a cumulus ensemble is in quasi-equilibrium with the large scale processes, we cannot uniquely relate the statistical properties of the ensemble to the large-scale variables." AS74, p691.

AS74 used the example of an ensemble of convection forced externally to introduce the assumption

of equilibrium for convective parameterisations. Through this assumption the cloud base mass flux of the convective ensemble can be related directly to the forcing and closure for the parameterisation can be determined. The fundamental assumption of equilibrium from AS74 is used either implicitly or explicitly in many parameterisation schemes to link the sub-grid cloud scheme to large-scale dynamics. It is the investigation of the validity (or otherwise) of the key assumption that $\tau_{adj} \ll \tau_{ls}$ that is the main aim of this thesis.

1.3.1 Convective parameterisations

This section provides an overview of some existing convective parameterisations to highlight the methods through which the equilibrium assumption of AS74 is used in practice. Firstly, parcel theory is briefly introduced as this is often used in convective parameterisations to determine triggering or to determine the intensity of convection in the closure. Then, adjustment schemes are discussed and finally mass flux parameterisations will be re-addressed by taking a couple of specific examples.

1.3.1.1 Parcel theory

For a given large-scale atmospheric thermodynamic structure, parcel theory is often used to determine the stability of a profile to convective ascent. A hypothetical parcel is released at a specified level, often near the surface, with a small temperature perturbation. The parcel will ascend dry adiabatically until it reaches a height at which it is saturated. The parcel then ascends along a moist adiabat.

The profile is defined as unstable to convection at a given level if the stability of the parcel, determined by the virtual potential temperature gradient, is less than the stability of the large-scale profile. If the profile is convectively unstable then rising air, such as that represented by the parcel, will continue to rise. This test of the stability of the large-scale profile can be used to define the triggering of convective parameterisations, as will be discussed in the following sections.

Parcel theory is also used to determine the amount of convection that might result given the thermodynamic structure of the large-scale environment. A measure of the potential energy in a profile (either for convection or as an obstacle to convection) in a given layer, is proportional to the vertically integrated virtual temperature difference between the parcel and the large-scale environment. Positive values of this integral give rise to positive energy for the convection process. This is termed

Convective Available Potential Energy (CAPE). On the other hand negative temperature difference gives rise to negative energy, which inhibits convection, Convective INhibition (CIN). Additional energy must be provided to overcome the CIN but when convection does triggers then CAPE can be released. CAPE is often used in mass flux convective parameterisations in the closure assumption, the intensity of the convection being related to the value of CAPE [1].

1.3.1.2 Adjustment schemes

Adjustment schemes are justified by two main physical hypotheses: 1) convection acts to reduce convective available potential energy (CAPE), which it may reasonably be assumed to achieve by driving the vertical profile towards a state that is neutral to moist convection; 2) convection occurs on timescales which are shorter than those characterising the large-scale environment so it may be assumed that (comparatively) convection occurs instantaneously. This requires a direct application of the temporal scale separation and the equilibrium assumption. If one accepts the physical justification, then adjustment schemes are conceptually very simple and do not require the determination of a large number of variables in the computation, so making them efficient for GCMs.

Convective adjustment involves the calculation of the model atmosphere lapse rate. When this lapse rate exceeds some critical value the parameterisation adjusts the lapse rate back to the critical lapse rate whilst conserving dry or moist static energy. In dry atmospheres the critical lapse rate is simply the dry lapse rate of 9.8 $K\ km^{-1}$. However, Manabe and Strickler (1964) noted that the globally averaged lapse rate was closer to 6.5 $K\ km^{-1}$ and used this as the critical value. Using this critical profile in a 1D radiative-convective model, the authors showed that convective cooling was required at lower levels and warming in the troposphere, hence removing the instability (their figure 4). It was shown that this type of scheme improved the vertical distribution of temperature compared to considering radiative effects alone. The process of convective adjustment forces the atmospheric profile to a reference state, at each model timestep, and for this reason is called a *hard adjustment*. Most regions of the atmosphere, however, contain significant moisture and therefore the lapse rate should be a moist adiabatic lapse rate, rather than a dry adiabatic lapse rate or the linear lapse rate as used by Manabe and Strickler (1964).

[1] CAPE is a special case of the cloud work function discussed in Section 1.3. For a non-entraining parcel, $\lambda = 0$ and $CAPE = A(\lambda = 0)$.

Manabe *et al.* (1965) developed moist convective adjustment to improve on convective adiabatic adjustment. Where the atmospheric lapse rate exceeds the moist adiabatic lapse rate, and the atmosphere is saturated, then the profile is adjusted to a moist adiabat whilst moist static energy is conserved. All excess moisture is assumed to rain out. This scheme was found to be an improvement on Manabe and Strickler (1964) but still had some limitations.

In particular, the requirement that the profile is saturated results in instability building up at the grid scale and large precipitation rates occurring when the scheme is finally triggered. Real convective precipitation occurs before the environmental relative humidity reaches 100 %. Fundamentally, convection occurs due to instability, predominantly in the lower troposphere, not the exceedence of some lapse rate. This dependence on a lapse rate means that moist convective adjustment schemes often underestimate the depth of the convective layer by not permitting convection to penetrate into layers that are convectively stable, but influenced by lower layers. The resulting saturated profile will subsequently trigger explicit clouds.

Adjustment schemes do not allow for the proper interaction between convection and the large-scale environment through the role of moisture. Moisture is obviously an important field in climate simulations and adjustment schemes do not allow convection to cause large-scale subsidence or detrainment of moist, cloudy air into the environment. The adjustment criteria do not allow a role for large-scale forcing such as moisture convergence and boundary layer and surface features in determining convection.

Fundamentally, the physical basis for hypothesis (1) of an adjustment scheme based on a reference profile is not known. Whilst convection may often achieve moist adiabatic profiles, particularly in the tropical free troposphere, it is not clear that this is globally applicable. Furthermore, the instantaneous nature of the parameterisation does not allow for simulation of cloud lifecycles which are important for the time evolution of the convective characteristics (Section 1.2.1). Hypothesis (2) implies that convection responds directly and instantaneously to the exceedence of a critical lapse rate.

Improvements to adjustment schemes

Modifications and improvements to hard adjustment schemes include, for example, Kuo (1974) and Betts and Miller (1986) which will be discussed in more detail here. These are often termed *soft adjustment* as they do not have the rigorous conditions of the previous schemes.

Kuo (1974) can be considered an adjustment scheme with a finite adjustment timescale (Arakawa, 2004) in that it adjusts the temperature and moisture of the large-scale environment towards the profile within the clouds, determined by a 1D cloud model. However, the adjustment timescale is different for the heating and moistening effects of convection (see equations (16) and (17) of Arakawa, 2004). Convection is triggered at a grid point if there is sufficient large-scale moisture convergence and buoyancy. Moisture convergence (M_q, equation 1.3) is partitioned into two parts, one which moistens the atmosphere and the other which precipitates (equation 1.4, where b is a prescribed constant). The timescales on which the parameterisation adjusts the environment (i.e. the closure timescales) are set by M_q and by b. The challenge then is to choose b related to the large scale conditions in a physically meaningful manner, and a number a methods have been proposed, e.g Anthes (1977), Donner *et al.* (1982), Krishnamurti *et al.* (1983). The definition of b completes the method through which a soft equilibrium is imposed between the convective scales and the large-scale forcing.

$$M_q = -\frac{1}{g}\int_0^{p_s} \underline{\nabla}\cdot(\underline{\mathbf{v}}\, q)dp + (F_q)_s \tag{1.3}$$

$$M_q = \begin{cases} bM_q + & \text{the moistening part} \\ (1-b)M_q & \text{the precipitating part} \end{cases} \tag{1.4}$$

where $\underline{\mathbf{v}}$ is the velocity field, $(F_q)_s$ is the surface moisture flux, p_s is the surface pressure, q is the water vapour mixing ratio and g is the acceleration due to gravity .

This scheme is an improvement on Manabe *et al.* (1965) as the cloud model allows a more physical determination of the height of cloud and cloud depth. It also ties convection to the large-scale environment through M_q. However, this in itself has been criticised, as in Arakawa (2004), due to arguments of causality. It has been argued that moisture convergence is a result of, rather than a driving force for convection (Emanuel *et al.*, 1994). Also, as a result of defining the amount of convection dependent on M_q the Kuo scheme is effectively limited to representing deep convection, more likely to be associated with large-scale convergence. This usually requires the Kuo scheme to be coupled with a separate scheme for shallow convection as in Kuo (1974) or Tiedtke (1989).

Compared to Manabe *et al.* (1965), the Kuo scheme requires more variables to calculate the adjusted profile, which creates two issues. Firstly, there is a greater computational cost but more significantly there is an increase in the tunable parameters and in the definition of variables. For example, the increased complexity causes debate around the definition of b. The Kuo scheme fails to be an over-arching parameterisation as it does not capture both precipitating shallow and deep convection, which hints that the scheme is based on incorrect physical reasoning: real atmospheric convection does not distinguish between the two regimes.

Similarly to Kuo (1974), Betts and Miller (1986) also determine triggering based on instability in the lower layers, and separate shallow and deep convection. In Betts and Miller (1986) this is based on the depth of the unstable layer, with unstable layers deeper than 200 *hPa* treated by the deep convection scheme and shallow layers by a separate scheme. The shallow convection makes an adjustment towards a reference profile which is based on a moist adiabat. The adjustment occurs over a predetermined timescale to account for τ_{adj} having a finite value. Whilst it may be an improvement to have convection adjust over a period of time rather than on the scale of the timestep, this adjustment period may be seen as a tunable parameter.

In the deep convection scheme, the amount of convection is determined based on the requirement to offset the rate of destabilisation, using a similar method to that outlined for shallow convection by Betts (1973). The temperature and moisture are adjusted towards a reference profile. In a modification to the scheme, Janjic (1994) introduced a *cloud efficiency* which improved the ability of the cloud to transport enthalpy upwards whilst producing limited precipitation.

In contrast to the hard adjustment schemes, the Betts-Miller scheme adjusts the atmosphere 90 % of the way towards the reference profiles and does not adjust instantaneously but over a predetermined timescale.

In addition to the adjustment timescale, the Betts-Miller scheme also includes a stability parameter, which determines the slope of the reference profile, and a saturation parameter, which alters the reference relative humidity profile. In Betts and Miller (1986) these are determined through single column tests based on data derived from the GATE (GARP (Global Atmospheric Research Programme) Atlantic Tropical Experiment) field campaign (Thompson *et al.*, 1979). The chosen values of these parameters provide the best fit to data when forced with the "GATE wave" (the structure and amplitude of the adiabatic forcing) although it was noted that achieving this resulted in incorrect phase of the precipitation.

This scheme highlights some interesting points about soft adjustment schemes. Firstly, the nature of these schemes requires separation of shallow and deep convection, which is rather arbitrary. The schemes also inherently possess a number of parameters which either have to be predetermined (i.e. constant for convection at all times and in all places) or made to be dependent on the large-scale environment (implying that cloud parameters can be directly related to the large scale environment in which they exist, a supplementary closure assumption in the language of Arakawa, 2004). Predetermining these parameters means they will have been chosen, or *tuned*, to some particular data (e.g. the GATE field campaign) and it is not clear that these choices will then be applicable in other situations. Testing against other data sources improves the situation but does not solve the basic problem. Finally, it has been noted that designing and testing parameterisations for certain atmospheric variables, like diabatic heating, does not guarantee that scheme will be correct for other atmospheric variables, as shown in Betts and Miller (1986).

1.3.2 Mass flux schemes

Mass flux schemes differ from adjustment schemes in that they aim to describe the sub-grid clouds themselves in a more physically consistent manner. As discussed in Section 1.3, a mass flux parameterisation has three basic components: firstly, the trigger, which determines when convection occurs and hence when to invoke the parameterisation; secondly, the cloud model, which represents the in-cloud mass flux M_c and the in-cloud thermodynamic variables; and, finally, the closure assumption, which determines how the in-cloud variables found in the cloud model relate to the large-scale environment. The closure assumption from AS74 suggested that equilibrium should be invoked between the sub-grid convection and the large-scale forcing. Mass flux schemes are generally the preferred type of parameterisations for operational meteorological centres.

Gregory and Rowntree (1990) represent shallow, mid-level and deep convection, both dry and moist. This scheme is used in the UK Meteorological Office Unified Model. The scheme uses a 1D bulk cloud model to represent the ensemble and takes account of clouds that detrain below the level of neutral buoyancy by *forced detrainment*. A bulk model is used in contrast to the spectrum of clouds discussed by AS74. Using a spectrum of clouds, a plume model, is computationally demanding and a bulk model is argued to represent the effect of the ensemble of clouds without explicitly representing all cloud types. The bulk cloud is thus a single "cloud" which represents the combined effect of all cloud types. Closure, and hence equilibrium, is enforced by making cloud base mass

flux proportional to the instability in the lowest levels. More recently this scheme has been modified such that the convective intensity is determined from the amount of CAPE at the large scale and, hence, is similar conceptually to the modified Tiedtke parameterisation.

Tiedtke (1989) also developed schemes for shallow, mid-level and deep convection and these have been implemented in the European Centre for Medium-Range Weather Forecasting (ECMWF) model. An non-entraining parcel ascent is used in a 1D bulk cloud model to calculate the depth of the cloud layer and to distinguish between shallow and deep convection. Deep convection is triggered if the large-scale moisture convergence is larger than the surface evaporation. The entrainment rate is set to be small in the cloud model. If the opposite occurs and surface evaporation exceeds moisture convergence then shallow convection occurs and the cloud model uses a larger value of entrainment. The cloud model is a bulk scheme following Yanai *et al.* (1973) where shallow, mid-level and deep clouds are represented by different entrainment and detrainment rates. The closures to the parameterisation are given by the large-scale, low-level moisture convergence for deep convection and by the evaporation rate for the shallow scheme. Deep convection detrains only at the level of neutral buoyancy. It is worth noting that this bulk scheme prevents more than one cloud type occurring in each grid box.

The scheme was modified by Gregory *et al.* (2000) to avoid 'switching' between the shallow and deep convection schemes. In Gregory *et al.* (2000) the type of convection is determined by the depth of the convection obtained from the parcel ascent; a depth of convection exceeding 200 *hPa* is deemed to be deep. The deep convection closure was changed to a CAPE scheme where CAPE is removed on a finite timescale, similar to Fritsch and Chappell (1980) (Gregory *et al.*, 2000). The closure timescale is dependent on grid length. Hence equilibrium is implied by relating the amount of convection to the CAPE available in the environment. Adapting the closure timescale to the grid length allows convection at different length scales to adjust at different timescales. The closure for shallow convection was unchanged.

The scheme was further modified by Jakob and Siebesma (2003) to improve the representation of updrafts, to make it consistent with ECMWF boundary layer scheme, and to change the parcel ascent to an entraining parcel model.

1.3.3 Recent development to parameterisation schemes

Either explicitly or implicitly the above parameterisation schemes have made an assumption of equilibrium between the large-scale forcing and the convective response. Whilst it might be reasonable to assume that convection occurs more rapidly than convective forcing mechanisms, it has yet to be conclusively proven whether τ_{adj} is sufficiently short compared τ_{ls} to validate an assumption of equilibrium. The assumptions in AS74 were more likely to be valid when numerical models had coarse horizontal resolution as the sub-grid convection may better have approximated a convective ensemble. In fact, recent studies have suggested that parameterisations may be one of the main weaknesses in numerical models (this is discussed further in Section 1.4.3).

Recent developments in parameterisations have begun to consider that convective clouds have a lifecycle and do not necessarily adjust instantaneously to a change in forcing. Some parameterisations, so-called relaxed schemes, include a closure timescale to delay the onset of convection. For example a CAPE closure timescale has been used to release the convection over a period of time, and there are 'relaxed' versions of other schemes discussed in Section 1.3.1. A closure timescale is now used both in the UK Meteorological Office and and ECMWF models. Other studies such as Pan and Randall (1998) and Piriou *et al.* (2007) have introduced parameterisations with explicitly calculated prognostic closures. Pan and Randall (1998) relate the entrainment rate to precipitation while Piriou *et al.* (2007) use a closure based on the cumulus kinetic energy present. Both studies stress the interaction between convection and microphysical processes, and highlight the dependence of convection on previous levels of convection.

Despite these new parameterisations, the physical basis for an equilibrium assumption is still not known. Studies that have tested the assumption of equilibrium through observations and numerical modelling experiments will be discussed in Section 1.4. Although some of these studies have implicitly investigated the validity of a temporal scale separation, the direct testing of this assumption will form the basis of this thesis.

1.4 Justification for the quasi-equilibrium assumption

Section 1.3.1 described a representative selection of convective parameterisations which invoke various assumptions based around the concept of an equilibrium. Indeed, almost all convective

parameterisations which have been developed exploit an equilibrium assumption. It is therefore important to test the validity of the equilibrium assumption and assess the timescales for which it is valid. Attempts to do so have been made through both observational analysis and numerical modelling experiments. This section introduces studies that have addressed the validity of the equilibrium assumption in terms of the condition $\tau_{adj} \ll \tau_{ls}$ through observations (Section 1.4.1) and modelling studies (Section 1.4.2).

1.4.1 Testing quasi-equilibrium assumption through observations

Brown and Bretherton (1997) tested a 'strict' form of the equilibrium assumption (SQE), that the vertical temperature profile is moist adiabatic. SQE is therefore relevant to the justification of adjustment schemes. Given this assumption, changes in CAPE will be negligible and the cloud work function (A), as expressed by AS74, will not change significantly in time. Furthermore, if there is sufficient convection and the tropospheric temperature is tied to a moist adiabat, the profile above the boundary layer will be strongly coupled to the potential temperature in the boundary layer. The authors examined microwave sounding data and ship-gathered boundary layer data over an 11 year period for 30 ^oN to 30 ^oS over the tropical oceans on timescales of a month and longer, and spatial scales longer than $\mathscr{O}(300\ km)$. It was shown that there was correlation between the boundary layer and the tropospheric temperatures but that this was not as strong as SQE theory suggested. However, the correlations improved when considering only the strongest convection, suggesting that an SQE assumption is most likely to be valid for the deepest convection. Correlations increase when larger spatial areas are considered. The correlations of atmospheric temperature and boundary layer temperature were larger than those of atmospheric temperature and sea surface temperatures (SST), suggesting a role for the boundary layer in mediating exchanges between the surface and the free troposphere.

The results in this study did not fully support SQE, even at long temporal and spatial scales. The strongest correlations were found on timescales longer than six months, although there were still positive correlations on shorter timescales. There was evidence to support the coupling between the boundary layer and the free atmosphere in terms of the control by the boundary layer on convection in the free troposphere. However, this study did not investigate shorter timescales which are more relevant to convective parameterisations. The study hinted that there may be correlations on timescales less than five days, although the correlation was not seen on timescales of 10-30 days.

There has also been debate about how fluctuations in CAPE in the troposphere relate to fluctuations in the boundary layer. For example, Zhang (2002, 2003) found that there was strong coupling between the boundary layer and the free troposphere, with variability in the boundary layer causing variations in CAPE above. Hence, deviations from equilibrium were found to be dependent on changes within the boundary layer. This relationship was found to hold in extra-tropical, continental regions (Zhang, 2002) and tropical oceanic regions (Zhang, 2003). The studies by Zhang (2002, 2003) are in contrast with those of Raymond (1995) and Emanuel (1995) who proposed a *boundary layer quasi-equilibrium* in which the boundary layer exhibits an equilibrium with the surface fluxes and the downward fluxes from convection. All fluctuations in CAPE are given by variations in the large-scale forcings. However, in the limit of the strict quasi-equilibrium of Brown and Bretherton (1997), then the results of Zhang (2002, 2003) also imply boundary layer quasi-equilibrium.

Another observational study by Donner and Phillips (2003) reconciled the ideas of Raymond (1995); Emanuel (1995) and Zhang (2002, 2003) by determining, if the boundary layer does control the fluctuations in tropospheric CAPE, on what timescales does that control apply. The authors investigated observations over a mid-latitude continental region, the eastern Atlantic and the western Pacific. It was found that results supported Zhang (2002, 2003), in that fluctuations in CAPE were controlled by the boundary layer in all datasets. However, there was evidence that on timescales of half a day or greater there were less fluctuations in the boundary layer and therefore on these timescales boundary layer quasi-equilibrium may hold, consistent with Raymond (1995). It was found that for timescales of 24 *hr* or longer that an assumption of boundary layer quasi-equilibrium was reasonable and therefore that free tropospheric CAPE is controlled by the large scale. The authors point out that through nonlinear interactions between the mean flow and convection, " inaccurate closures at sub-diurnal timescales can lead...to inaccurate treatment of longer timescales as well", p(7)-9.

These studies have shown that on longer temporal and spatial timescales an assumption of quasi-equilibrium may be valid. It has also been shown that deviations away from this equilibrium may be related to changes in the boundary layer modifying the CAPE in the free troposphere. However, due to constraints on the sampling of the observational data it is not possible to determine whether the quasi-equilibrium assumption is valid on shorter timescales. From the point of view of a parameterisation based on the quasi-equilibrium assumption it is most important to determine whether quasi-equilibrium remains valid on shorter timescales, close to the rate at which a parameterisation is activated.

1.4.2 Testing quasi-equilibrium through numerical modelling of radiative-convective equilibrium

Observations are necessary to provide an understanding of processes in the real atmosphere. However, the number of observations that can be taken in time and space are heavily limited. There are usually insufficient data to analyse a full cloud ensemble directly, such as represented by Figure 1.2. One solution is to use numerical models to 'fill the gaps' between the observations and provide more data. Cloud-resolving models (CRMs) can be used to represent a convective ensemble as in Figure 1.2, being run at sufficient resolution to represent the individual clouds within the ensemble. In this way data can be generated for a complete convective ensemble. It is the mean effect of this convective ensemble that the parameterisation is required to represent. The cloud-resolving model can be forced with data from observational campaigns (for example, tropospheric cooling rates or surface fluxes), and the model can be used to simulate variables that may be hard to observe in the real atmosphere, such as profiles of temperature, moisture tendencies and mass flux.

The additional data provided by CRMs makes them suitable to develop and test parameterisations and conceptual models. By prescribing a time-invariant forcing a CRM can be run to a state of radiative-convective equilibrium (RCE). The specification of radiation is important as longwave cooling is key method of forcing convection. At RCE the convective ensemble is in equilibrium with the forcing and (by construction) satisfies that assumption from AS74. A study of the properties of the convective ensemble show characteristics which a parameterisation must capture and so can be used to develop the parameterisation. In another sense, a parameterisation is designed to represent the characteristics of a convective ensemble and so its performance can be tested against data from a CRM. This is often achieved by comparing results for a single column of a numerical model, with prescribed forcing, to a CRM with the same forcing.

The usefulness of CRM simulations in understanding convective ensembles can be seen by considering Figure 1.3 for example. The timeseries shows the temporal-evolution of mass flux near cloud base in response to a step change in the prescribed cooling rate at day 11. A parameterisation relying on a strict equilibrium would only attempt to represent the convective response seen here after $\gtrsim$ 16 days. Note also that a convective parameterisation would usually attempt to represent the mean value of the mass flux, and not the fluctuations about the mean state which are seen in Figure 1.3 and also in other studies (Tompkins and Craig, 1998a; Tompkins, 2000). Studies such as Plant and Craig (2008); Cohen and Craig (2006) have presented theories to explain the fluctuations and

incorporate their effects into parameterisations.

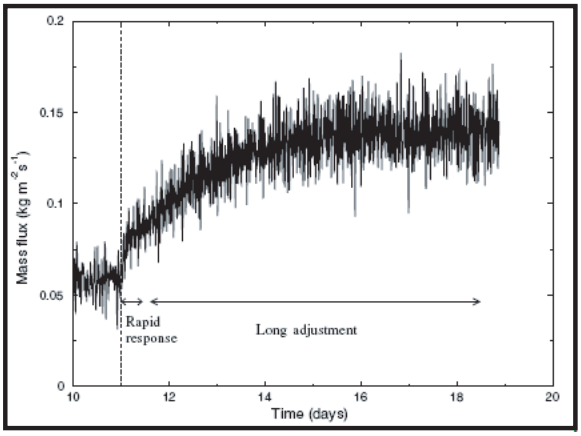

Figure 1.3: *Timeseries of mass flux at* 2.4 *km after a step-function perturbation to the radiative forcing from* $-8\ K\ day^{-1}$ *to* $-16\ K\ day^{-1}$ *has been applied at day 11. (After Cohen and Craig (2004).)*

A CRM can also be used to investigate the detailed time-evolution of the convective ensemble. Cohen and Craig (2004) showed in Figure 1.3 that the convective ensemble responded on two timescales to the step change in the forcing. Firstly, there is a rapid response in the convective ensemble which was determined to be about 1 *hr*. The authors suggest that this is due to the time that gravity waves take to pass between the clouds. The longer adjustment is due to the time taken for moisture to mix through the depth of the troposphere. Cohen and Craig (2004) regard the 1 *hr* timescale as the time convection takes to respond to a change in forcing: i.e. the τ_{adj} in AS74. The authors hypothesise that for the quasi-equilibrium assumption to be valid the timescale of the large-scale forcing, τ_{ls}, must be significantly larger than this 1 *hr* adjustment timescale. As this is likely to be true for most forcings then the quasi-equilibrium assumption may be considered valid. However, the role of the long adjustment timescale in Figure 1.3 on the evolution of the convection is not explicitly considered.

A study of the diurnal cycle by Petch *et al.* (2002) investigated a convective ensemble in a CRM with a repeating series of time-varying surface and atmospheric forcings to represent several successive diurnal cycles. The authors were interested in assessing the effects of model resolution on the development of convection, and in the interests of creating robust results ran their simulations for several successive days. Figure 1.4 shows four days of the surface precipitation. The original aim was to composite the results from the individual days. However, it was found that the characteristics of the convective response were not necessarily consistent day-to-day. For example, the acknowledged effect of coarse model resolution is to delay the onset of convection and to increase

its initial intensity when convection does develop. However, it was noted that at 125 *m* resolution (the highest resolution studied), the convection on the third day developed later than for coarse resolution. This occurred because there had been increased precipitation on day two, seen in the double peak (Figure 1.4), which reduced the precipitable water on day three. It was noted that care was needed in interpreting composite plots from these studies as there is a "strong feedback of previous days' events on the subsequent development of convection", p2039.

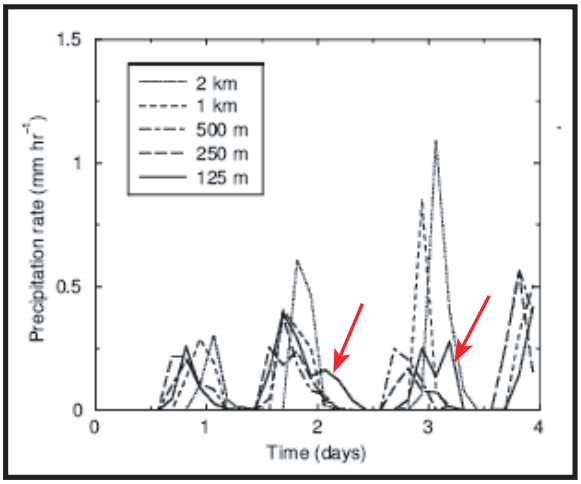

Figure 1.4: *Timeseries of surface precipitation rate from four-day semi-idealised simulations. Results are plotted for horizontal resolutions of* 2 *km,* 1 *km,* 500 *m,* 250 *m and* 125 *m. The lines for* 125 *m horizontal resolution are highlighted with red arrows. (After Petch* et al. *(2002).)*

The nature of this feedback described by Petch *et al.* (2002) suggests that convection is not directly related simply to the current amount of forcing as AS74 theory suggests but rather that, in some manner, convective activity is also is related to previous levels of convection. This may be related to the Cohen and Craig (2004) result that convection responded rapidly, within 1 *hr*, to a step change in forcing but that complete adjustment to the forcing took much longer. If the current convection cannot be related to the current large-scale forcing then the quasi-equilibrium assumption is no longer valid and the parameterisation of convection becomes more complex. As AS74 acknowledged, if the temporal scale separation ($\tau_{adj} \ll \tau_{ls}$) is not valid then the statistical properties of the convection (the convective ensemble) cannot be related to the large-scale forcing. When the scale separation is not valid then the previous levels of forcing, and the associated convective response, are not encoded in the large-scale environment. It is then not possible to parameterise diagnostically using information about the large-scale forcing only. In these situations a parameterisation must be formulated with an alternative technique and make different assumptions to the quasi-equilibrium assumption.

1.4.3 Testing quasi-equilibrium in numerical climate models

As highlighted by the CRM studies described in Section 1.4.2, it has been suggested that the real atmosphere may not always fulfil a quasi-equilibrium assumption, and that this may be a fundamental deficiency of current convective parameterisations. If so, one might expect to find associated deficiencies in atmospheric numerical models.

A study by Yang and Slingo (2001) directly compared observations to results from a climate model to assess the timing of precipitation over the tropics in the model. Precipitation over the tropics is predominantly convective and therefore generated by the convective parameterisation. The authors extracted from both data sources the phase (timing) of the diurnal harmonic of precipitation. The diurnal cycle is a dominant mode of variability in the tropical atmosphere and is particularly relevant for convection. Figure 1.5 contrasts results for differing seasons, although the main features are similar in both seasons. Over tropical land regions observations show that the strongest precipitation tends to occur between 1700 and local midnight. For tropical oceans the picture is more variable, particularly near coasts, but away from the effects of land, precipitation occurs around 0600.

The model has particular difficulty in representing the timing of precipitation in the land-based convective regions. The time of the maximum precipitation is close to local midday, typically 8 *hr* earlier than observations suggest. The tropical oceans also have convection occurring too early, around midnight. It can be seen that, in the case of land-based convection, precipitation is occurring close to the peak of the forcing due to incoming shortwave radiation. The convective parameterisation is causing convection, and hence convective precipitation, to develop closely in phase with the forcing. This is consistent with a quasi-equilibrium-based parameterisation scheme that relates the level of convection to the current forcing, such as suggested by AS74. However, the observations in Figure 1.5(a) suggest that this is not valid.

In discussing the results of this study Yang and Slingo (2001) state:

> " It is possible that the convective parameterisation may need to carry a history of the life-cycle of the cloud systems, suggesting major changes in our current approach to convective parameterisation." p800.

Hence, exploiting a quasi-equilibrium assumption in a climate model may be problematic in terms of producing the correct diurnal cycle of convection over land. It may be necessary for a convective

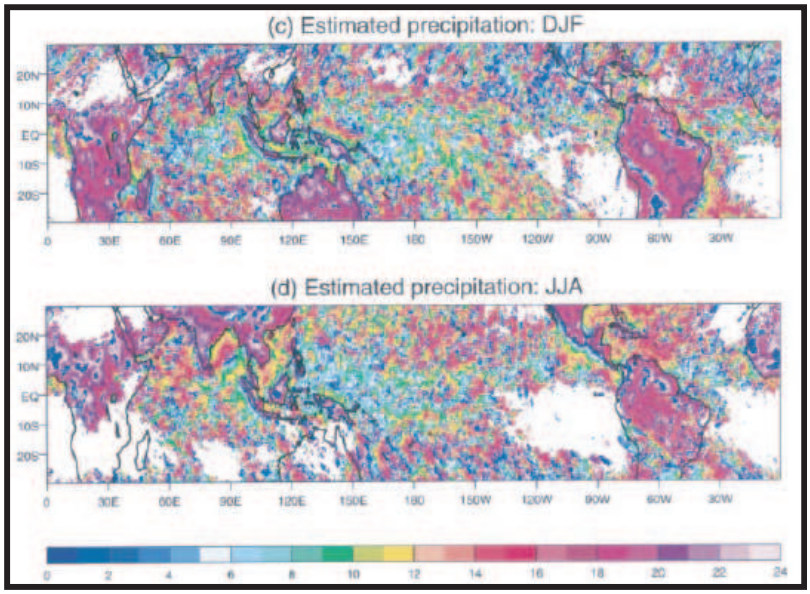

(a) Observed

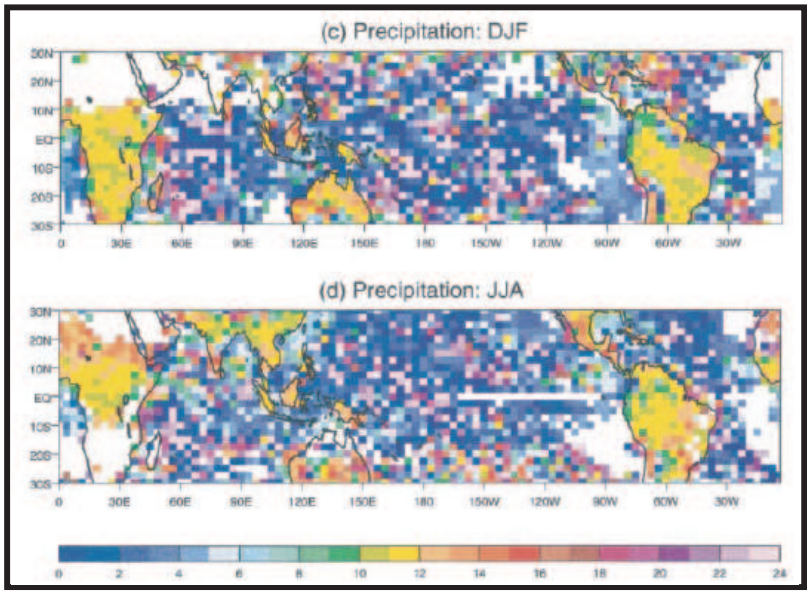

(b) Modelled

Figure 1.5: *Seasonal mean phase of the diurnal harmonic of a) observation-estimated precipitation and b) modelled precipitation for December, January, February (DJF) and June, July, August (JJA). Local time of maximum is given. (After Yang and Slingo (2001).)*

parameterisation to have some time dependence.

To determine the applicability of the quasi-equilibrium assumption to modelling real convection, in a full climate model as opposed to a CRM at radiative-convective equilibrium, it is necessary to test the validity of the temporal scale separation. Cohen and Craig (2004) showed that convection

responds on (at least) two different timescales to a step change in tropospheric cooling, but real atmospheric convective forcing mechanisms are temporally-evolving rather than step changes. It is necessary to investigate how convection responds to different timescales of the forcing in order to fully assess when $\tau_{adj} \ll \tau_{ls}$ is valid.

A recent study by Kuang (2008) investigated convection in a CRM by forcing it with large-scale gravity waves of different wavelengths but fixed amplitude. A simulation of RCE is produced in the first instance and is then coupled to the gravity wave forcing. Figure 1.6 shows timeseries of the surface precipitation for the time when gravity wave forcing is applied. At RCE the precipitation has a mean value of 9.1 $mm\ (day)^{-1}$ and a standard deviation of 0.6 $mm\ (day)^{-1}$. It can be seen that with long forcing wavelengths the convection is similar to that at RCE. As the wavelength shortens the convective response is modified in three ways. Firstly, the shape of the gravity wave forcing becomes more apparent in the precipitation timeseries. Secondly, amplitude of the precipitation becomes more variable in response to forcing cycles of the same amplitude. Finally, the fluctuations that were observed in the standard deviation at RCE reduce with decreasing wavelength.

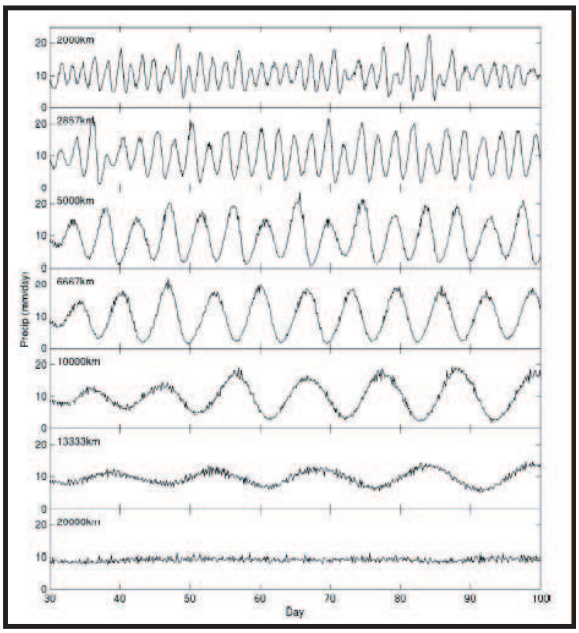

Figure 1.6: *Domain-averaged precipitation as a function of time after coupling to a gravity wave forcing activated for wavelengths of (top to bottom) 2000, 2857, 5000, 6667, 10 000, 13 333 and 20 000 km. (After Kuang (2008).)*

Kuang (2008) present an interesting methodology. The idealised CRM simulations, where one time-varying forcing mechanism has been isolated, show a wide variety of responses for variations

in the timescale of the forcing. The author shows that for a system which is forced by a series of repetitive cycles, of the same amplitude, that responses can be obtained which are non-repetitive, having amplitudes that are different cycle-to-cycle. The technique of investigating the convective response to a single time-varying forcing mechanism will be used in this thesis. This study will focus on convection forced from the surface, as in the example of the diurnal cycle. By changing the length of the forcing cycle different convective responses may be observed.

1.5 Thesis questions

The aim of this thesis is to investigate and quantify the validity of the quasi-equilibrium assumption when a convective ensemble is forced by a time-varying surface forcing. In particular, the scale separation assumption may break down as the forcing timescale is reduced below some limit to be determined. Furthermore, it will be determined whether situations for which a quasi-equilibrium may not be valid can be understood in terms of a memory within the convective system. In the course of this investigation a convective ensemble will be forced at timescales where an equilibrium is achieved and at timescales where it is not. Analysis of, and direct comparison between, these two extremes will enable the identification of physical mechanisms that may cause a convective system to exhibit memory. Specifically, the following questions will be addressed in this study:

Q1. How can a state of equilibrium usefully be defined when the forcing is time-varying? Quasi-equilibrium thinking suggests that convection at each point in time is related to the current forcing. Can this idea be applied for a given time-varying convective response? And if not, how might the ideas from theory be adapted?

Q2. Given a useful definition of an equilibrium from Q1, for what values of forcing timescale is the equilibrium assumption valid? Do situations, where the assumption is not valid, resemble situations where a system has memory?

Q3. In situations where an equilibrium assumption is not valid, what physical mechanisms may be causing the convective response to differ from that expected for the current forcing?

The answers to these questions will be sought through a combination of conceptual analysis of the solution to an analytic model, and investigations of realistic convective ensembles simulated with a cloud-resolving model (CRM). In both cases the convective response is examined for a time-varying

forcing in order to test quasi-equilibrium assumptions. The analytic model has an explicit memory timescale which can be modified in conjunction with the forcing timescale. This permits direct quantification of the relationship between the memory timescale and the forcing timescale. Through analysis of the convective response in the analytic model a metric for defining an equilibrium is introduced, and used to assess for which memory and forcing timescales equilibrium is observed. Whilst the analytic model allows the simplification of convective processes, and hence the direct investigation of memory, it does not represent many of the complexities of real convective systems, most notably the role of moisture. Therefore, a CRM is used in order to examine the response of a realistic convective system, which includes moisture and detailed physical processes. The definition of equilibrium introduced for the analytic model can be used to analyse the response of the CRM. Direct comparison between the two models enables the role of memory to be discussed. Furthermore, the CRM results, being representative of atmospheric convection, can be used to examine physical mechanisms that may cause memory in convective systems.

1.6 Thesis layout

This thesis is laid out as follows. Chapter 2 introduces an analytic model with a memory timescale. The model is used to investigate the response of highly-idealised convection, in a system which has memory, to a time-varying surface forcing. The results are quantified in terms of the characteristics of the convective response and the relationship between the memory timescale and the forcing timescale. A new metric is introduced to define the equilibrium of the convective response and the characteristics of the response are categorised into different regimes based on this metric.

Chapter 3 introduces the CRM that will be used for the simulations of realistic convection. The setup of the model is specified in some detail, and those choices which are different from other CRM studies of convection are highlighted, for example, the method of forcing the CRM. Statistics of the cloud ensemble are discussed and the sensitivities of the cloud characteristics to the highlighted model setup choices are investigated.

In Chapter 4 the response of the same CRM is then investigated in response to a range of forcing timescales. Comparisons are made between the convection in the CRM and that observed in the real atmosphere. The convective response is quantified and discussed in terms of the metric and regimes discussed in Chapter 2. This enables identification of the forcing timescales at which the

convective response may be affected by memory.

Chapter 5 contrasts the convective response in the CRM forced at timescales that are affected by memory to those that do not seem to have memory effects. The domain-mean fields and cloud fields are discussed in order to isolate the mechanism whereby memory exists. Finally, the conclusions of this work are discussed in Chapter 6. In this chapter there is also some discussion of the limitations of this work and further investigations are suggested. Implications of this work for convective parameterisations are also presented.

CHAPTER 2

An analytic model with memory

2.1 Introduction

Chapter 1 discussed the assumption of equilibrium between the convective response and the large scale forcing, which is often made in parameterisation schemes. Here, we are not concerned with the exact nature and representation of the large scale forcing, which depends on the parameterisation in question, but with the validity of such an assumption. It was highlighted that parameterisation schemes fail to capture some features of tropical meteorology, such as the diurnal cycle. One suggested reason may be the role of memory in the atmosphere altering the response of convection to a given forcing.

This chapter will introduce an analytic model which has memory, in the form of a memory timescale. This model represents the convective response of the atmosphere when the system is forced by constant tropospheric cooling and time-varying surface temperatures. The model consists of a 1D second-order differential equation set which is solved through stand-alone numerical integration. Investigation will focus on the relationship between the timescale of the forcing and the memory timescale. The convection will be characterised in terms of the relative values of these timescales and hence the convective response due to the presence of memory will be characterised.

The analysis techniques presented in this chapter will form the basis of further investigations of the response of a convective ensemble to a time-varying forcing in Chapter 4.

2.2 Analytic model

The use of analytic models in atmospheric science is a well-established tradition. Analytic models enable the simplification of complex processes so that the underlying, fundamental mechanisms can be examined. For example, the representation of the Madden-Julian oscillation (MJO) by a Kelvin wave first proposed by Madden and Julian (1971) has formed the basis for many theories

which improve our understanding of the interaction of the MJO and the tropical environment. Also, Stommel and Arons (1961) proposed one of the first dynamical models of abyssal ocean circulation and, whilst it only partially explained deep circulations, it was successful at predicting western boundary currents.

The analytic model used here is designed to represent the convective response caused by atmospheric destabilisation due to a temperature difference between the surface and the atmosphere above. An analytic model is proposed which models the convective activity occurring in a system in response to a time-varying surface temperature when the atmosphere is forced with a constant cooling rate. When convection occurs a heating rate, which represents the latent heat release due to the convection, is fed back to the atmosphere. Therefore, in this analytic model the atmospheric temperature is defined by the action of the constant atmospheric cooling rate (*COOL*) and the convective heating (Q_1).

Let T represent the atmospheric temperature which evolves as:

$$\frac{d\,T}{d\,t} = COOL + Q_1 \tag{2.1}$$

Here the cooling rate represents either radiative or advective temperature forcing or both. Whilst the source of *COOL* is not specified, its value is chosen to be representative of typical atmospheric cooling rates in the tropics. Cooling rates of $-2\ ^oC\ day^{-1}$ are typical of values used in idealised cloud-resolving modelling studies (and a similar value will be used in Chapter 4). This magnitude of cooling rate was used in modelling studies by, for example, Tompkins and Craig (1998a) and Stirling and Petch (2004). Similar values have been found in observational studies: for example by Wu *et al.* (2007) and Xu *et al.* (2002). In this model the cooling rate is chosen to be consistent with these studies, i.e $COOL = 2\ ^oC\ day^{-1}$, with the caveat that 'day' is to be interpreted as the timescale of the forcing, which is discussed further in Section 2.4. (The forcing timescale will have a range of values in the results presented here. This includes a forcing timescale of 24 *hr*, the length of the diurnal cycle, but it will also take other values.) Q_1 here is taken as a direct measure of convective heating, following convention. It is also directly proportional to convective mass flux (Emanuel, 1994), although explicit definition of Q_1 is not required here.

Within the model it is assumed that the convective heating does not respond instantly to a change

in the forcing but rather evolves over time towards a rate R. The evolution towards R occurs over a memory timescale t_{mem} (equation 2.2). R and Q_1 would represent the same convective heating rate if there was not memory within the system. Therefore, Q_1 is the convective heating rate given that the system has memory. The terminology of a memory timescale is used to imply that there is feedback within the system. With large t_{mem} the convection adjusts gradually and so $\frac{d\,Q_1}{d\,t}$ is small. With a small value of t_{mem} the convection adjusts rapidly as the rate of change of convective heating is large. As this model is representing a convective system, t_{mem} is a timescale that represents the time convection would take to *adjust* to changes in forcing. Hence, it can be interpreted as a memory in the system, even though there is no direct dependence of current levels of convection on previous convection.

$$\frac{d\,Q_1}{d\,t} = \frac{R - Q_1}{t_{mem}} \tag{2.2}$$

In the spirit of a conventional CAPE closure (see discussion in Section 1.3.1) we assume that if all the forcing were to be removed, R would act to achieve a convectively neutral atmospheric temperature T_n with a closure time t_{close} (equation 2.3). The closure timescale represents the time it takes convection to *develop* in response to a change in forcing. Without a closure timescale the convection would stabilise the atmosphere instantaneously in response to the forcing.

$$R = \frac{T_s - T_n}{t_{close}} \tag{2.3}$$

The surface temperature (T_s) is made to vary in time, with half of the forcing cycle given by a positive sinusoid and the other half fixed to zero. The period of the forcing cycle is called the forcing timescale, τ. In this thesis the word *period* is generally replaced by *timescale* as the focus of the study is relationship between forcing timescale and convection. The forcing timescale is, therefore, taken to be the time from peak to subsequent peak. Peak values of surface temperature are 5 ^oC giving a diurnal temperature range of 5 ^oC, which is consistent with observations of the diurnal range of tropical surface temperatures (Lin *et al.*, 2000).

2.2.1 Characteristics of model

The system of equations, as they are stated above, has a response shown in Figure 2.1(a) for t_{mem}= $t_{close} = 1\ hr$, $\tau = 24\ hr$. Figure 2.1(a) shows a sample forcing cycle after the system has reached a well-adjusted state and the response is therefore the same cycle-to-cycle. The adjustment process will be discussed further in Section 2.3.1.

The response is characterised by both positive and negative values of R and Q_1. At $time = 0$ the surface is fixed at 0 ^oC and the resulting convection is caused by the cooling in the atmosphere creating a temperature difference between the atmosphere and the surface. As T_s increases (at $time = 0.25$), stronger convective instability results. This causes R to increase and, on the timescale of t_{close}, Q_1 heats the atmosphere to try to remove the instability. The heating by Q_1 increases the atmospheric temperature (e.g. at $time = 0.3$) which reduces the temperature difference between the temperature and the surface. As a result R reduces and Q_1, therefore, subsequently reduces. At the point where $T = T_s$, R become negative and negative values of Q_1 result (at $time = 0.5$).

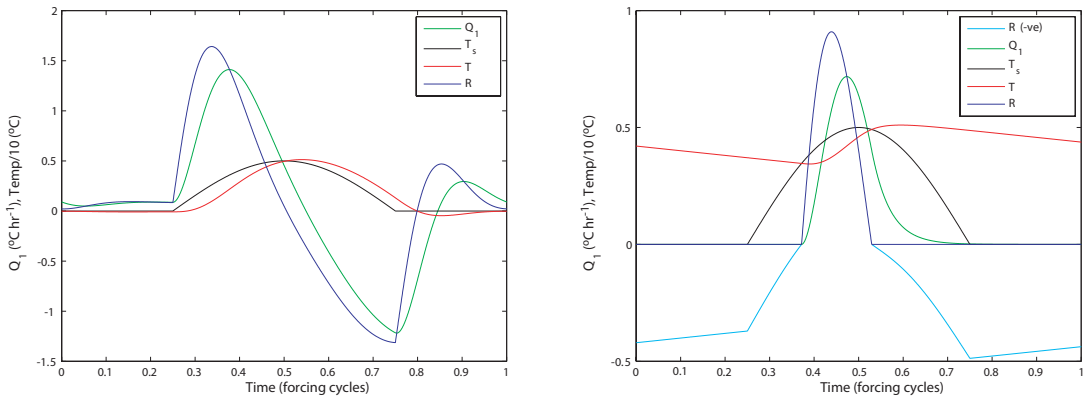

(a) Without traps (b) With traps

Figure 2.1: *Use of trap in the analytic model using $t_{mem} = t_{close} = 1\ hr$, $\tau = 24\ hr$. Analytic model response a) without the trap used and b) with the trap used. Both a) and b) show one forcing cycle after all initial adjustments have been removed and the convection is considered well-adjusted to the forcing. $T_s/10$ black line, $T/10$ red line, Q_1 green line and R blue line. In b) the light blue line is the negative portion of R that would be calculated from equation 2.3. Note different y-axis.*

Figure 2.1(a) shows that the characteristics of the system include negative values of Q_1. These occur when the surface temperature is less than the atmospheric temperature. In reality convection could not occur when there is a positive temperature gradient with height. In particular, in the atmosphere, convection would not occur as the resulting stability at lower levels would cause a layer

of Convective INhibition (CIN). As convection would not occur in this situation negative values of Q_1 in Figure 2.1(a) are not physically meaningful. They result from the model representing convection due to a temperature difference between the model levels without consideration of the direction of the temperature gradient. The use of a 'trap' which prevents negative values of Q_1 is therefore appropriate. This represents the physical criteria that surface temperature must be warmer than the atmospheric temperature for convection to occur and that when convection does occur this causes positive atmospheric heating (positive Q_1). The trap is written in equation 2.4:

$$R = 0 \ \ if \ \ T_s \leq T \tag{2.4}$$

The system response when this trap is used is seen in Figure 2.1(b). Here the constant cooling reduces the atmospheric temperature and R is negative, but increasing. As the surface temperature starts to increase at $time = 0.25$ R increases more rapidly. Due to the trap, which mimics the presence of CIN, there is no convection and Q_1 remains zero. As the surface warms $T_s - T$ decreases until $R = 0$ when $T_s = T$ (at $time \approx 0.35$). At this point convection occurs and Q_1 becomes positive. Whilst $T_s \geq T$ convective heating increases the atmospheric temperature. At $time \approx 0.5$ this forces the atmospheric temperature to be greater than the surface temperature. The trap is then activated and R is switched off. The convection then decays to zero on the timescale t_{mem}. When the convection has switched off the atmospheric temperature evolves, again, only through the cooling rate.

It is suggested that Figure 2.1(b) is broadly representative of a convective system whereas Figure 2.1(a) does not reflect the processes seen in the real atmosphere. The atmospheric response to temperature is highly nonlinear with convective processes occurring only when the surface temperature is warmer than the atmospheric temperature. The nonlinearities stem from the interaction between the activation of the trap and the convective response. The difference between the atmospheric and surface temperature determines when the trap is activated but the activation of the trap has a direct effect on the nature of the convective response, modifying the atmospheric temperature. Hence, due to the inclusion of this trap the model cannot be solved analytically but must be integrated numerically. This nonlinear behaviour can produce much richer behaviour than the second-order differential equation without the trap, and this behaviour is investigated further in this chapter.

The following section will discuss the model setup in terms of the numerical choices made. Section 2.4 will discuss the model results first by determining the effect of t_{close} on the solution and then the effect of t_{mem}. Furthermore Section 2.4 will introduce a method for characterising the convective response. Section 2.5 will present a study of the sensitivity of the results for t_{mem} and τ to t_{close}. Finally, Section 2.6 will characterise the types of response that may be expected for different values of t_{mem} and τ.

2.3 Model setup

In this section the choice of parameters used in the analytic model will be discussed. These include the choices of initial values of atmospheric temperature and convective heating, and the model timestep. Suitable values of t_{mem} and t_{close} will be discussed in Section 2.4.

2.3.1 Choice of initial values

In the first instance the model needs to be initialised with values of T and Q_1. Ideally the choice of these variables would not affect the model solution once converged and if possible the initial choice of T and Q_1 will limit the time the model takes to converge to a final solution. It is not immediately apparent what values of Q_1 the system will attain, so inital values of Q_1 are simply set to zero. Similarly, the value of atmospheric temperature that the system attains cannot be anticipated *a priori* and so the convergence of the system will be tested with values of $T = 0$ and $5\ ^oC$. Figure 2.2 shows the results for these two values when t_{mem}= 24 *hr*, t_{close}= 1 *hr*, τ= 24 *hr*. This combination of values is found to produce a large inital response in Q_1 and so it is anticipated that the system would take a long time to converge. The effect of the initial value of T can be seen in the first 10 days of the response. After 10 days the solution is almost independent of the initial T and is well-adjusted to the forcing. In this final state the convective response has converged and is the same for each forcing cycle. A longer simulation would not change the characteristic shape of the response.

As the final well-adjusted state is independent of the initial temperature chosen the results in this chapter are presented for an initial temperature of 5 °C. Characteristics of the convective response or composites of the response are computed and discussed after the first 15 forcing cycles have been removed to ensure the system is not responding to the inital conditions and that the system has converged to the well-adjusted state.

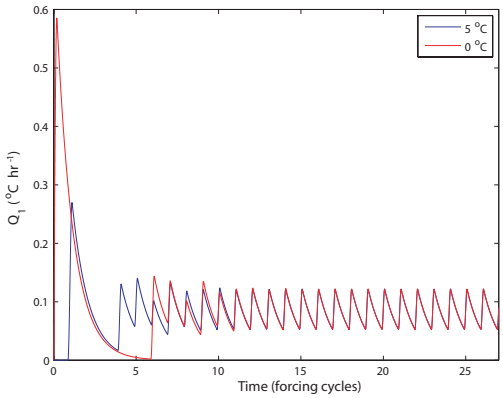

Figure 2.2: *Effect of choice of initial atmospheric temperature (T) on solution to analytic model using $t_{mem} = \tau = 24$ hr, $t_{close} = 1$ hr. Timeseries of Q_1 for two different initial values of T, 5 °C (blue line) and 0 °C (red line).*

2.3.2 Choice of model timestep

In order to compute the numerical solution to this system of equations, the model is discretised using a 1st order, forward in time, finite difference approximation scheme such that equations 2.1 and 2.2 become equations 2.5 and 2.6 respectively:

$$T(i) = T(i-1) + \Delta t\,(COOL + Q_1(i-1)) \tag{2.5}$$

$$Q_1(i) = Q_1(i-1) + \left(\frac{\Delta t}{t_{mem}}\right)(R(i) - Q_1(i-1)) \tag{2.6}$$

where i denotes the value at the current timestep and $(i-1)$ the value at the previous timestep. Δt is the model timestep and all other terms are discretised versions of those in equations 2.1 and 2.2.

This model has an explicit timestep, and therefore a suitable value of Δt must be chosen before the model can be investigated. The precise choice of Δt should not significantly modify the solution to the model. Figure 2.3 shows the solution for Q_1 for two different values of Δt. The response for a large value of Δt (Figure 2.3(a)) is contrasted to that for a small value of Δt (Figure 2.3(b)). The model response is also compared for other values of Δt within this range and the results are summarised in Figure 2.3(c) and 2.3(d).

The effect of the length of the timestep is to alter the accuracy with which the sine wave forcing

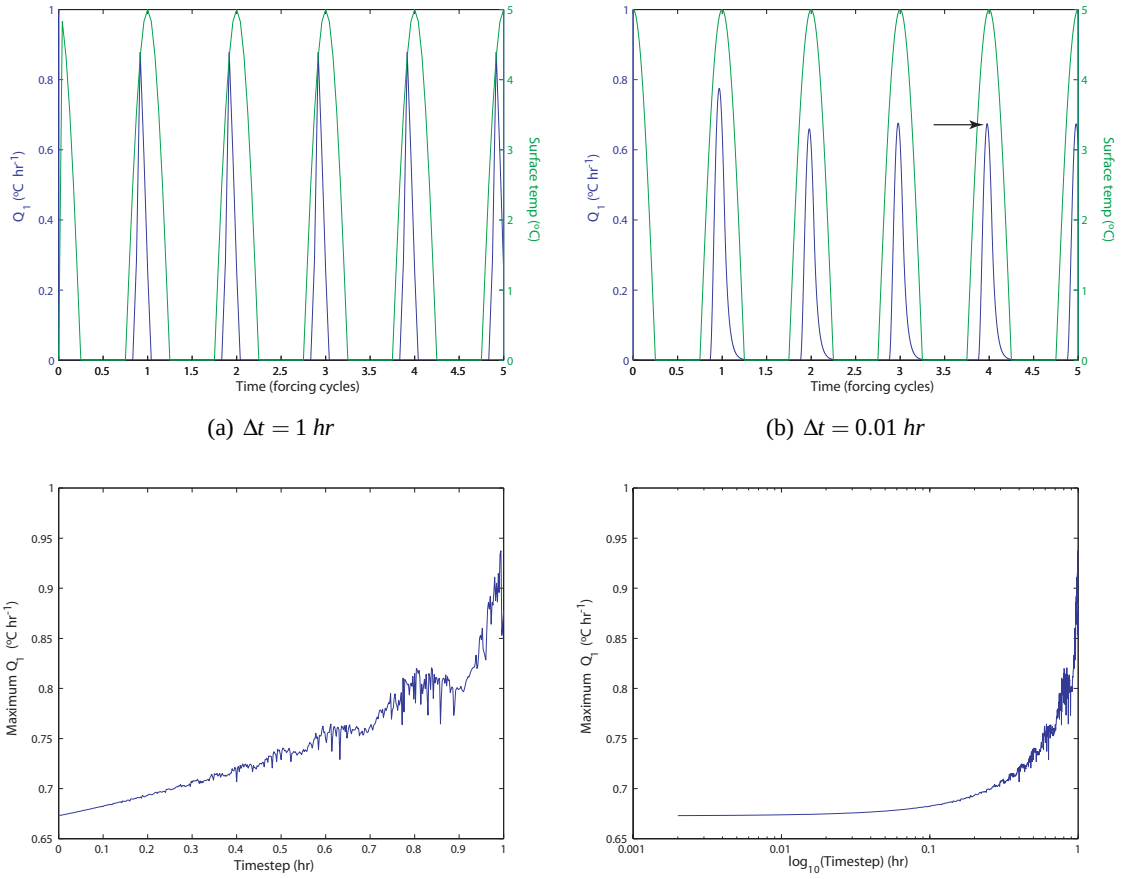

(a) $\Delta t = 1\ hr$ (b) $\Delta t = 0.01\ hr$

(c) Δt (d) $log_{10}(\Delta t)$

Figure 2.3: *Effect of model timestep on solution to analytic model using $t_{mem} = t_{close} = 1\ hr$, $\tau = 24\ hr$. a, b) Timeseries of Q_1 (blue line) for two different values of timestep. Superimposed are timeseries of the surface temperature (green line). In a) there are 24 data points in a forcing cycle and in b) there are 2400. c) Timeseries of maximum value of Q_1 for a range of timesteps. d) Shows the same data as c) but with a logarithmic x-axis in order to show the convergence for small model timesteps. Maximum Q_1 is defined as the maximum value of Q_1 achieved over 12 cycles when the system is in the well-adjusted state. The timing of maximum Q_1 is indicated by arrow in b). Note, however, maximum Q_1 is only found in the well-adjusted state.*

of T_s can be represented. Figure 2.3(a) shows that with a coarse timestep the model has difficulty in capturing the peak of the forcing, producing an overly 'pointed' sinusoidal shape around the maximum. With higher temporal resolution (Figure 2.3(b)) the characteristic shape of the sine wave is better resolved, being more 'rounded' near the maximum. Under-resolving the forcing causes the response, Q_1, to 'overshoot' the value of Q_1 seen at higher resolution. Also, the 'tail' seen at higher temporal resolution (Figure 2.3(b)) cannot be seen when the timestep is too long.

A metric is suggested to determine how the choice of timestep affects the convective response.

When the response has reached its well-adjusted state the maximum value of Q_1 is found over the following 12 cycles. The location of this maximum is shown by the black arrow in Figure 2.3(b). Figure 2.3(c) shows that reducing the timestep reduces the maximum value of Q_1, due to improving the resolution of the forcing function. Figure 2.3(c) shows that at Δt greater than about 0.4 *hr* the response is heavily dependent on the choice of Δt as the model struggles to resolve the forcing and the response. Below 0.4 *hr* the convective response is less sensitive to Δt. Figure 2.3(d) shows that for very short Δt (< 0.03 *hr*) the solution has converged as the representation of the sine wave is improved. A value of $\Delta t = 0.01$ *hr* will be used here for the integration of analytic model as the response is well-defined and the model remains efficient to run. This provides sufficient resolution to represent the forcing function for all examined values of the forcing timescale. At the shortest forcing timescale investigated, $\tau = 1$ *hr*, there are 100 data points representing the sine wave which still provides sufficient resolution.

2.4 Model results

In this section results of the analytic model will be discussed using different values for forcing timescale, t_{close} and t_{mem}. The investigation of forcing timescale is particularly important as characterising the convective response dependent on the rate at which the system is forced is a focus of this work and a specific thesis question (Section 1.5).

The model is set up using variables defined in previous sections. A summary of the variables used is given in Table 2.1. The range of forcing timescales is chosen for the most part to represent the diurnal and sub-diurnal timescales on which convection may be forced. No attempt is made here to represent the longer forcing timescales except in sensitivity studies in Section 2.5. t_{mem} is also chosen to have timescales in diurnal and sub-diurnal ranges so that contrasts can be made between τ and t_{mem} when they are similar and when they are very different. There is little literature to use to determine the range of t_{close}. However, in operational convective parameterisations t_{close} is usually in the range $0.5 - 2$ *hr* dependent on model grid resolution. For the Met Office Unified Model $t_{close} = 2$ *hr* in the climate model and 0.5 *hr* in high resolution Numerical Weather Prediction. Therefore the response of the model to t_{close} in this range will be discussed. However, in Section 2.4.1 $t_{close} = 20$ *hr* will also be used to represent a 'large' t_{close}. The values that are used for the majority of the analysis are listed in Table 2.1.

Variable	Value
Forcing timescale (τ)	$1-24\ hr$
t_{mem}	$1-24\ hr$
t_{close}	$0.5-2\ hr$
COOL	-2 °C day^{-1}
Maximum T_s	5 °C
Initial Q_1	0 °C day^{-1}
Initial T	5 °C

Table 2.1: *Summary of variables used in analytic model.*

In this section the shape of the response timeseries and the effects of different values of closure timescale and memory timescale will be discussed in Sections 2.4.1 and 2.4.2, respectively. Then, in Section 2.4.3 a method of characterising the time-evolution of the response for different values of t_{mem} will be introduced.

2.4.1 Different values of closure timescale

As stated in Section 2.2, R is the heating rate that would adjust the atmosphere from a convectively unstable to a convectively neutral temperature, if there were no further destabilising force acting. t_{close} is a timescale which characterises the rate at which convection can develop in response to a destabilising forcing. In a convective parameterisation this is referred to as a *closure timescale* and specifies how rapidly instabilities are removed. A traditional, diagnostic parameterisation makes no distinction between the quantities R and Q_1. When the convective heating produced in the parameterisation is based on the level of CAPE present, the CAPE *closure timescale* defines how quickly CAPE is removed. In the parameterisation framework the role of t_{close} is only loosely tied to characteristics of the real atmosphere. However, it is still useful to understand the role of t_{close} in the evolution of the solution of the analytic model.

Figure 2.4 shows the effect of t_{close} on the response of the system. The shape of the response on the panels should be contrasted with Figure 2.1(b). With a large value of t_{close} (Figure 2.4(a)) the atmospheric temperature adjusts to the surface temperature over a longer period (see equation 2.3). To maintain convective heating equation 2.3 shows that $T_s - T_n$ must be positive for much of the time and in the well-adjusted state T fluctuates around zero. With a smaller t_{close} (Figure 2.4(b)) the

atmosphere adjusts more rapidly to the surface temperature. As a result the atmospheric temperature can be larger than zero (more positive) and convective heating occurs for a more limited time.

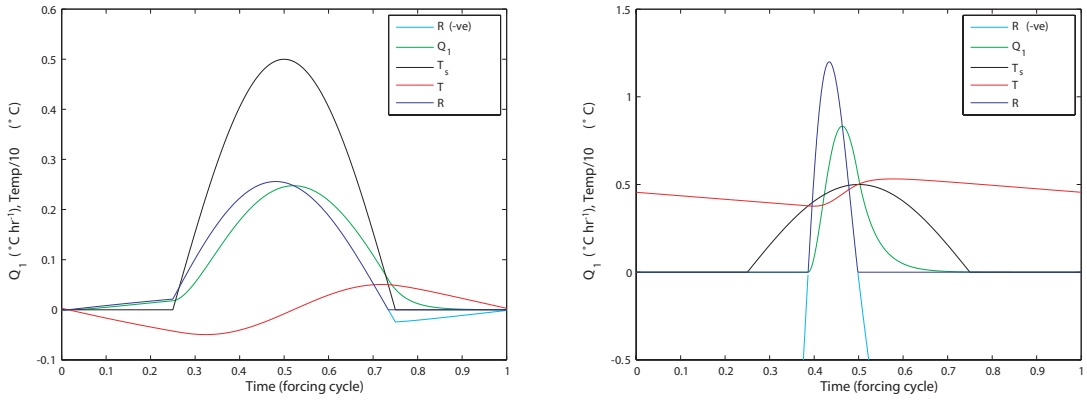

(a) t_{close}= 20 *hr* (b) t_{close}= 0.5 *hr*

Figure 2.4: *Effect of t_{close} on solution to analytic model with t_{mem}= 1 hr, τ= 24 hr. Timeseries of various variables for different values of t_{close}. a) t_{close} = 20 hr, b) t_{close} = 0.5 hr. Both a) and b) show one forcing cycle after all initial adjustments have been removed and the convection is in the well-adjusted state. $T_s/10$ black line, $T/10$ red line, Q_1 green line and R blue line. Light blue line is the negative portion of R. Note different scales on y-axis.*

The results here show that the convective response is dependent on t_{close} as it defines the rate at which convection removes instabilities. Instinctively, a realistic value of closure timescale is likely to be closer to 0.5 *hr* than 20 *hr* as convection occurs in the atmosphere for relatively short periods of time. It is for only limited periods that the surface temperature exceeds the atmospheric temperature. The role of t_{close} in modifying the convective response will, therefore, have to be considered when the effect of the memory timescale and forcing timescale are investigated.

2.4.2 Different values of memory timescale

Due to the characteristics of the response the effect of memory timescale is best visualised by examining the system response on several successive cycles. As described in Section 2.2, t_{mem} defines how rapidly the convection adjusts to changes in forcing. Thus, even though there is no explicit dependence of the current convective response on previous levels of forcing, the role of t_{mem} makes the system behave as if there was memory in the system. If t_{mem} is large then the convective response will depend on previous levels of forcing and is not simply related to the current forcing, as a parameterisation may suggest.

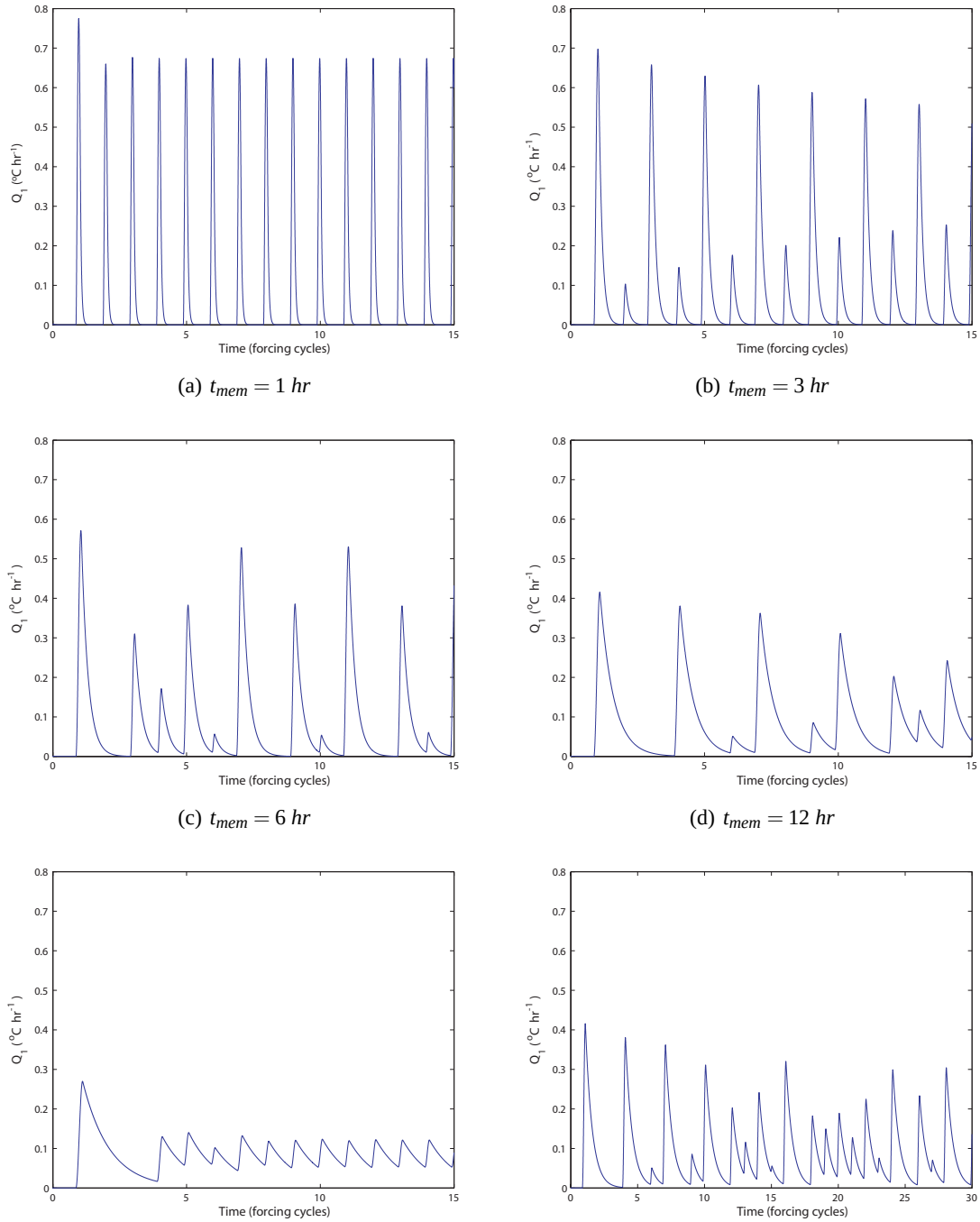

(a) $t_{mem} = 1\ hr$ (b) $t_{mem} = 3\ hr$

(c) $t_{mem} = 6\ hr$ (d) $t_{mem} = 12\ hr$

(e) $t_{mem} = 24\ hr$ (f) $t_{mem} = 12\ hr$

Figure 2.5: *Effect of t_{mem} on solution to analytic model with t_{close}= 1 hr, $\tau = 24$ hr. Timeseries of Q_1 for various values of t_{mem}: a) $t_{mem} = 1$ hr, b) $t_{mem} = 3$ hr, c) $t_{mem} = 6$ hr, d) $t_{mem} = 12$ hr, e) $t_{mem} = 24$ hr, f) extended timeseries with $t_{mem} = 12$ hr.*

Figure 2.5 shows the effect of t_{mem} on the convective response, Q_1. The response is seen to be strongly dependent on the value of t_{mem}. For values of t_{mem} small in relation to τ (e.g., Figure2.5(a)) Q_1 rapidly attains a response which is repetitive and matches the pattern of the forcing. The char-

acteristic shape of the forcing cycle is clearly visible so the response is closely tied to the forcing.

Similarly, when t_{mem} is relatively long the response settles down into a steady state (Figure2.5(e)). However, this response is fundamentally different from that with a short t_{mem}. The response here, in essence, happens over a greater period of time, resulting in a slowly varying Q_1. Hence the response is never zero but also never reaches the large values of Q_1 seen in Figure 2.5(a). The regularity of the response comes from the superposition of the forcing characteristics over a smoothed, slow response. It is anticipated that for very large t_{mem} the response will be characterised by a constant value with the forcing characteristics seen as small scale noise about this mean.

For both short and long t_{mem} (Figures 2.5(a) and 2.5(e)) the response has been characterised as somewhat predictable, although the evolution of the forcing may be strongly or weakly visible respectively. The predictability stems from the same total convection that occurs in response to each cycle of the forcing. If t_{mem} is small, the system has little memory of previous convection and therefore the current convection depends predominantly on the current level of forcing. As the same total forcing occurs for each cycle so the response has the same total convection. If t_{mem} is large, the system has a long memory, causing the current level of forcing to be less significant than its long-term mean.

Between these extreme cases the response is somewhat different in character (Figures 2.5(c), 2.5(d) and 2.5(f)). When $t_{mem} = 3\ hr$ (Figures 2.5(b)) the period of the response is double the period of the forcing but over a long time tends to the period of the forcing. There will be further discussion of the response to intermediate forcing timescales in Section 2.4.3. As t_{mem} increases further beyond 1 *hr* the response becomes non-repetitive and no longer matches the evolution of the forcing. Some forcing cycles include large convective heating whilst for other cycles there is less, or no, convection. For 'moderate' t_{mem} there is feedback within the system, so that larger total convection in some cycles may cause convection to be suppressed in subsequent cycles. Despite the same forcing on each forcing cycle, for these values of t_{mem}, there is sufficient memory to cause different levels of convection in the response across different cycles. Figure 2.5(f) shows that these characteristics may persist with time and that the system does not settle down to a steady, repetitive state even when the response is far removed from the effects of the initial conditions and is in the well-adjusted state.

A summary of the results for different memory timescales can be seen in Figure 2.6. Figure 2.6(a) and 2.6(b) show composite mean Q_1 over 12 successive forcing cycles in the well-adjusted state (i.e after 15 cycles have been removed to account for initial adjustments, see Section 2.3.1). When t_{mem}

is short (Figure 2.6(a)) the response is identical from cycle-to-cycle, as shown by the small standard deviation about the composite Q_1. In contrast having 'moderate' t_{mem} causes different total convection to occur cycle-to-cycle in the response, as shown by the considerable standard deviation about the composite Q_1 timeseries (Figure 2.6(b)). In Section 2.4.3 the mean and standard deviations of the total response over successive forcing cycles will be used to characterise the convective response over a wider range of parameter space.

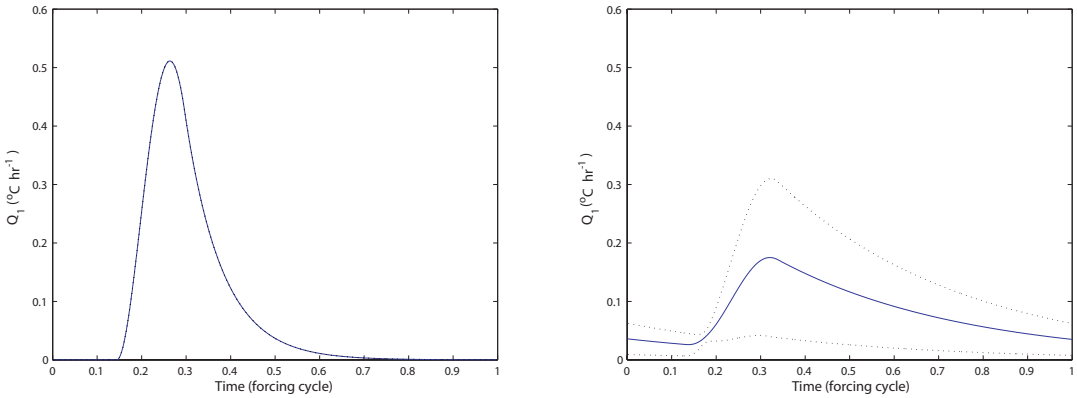

(a) $\tau = 24$ *hr*, $t_{close} = 1$ *hr*, $t_{mem} = 2$ *hr* (b) $\tau = 24$ *hr*, $t_{close} = 1$ *hr*, $t_{mem} = 10$ *hr*

Figure 2.6: *Effect of t_{mem} on solution to the analytic model with $t_{close} = 1$ hr, $\tau = 24$ hr. Composite timeseries of mean Q_1 (blue line) with standard deviation (black, dotted line). a) $t_{mem} = 2$ hr, b) $t_{mem} = 10$ hr. In a) the standard deviation is so small that the dotted and solid lines are difficult to distinguish by eye. Panels show composites computed over 12 successive cycles after all initial adjustments have been removed and the convection is in the well-adjusted state.*

2.4.3 Characterising the response for different values of memory timescale

A metric is suggested to measure the cycle-to-cycle variability of convective heating, and thereby the effect of memory. The total time-integrated Q_1 is found in response to each of 12 forcing cycles in the well-adjusted state (see Section 2.3.1); i.e. after the 15 initial cycles are removed. This is the heating due to convection over 1 cycle and will be written as ΔT_{conv}. From this the mean and standard deviation of ΔT_{conv} is found over the 12 cycles, $\overline{(\Delta T_{conv})}$ and $\sigma(\Delta T_{conv})$ respectively. The second variable is useful to characterise the response for different values of t_{mem} (Figure 2.7). As might be expected, it can be seen that the $\overline{(\Delta T_{conv})}$ is the same regardless of t_{mem}, which implies that the same total convection is required to balance the same total forcing. $\overline{(\Delta T_{conv})}$ can be calculated from the applied cooling by the following: averaged over sufficient forcing cycles the convective heating balances the cooling such that $\Delta T_{conv} = COOL \times \tau$, where COOL is normalised by the

forcing timescale (see Section 2.2). As $COOL = -2\ ^oC\ day^{-1}$, where 'day' is the forcing timescale, this explains why $\overline{(\Delta T_{conv})} = 2\ ^oC$ for all t_{mem}. However, the effect of memory is seen in $\sigma(\Delta T_{conv})$.

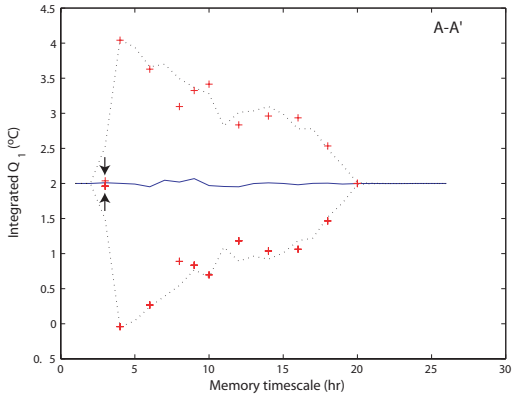

(a) $\tau = 24\ hr, t_{close} = 1\ hr$

Figure 2.7: *Effect of t_{mem} on solution to the analytic model with $t_{close} = 1\ hr$, $\tau = 24\ hr$. $\overline{(\Delta T_{conv})}$ (blue line) with $\sigma(\Delta T_{conv})$ (black, dotted line) for a range of t_{mem}. Values are computed over 12 successive cycles after 15 initial cycles have been removed. The sensitivity to the time period for which the calculations are made is shown by the red pluses, which represent $\sigma(\Delta T_{conv})$ computed over 12 successive cycles after 88 initial cycles are removed. The black arrows highlight that for t_{mem}= 3 hr the response is sensitive to the time period for which the calculation is made. The plot represents A-A' on Figure 2.9(b). t_{mem} is plotted in intervals of 1 hr.*

The magnitude of $\sigma(\Delta T_{conv})$ is found to be dependent on t_{mem}. With small memory timescales, $\sigma(\Delta T_{conv})$ is small, as seen in the timeseries of Q_1 in Figure 2.5(a). As t_{mem} increases the standard deviation also increases. For very large t_{mem}, $\sigma(\Delta T_{conv})$ again becomes small and the timeseries response is similar to that seen in Figure 2.5(e). The most interesting responses occur between the extremes of t_{mem} and these will be discussed in further detail.

The effect of memory can be seen at t_{mem}= 3 *hr*. Here the response was seen to have doubled the period of the forcing (Figure 2.5(b)). This produces large differences in the total convection cycle-to-cycle, as seen by the large values of $\sigma(\Delta T_{conv})$ at t_{mem}= 3 *hr* in Figure 2.7. However, from Figure 2.5(b) it was suggested that Q_1 is converging to a solution, although that convergence is not reached within the 27 cycles examined. This is confirmed from the sensitivity to the time period for which $\sigma(\Delta T_{conv})$ is computed, shown by the red pluses on Figure 2.7. By examining $\sigma(\Delta T_{conv})$ over a longer period of time the system does adjust to a state with the same total convection in each forcing cycle. However, for the other values of t_{mem} plotted on Figure 2.7, $\sigma(\Delta T_{conv})$ has converged after 27 cycles. Therefore, examining integrated Q_1 beyond 15 cycles is sufficient for all other cases. For 'moderate' values of t_{mem} we can usefully discuss two regimes with different

characteristics.

For $t_{mem} = 4-5$ *hr* the largest values of $\sigma(\Delta T_{conv})$ are seen (Figure 2.7) and this is independent of the cycles used, as can be seen by comparing the black, dotted line to the red pluses. The timeseries of Q_1 at these t_{mem} are shown in Figure 2.8. In the case of t_{mem}= 4 *hr* the system settles into a regime where alternate forcing cycles are missed in the pattern of Q_1 (Figure 2.8(a)), thus giving rise to the very large $\sigma(\Delta T_{conv})$ in Figure 2.7. Similarly, for t_{mem}= 5 *hr* forcing cycles are missed in the response although the pattern is no longer as simple as alternate cycles. There is repetition in the system but on several different timescales. The responses seen for $t_{mem} = 4-5$ *hr* are not expected to be found in real atmospheric convection as the response requires an exact balance between the variables, which is unlikely to be achieved in complex convective systems.

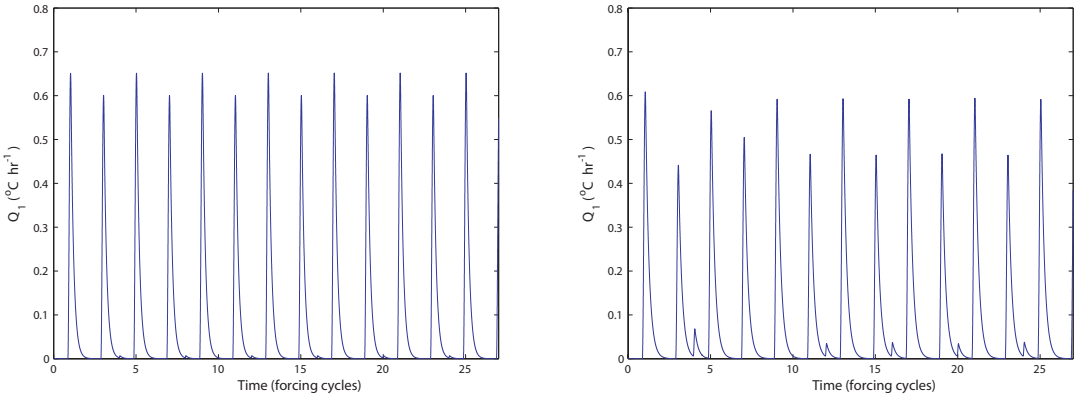

(a) t_{mem}= 4 *hr* (b) t_{mem}= 5 *hr*

Figure 2.8: *Effect of t_{mem} on solution to analytic model with $t_{close} = 1$ hr, $\tau = 24$ hr. Timeseries of Q_1 for different values of t_{mem}: a) $t_{mem} = 4$ hr, b) $t_{mem} = 5$ hr.*

As t_{mem} increases the characteristics seen in Figure 2.8 break down and responses become non-repetitive (compare Figure 2.8 to Figures 2.5(c), 2.5(d) and 2.5(f)). In the range $t_{mem} \sim 10 - 16$ *hr*, where there is 'moderate' memory, the feedback in the system causes large values of standard deviation of Q_1.

In the limit as t_{mem} becomes large compared to the forcing timescale, $\sigma(\Delta T_{conv})$ again becomes small as the system again becomes repetitive and the same total convection occurs in response to each forcing cycle (Figure2.5(e)).

This section shows that the metric $\sigma(\Delta T_{conv})$ can be used to distinguish characteristics of the system response, although examination of the timeseries of Q_1 is required to verify the reason for larger values of $\sigma(\Delta T_{conv})$; e.g. to distinguish between the occurrence of period-doubling (Figure 2.8)

and a non-repetitive response (Figure 2.5(f)). With this caveat, however, the response will be characterised by $\sigma(\Delta T_{conv})$ and this variable will be used to investigate the sensitivity of the response characteristics for other combinations of τ, t_{mem} and t_{close}.

2.5 Sensitivity of convective characteristics

So far the discussion of the effect of memory on a convective system has focussed on altering the memory timescale in relation to a fixed forcing timescale for a given value of closure timescale. This has shown different response timeseries and these have been characterised using the mean and standard deviation of integrated Q_1. The aim of this section is to test the robustness of the results in Section 2.4.2 to the value of t_{close} and in doing so develop a broader representation of the relationship between the memory timescale and the forcing timescale. Then the convective response to a range of forcing timescales will be tested, at a fixed value of t_{close}, for different t_{mem}.

2.5.1 Sensitivity to closure timescale

As noted in Section 2.4 within parameterisations of convective systems there is comparative agreement on convective closure timescales and the response of the analytic model will be tested in this range ($0.5-2$ *hr*). Figure 2.9 shows $\sigma(\Delta T_{conv})$ for t_{close} in this realistic range. This represents a small subset of variable space that could potentially be studied using this analytic model but the aim has been to constrain the choice of variable to those seen in realistic atmospheric convective systems. The responses previously discussed (Figure 2.7) have been for $t_{close}=1$ *hr* and $\tau=24$ *hr* and these lie on the line A-A'. In Figure 2.9(b)) A-A' represents the portion $1 \leq t_{mem} \leq 7$ *hr* shown in Figure 2.7. It is not practical to consider in detail all combinations of $1 \leq t_{mem} \leq 24$ *hr* and $1 \leq \tau \leq 24$ *hr*. However, cross-sections such as A-A', B-B', C-C' and D-D' have been investigated for a wider range of values of τ and t_{mem}.

With larger values of t_{close} the combinations of t_{mem} and τ that produce a large $\sigma(\Delta T_{conv})$ shift towards larger values of t_{mem} and τ. Thus, Figure 2.9 shows that at longer values of t_{close} the system is less influenced by t_{mem} for the same values of τ. As t_{close} determines how long the system takes to develop convection then increased values of t_{close} damp the ability of the system to respond to t_{mem}. Values of t_{mem} and τ need to be larger to show an impact on the system. Specifically, results will be discussed below for the cross-sections through variable space B-B', C-C' and D-D'. Comparison

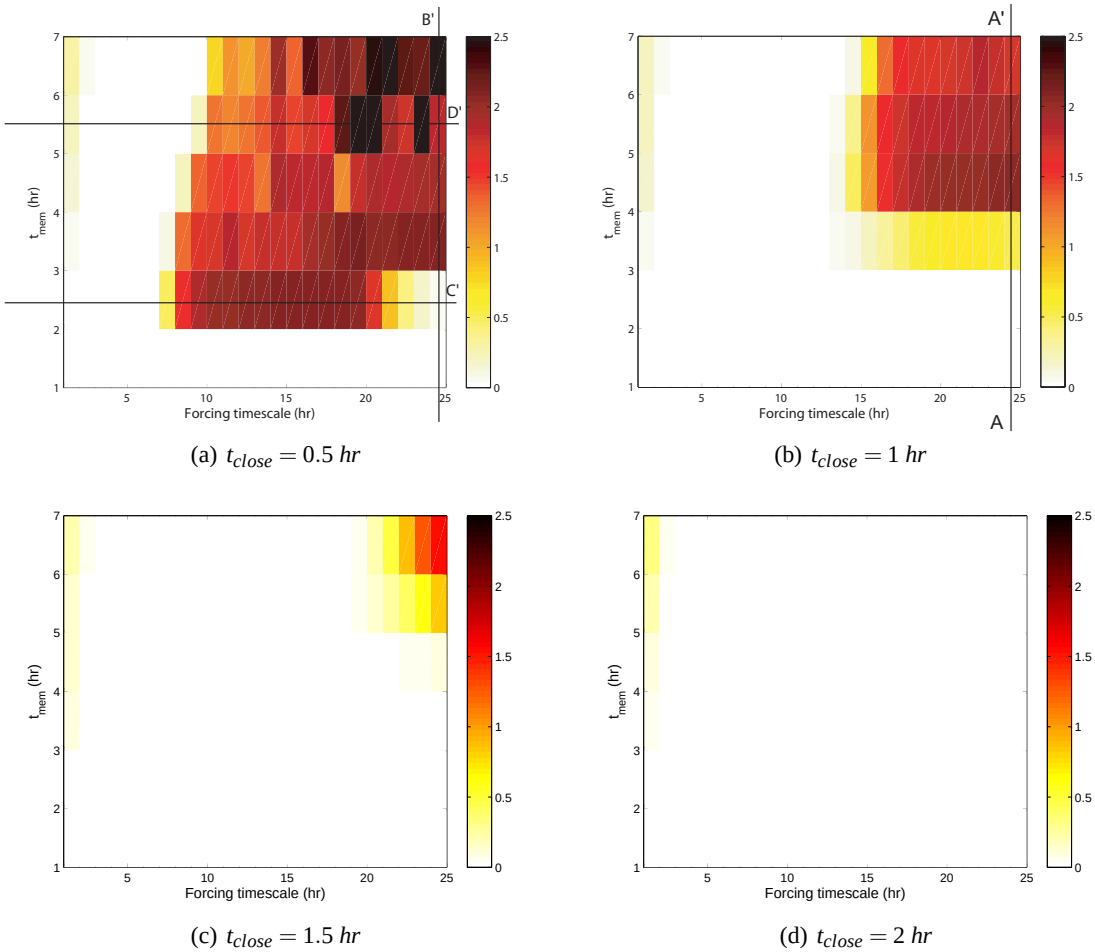

(a) $t_{close} = 0.5\ hr$ (b) $t_{close} = 1\ hr$

(c) $t_{close} = 1.5\ hr$ (d) $t_{close} = 2\ hr$

Figure 2.9: *Effect of t_{mem} and τ on solution to the analytic model. Plotted is $\sigma(\Delta T_{conv})$ for different values of t_{close}. a) t_{close}= 0.5 hr, b) t_{close}= 1 hr, c) t_{close}= 1.5 hr, d) t_{close}= 2 hr. Lines A-A', B-B', C-C' and D-D' represent cross sections indicated on Figures 2.7, 2.10, 2.12(a) and 2.12(b) respectively.*

of A-A' with B-B' shows the effect of t_{close} on the system response. Section 2.5.2 discusses the comparison of C-C' with D-D' to show the effect on the convective response of increased t_{mem}, for fixed t_{close}, for a range of forcing timescales.

Figure 2.10 shows the cross-section through B-B' with $\tau = 24\ hr$ and $t_{close} = 0.5\ hr$ for a range of t_{mem}. This should be compared to Figure 2.7 which is represented by the cross-section A-A' in Figure 2.9. The characteristic shape of the plots are similar for both values of t_{close}. Due to the shorter value of t_{close} in Figure 2.10, t_{mem} can be shorter and still produce the same characteristic response. Hence, in Figure 2.10 the small value of $\sigma(\Delta T_{conv})$ at $t_{mem} = 1\ hr$ is representative of a response which is repetitive with the convective response following the pattern of the forcing, similarly to Figure 2.5(a).

The response observed at $t_{mem} = 4-5\ hr$ when $t_{close} = 1\ hr$ can be seen for t_{mem}= $2-3\ hr$ in

Figure 2.10. Here there is the effect of period-doubling and missed cycles which are similar to those seen in Figure 2.8. This response breaks down and becomes non-repetitive for $3 \leq t_{mem} < 30$ *hr* when $t_{close} = 0.5$ *hr*. The value of $\sigma(\Delta T_{conv})$ starts to reduce for increasing t_{mem} and the response resembles Figures 2.5(d) and 2.5(f). When $t_{mem} \geq 30$ *hr*, $\sigma(\Delta T_{conv})$ is small as the system becomes repetitive due to large memory within the system and the response resembles Figure 2.5(e). Generally the response in Figure 2.10 is more noisy than Figure 2.7. This is due to the smaller value of t_{close} which does not damp the system to the same extent as seen in Figure 2.7. Hence, the effect of t_{mem} is stronger.

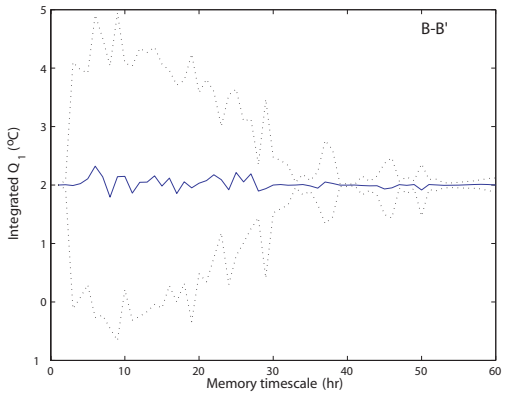

(a) $\tau = 24$ *hr*, $t_{close} = 0.5$ *hr*

Figure 2.10: *Effect of t_{mem} on solution to the analytic model with $t_{close} = 0.5$ hr and $\tau = 24$ hr. Plotted is $\overline{(\Delta T_{conv})}$ (blue line) with $\sigma(\Delta T_{conv})$ (black, dotted line) for a range of t_{mem}. The values are computed for 12 successive cycles after 15 initial cycles have been removed. The plot represents B-B' on Figure 2.9. t_{mem} is plotted in intervals of 1 hr.*

In fact the shape of Figure 2.10 is very similar to Figure 2.7. The role of t_{close} in modifying the response between when $t_{close} = 1$ *hr* and $t_{close} = 0.5$ *hr* can be seen in Figure 2.11. Here, Figure 2.7, where $t_{close} = 1$ *hr*, is shown with Figure 2.10, where $t_{close} = 0.5$ *hr* superimposed. The *x*-axis, t_{mem}, is shown as $t_{mem} \times t_{close}$. The two plots collapse quite well, particularly for large t_{mem}. This suggests that at large t_{mem} it may in fact be the relationship between the closure timescale and the memory timescale, i.e. the product of t_{mem} and t_{close}, which characterises the response of the system at a given value of forcing timescale. At small values of t_{mem} this relationship is less clear in Figure 2.11.

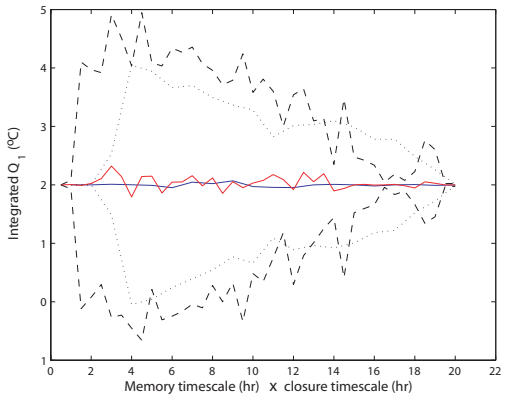

(a) $\tau = 24\ hr$

Figure 2.11: *Figure 2.7 with Figure 2.10 superimposed, where x-axis is multiplied by t_{close}. For $t_{close} = 1\ hr$, $\overline{(\Delta T_{conv})}$ (blue line) with $\sigma(\Delta T_{conv})$ (black, dotted line) and for $t_{close} = 0.5\ hr$, $\overline{(\Delta T_{conv})}$ (red line) with $\sigma(\Delta T_{conv})$ (black, dashed line).*

2.5.2 Sensitivity to memory timescale

This section looks at the effect of t_{mem} on the characteristic response for a range of forcing timescales, for $t_{close} = 0.5\ hr$. This value of t_{close} is taken to be indicative of the response for other t_{close}. In Figure 2.12(a) the effect of short t_{mem} (2 hr) on the system can be seen for a range of τ. When τ is small, $\tau \leq 8\ hr$, the response is repetitive cycle-to-cycle producing small $\sigma(\Delta T_{conv})$. Here t_{mem} is similar to τ and so there is a strong memory effect. The response is like Figure 2.5(e). $\sigma(\Delta T_{conv})$ is large for $8 \leq \tau \leq 18\ hr$. Analysis of the timeseries of Q_1 shows that the response in this range, misses forcing cycles or becomes repetitive on timescales greater than the forcing timescale. In fact, the entirety of the increase in $\sigma(\Delta T_{conv})$, for these parameters, is due to responses that are similar to Figure 2.8. When $\tau \geq 18\ hr$ the response is again repetitive as t_{mem} is much shorter than τ. The system adjusts to the forcing and the shape of the response is characterised by the forcing (see Figure 2.5(a)). For this combination of variables the response never becomes non-repetitive and never resembles Figure 2.5(f).

With a larger value of t_{mem} (5 hr) the response for different values of τ can be seen in Figure 2.12(b). When $\tau \leq 3\ hr$ the response never fully adjusts to the forcing and is not considered further here. For $3 \leq \tau \leq 10\ hr$, the response is repetitive, producing small $\sigma(\Delta T_{conv})$, due to the strong memory effect, which has been previously discussed (see Figure 2.5(e)). $\sigma(\Delta T_{conv})$ then increases and the response becomes non-repetitive, resembling Figure 2.5(d) and 2.5(f) for $10 \leq \tau \leq 13\ hr$. The effect of period-doubling and repetition on timescales greater then the forcing timescale is observed for

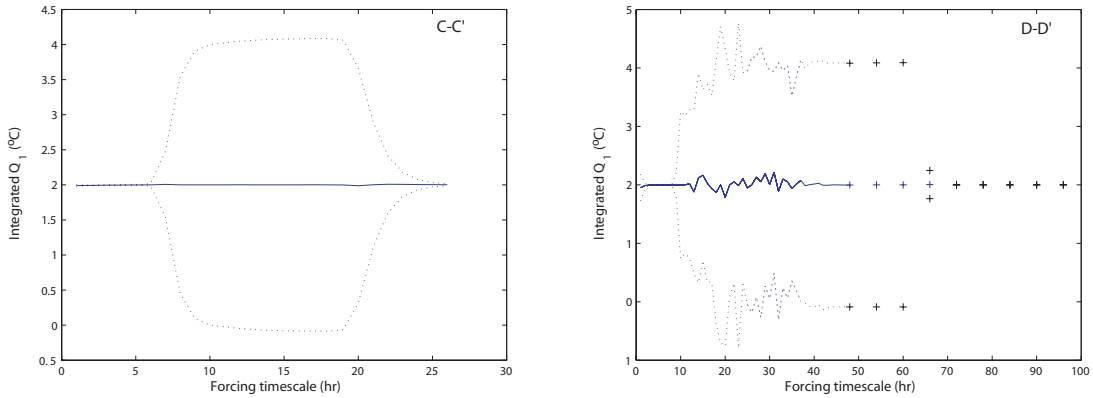

(a) $t_{close} = 0.5$ *hr*, $t_{mem} = 2$ *hr* (b) $t_{close} = 0.5$ *hr*, $t_{mem} = 5$ *hr*

Figure 2.12: *Effect of τ on solution to the analytic model with a) $t_{close} = 0.5$ hr and $t_{mem} = 2$ hr and b) $t_{close} = 0.5$ hr and $t_{mem} = 5$ hr. Plotted is $\overline{(\Delta T_{conv})}$ (blue line) with $\sigma(\Delta T_{conv})$ (black, dotted line) for a range of t_{mem}. The values are computed for 12 successive cycles after 15 initial cycles have been removed. a) and b) represent C-C' and D-D' on Figure 2.9 respectively. τ is plotted in intervals of 1 hr. In b) blue and black crosses represent the continuation of the blue and black lines respectively but for τ plotted in intervals of 6 hr.*

14 *hr* $\leq \tau \leq$ 60 *hr*. For even larger values of τ the response is repetitive due to a small memory in the system and $\sigma(\Delta T_{conv})$ is small. Here the response is similar to Figure 2.5(a).

2.6 Summarising model regimes

The understanding of the characteristics of the response of the analytic model gained from Sections 2.4 and 2.5 are presented in this section to form an overview. Figure 2.13 provides a summary, given a certain t_{close}, of the characteristics discussed in this chapter and the relationship between t_{mem} and τ at which they occur. The regimes A-E are summarised below:

- **A: System 'never' adjusts to forcing**

  The forcing timescale is short compared to the memory timescale. The effect of the closure timescale is strongly felt and the system takes a long time to respond to the forcing and does not fully achieve adjustment. This has not been considered in any detail in this chapter as it is not considered relevant to atmospheric convection. An example is not shown.

- **B: System oscillates about mean response**

  The forcing timescale is of the same order as the memory timescale. The system adjusts to

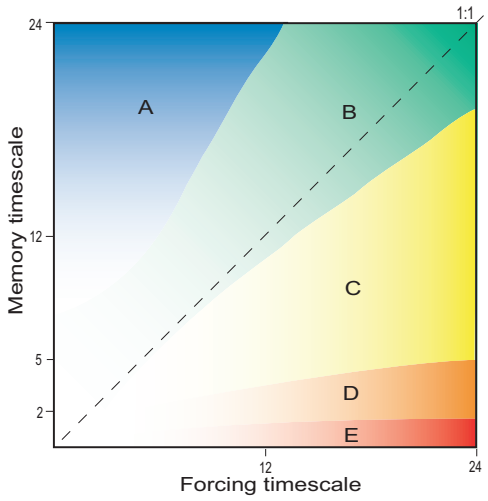

Figure 2.13: *Schematic showing qualitative characteristics of system as a function of t_{mem} and τ for given t_{close}. The shaded areas show where key characteristic responses (regimes) are observed. Where there is no shading, near the origin, the determination of a particular regime is less clear. See text for explanation of the characteristics defined by letters A-E. The schematic provides an indication of regime type at certain timescales but no attempt has been made to test longer timescales (except that in Figure 2.12(b)). The numerical timescales are shown for $t_{close} = 1$ hr and are indicative, rather than quantitative, of the regime type at certain t_{mem} and τ.*

the forcing and the response is repetitive. It is characterised by a mean response, due to strong memory in the system, with the variation of the forcing superimposed as a perturbation about that mean. This is typified by Figure 2.5(e).

- **C: System response is non-repetitive**

  The forcing timescale is longer than the memory timescale. The system adjusts to the forcing but the response is non-repetitive. This 'moderate' memory causes feedback within the system. This is typified by Figure 2.5(d) and 2.5(f).

- **D: System response is repetitive at different timescales**

  For a range of memory timescales the system adjusts to the forcing but the response settles into a regime where cycles are missed on different timescales (Figure 2.8). This bi-modal characteristic represents the model transition between inherently repetitive and non-repetitive regimes.

- **E: System response is repetitive**

  The forcing timescale is long compared to the memory timescale. The system adjusts to the forcing and the response is repetitive. It is characterised by the evolution of the forcing as

there is very limited memory in the system. This is typified by Figure 2.5(a).

Figures 2.13 and 2.11 highlight that these characteristic regimes are not specific to the absolute values of t_{mem} and τ but their relative values.

2.7 Summary and discussion

This chapter introduced an analytic model of atmospheric convection based on a second order ODE. The model represents the time-evolution of both surface and atmospheric temperature. The analytic model is forced by a time-varying surface temperature and a constant atmospheric cooling. Due to imbalance between these forcing mechanisms atmospheric instability results. The model determines the rate at which convection would remove this instability, subject to a memory timescale and a closure timescale. The model was constrained such that convection only occurs when the surface temperature exceeds the atmospheric temperature, in order to represent the non-linear behaviour of the real atmosphere. The analytic model was forced with realistic time-varying, surface temperature and longwave cooling and the characteristic responses were investigated for a range of memory timescales, closure timescales and forcing timescales.

A diagnostic metric $\sigma(\Delta T_{conv})$ was presented to characterise the convective response. This represents a measure of the difference in the total convective response between subsequent cycles and can be used to compare the response for different values of memory timescales, closure timescales and forcing timescales. For different values of memory timescales in relation to the forcing timescale a range of characteristic convective responses were found.

When the memory timescale was much smaller than the forcing timescale the response looked very like the forcing as the memory timescale had limited effect. The response was repetitive and $\sigma(\Delta T_{conv})$was small. For memory timescales much longer than the forcing timescale the response was also repetitive and had small $\sigma(\Delta T_{conv})$. However, the time-evolution of the convection has different characteristics. The response achieved a mean convective response and the variation of the forcing was superimposed as a perturbation about that mean. Here, the memory acts to 'smooth' the convective response such that the characteristic shape of the forcing is not obvious. Between these extremes, for moderate memory timescales, the response is non-repetitive and $\sigma(\Delta T_{conv})$ is larger. There is feedback within the system that prevents the convection reaching a state where the response is the same cycle-to-cycle. A full discussion of these characteristics is found in Section

2.6.

The closure timescale was found to modify the memory and forcing timescales at which key characteristics were observed but similar characteristics were found if memory timescales were re-defined as $t_{mem} \times t_{close}$ for long t_{mem}. This is consistent with equations 2.2 and 2.3.

The analytic model presents a very simple representation of atmospheric convection, although it has been shown it retains some important characteristics of the real atmosphere. The model does not contain moisture and, therefore, does not represent one of the fundamental processes in the real atmosphere, latent heat release. It also does not have an atmospheric boundary layer between the surface and free atmosphere. For this reason there is no phase shift between the forcing and the convective response which is seen in observations of the real atmosphere. It will be important to look at the characteristics of the convective response in a realistic model of convection, which has these properties.

In a realistic convective model the memory timescale will be set by the variables and physical processes within the model. As the memory timescale is intrinsic to the convection only the forcing timescale can be directly controlled. However, through examining the time evolution of the convective response and the standard deviation of the total convection for different forcing timescales it will be possible to determine if the characteristics found in the analytic model can still be observed. From this the role of memory in the evolution of convection can be determined.

CHAPTER 3

Cloud resolving model setup and specification

3.1 Introduction

As discussed in Chapter 1, convection interacts with the large-scale on a range of timescales from the diurnal timescale and longer forcing timescales, to short timescales such as the lifetime of a convective cloud. In Chapter 2 it was shown in an analytic model that the response of a convective system with memory to a time-varying forcing is sensitive to the timescale at which the system was forced. To fulfil the aims of this thesis it is necessary to investigate whether similar behaviour occurs for a realistic convective ensemble.

The characterisation and discussion of the convective response to a time-varying forcing is presented in Chapter 4. This chapter presents an experimental setup suitable for use in such an investigation. The suitability of the setup will be tested in a control simulation of radiative convective-equilibrium (RCE), with time invariant surface fluxes, which will then be used to provide the initial conditions for the simulation with time-varying surface forcing.

Firstly, the numerical model used will be introduced and the decisions made for the overall model setup will be discussed. The initial setup for the control simulation will then be presented. The convective characteristics of the control simulation will then be discussed at RCE in terms of the thermodynamic structure and the cloud field. The sensitivities of the cloud characteristics to key setup choices will also be investigated.

3.2 Model description

3.2.1 Model methodology overview

Numerical simulations of realistic convection are presented using the UK Meteorological Office Large Eddy Simulation (LES) model, version 2.3. This model is a stand alone numerical model

which can be used to represent a convective ensemble. The model is run as a Cloud Resolving Model (CRM) in that it resolves elements which are 'cloud-like' within regions that essentially represent the mean atmospheric state away from the cloud. There is debate about the correct terminology used to describe this type of model. 'Cloud-permitting' or 'cloud system-resolving' models usually refer to models with a grid spacing of $4-5$ *km* down to scales of 1 *km*, such as the UK Meteorological Office forecast model when run at 4 *km*. The term 'cloud-resolving' is often applied to higher resolution simulations where the resolution is between $100-200$ *m*. As there is gap in the terminology, the term 'cloud-resolving' is preferred here since individual clouds of varying sizes (typically $3-10$ km^2) can be identified within the domain. This LEM has been used to investigate a wide range of turbulent and convective processes. These include the evening transition of the boundary layer (Beare *et al.*, 2006), development of convection in the diurnal cycle (Stirling and Petch, 2004; Petch, 2006), and moist boundary layers, including shallow cumulus (Grant and Lock, 2004) and stratocumulus cloud (e.g Lock, 2006). The LEM has also been used in studies of deep convection, from isolated cells to mesoscale convective systems (Gray, 2000).

LES is a technique developed for the study of turbulent processes where the larger scale turbulent motions, or eddies, responsible for most of the energy and transport are explicitly resolved by the model. Smaller scale motions, which may be assumed to dissipate energy, are parameterised. For example, numerically representing the Navier-Stokes equations for a highly-turbulent flow with high Reynolds number, would require very high spatial resolution to fully capture the dissipative terms. Simulating at sufficiently high resolution would then place restrictions on the maximum large-scale length scale that could be considered.

With an LES simulation this problem is addressed by separating the equations into resolved and sub-grid scale components, assuming that an appropriate scale exists. The resolved scale is where the majority of the turbulent energy exists and for a convective system this is the large-scale cloud motions. Energy lost from the resolved scale is transferred to the sub-grid components where it is predominantly dissipated. In a convective system the sub-grid scheme acts to provide boundary layer turbulent mixing and entrainment and detrainment within clouds. In this CRM the grid length is used to separate the resolved flow from that represented by the sub-grid components. One of the challenges of CRM modelling is selecting a suitable resolution where the convective processes are sufficiently-well resolved. Model resolution will be discussed further in Section 4.3.2.

The principles behind LES simulations differ somewhat from Reynolds Average Navier-Stokes (RANS) solution. LES implies some filter where larger scales are explicitly represented and smaller

scale structures are presented by the sub-grid scheme. The grid length may be considered as a filter. Provided that the filter is in the inertial sub-range then the solution will be independent of the grid length. Hence the challenge is to determine the filter scale. RANS separates the flow into a mean component and a fluctuating component. The mean component is explicitly represented and the fluctuations are parameterised. The parameterised component represents an ensemble of possible realisations of the flow. Hence a RANS solution is independent of grid length, excepting the method of parameterisation is chosen based on model resolution (Nieuwstadt and van Dop, 1982).

3.2.2 Overview of CRM

The full details of the CRM setup can be found in Gray (2000) or Derbyshire *et al.* (1994) although useful scientific documentation can also be found in Gray *et al.* (2001). Here only an overview of the CRM setup is given.

The model solves the full primitive equations with anelastic, Boussinesq approximations. The anelastic approximations allow for variations with height of reference profiles of pressure, temperature and density and are an appropriate approximation for convective systems where the buoyancy of clouds is defined by density perturbations.

The sub-grid scheme parameterises the small dissipative eddies which are not explicitly resolved in the model. This scheme is based on a first order Smagorinsky-Lilly approach with two major modifications outlined in Mason (1989) and Derbyshire *et al.* (1994). In a classical Smagorinsky-Lilly scheme the sub-grid momentum flux is dependent on both a basic mixing length and the tensor strain. The first modification in the CRM scheme is that the sub-grid momentum and scalar fluxes are also dependent on a point-wise moist Richardson number. The Richardson number is a fundamental measure of stability in turbulent atmospheric flows. The inclusion of a moist Richardson number permits the scheme to take into account the sub-grid buoyancy production and dissipation effects, including the effect of moisture. Secondly, the basic mixing length is modified so that near ground it is dependent on distance from the surface with a smooth transition to the basic mixing length in the interior of the flow. In the CRM the basic mixing length is given by $c_s\Delta$ (where Δ is the grid length) and may be considered as the spatial scale over which the sub-grid scheme mixes. Practically, the basic mixing length is set in the model with $c_s = 0.23$, although altering c_s is required for very coarse Δ.

In addition to providing a representation of the cloud-scale dynamics and the sub-grid components, to be truly classified as a *cloud* resolving model a representation of the in-cloud microphysical processes is required. The CRM is able to represent three-phase microphysics which include single-moment mixing ratios of water vapour, liquid water, rain and ice processes (ice, snow and graupel), as well as double-moment number concentrations of the ice variables. The scheme is based on Lin *et al.* (1983) and Rutledge and Hobbs (1984) with limited subsequent alterations and modifications. The double-moment part of the scheme is described by Ferrier (1994) and Ferrier *et al.* (1995). A recent description and testing of the scheme can be found in Brown and Swann (1997). By using double-moment schemes, rather than single-moment, the number of adjustable coefficients is reduced and increased physical realism is added by allowing the particle mass concentration and number concentration to deviate from a monotonic relationship. Double-moment schemes have been shown to represent ice processes which are important for the development of precipitation that are not well represented by single-moment schemes.

The CRM uses an Arakawa C-grid (Arakawa and Lamb, 1977) in the horizontal and Lorenz grid in the vertical. The C-grid is used as it gives good accuracy for all wavelengths when Δ is less than the radius of deformation, which is true for all LEM simulations. (The radius of deformation is given in Held (1999) as $\lambda = \frac{NH}{f_c}$ where H is depth scale of the convection, N is the Brunt-Vaisala frequency, and f_c the Coriolis parameter. For typical LEM values of these parameters Δ is less than λ. In this study $f_c = 0$ and therefore Δ is less than ∞.) Each velocity component is staggered in its own direction and scalars (temperature, moisture and pressure) are held on the centre point. The model timestep is internally altered to ensure advective CFL and diffusive stability is maintained but also that the model is run as efficiently as possible. Timestep values in this study vary from $0.5\ s$ at times of strong convection to $3-4\ s$ when there is very limited convective activity.

To avoid the reflection of gravity waves from the rigid lid of the domain, which may interact unrealistically with the convection, a Newtonian damping layer is applied at the top of the domain. All prognostic variables are relaxed to their horizontal means over the depth of damping layer (H_D) on a timescale given by τ_{damp}. The height at which damping begins is z_D and the rate of damping at any given height is given by:

$$\frac{1}{\tau_{damp}}\left[exp\left(\frac{z-z_D}{H_D}\right)-1\right] \tag{3.1}$$

Further details of model setup in the context of this study will be given in the subsequent Section 3.3.

3.3 Experimental design

There are two traditional forcing mechanisms for the CRM. Either a surface temperature (and possibly moisture) or else surface fluxes are specified. The choice has been made here to force the system through prescribed surface fluxes, although sensitivity to this choice will be discussed in Section 3.8.1. It is the timescale of the surface fluxes which will be modified in Chapter 4. Forcing timescales will vary in the range $1 - 36$ *hr* to include timescales close to the convective lifetime and the diurnal cycle.

The diurnal cycle of convection, as an example of convection responding to a time-varying forcing, has been investigated in a CRM in studies such as Chaboureau *et al.* (2004), Guichard *et al.* (2004), Petch (2004), Stirling and Petch (2004) by coupling the surface fluxes with a constant longwave cooling. The work here will follow in this tradition, although it will extend the range of timescales considered, for reasons described below. Studies such as Tompkins and Craig (1998a) and Bretherton *et al.* (2005) have used an interactive radiation scheme together with surface fluxes. There is discussion in Section 3.4 on the effect of simplifying the radiation scheme to a prescribed longwave cooling profile.

For the purposes of this study, forcing the system through prescribed surface fluxes and longwave cooling has the following advantages:

• The convective response, in the context of the diurnal cycle, is reasonably well-understood and hence can be used as a baseline to understand the response when forced with other forcing timescales which do not have direct physical analogues.

• The forcing timescale can be simply controlled through one forcing mechanism. For example, whilst convection is often linked to regions of large-scale convergence it is not immediately apparent how a convergence rate should be modified to provide a time-varying forcing. Another method of forcing convection on different scales is presented in Kuang (2008) who externally forced a CRM with equatorial waves of different wave number.

• The total energy balance of the system, through the surface sensible and latent heat fluxes and

large scale cooling, is known and can be designed to be in balance. As simulations with long forcing timescales will be run for longer than those with shorter forcing timescales, if there was a net imbalance between heating and cooling then this would become more apparent. Direct comparison with different forcing timescales would not then be possible.

As outlined above there are two phases to the model setup, which are summarised in Figure 3.1. A control simulation is used to produce a steady state RCE. This equilibrium state is used to provide a realistic convective field with which to initialise the simulations using a time-varying forcing. For the control simulation both the surface fluxes and the longwave cooling are held constant in time; with time-varying surface fluxes, the longwave cooling remains constant in time. This is consistent with the diurnal cycle situation over land where convection is driven by time-varying surface fluxes. Other studies of RCE discussed in Section 3.4, which prescribe surface temperature (often with a saturated surface), are reminiscent of ocean-type convective situations.

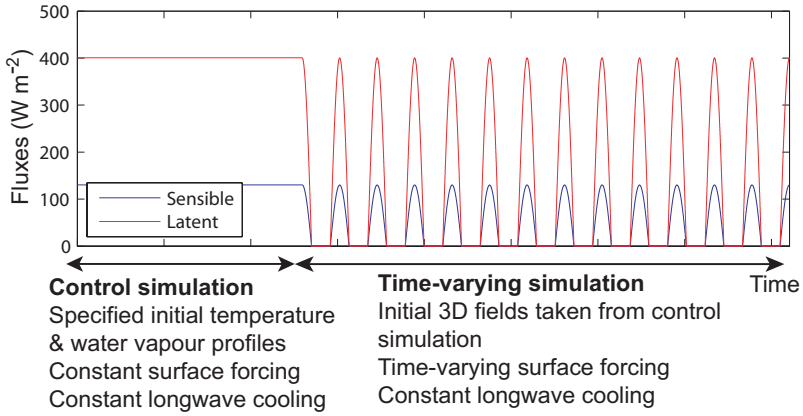

Figure 3.1: *Schematic of experimental setup showing a control simulation of RCE used as initial conditions for time-varying experiments. The characteristics of the control run will be discussed in this chapter and the time-varying runs will form the basis of chapter 4.*

This chapter will focus on the RCE control simulation which forms the basis and a useful point of comparison for the time-varying simulations. The characteristics of the control simulation will be discussed in Section 3.5. Chapter 4 will then focus on discussion of the characteristics of the convection forced on different timescales.

3.3.1 Defining system energy balance

As stated above specifying surface fluxes and a longwave cooling profile allows the total energy supplied to the system to be calculated and controlled *a priori*. The longwave cooling profile directly balances the surface fluxes, as specified through the moist static energy in the system. When the surface fluxes are constant with time, as in the control simulation, the cooling profile is in direct balance at all times. With a time-varying forcing the cooling profile is designed to balance the amount of heating provided by the surface fluxes, over a complete forcing cycle. As there is no net heating or cooling over times greater than the forcing timescale the convective response for different forcing timescales can be compared.

Equation 3.2 shows that the time variation of h, the moist static energy, is dependent on the applied sensible and latent heat fluxes (F_S and F_L respectively) and the applied longwave cooling F_{rad}.

$$\int_0^{z_t} \rho \frac{\partial h}{\partial t} dz = F_S + F_L + F_{rad} \tag{3.2}$$

$$\text{where} \qquad h = c_p T + gz + L_v q \tag{3.3}$$

where z_t is the top of the convective layer and all other symbols have their usual meaning.

For time invariant h it is required that $F_S + F_L + F_{rad} = 0$. With constant surface fluxes, F_S and F_L balance F_{rad} at all times. When the forcing varies in time, F_S and F_L in equation 3.2 should be replaced by $\frac{1}{\tau}\int_0^\tau F_S\, dt$ and $\frac{1}{\tau}\int_0^\tau F_L\, dt$, where τ is the forcing timescale. Thus, the surface forcing is balanced over a complete forcing cycle. The rates of longwave cooling required are different in the control and time-varying phases. This will be discussed further in Section 4.4.2.

Given the longwave cooling rate (F_{rad}) a vertical cooling profile is created using Equation 3.4. The profile chosen is shown in Figure 3.2, with the tropospheric cooling rate ($\dot{T}$) selected such that Equations 3.2 and 3.4 are satisfied. The profile represents a constant longwave cooling in the troposphere, linearly decreasing to zero at the tropopause, and zero in the stratosphere.

$$F_{rad} = \int_0^{z_t} \rho c_p \dot{T} dz \tag{3.4}$$

$$\text{where} \qquad \dot{T} = \left.\frac{\partial T}{\partial t}\right|_{rad} \tag{3.5}$$

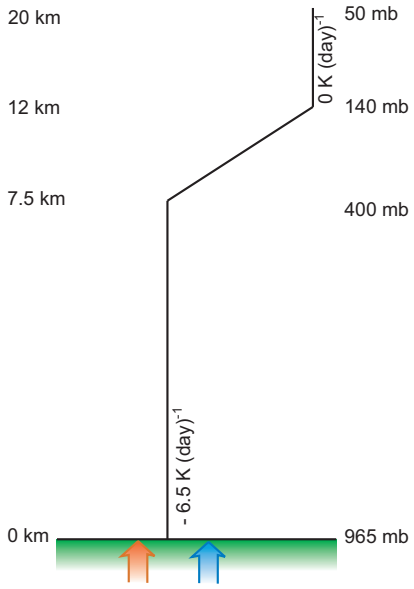

Figure 3.2: *Schematic of model setup with a horizontally-uniform longwave cooling profile and surface sensible and latent heat fluxes. The tropospheric cooling rate of* $\dot{T} = -6.5\ K\ (day)^{-1}$ *applies for the control part of the simulation, and is chosen to satisfy equations 3.4 and 3.2.*

3.4 Overall model setup

The experimental procedure has two parts – the control simulation and the time-varying simulation. As discussed in Section 3.3.1 there are differences in both the surface forcing and the longwave cooling, which make these two parts inherently different. However, there are many choices in the model setup which are the same for both parts. These will be discussed and summarised here.

Radiation

The longwave cooling profile implemented here has the same vertical structure in both parts of the simulation and is shown in Figure 3.2. A homogeneous, non-interacting radiative profile is a substantial simplification of the physical interaction between clouds and radiation. For example, Tao *et al.* (1996) found that the effect of interactive radiation caused infrared cooling at cloud top

and cloud base which served to de-stabilise the cloud layer and enhance precipitation. There was also an effect from the differential heating in the horizontal between cloudy and non-cloudy areas, causing convergence into the cloudy regions, but this effect was found to be less significant than the large-scale longwave cooling. Held *et al.* (1993) found that convection substantially organised itself over a 50 day period. Xu and Randall (1995) however, found it more difficult to distinguish a direct impact of interactive or non-interactive radiation. However, all of these results were for 2D simulations which cannot capture the 3D nature of clouds and their interaction with radiation. A 3D simulation of RCE with interactive radiation (Tompkins and Craig, 1998a) showed that convection organised into bands after four days and that this organisation was sensitive to both the radiation scheme and also to the wind-dependent surface fluxes. Similarly, a recent study by Bretherton *et al.* (2005) showed that in a 3D CRM, without wind shear or rotation, convection organised in ten days into distinct convective and non-convective regions. The system fed-back on itself maintaining the convective precipitation and drying the surrounding regions.

This study has chosen to implement a constant longwave cooling profile for three main reasons. The inclusion of an interactive radiation scheme increases the computational cost, dependent on how frequently the scheme is implemented. (At the spatial resolution used here the implementation of a radiation scheme every 15 *mins* roughly doubles the computational time (S. Weinbrecht, *pers. comm.*)). Second, the interactive radiation scheme can introduce organisation, producing an ensemble of convection which is no longer randomly distributed in space. One of the aims of this study is to investigate how convection responds when forced at different timescales. It is based around the idealised concept of a randomly distributed ensemble of convection which forms the basis for much quasi-equilibrium thinking (Section 1.3). An organised system may not have the same sensitivities as a random ensemble in response to changes in the forcing timescale. Finally, as discussed in Section 3.3.1 the specification of a constant longwave cooling profile allows the timescale at which there is energy balance in the system to be directly controlled. This would not be possible with an interactive radiation scheme.

Wind shear and rotation

Organisation of convection has also been linked to the presence of wind shear and rotation. For example, Robe and Emanuel (2001); Rotunno *et al.* (1988); LeMone *et al.* (1998) examined the role of wind shear in both CRM studies and the real atmosphere and found that, whilst the exact extent to which wind shear organised convection depended on the strength of the shear and the height of strongest shear, shear is capable of organising convection into lines and arcs. Experiments

modifying the rotation rate, i.e. the Coriolis force, showed that with increased rotation more energy cascaded up to larger scales than with smaller rotations, suggesting that rotation plays a role in increasing organisation of convection (Vallis *et al.*, 1997). Due to the organisational effects of wind shear and rotation they are not included in these simulations.

Model dimensionality

The role of model dimensionality has been found by some studies to have limited effects on RCE (Tao *et al.*, 1987; Grabowski *et al.*, 1998). Tompkins (2000) however, found differences when using different dimensions. In 2D the boundary layer was warmer and more moist, with a warmer atmosphere above, than a comparison 3D simulation. It was suggested that the warmer boundary layer in the 2D simulation was caused by stronger surface winds creating stronger fluxes and hence transporting more heat from the surface into the boundary layer. In 3D the speed of spreading cold pools decreases with distance from the source but, the artificial restriction to 2D causes the surface wind speeds to be maintained. Hence, although mean wind speeds are the same in both cases the perturbations, and fluxes of heat, are stronger in 2D. With a larger domain convective organisation also occurred in the 2D case. This produced a drier atmosphere as areas without convection become very dry and therefore inhibit further convection, thus creating a positive feedback. Bretherton and Smolarkiewicz (1997) suggested that the subsidence region around the clouds is enhanced in 2D, resulting in increased organisation. For similar reasons to the difference in cold pool dynamics between 2D and 3D simulations, there are also stronger convergence and divergence patterns in 2D than 3D which may modify the cloud characteristics.

A further limitation of 2D simulations is the artificial development of strong wind shear, which moves downwards with time, in simulations for which the horizontal wind field is unconstrained. In order to test this effect explicitly a simulation for RCE was performed with a similar setup to the control simulation (Section 3.5.1), except that it is 2D and the domain is 128 *km*. Figure 3.3(a) shows that the horizontal shear is seen to increase with time and move downwards. This has also been observed in studies such as Held *et al.* (1993) and Tompkins (2000). It was found by Mapes and Wu (2001) that in 3D the momentum transported by turbulent eddies acted to dampen the horizontal winds whereas in 2D the eddies did not suppress the wind speeds to the same extent. The wind shear generated can have a profound effect on the characteristics of the convection. In Figure 3.3(b) the presence of wind shear causes convection to trigger strongly in only one area and to slant with height. The development of these artificial winds can be suppressed either by constraining the wind to zero (Tompkins, 2000) or imposing a chosen wind profile (Held *et al.*, 1993). Other

methods of suppressing the strong winds were experimented with. These were found to modify their intensity or slow their development but did not remove them sufficiently. Furthermore, artificially controlling the wind profile places additional constraints on the development of the convection and therefore a 3D domain is chosen for this study.

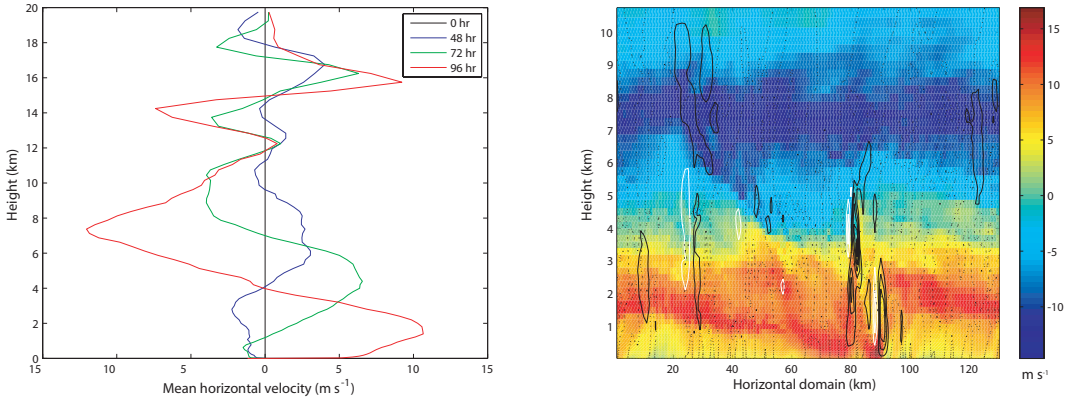

(a) Mean horizontal wind (b)

Figure 3.3: *Effect of 2D dimensionality on horizontal winds at RCE for a domain length of* 128 *km, with* 1 *km horizontal resolution. a) Vertical profile of domain-mean horizontal winds at* 48 *hr intervals. b) Horizontal and vertical velocity after* 96 *hr. The colours show horizontal velocities and the contours vertical velocity where upward motion is black, downward motion is white and the zero vertical velocity contour is dotted black. The contour interval is* 1 $m\ s^{-1}$. *Note the difference in the y-axis.*

Domain size

The issue of domain size is related to the choice of horizontal resolution in that the simulation must be large enough to include several convective clouds, and their associated subsidence, but those clouds must be reasonably well-resolved. A sufficiently large ensemble of convective clouds will produce a domain-mean equilibrium state with small temporal fluctuations. If the domain is too small then intermittency will occur as the environment can be temporarily pushed into a convectively stable state (Tompkins, 2000). The aim is to have a domain that has sufficient clouds which are themselves adequately resolved. The compromise that must be made is between the computational expense of increased domain size and increased horizontal resolution.

Spatial resolution

Studies such as Bryan *et al.* (2003) suggest that for LEM simulations of deep convection to truly resolve the large eddies, horizontal resolutions of $\mathcal{O}(100\ m)$ are required. This is not computationally possible for this study. Recent studies of resolution requirements for CRMs, such as Petch (2006), have suggested resolutions of the order of $200 - 250\ m$ are required to represent the development

from shallow to deep convection. The aim in this study is to focus on the deep convective regime rather than the details of the transition to that regime. Hence, a coarser resolution can be employed. Tompkins and Craig (1998a) suggest that in order to marginally resolve deep convective cores a resolution of 2 *km* is required. They also estimate that, to have continuous convection somewhere in the domain, a grid of 50×50 points is required, although this is dependent on the model cooling rate. This argument was used to justify the choice of domain size in Cohen and Craig (2004) and can also be applied to motivate the choice of domain size here. A horizontal resolution of 1 *km* is chosen which should adequately resolve the *deep* convective cores. It is also the aim of the UK Meteorological Office to more towards 1 *km* horizontal resolution weather forecasts partly for the improved resolution of convective systems. A domain size of 64×64 grid points, hence 64×64 km^2, is chosen here. The horizontal resolution is therefore sufficient, compared to the literature, to represent the type of convection studied. However, the domain size is slightly smaller than some previous studies. The sensitivity of the characteristics of the convection to the domain size will be discussed in Section 3.8.2.

The vertical domain uses a stretched grid with higher resolution near the surface where eddies are smaller and coarse resolution in the free troposphere where circulations are larger. 76 levels are used to provide good representation in the vertical, since Tompkins and Emanuel (2000) showed that vertical profiles of temperature and moisture were sensitive to vertical model resolution, particularly in the boundary layer. Lean and Clark (2003) showed that $\mathcal{O}(100)$ levels were required to represent complex vertical structures. A resolution of 25 *m* is used close to the surface, around 50 *m* through the bulk of the boundary layer, stretching to 250 *m* in the free troposphere and 500 *m* near the tropopause.

3.5 Control simulation

In this section the setup and results for the control simulation, which is at RCE, will be discussed. The characteristics and sensitivity of key atmospheric diagnostics to the chosen setup will then be discussed.

3.5.1 Control simulation setup

The forcing and setup chosen are based on a EUROCS (European Cloud Systems Project) case study (Guichard *et al.*, 2004). This case study was designed specifically to address the issues of modelling the diurnal cycle of deep convection over land, driven by boundary layer heating. It is based on a continental situation, with observations from over the Southern Great Plains, USA, during summer 1997 by an Atmospheric Radiation Measurement programme intensive observation period, which itself formed the basis of the GEWEX (Global Energy and Water-cycle Experiment) cloud system study (GCSS) working group-4 Case 3 (Xu *et al.*, 2002; Xie *et al.*, 2002). For this case study convective events were linked directly to local diurnal heating and were little affected by the advection of mesoscale systems into the domain. Using data from from a field campaign provides realistic forcing mechanisms, with the view to developing realistic convection. As these data have already been used in the EUROCS case study there is a wealth of data against which to compare results.

The case study provides characteristic surface forcing timeseries of sensible and latent heat fluxes, and initial profiles of temperature and water vapour. The EUROCS case study also employed time-series for the large-scale vertical advection of heat and moisture although these are not used in the present study. It was noted by Chaboureau *et al.* (2004); Guichard *et al.* (2004) that these advection terms have limited influence on the evolution of the convection and it is anticipated that excluding them will not significantly effect results. It is necessary to maintain balance between the forcings (see Section 3.3.1) and the introduction of additional forcings, such as advection terms, would disrupt this balance.

The initial profiles of temperature and water vapour for the control simulation are shown in Figure 3.4. These are the initial profiles from the EUROCS case study. The system is forced using constant sensible and latent heat fluxes that are equal to the maximum values that are applied in the time-varying surface forcing simulations (the specific model setup used for the time-varying simulations will be discussed in Chapter 4). The values are 130 $W\ m^{-2}$ and 400 $W\ m^{-2}$ for sensible and latent heat respectively. As discussed in Section 3.3 the longwave cooling required to balance these fluxes (equation 3.3) is calculated and then a cooling profile is created with values as shown in Figure 3.2. The system should then adjust over time to a state of RCE.

It is anticipated that by specifying initial profiles of temperature and water vapour that are appropriate for the forcing, the system will adjust fairly rapidly to RCE. The majority of RCE simulations

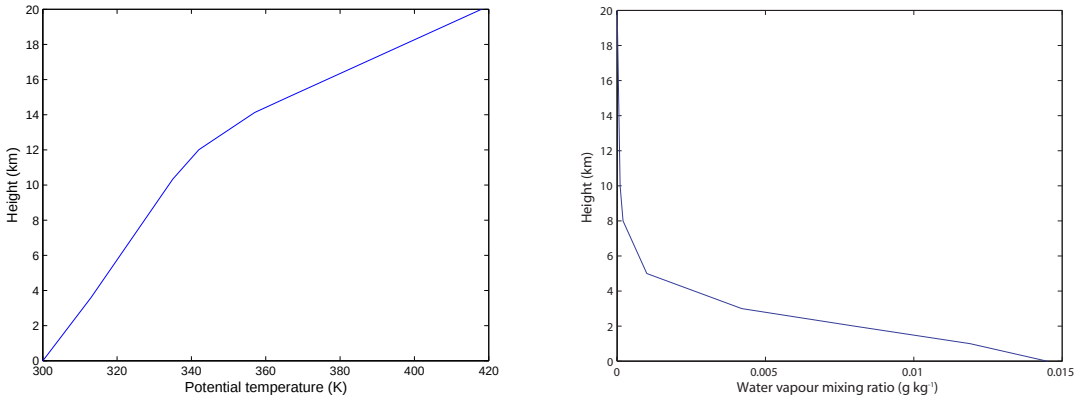

(a) Potential temperature (b) Water vapour mixing ratio

Figure 3.4: *Initial vertical profiles of potential temperature and moisture applied at start of control simulation.*

(Cohen and Craig, 2004, 2006; Bretherton *et al.*, 2005; Tompkins, 2000; Tompkins and Craig, 1998b,a) force a convective ensemble with either an interactive radiation scheme or else with prescribed longwave cooling over a fixed surface temperature. In these situations the adjustment to RCE can take typically $10-20$ *days*. The long adjustment periods are due to the time required to develop a surface wind field which drives sufficiently strong surface fluxes. By prescribing the surface fluxes, convection should develop more rapidly allowing the control simulation to adjust to RCE in a shorter period of time. Hence it is suggested that RCE simulations of 'land-type' convection will adjust to equilibrium more rapidly than 'ocean-type' convection.

A summary of the model setup used in the control simulation is given in Table 3.1.

Sensible heat flux (F_S)	130 $W\ m^{-2}$
Latent heat flux (F_L)	400 $W\ m^{-2}$
Longwave cooling ($\dot{T}$)	$-6.5\ K\ day^{-1}$
Horizontal resolution	1 km
Number of vertical levels	76
Vertical resolution	Stretched grid from 25 m in boundary layer to 500 m near tropopause
Boundary conditions	Bi-periodic, rigid lid, zero slip surface
Newtonian damping layer coefficients	$\tau_{damp}^{-1} = 0.001\ s^{-1}$, $z_D = 16\ km$, $H_D = 3\ km$
Wind shear imposed	none
Coriolis parameter	zero

Table 3.1: *Summary of variables used in control simulation.*

3.6 Characteristics of control simulation

At the end of the control simulation a well-adjusted, realistic convective ensemble should have developed. It will be useful to discuss the characteristics of the ensemble in RCE, first to verify that the effect of initial conditions has been removed (Section 3.6.1) and second to check that the simulated convection is consistent with observations of convective systems (Section 3.6.2).

3.6.1 Timeseries of control simulation

Timeseries of the convective response are shown by the cloud base mass flux and the surface precipitation. The cloud base mass flux is the mass flux through a horizontal level such as that shown in Figure 1.2. The cloud base is the height of the lowest moist point in the domain, where $q_l > 1 \times 10^{-5} kg\ kg^{-1}$. The cloud base mass flux is calculated from equation 1.1 at this height for all grid points where $q_l > 1 \times 10^{-5} kg\ kg^{-1}$ and $w > 1\ m\ s^{-1}$. The cloud base mass flux is given per unit area by dividing by the area of the domain.

Figure 3.5 shows timeseries of the adjustment of the control simulation to the forcing. Cloud base mass flux and surface precipitation adjust fairly rapidly (within 50 *hrs*) to a quasi-steady state with high frequency fluctuations about their mean values. This adjustment time is much shorter than the 12 *days* found by Cohen and Craig (2004) or the 30 *days* found by Tompkins and Craig (1998b). It has been suggested that this adjustment timescale is dictated by the rate at which the model adjusts the thermodynamic profiles through the mixing of water vapour in the subsidence region around the cloud (Emanuel *et al.*, 1994). With the initial vertical profiles in this study chosen to be appropriate to the convective environment being studied, the relatively short adjustment is primarily due to model spin-up as it develops a wind field and spatial variations in the thermodynamic fields. The total vertically integrated water vapour (Figure 3.5(c)) takes a little longer to adjust and shows a slight drift even after 5 *days*, but as the drift is smaller than the fluctuations in the water vapour field this is not significant.

3.6.2 Vertical profiles of control simulation

Figure 3.6 shows domain mean vertical profiles of key thermodynamic variables at 144 *hr* as after this time, it can be seen in Figure 3.5 that there is no further variation in the mean state. The

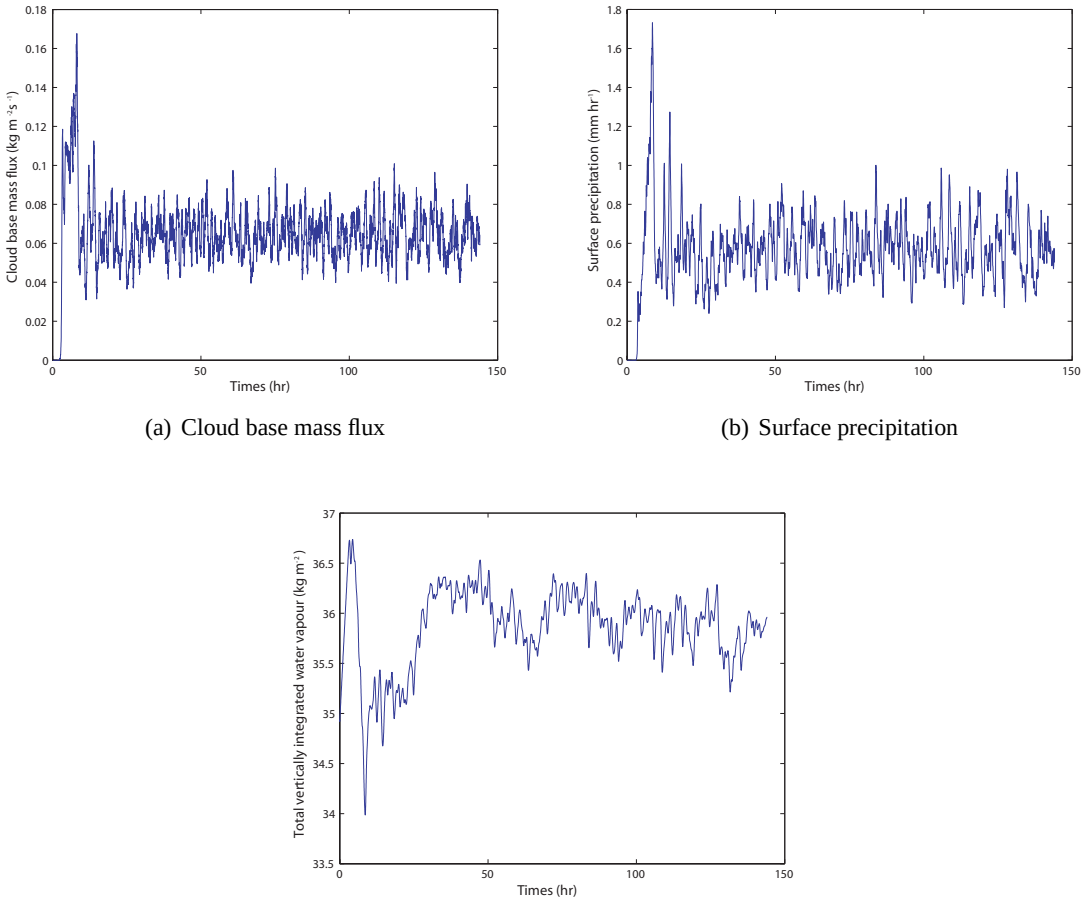

(a) Cloud base mass flux

(b) Surface precipitation

(c) Water vapour

Figure 3.5: *Timeseries of domain-mean a) cloud base mass flux, b) surface precipitation and c) total vertically integrated water vapour for the control simulation.*

potential temperature profile (Figure 3.6(a)) shows a well-mixed boundary layer in the lowest 1 *km*. Above this potential temperature increases with height. Similar profiles form the basis of the Betts-Miller parameterisation (Section 1.3.1.2). Below the tropopause at 12 *km* the profile is close to a moist adiabat (see Section 4.3.3). The profiles is similar to those found by Holloway and Neelin (2007). The largest moisture values are found in the boundary layer, decreasing with height through the troposphere and with no water vapour found above the tropopause (Figure 3.6(b)).

Figure 3.6(d) is consistent with relative humidity profiles seen in observations over oceans (Liu *et al.*, 2000) and in the tropics (Sun and Lindzen, 1993). The minimum of relative humidity seen at 7 *km* is also seen in such observations. The increased relative humidity between $8-12$ *km* can be attributed to detrainment from deep convection (Tompkins and Craig, 1998a). Moist static energy (Figure 3.6(c)) shows a minimum at $\approx 2-3$ *km*. This is typical of tropical soundings

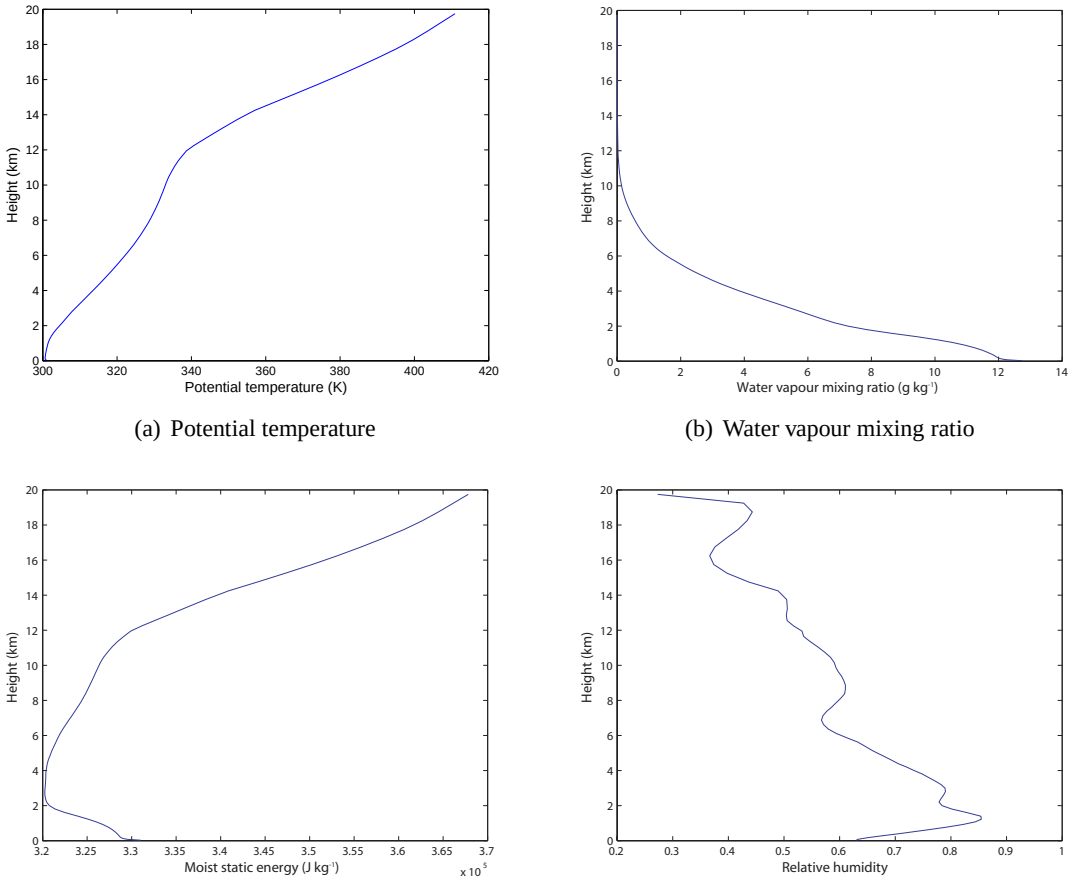

(a) Potential temperature

(b) Water vapour mixing ratio

(c) Moist static energy

(d) Relative humidity

Figure 3.6: *Vertical profiles of domain-mean a) potential temperature, b) moisture, c) moist static energy and d) relative humidity after* 144 *hr of the control simulation. These are the initial profiles used at the start of the time-varying simulations.*

and is thought to mark the transition between the shallow cumulus layer and the upper part of the atmosphere which contains deep convection (Shutts and Gray, 1999). Although these data are used in the control simulation taken from observations at mid-latitudes the meteorology of this area, in summer, can be similar to that in the tropics due to flow from warmer, more moist regions near the Gulf of Mexico.

Profiles of the updraft and downdraft mass fluxes are shown in Figure 3.7. In this figure the updrafts and downdrafts are defined using vertical velocity criteria of $w \geq 1\ m\ s^{-1}$ and $w \leq -1\ m\ s^{-1}$ respectively. This implies that clouds form where there is upwards motion and focusses on the cores of the clouds, where there are strong vertical velocities. This definition is rather arbitrary, although it is regularly used in CRM studies and is based on the aircraft observational study of LeMone and Zipser (1980). It equates to a definition of a cloud core, as discussed in Siebesma and

Cuijpers (1995). The sensitivity of cloud statistics to this definition is discussed further in Section 3.7.

Figure 3.7 shows the vertical profile of updraft mass flux, which is similar to that of Tompkins and Craig (1998a); Gray (2000); Plant and Craig (2008); Grabowski *et al.* (1998). There is a strong peak in the updraft and downdraft mass fluxes in the boundary layer which is not widely reported as a feature of RCE simulations. A similar strong peak can also be seen in the vertical velocity variance (Figure 3.8). Khairoutdinov and Randall (2006) also found a strong peak below cloud base in their simulations of the diurnal transition. It was suggested that this peak is caused by the strong variability in boundary layer plumes, which were comparatively well-resolved. Khairoutdinov and Randall (2006) used a horizontal resolution of 100 *m* and a vertical resolution of 50 *m* in the boundary layer. Although the horizontal resolution used here is much coarser than Khairoutdinov and Randall (2006) the vertical resolution near the surface is finer. Here the horizontal resolution is also finer than other studies reporting updraft mass flux profiles. Therefore, the boundary layer peak in updraft mass flux and vertical velocity variance is attributed to boundary layer plumes.

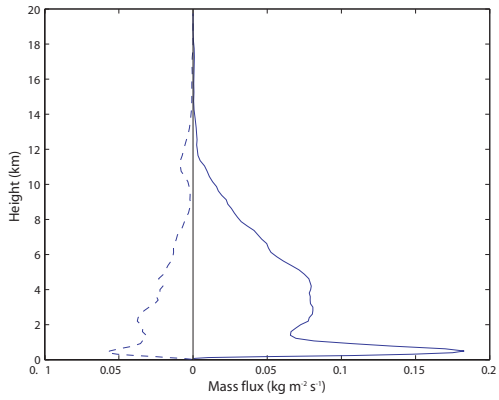

Figure 3.7: *Vertical profiles of domain-mean updrafts (solid line) and downdrafts (dashed line) after* 144 *hr of the control simulation.*

3.6.3 Spatial characteristics of cloud field

Figure 3.9 shows model snapshots which illustrate the horizontal and vertical cloud structure. At any given time there are typically $\approx 15-20$ clouds observed within the domain (Figure 3.9(a)). (The exact number would depend on the cloud definition used, see Section 3.7.) These clouds have a wide variety of sizes, ranging from single cell clouds of $1-2$ km^2 to larger multi-cell complexes.

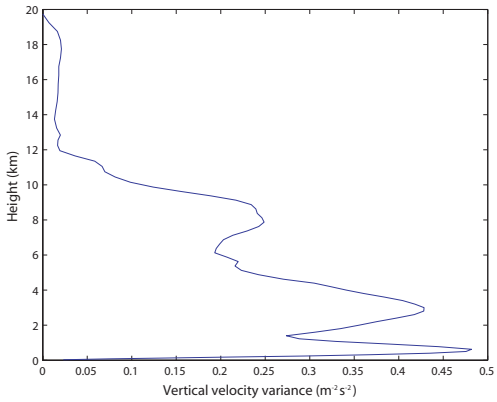

Figure 3.8: *Vertical profile of domain-mean vertical velocity variance after* 144 *hr of the control simulation.*

It is reassuring to see clouds larger than a single grid square as this suggests the dynamical processes involved in cloud development should be partially captured by the resolved scales and are not entirely dependent on the parameterised, sub-grid processes. Despite the stated aim to reduce large scale organisation by using three dimensions and excluding wind shear and rotation (Section 3.4) a line of convection can nonetheless be seen in Figure 3.9(a), orientated south-west to north-east between (35, 20) and (55, 40). (As there is no rotation in these simulations north, south, east and west are arbitary, but used for convenience.) This is found not to be an isolated occurrence; organisation is observed at other times. Further discussion of organisation and its role in the convective ensemble can be found in Section 5.3.1.

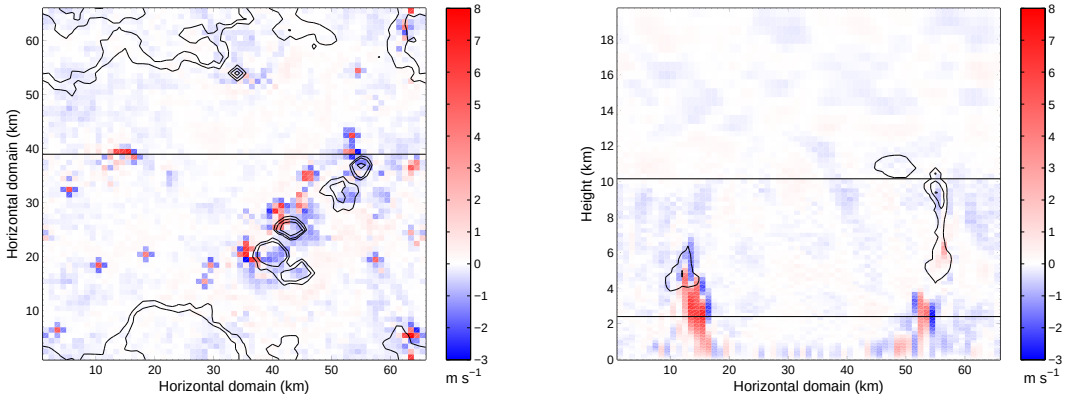

(a) (b)

Figure 3.9: *Horizontal and vertical cross sections of vertical velocity and ice mixing ratio. a) Horizontal cross section of vertical velocity at* $z = 2.4$ *km, superimposed with contours of the ice mixing ratio at* $z = 10.1$ *km. These heights are shown as lines in (b). Mixing ratio contours at 0.1, 0.2 and 0.4 g* kg^{-1}*. b) Vertical cross section, the location of which is shown as a line in (a). Mixing ratio contours at 0.005, 0.05 and 0.1 g* kg^{-1}*.*

Figure 3.9(a) shows that the majority of the larger convective cells become deep (they are producing cirrus anvils at high levels). Also seen are large ice shields that are not apparently associated with convection at low levels. These have persisted while the deep convective cells from which they originated have decayed. This demonstrates that there are processes, which whilst initiated by cumulus cloud processes, actually act on timescales longer than the cloud lifetime. This is an example of a process that persists in the convective ensemble. There will be further discussion about the role of such processes in the evolution of subsequent convective systems in Section 5.4.2.

The vertical cross section (Figure 3.9(b)) shows convection at different stages of development. Below 1 *km* a large number of shallow plumes are visible. Above the boundary layer (2 *km*) there are a limited number of larger, deeper cells. This transition layer was observed in the moist static energy field (Figure 3.6(c)). The deep cumulus clouds extend to the tropopause and develop ice cloud above their cores. Due to the comparatively coarse resolution used, small shallow boundary layer clouds will not be discussed in detail. Investigation will focus on the deep convection above 2 *km*.

3.7 Cloud characteristics of the control simulation

It is useful to determine statistics for the cloud field over a period of time, not least to verify that the characteristics observed at one snapshot in Section 3.6.3 can be generalised to other times. The cloud field will be quantified here in terms of the average number of clouds in the domain ($\langle N \rangle$), the average size of a cloud ($\langle A \rangle$) and the mean mass flux per cloud ($\langle m \rangle$). These statistics are useful to show that sufficient clouds are represented with a plausible distribution. Furthermore, these statistics will form the basis of more in-depth analysis in Chapter 5, which will discuss the organisation of the convection in relation to these variables.

In the first instance a method for partitioning between cloudy and non-cloudy grid points is required. This has been approached differently in observational studies and CRM studies. Early observational studies investigated clouds from aerial photographs. For example, Plank (1969) visually identified clouds, classifying them by their diameter and found that early morning convection had an exponential distribution, although this distribution was less clear later in the day. Recent advances in satellite imaging have led to more objective cloud classification. Futyan and Genio (2007) identified clouds at different stages of development based on a combination of cloud top temperatures

and radius.

In CRM studies a cloud is often defined as where the vertical velocity at a grid point exceeds a threshold, e.g $w > 1\ m\ s^{-1}$, (Cohen and Craig, 2006) although other definitions have also been discussed. Cohen and Craig (2006) compared a moisture definition ($q_l > 0$) with the vertical velocity definition and found that it did not alter the characteristics of the cloud ensemble considerably. An exponential distribution of cloud mass flux was found. Khairoutdinov and Randall (2006) used a definition based on the exceedence of a moist static energy threshold. Other cloud distributions have been identified, such as log-normal, power law and double power law distributions. However, direct comparison between studies is often made difficult by the range of cloud sizes studied and and the contrasts in resolution between satellite observed or modelled cloud fields.

Here two different cloud definitions will be used. Firstly, clouds will be defined by a vertical velocity threshold (introduced in Section 3.6.2) where $w > 1\ m\ s^{-1}$. Secondly, clouds will be defined by buoyancy, where buoyancy is defined by B in equation 3.6. According to this definition clouds are buoyant, moist and upward moving, i.e $\theta_v' > 1 \times 10^{-5}\ K$, $q_l > 1 \times 10^{-5}\ kg\ kg^{-1}$ and $w > 1 \times 10^{-5}\ m\ s^{-1}$.

$$B = g\frac{\theta_v'}{\overline{\theta}} \tag{3.6}$$

$$\text{where} \qquad \theta_v' = \theta' + 0.61\overline{\theta}q_v' - \overline{\theta}q_l - \overline{\theta}q_r$$

Here θ_v' is the virtual potential temperature perturbation from its horizontal mean value ($\overline{\theta}_v$), q_v' is similarly the water vapour mixing ratio perturbation, q_l is the liquid water mixing ratio and q_r is the rain water mixing ratio.

Once the location of cloudy grid points in the domain has been determined it is then necessary to determine which can be considered to be part of the same cloud. This process is called segmentation. Adjacent cloudy grid points are considered part of the same cloud. Cloudy points, it is assumed, can be connected to any of the surrounding eight grid points (Figure 3.10(b)). Four-point segmentation may also be assumed (Figure 3.10(a)). A comparison of the two methods discussed in Kuo *et al.* (1993) concluded that the choice of method had little effect on the cloud statistics observed. The cloud may have any size, so that all connected points are part of the same cloud.

(a) 4-point segmentation (b) 8-point segmentation

Figure 3.10: *Two methods of cloud segmentation. The middle grid point in red is cloudy. a) Four-point segmentation considers the four surrounding points in purple as potentially part of the same cloud. b) Eight-point segmentation considers the eight surrounding points in purple and blue as potentially part of the same cloud.*

Qualitatively, clouds of similar size and location are observed with the two different definitions of a cloud (Figure 3.11). This suggests that these definitions are detecting the same clouds. The largest discrepancies occur in the precise location of small, single cell clouds and in the precise arrangement of grid points in the larger clouds. However, it is not expected that these details will make a substantial difference to the statistics calculated for the cloud field. The effect of the different definitions on cloud statistics can be seen in Figure 3.12.

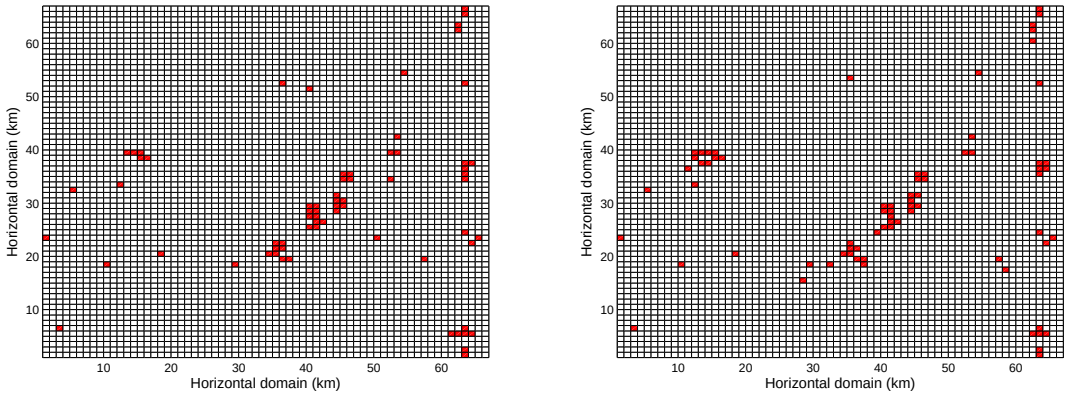

(a) Buoyancy definition (b) Vertical velocity definition

Figure 3.11: *Effect of cloud definition on the cloud classification of the horizontal cross section in Figure 3.9(a). The location of grid points flagged as a cloud (red) at a height of* 2.4 *km for a) a positive buoyancy definition and b) vertical velocity definition. See text for further description of the definitions used.*

Figure 3.12 shows statistics for the clouds in the RCE control simulation using the two cloud definitions. Fewer clouds are detected below cloud base using the buoyancy definition (Figure 3.12(a)). The larger number of clouds seen with the vertical velocity definition below 2 *km* occurs because

it detects small, upward moving cells in the boundary layer. It is not reasonable to classify such cells as clouds. The buoyancy definition does pick out the base of the deep convective clouds at $1-2$ *km*, which corresponds to the minimum in the moist static energy profile at this height (see Figure 3.6(c)). At all heights there are fewer clouds found using the buoyancy definition than the vertical velocity definition, suggesting that the former focusses more strongly on the core region of clouds and is therefore not finding smaller, weaker clouds.

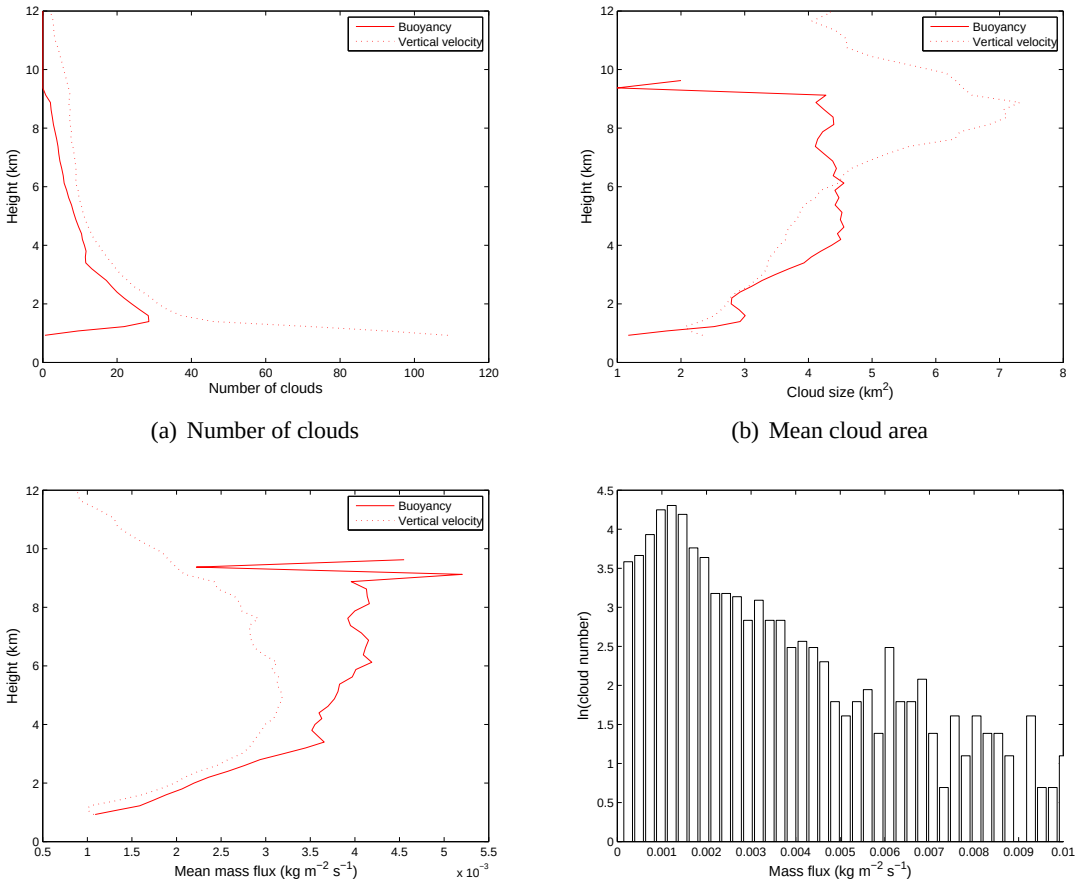

(a) Number of clouds

(b) Mean cloud area

(c) Mean mass flux per cloud

(d) Probability distribution of mass flux per cloud

Figure 3.12: *Cloud statistics as a function of height for the RCE control simulation. The statistics are taken over a period of* 240 *hr, sampled every* 5 *hr, using two cloud definitions. a) Number of clouds in domain, b) mean area of cloud and c) mean mass flux per cloud. In each panel, statistics obtained from the buoyancy definition are shown with a solid line and those from the vertical velocity with a dotted line. d) Shows the natural logarithm of the probability distribution of mass flux per cloud using a buoyancy definition at* 3 *km. In d) the distribution for large values of mass flux, where there are 2 clouds or fewer in each bin, are not shown.*

The size of the observed clouds also depends on the cloud definition used (Figure 3.12(b)). Looking first at the results with the buoyancy definition, there is an increase in cloud size with height below

4 *km* as the cloud entrains environmental air and becomes larger. Above 4 *km* the cloud size is almost constant with height, i.e. the cloud core area no longer increases. Just below 2 *km* there is a local minimum in cloud size, which is co-incident with the transition between shallow and deep convection that is seen in Figures 3.12(a) and 3.6(c). This suggests that diagnostics computed to study deep convection should be taken above 2 *km*. With a vertical-velocity-defined cloud, the cloud size increases throughout the depth of the troposphere. Here the area defined to be within the cloud is larger in the upper troposphere, encompassing all the air moving up around the buoyant centre of the cloud.

The size of the clouds has a direct effect on the mean mass flux per cloud. Figure 3.12(c) shows that, with the buoyancy definition, as the size of the clouds remain constant with height above 4 *km* so the mean mass flux per cloud is also nearly constant with height: i.e. the cloud core has a near-constant mass flux. This suggests that the buoyancy definition is, indeed, a definition of the cloud core. There is limited entrainment of environmental air into the core modifying the strength of the clouds. With a vertical velocity definition the mean mass flux per cloud decreases as the size increases, so the cloud is considered to be larger but the outer portions of the cloud have weaker vertical velocities.

Figure 3.12(d) shows the probability distribution of mass flux per cloud for the control simulation. Previous studies have shown that clouds exhibit a range of different distributions, including studies of RCE which have shown an exponential distribution of cloud mass flux, for example Cohen and Craig (2006) and also by Plank (1969). The distribution here, using a buoyancy definition, also fits an exponential type distribution, although compared to distributions seen in Craig and Cohen (2006) there is a decrease in the number of clouds at low values of mass flux. This is partly due to the buoyancy definition focussing on the core of the clouds which are fundamentally stronger and excluding the smaller, weaker cells. Also, small cloud mass fluxes result from clouds close to the grid scale and therefore the fit to an exponential distribution may be sensitive to horizontal resolution used.

The similarity between the cloud statistics observed here and those in previous studies suggests that fundamental theories from literature should be applicable to the ensemble of convection simulated here (Section 5.3). The following section verifies that the statistics are not overly sensitive to some of the setup choices made.

3.8 Sensitivity experiments

This section will discuss the sensitivity of the cloud statistics presented in the previous section to the method of forcing the system and the size of the model domain. Sensitivity to model resolution with time-varying surface forcing will be discussed in more detail in Section 4.3.2. Most CRM studies of RCE force the model by constant longwave cooling, whilst holding the surface temperature fixed. As discussed in Section 3.3.1, to facilitate control of the energy balance during the time-varying simulations, here the system is forced with surface fluxes and constant longwave cooling. The effect of the choice of forcing mechanism on the state of RCE, will be determined in this section by directly contrasting cloud statistics obtained using the two contrasting forcing mechanisms. Moreover, it is essential that a sufficiently large number of clouds is simulated so that cloud statistics within the domain are not artificially constrained. A larger domain (128×128 km^2) will be used to assess whether the cloud statistics within the smaller domain are indeed sufficient.

3.8.1 The effect of forcing mechanism

Equilibrium timeseries when the convective system is forced by different methods are shown in Figure 3.13. The model setup when the system is forced with constant fluxes and longwave cooling is discussed in Section 3.5.1. This is termed the *'flux-forced'* RCE. When constant surface temperature and longwave cooling are used the longwave cooling rate and profile are the same as in the flux-forced RCE, while the surface temperature is held fixed to the domain-mean surface temperature obtained from the flux-forced RCE. To ensure that the two simulations are directly comparable the surface water vapour mixing ratio is also held fixed to the domain-mean water vapour mixing ratio from the flux-forced RCE simulation. The surface is therefore not saturated (recall that the flux-forced RCE is based on observations from over land) in contrast with previous RCE studies of ocean-based convection over a fixed SST. The surface fluxes are allowed to evolve over time, producing a simulation which will be referred to as *'temperature-forced'* RCE. All other setup details remain unchanged.

Figure 3.13(a) shows that the temperature-forced RCE produces total surface fluxes that are identical to the value specified when flux-forced to within one standard deviation. The Bowen ratio, which defines the ratio of sensible heat flux to latent heat flux, is the same for both RCE. Figure 3.13(b) shows that that the two RCE states have similar cloud base mass fluxes, although when

flux-forced the cloud base mass flux is slightly weaker. In addition the two RCE states have very similar mean vertical profiles (not shown).

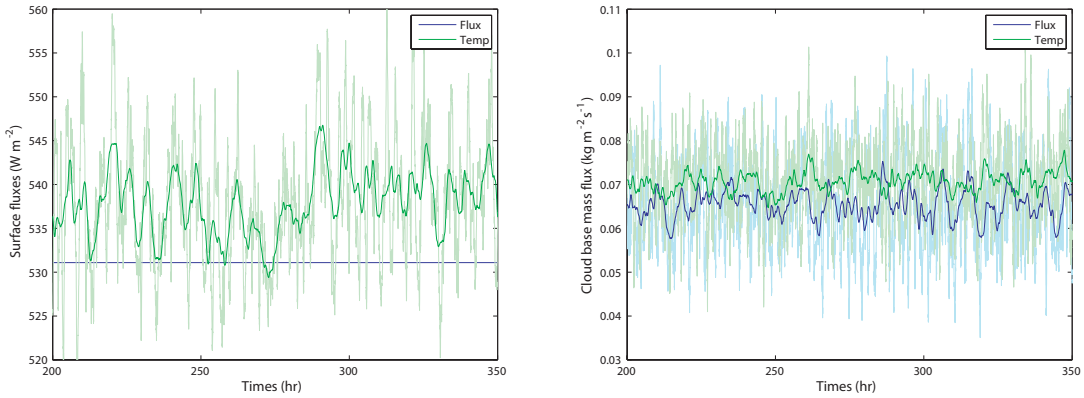

(a) Surface fluxes (b) Cloud base mass flux

Figure 3.13: *Timeseries of a) surface fluxes (sensible + latent) and b) cloud base mass flux when RCE is forced by two forcing mechanisms. The blue line shows flux-forced RCE and the green line temperature-forced RCE; see text for discussion. The dark lines are* 80 *min running means through the instantaneous values given by the light lines.*

The difference in the cloud statistics using different forcing mechanisms can be seen in Figure 3.14. When temperature-forced there are consistently more clouds in the domain than when flux-forced, regardless of the cloud definition (Figure 3.14(a)). The cloud base detected remains at $1-2$ *km*. When temperature-forced the clouds are generally smaller (Figure 3.14(b)) and weaker (Figure 3.14(c)). Hence, the overall characteristics, summed over the full ensemble, remain similar.

In summary, whilst the domain-mean characteristics are similar, regardless of the forcing mechanism of RCE, there is a tendency for a larger number of clouds which are smaller and weaker when temperature-forced. Discussion of the reasons for this may be found in Chapter 5.

3.8.2 The effect of domain size

It is thought that a truly idealised situation of an infinite domain size would permit the convective ensemble to achieve true radiative-convection *equilibrium*: the system would achieve a constant steady state. Since an infinite domain cannot be modelled computationally, the finite domain size results in the convective system achieving a mean state when averaged over space, but with fluctuations about that mean. The size of the fluctuations are directly related to domain size, in that larger domains have smaller fluctuations about the mean. It is important to check that the model setup

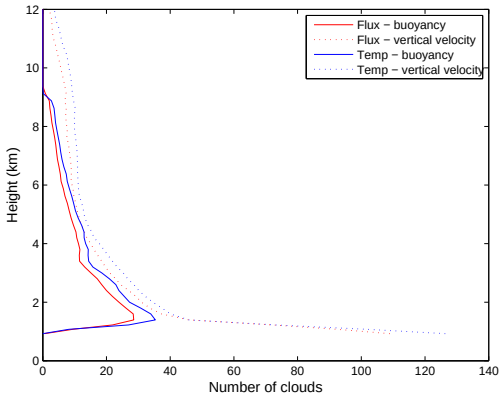

(a) Number of clouds

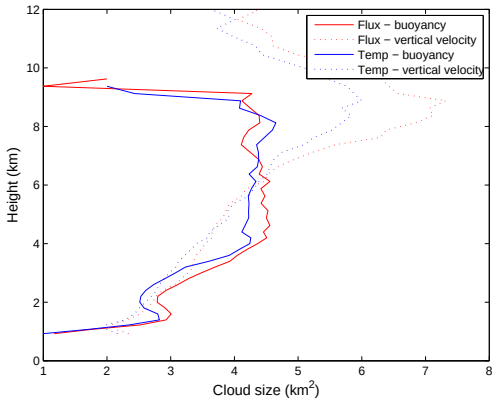

(b) Mean cloud area

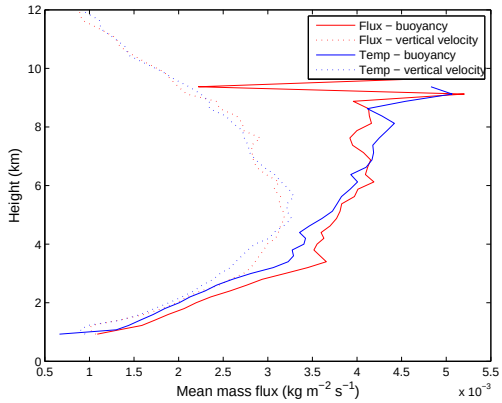

(c) Mean mass flux per cloud

Figure 3.14: *Cloud statistics as a function of height at RCE. The statistics are taken over a period of* 240 *hr, sampled every* 5 *hr, using two cloud definitions, for two forcing mechanisms. a) Number of clouds in domain, b) mean area of a cloud and c) mean mass flux per cloud. For each panel statistics for a buoyancy definition are shown with a solid line and vertical velocity with a dotted line. Statistics for flux-forced RCE are shown in red and for temperature-forced RCE in blue.*

has a sufficiently large domain for these fluctuations to be tolerably small. This section directly contrasts the RCE with a large domain of 128×128 km^2, to the RCE with the standard 64×64 km^2 domain for both forcing mechanisms. In particular, the aim is to check that the fluctuations do not overly modify the observed equilibrium state to the extent that the RCE state cannot clearly be identified. Figure 3.15 confirms that with a larger domain fluctuations about equilibrium are reduced, but that both large and small domain RCE simulations produce a similar mean state.

Tompkins (2000) showed that at small domain sizes intermittency could occur, as there would be some times when there was no convection in the domain. This intermittency was not improved with increased resolution but was solely dependent on the domain size. It occurred due to the domain

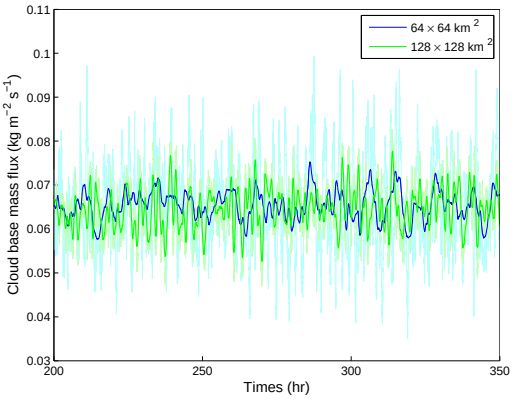

Figure 3.15: *Timeseries of cloud base mass flux when RCE is simulated using two domain sizes. The blue line shows a* 64×64 *km*^{2} *domain at RCE and the green line shows a* 128×128 *km*^{2} *domain at RCE when flux-forced. The dark lines are* 80 *min running means through the instantaneous values given by the light lines.*

size artificially modifying the spectrum of clouds present in the domain. Hence it is necessary to investigate the extent to which domain size modifies the simulated RCE by altering the cloud statistics.

Figure 3.16 shows cloud statistics at two different domain sizes, using the buoyancy definition. It shows that there are fewer clouds per unit area when RCE is flux-forced with the larger domain compared to the smaller domain (Figure 3.16(a)). This reduction in cloud number density with increased domain size is not seen when RCE is temperature-forced. When flux-forced the increased domain size increases both the mean size of the clouds and the mean mass flux per cloud (Figure 3.16(b) and 3.16(c)). There is no marked change in the mean size of the clouds or the mean mass flux per cloud when temperature-forced. It is not immediately clear why there is a greater difference in the cloud statistics when the domain is flux-forced compared to temperature-forced although there is a differing role for the cold pools between the two model setups. This is discussed further in Section 5.3.1.

This tendency to fewer, larger and stronger clouds in the flux-forced RCE with the larger domain, can also be seen in the probability distribution (compare Figure 3.17(a) to Figure 3.17(b)). With a smaller domain there are more clouds with mass flux $\lesssim 0.002$ *kg* m^{-2} s^{-1} whereas with the the larger domain there are more clouds with a mass flux $\gtrsim 0.012$ *kg* m^{-2} s^{-1}. As the domain-mean mass flux is almost identical at the different domain sizes, it may be anticipated that if there is an increase in the number of larger clouds there must be a decrease in the number of smaller clouds

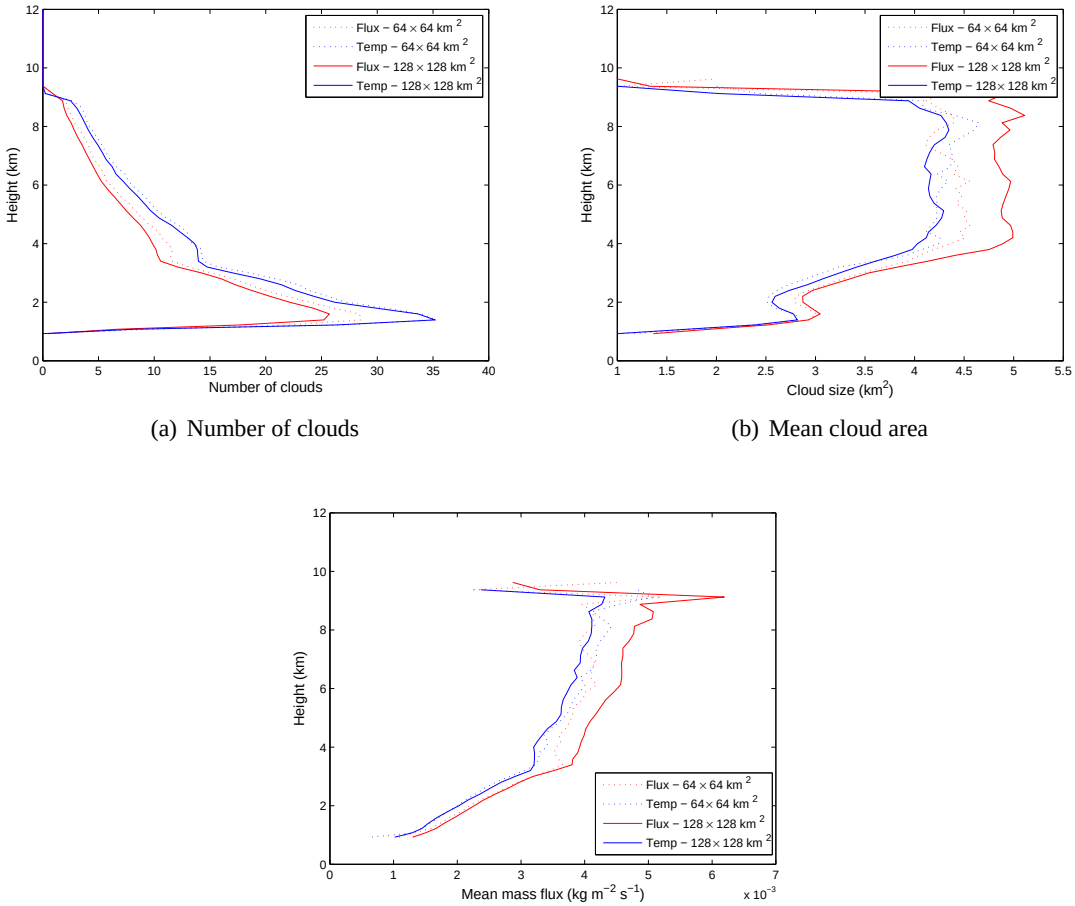

(a) Number of clouds

(b) Mean cloud area

(c) Mean mass flux per cloud

Figure 3.16: *Cloud statistics as a function of height at RCE. The statistics are taken over a period of* 240 *hr, sampled every* 5 *hr, using two forcing mechanisms, for two different domain sizes. A buoyancy cloud definition is used. a) Number of clouds in domain, b) mean area of cloud and c) mean mass flux per cloud. For each panel statistics for a domain size of* $128 \times 128\,km^2$ *are shown with a solid line and those for* $64 \times 64\,km^2$ *with a dotted line. Statistics for flux-forced RCE are shown in red and for temperature-forced RCE in blue. In a) the number of clouds has been normalised to the area of the smaller domain in order to permit comparison of domains of different sizes.*

to compensate. It is also suggested that the increased domain size, and the re-distribution of cloud mass flux, improves the fit of the cloud ensemble to an exponential distribution, seen by comparing Figure 3.17(a) to Figure 3.17(b). It is likely that the smaller domain is representing an exponential distribution but is slightly under-sampling the spectrum of larger clouds.

Table 3.2 shows a summary of these data presented in Figures 3.14 and 3.16 for the cloud field at 3 *km*. It shows the mean and standard deviations for each combination of forcing mechanism, domain size and cloud definition. There is generally a smaller difference in the cloud statistics with

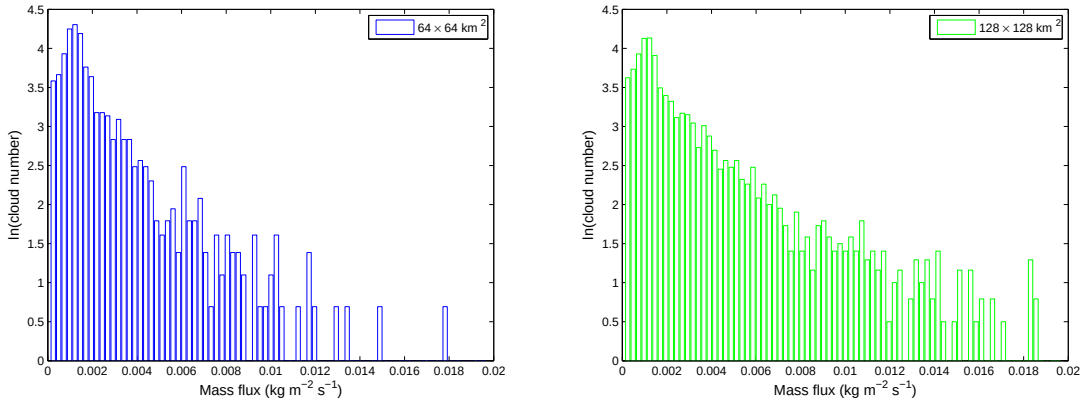

(a) $64 \times 64\ km^2$ (b) $128 \times 128\ km^2$

Figure 3.17: *The natural logarithm of the probability distribution of mass flux per cloud using a buoyancy definition at* 3 *km for domain sizes a)* $64 \times 64\ km^2$ *and b)* $128 \times 128\ km^2$ *when flux-forced. a) Is the same as Figure 3.12(d) but showing all clouds present in the domain.*

increased domain size than is found by altering the forcing mechanism. In general fewer clouds form when flux-forced but the clouds are more variable in size and mass flux. Regardless of the forcing mechanism or domain size a buoyancy definition finds fewer clouds that are slightly larger and stronger than with a vertical velocity definition.

	$w > 1\ m\ s^{-1}$			Buoyant cloud definition		
RCE simulation	$\langle N \rangle$	$\langle m \rangle$ $(kg\ m^{-2}\ s^{-1})$	$\langle A \rangle$ (km^2)	$\langle N \rangle$	$\langle m \rangle$ $(kg\ m^{-2}\ s^{-1})$	$\langle A \rangle$ (km^2)
Flux-forced $64 \times 64\ km^2$	21.0	0.0027 $\pm$0.0043	3.3 $\pm$4.4	15.1	0.0032 $\pm$0.0043	3.5 $\pm$4.2
Temperature-forced $64 \times 64\ km^2$	25.3	0.0025 $\pm$0.0036	2.9 $\pm$3.6	18.5	0.0028 $\pm$0.0035	3.1 $\pm$3.3
Flux-forced $128 \times 128\ km^2$	20.9	0.0027 $\pm$0.0047	3.3 $\pm$4.8	14.2	0.0032 $\pm$0.0046	3.5 $\pm$4.4
Temperature-forced $128 \times 128\ km^2$	23.7	0.0025 $\pm$0.0036	3.1 $\pm$3.6	17.1	0.0029 $\pm$0.0034	3.2 $\pm$3.4

Table 3.2: *Summary comparison of cloud statistics, mean and standard deviation, for the RCE control simulation (flux-forced* $64 \times 64\ km^2$*) compared to the other RCE simulations (flux-forced* $128 \times 128\ km^2$*, temperature-forced* $64 \times 64\ km^2$ *and temperature-forced* $128 \times 128\ km^2$*). These data are for the cloud field at* 3 *km presented in Section 3.8.*

This section confirms that increased domain size does effect the equilibrium state of RCE by reducing the fluctuations about the mean response. It has been shown that this is due to the representation

of a larger spectrum of clouds with a larger domain. The statistics of the clouds are less sensitive to domain size than they are to forcing mechanism.

3.9 Summary and discussion

The chapter introduces an LES model which was run as a CRM. This model, from the UK Meteorological Office, is shown to be suitable to investigate the characteristics of a convective ensemble. It forms the basis of the 'realistic' convective modelling work in this study. The model has been forced in two phases, a control simulation of RCE and a time-varying simulation (which will be discussed in Chapter 4).

This model is suitable for studying cloud processes as the CRM is designed resolve large, cloud-scale, eddies and parameterise the small-scale processes, such as sub-grid turbulence, details of which are assumed to be 'less' important for cloud development. In addition the CRM has been developed to include moisture and microphysical processes. The CRM can represent both liquid and ice processes and the conversions between rain and ice and also conversions to and from water vapour.

In specifying a model setup the choice has been made to develop a cloud ensemble that is as homogeneous and random (non-organised) as possible. For this reason a 3D domain with horizontally uniform forcings is used, and there is no wind shear or rotation applied. An additional consideration is given to the method by which the model is forced. For the long time-varying simulations it will be necessary to maintain a balance between heating and cooling rates. This is to avoid simulations with longer forcing timescales drifting compared to simulations with shorter forcing timescales. i.e. experiencing more net warming/cooling. The forcing is therefore achieved by prescribing surface fluxes and balancing this with a constant longwave cooling. This is a deviation from the methodologies often used in CRM studies. The exact longwave cooling required is different for the control and time-varying phases.

The control simulation, which is flux-forced, has initial conditions and surface fluxes taken from observational data used in the EUROCS case study. The longwave cooling profile is designed to balance this forcing. Timeseries of cloud base mass flux and precipitation show the convective ensemble rapidly adjusts (within 50 *hrs*) to a realistic RCE. The thermodynamic structure, in terms of temperature and moisture, is reminiscent of tropical soundings, despite the case study being

based on mid-latitude observations. Hence, without additional external forcing, the convection within the cloud ensemble has the thermodynamic structure of generic convection. The final state of the complete 3D control simulation is used to provide the initial conditions for the time-varying simulations.

The statistics of the cloud ensemble are shown to be similar to those found in other studies of RCE. The cloud distribution is seen to be exponential although at small cloud sizes the fit is less clear. This is likely to be because close to the grid length cloud features are not well-resolved. A buoyancy definition focusses on the core of a cloud. This reduces the number of clouds identified at RCE and those found are larger and stronger. The identified clouds may be larger as the buoyancy definition is a more stringent definition in terms of whether grid points are classified as part of the same cloud. Hence grid points separated into two clouds with a vertical velocity definition may be linked as one larger cloud with a buoyancy definition.

It is shown that increasing the domain size increases the number of clouds overall at RCE and re-distributes the cloud mass fluxes. There is a broader spectrum of clouds with the larger domain although the shape of the distribution does not change considerably. It was seen that altering the forcing mechanism had a greater effect on the cloud statistics than changing the domain size. Cloud definition also affects the exact values of the cloud statistics but with both cloud definitions the differences in cloud statistics, due to the model setup, were of similar magnitudes. For the majority of this study a buoyancy definition will be used. This defines a cloud more similar to the type of cloud considered in convective parameterisation schemes than that given by a vertical velocity definition.

CHAPTER 4

Experiments with finite forcing timescales

4.1 Introduction

Chapter 3 introduced a cloud-resolving model which was used to investigate the properties of a convective ensemble at radiative-convective equilibrium (RCE) when forced by time invariant surface fluxes. These were found to be similar to the convective characteristics observed in a more 'traditional' simulation which has an identical setup but has time invariant surface temperature. The final RCE from the flux-forced simulation, the control simulation, is used in this chapter to initialise a series of simulations with time-varying surface fluxes. This will permit the investigation of the response of a convective ensemble to changes in forcing timescale which is an aim of this thesis.

The details of modifications to the model setup required when time-varying forcing is used will be detailed first. Then results will be analysed, in the first instance, by discussing the characteristics of a time-varying simulation when the forcing timescale is 24 *hr*. Analogies will be made with the diurnal cycle in analysing the response at this forcing timescale. Sensitivity to model resolution is discussed at 24 *hr* forcing timescale with regard to the development of convection. The characteristics of the convective response when different forcing timescales are used will then be contrasted. Investigation will focus on explaining the differences in the responses at different forcing timescales.

4.2 Time-varying simulation setup

Many aspects of the overall model setup with time-varying forcing are the same as for the control simulation described in Section 3.4. This section provides the specification of those aspects of the model setup with the time-varying forcing that are different to the control simulation.

Model resolution, domain size, boundary conditions and other setups are the same between the two model phases as shown in Table 3.1. The differences in the setup are in the forcing, both the

surface forcing and the longwave cooling. The surface forcing is made to vary in time with surface fluxes provided by the EUROCS case study introduced in Section 3.5.1. Chaboureau *et al.* (2004); Bechtold *et al.* (2004); Guichard *et al.* (2004); Petch (2004) used filtered and smoothed sensible and latent heat flux timeseries from the observational campaign. In contrast Stirling and Petch (2004) used idealised observed sensible and latent heat fluxes which vary sinusoidally during the day and are set to zero at night; as a result the maximum values used by Stirling and Petch (2004) are slightly different to those from the observations. Here sensible and latent heat fluxes are used which are the same as Stirling and Petch (2004). In this study it is the period of the sine wave that is altered to represent different forcing timescales. In the control simulation, the surface forcing was given by the maximum of the sine wave.

At the transition between the control simulation and the time-varying simulation the forcing is gradually switched off, as shown in Figure 4.1. This transition from maximum forcing to minimum forcing may be thought of as the transition between midday and midnight. After the transition the forcing cycle repeats. The exact number of forcing cycles for which the simulation is run depends on the length of the forcing cycle and will be discussed in Section 4.4.2. However, the aim is to have sufficient cycles to produce robust statistics. Times less than $time = 0$ (Figure 4.1), during the transition, will not be considered in discussion of the time-varying forcing. The control simulation, as described in Chapter 3, reached radiative-convective equilibrium. This chapter will discuss the transition of the convective response to the time-varying forcing (Section 4.4.2) and the response when adjusted (Section 4.6).

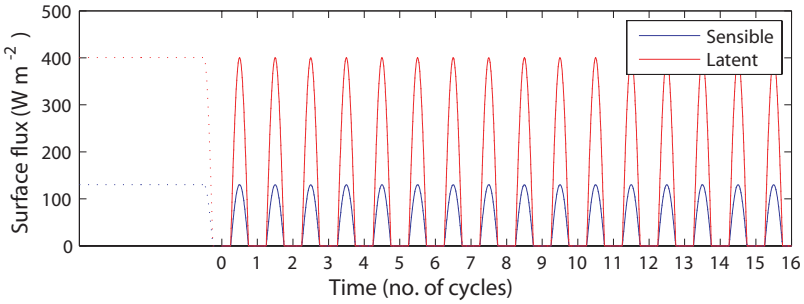

Figure 4.1: *Timeseries of surface fluxes of sensible (blue line) and latent heat (red line) for time-varying simulations. Times before* $time = 0$ *represent the control simulation and the period of transition to the time-varying simulation, when the forcing is switching off. The x-axis is given in units of the forcing cycle.*

The longwave cooling rate is chosen to balance the surface forcing over a complete forcing cycle

(equation 3.2), thereby setting the value of $\dot{T}$ for the cooling profile in Figure 3.2. $\dot{T}$ is computed as $-2.4 \times 10^{-5} K\ s^{-1}$ and is the same regardless of forcing timescale. This is equivalent to a cooling of $-2.1\ K\ (day)^{-1}$ for a forcing timescale of 24 *hr*.

A range of forcing timescales, τ, are chosen. These represent a range of timescales on which convection may be forced. An important timescale at which convection is forced is the diurnal timescale, 24 *hr*, and this is investigated in detail. A value of $\tau = 36$ *hr* is chosen to represent forcings on longer timescales. Computational constraints on the time simulations take to run, and the ability of the model to represent the stable atmosphere when the surface forcing is zero (Section 4.4.3), prohibit much longer timescales. If a forcing timescale of 48 *hr* is used, strong stability in the lower atmosphere occurs when the surface forcing is zero. The high temporal and spatial resolution required to represent this situation cause the model (run at 1 *km* resolution) to develop a computational instability. However, qualitatively the few results gathered at 48 *hr* showed that the characteristics of the response were similar to those at $\tau = 36$ *hr*. Forcing timescales close to the lifetime of a deep convective cloud are given by timescales of $1-3$ *hr*. A summary of the model setup for the time-varying simulations is given in Table 4.1. This only includes the details that are different to the control setup.

Peak sensible heat flux (F_s)	$130\ W\ m^{-2}$
Peak latent heat flux (F_L)	$400\ W\ m^{-2}$
Longwave cooling ($\dot{T}$)	$-2.4 \times 10^{-5} K\ s^{-1}$
Forcing timescale (τ)	$1-36$ *hr*

Table 4.1: *Summary of variables used in time-varying simulation.*

Whilst the aim is to investigate convection at a range of forcing timescales, the response will be initially discussed at $\tau = 24$ *hr*.

4.3 24 hr forcing timescale

This section presents a discussion of the characteristics of the time-varying simulation with a forcing timescale of 24 *hr*. Whilst the primary intention is to investigate how the characteristics of convection change when forced at a range of timescales, it is useful to have an initial focus on a system with similarities to the diurnal cycle. This enables the verification and comparison of the simulation against observations and the literature. The results in this section are presented for a

section of the 24 *hr* time-varying simulation which is fully-adjusted to the forcing. The reason for this will be discussed in more detail in Section 4.4.2. In a similar way to the initial adjustment period seen in Section 2.3.1, some time is needed for the convective system to adjust to a change in the pattern of the forcing.

4.3.1 Timeseries characteristics of 24 *hr* simulation

Timeseries of the characteristic convective response can be seen in Figure 4.2, for both the cloud base mass flux and surface precipitation rates. Cloud base mass flux shows positive values over most of the 'daytime' (i.e when the surface is being heated). There is a strong initial response to the forcing, seen as 'spikes' in the mass flux timeseries. Details of the 'spike' depend on resolution but its existence is due to the night-time fluxes which are fixed at zero and do not become negative. The effect of model resolution on this 'spike' will be discussed further in Section 4.3.2. As the daytime progresses the mass flux decreases from this initial strong response.

Figure 4.3(a) shows the composite of the cloud base mass flux timeseries over the 11 days in Figure 4.2(a). The main features from the timeseries can still be seen and it is possible to relate times in the response to times in the forcing. There is a delay of 2 *hr* between the start of the forcing and the start of the convection. This initiation of convection is a key aspect in the convective cycle and is termed the 'triggering'. Here the time of triggering is defined as the time at which the cloud base mass flux reaches 50 % of the mean maximum cloud base mass flux averaged over 11 successive days. The convection responds strongly throughout the forcing cycle but decays to zero as the forcing switches off.

The surface precipitation timeseries (Figure 4.2(b)) shows similar characteristics although there is not a strong 'spike' associated with the triggering of deep convection. From the composite time-series, Figure 4.3(b), it can be seen that the precipitation lags the mass flux. Precipitation occurs 2.5 *hr* after the start of the forcing. The delay in the precipitation is caused by the physical processes of precipitation development which dissociates the precipitation from the 'spike' at convective triggering which is seen in the mass flux. After triggering the precipitation composite has the same shape as the forcing.

Figure 4.2(c) shows the components of precipitation attributed to convective and stratiform clouds. The distinction between the two is given by the methodology used by Steiner *et al.* (1995) who de-

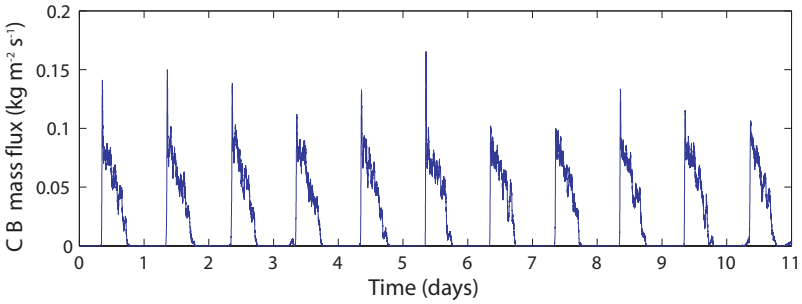

(a) Cloud base mass flux

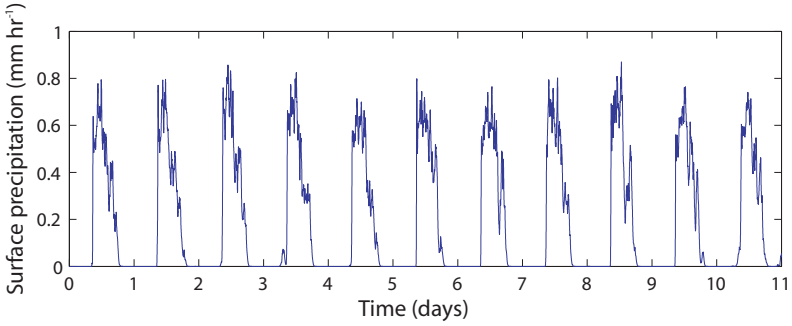

(b) Surface precipitation

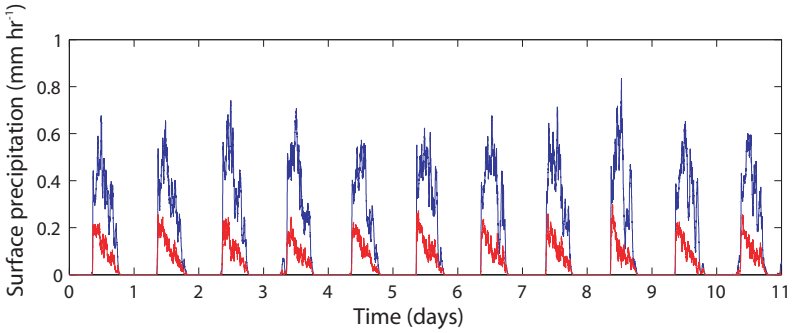

(c) Convective and stratiform precipitation

Figure 4.2: *Timeseries for τ= 24 hr simulation. a) Cloud base mass flux, b) surface precipitation and c) convective and stratiform components of the surface precipitation. The sum of convective (blue line) and stratiform (red line) surface precipitation in (c) gives the total surface precipitation in (b). The partitioning between stratiform and convective is discussed in Steiner* et al. *(1995)*

fine convective precipitation as either the strongest local rain rates or rain rates exceeding a threshold within the proximity of strong rain rate. All other rain is assumed to be stratiform in nature. It shows that the dominant source of precipitation is convective cloud and that this is also the most variable source of precipitation between the different days. There is three times less total stratiform precipitation per day.

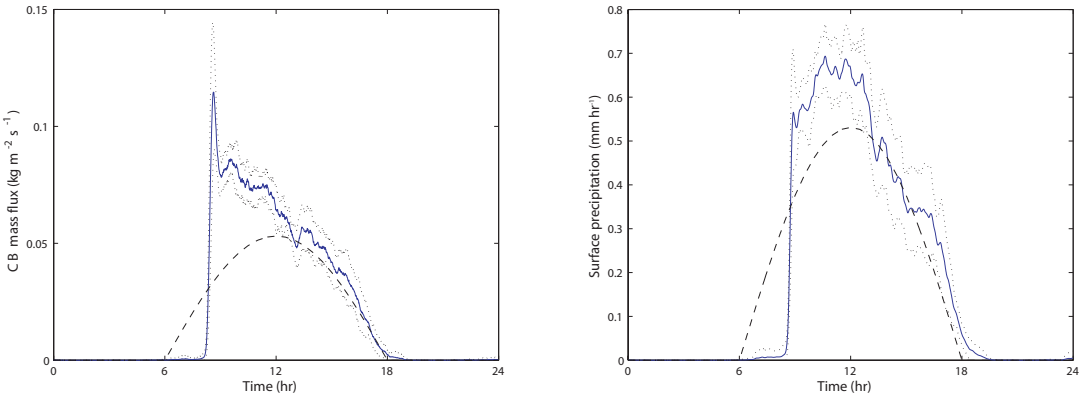

(a) Cloud base mass flux (b) Surface precipitation

Figure 4.3: *Composite timeseries for* 24 *hr. Mean (blue line) with standard deviation (black, dotted line) for a) cloud base mass flux and b) surface precipitation. Composite over 11 forcing cycles. Timeseries of surface forcing (sensible + latent heat flux) are shown for reference. Maximum reference surface forcing is* $530\ W\ m^{-2}$

4.3.2 Sensitivity to model resolution

Section 4.3.1 mentioned a possible role of model resolution in influencing convective characteristics at the time of triggering, as seen in the 'spike' in the cloud base mass flux timeseries. Petch (2006) discussed the minimum benchmark that a simulation requires to represent the transition of the diurnal cycle from shallow to deep convection. The author concluded that 3D simulation, at a horizontal resolution of 200 *m*, and a domain of $25 \times 25\ km^2$ was necessary in order 'to capture the most important processes'. As was discussed in Section 3.4 a horizontal resolution of 1 *km* has been chosen for this work and the aim in this section is to discuss the sensitivity of the convection to the exact choice of horizontal resolution when the forcing varies in time.

Sensitivity studies have been conducted for grid lengths of 2 *km* and 500 *m*, and compared to the 1 *km* case. The domain size remains at $64 \times 64\ km^2$. Figure 4.4 shows example horizontal cross sections of vertical velocity at a height of 3 *km* at the time of triggering for the three resolutions. Table 4.2 shows some key characteristics of the clouds observed at the time of triggering. With 500 *m* horizontal resolution the convection is seen to trigger in many locations with the average individual clouds around $2\ km^2$ in area but also existing at larger sizes. Around the clouds is a small region of strong, compensating downdrafts. The majority of the domain has near-zero vertical velocity as all the convective activity is focussed in the regions of cloud. Degrading the resolution, to a horizontal grid length of 1 *km*, produces a greater number of clouds. On average the clouds

are 1.2 km^2 (i.e close to the grid scale) but some clouds are larger. Each cloud has a downdraft field associated with it. By contrast at 2 *km* horizontal resolution, there are many fewer clouds and the majority of clouds occur at only one grid point. The strong vertical velocities associated with each cloud require large areas of downdraft to compensate and, as a result, there are larger areas of downward motion (Figure 4.4(c)). It is more difficult to associate each cloud with its own downdrafts.

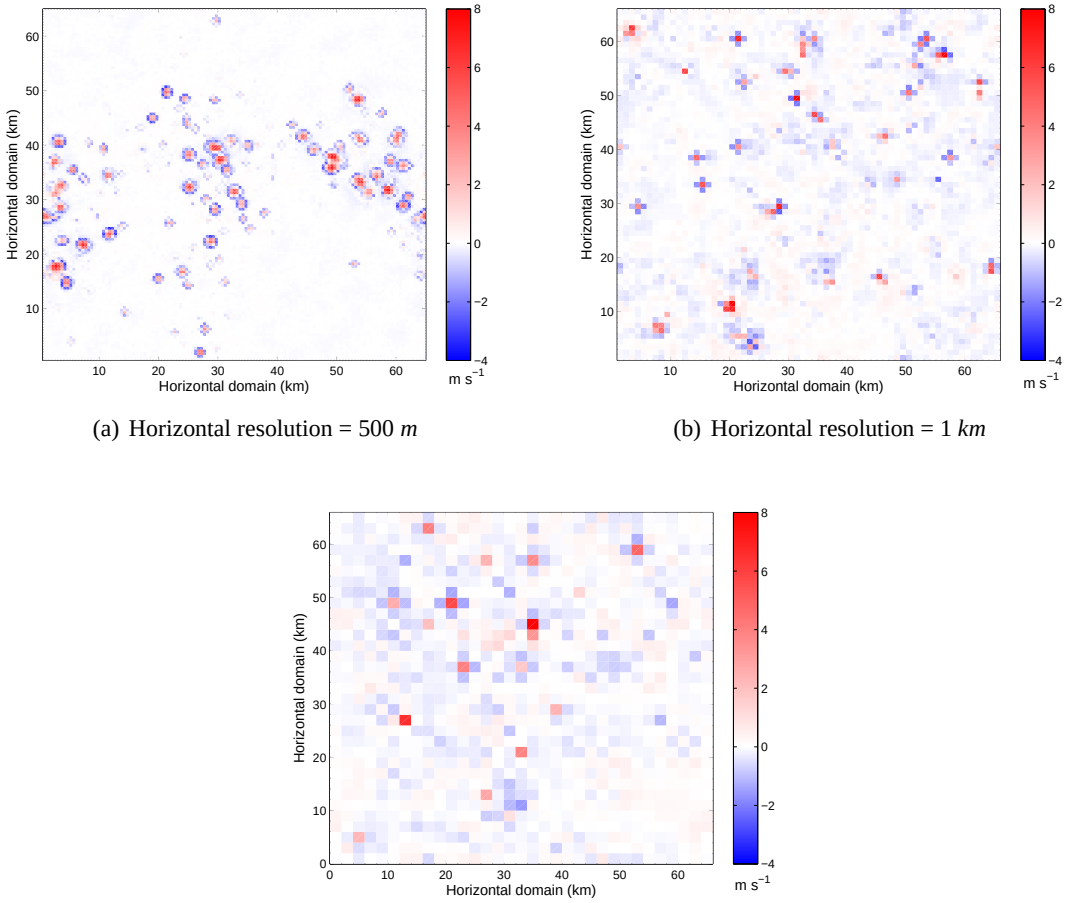

(a) Horizontal resolution = 500 *m*

(b) Horizontal resolution = 1 *km*

(c) Horizontal resolution = 2 *km*

Figure 4.4: *Horizontal section of vertical velocity at height $z = 3$ km for three horizontal resolutions: a)* 500 *m, b)* 1 *km and c)* 2 *km, at the time of triggering.*

Figure 4.5 shows the composite timeseries of cloud base mass flux and surface precipitation. It can be seen that there is strong triggering with all model resolutions. The cloud base mass flux shows a 'spike' at the time of triggering for all model resolutions. At the higher resolutions, for surface precipitation, the 'spike' at triggering is less pronounced, although there is still a strong response observed at 500 *m* resolution. When the resolution is coarse the sub-grid scheme has to represent larger sub-grid eddies. As the sub-grid processes become large enough to be resolved at the grid

	Buoyant cloud definition			
Horizontal resolution	$\langle N \rangle$	$\langle m \rangle$ ($kg\ m^{-2}\ s^{-1}$)	$\langle M \rangle$ ($kg\ m^{-2}\ s^{-1}$)	$\langle A \rangle$ (km^2)
500 m	46.2	0.0015 $\pm$0.0029	0.0672 $\pm$0.0189	2.2 $\pm$3.2
1 km	73.6	0.0010 $\pm$0.0007	0.0762 $\pm$0.0177	1.2 $\pm$0.5
2 km	16.8	0.0052 $\pm$0.0032	0.0883 $\pm$0.0447	4.4 $\pm$1.6

Table 4.2: *Comparison of cloud statistics at three different horizontal resolutions computed at the time of convective triggering at $z = 3$ km. Statistics are computed over 11 days with $\tau = 24$ hr. A buoyancy definition of a cloud is used. $\langle N \rangle$ is the average number of clouds in the domain, $\langle A \rangle$ is the average size of a cloud, $\langle m \rangle$ is the mean mass flux per cloud and $\langle M \rangle$ is the domain-mean cloud base mass flux. See Section 3.7 for a discussion of this cloud definition and the cloud statistics at RCE.*

scale convection triggers strongly in the domain. This was noted by Petch (2006) who looked at the development of convection over land in a CRM and found that coarser resolution changed the characteristics of the convective transition. However, here there is still a strong positive response in both the cloud base mass flux and precipitation, at the time of triggering, even at 500 m resolution indicating that there may also be a physical mechanism behind the response (see Section 4.3.3).

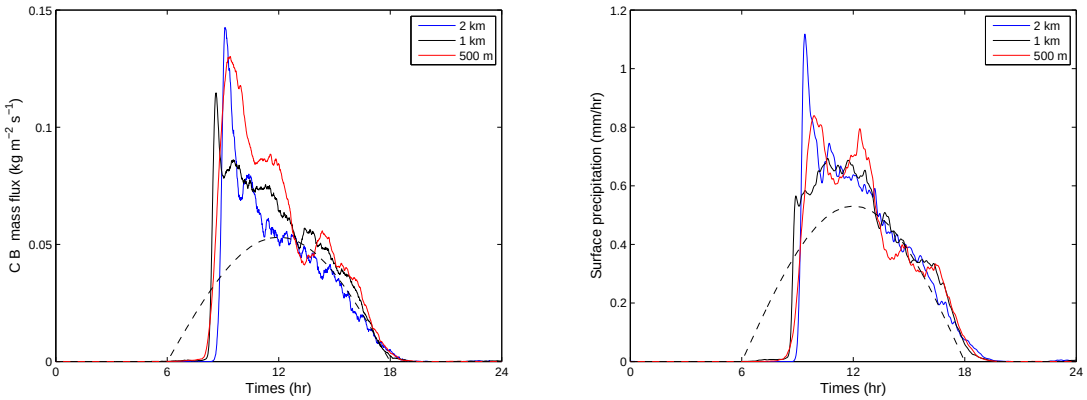

(a) Cloud base mass flux (b) Surface precipitation

Figure 4.5: *Comparison of mean cloud base mass flux for three horizontal resolutions,* 500 *m (red line),* 1 *km (black line) and* 2 *km (blue line) for, a) cloud base mass flux and b) surface precipitation. Composite over 11 days with $\tau = 24$ hr. Timeseries of surface forcing (sensible + latent heat flux) shown for reference. Maximum reference surface forcing is* 530 $W\ m^{-2}$.

The results in this section confirm previous results that horizontal resolution does have a significant

impact on characteristics of convective clouds and on the evolution of both the cloud base mass flux and the surface precipitation. Over-reliance on the sub-grid scheme, for example at 2 *km*, results in few clouds, of limited size which have, on average, larger mean mass flux. Results at 500 *m* and 1 *km* reflect findings of Smith and Jonas (1995) where clouds had sizes of $1.5-3$ *km*. The time evolution of the convective development seen in the cloud base mass flux and precipitation (Figure 4.5) also show that details are dependent on horizontal resolution. However, the focus of this study is the characteristics of deep convection and not specifically the transition *to* deep convection. It can be seen in Figure 4.14 that away from triggering clouds at a height of 3 *km* have an areas about 2.5 km^2 and that the exact statistics of the cloud field at the time of triggering are highly variable. Ideally a resolution of 500 *m* would be used but the choice is also restricted by computational considerations (Section 3.4). The results presented here suggest that the choice of a horizontal resolution of 1 *km* does not overly distort the characteristics of the convection at the time of triggering compared to a higher resolution and is certainly a considerable improvement over using a coarser resolution.

4.3.3 Vertical profiles of 24 *hr* simulation

Figure 4.6 shows vertical potential temperature profiles with $\tau = 24$ *hr*. Figure 4.6(a) shows the mean potential temperature at two times in the forcing cycle. The first is at dawn, just before the surface heating begins, and the second at sunset as the surface forcing switches off. These two profiles represent the full extent of the range of potential temperature, when the atmosphere is at its coolest and warmest. It can be seen that through the majority of the free troposphere the profiles are moist adiabatic. This is often observed in the tropical atmosphere, as discussed in Section 3.6.2. The effect of surface heating, during the day, is to increase the temperature throughout the depth of the troposphere with the profile remaining close to moist adiabatic. This suggests that the vertical profile is well-mixed by clouds and turbulent processes. At night the longwave cooling, being constant in height uniformly modifies the potential temperature profile, and therefore, the stability structure of the atmosphere, i.e. the dawn profile is still close to a moist adiabat. As the profile remains close to conditionally unstable, convection responds quickly once triggered. The convection is able to become deep, rapidly mixing throughout the depth of the troposphere. This explains the strong convective response discussed in Section 4.3.2 seen even at high spatial resolutions.

Figure 4.6(b) shows the evolution of the domain-mean potential temperature in the boundary layer,

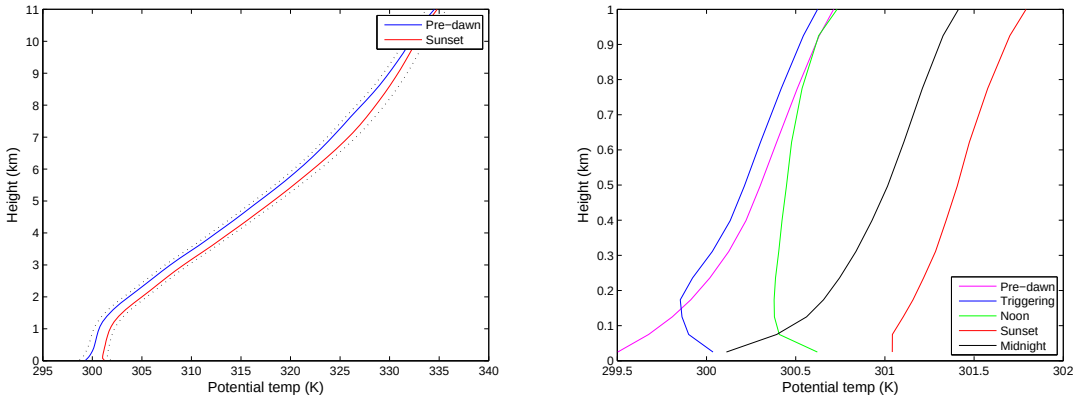

(a) (b)

Figure 4.6: *Domain-mean vertical profiles of potential temperature, composited over 11 days with* τ= 24 *hr. a) At two times in the diurnal cycle, just before dawn and at sunset. These represent the times in the forcing cycle when the system is at its coolest and warmest respectively. The superimposed black, dotted lines show two moist adiabatic profiles, for reference. b) Evolution of the boundary layer potential temperature at key moments through the diurnal cycle.*

the lowest 1 *km* of the troposphere, as this layer has the greatest temporal and spatial variability of potential temperature. At dawn the profile is stable near the surface. By the time that convection is triggered the surface layer has warmed, whilst the air above 200*m* is still cooling, creating an unstable profile near the surface. During the day, as the surface continues to warm, a well-mixed layer forms and deepens. At night the constant longwave cooling affects the full depth of the profile.

This section has provided an overview of the characteristics of the convective response when forced with $\tau = 24$ *hr*. It was shown that there were many similarities between the response in this simulation and the characteristics of the diurnal cycle.

4.4 Altering forcing timescales

As described in Section 4.2 the convective response is investigated when the system is forced with different values of forcing timescale. The shape of the forcing is the same as that in Figure 4.1 but with different lengths of forcing cycle. The longwave cooling is unaltered. This section will discuss the characteristics of the convective response for differing forcing timescales by examining the timeseries of cloud base mass flux and composites of cloud base mass flux. The analysis of the timeseries will prompt futher investigation of key aspects of the convection that change in response to the length of the forcing cycle.

The results here are presented for different values of forcing timescale, hence discussion of 'day', 'night', 'dawn' and 'sunset' are no longer directly applicable. These terms have strong connotations with specific times in the diurnal cycle (i.e when $\tau = 24$ *hr*). Instead, the preferred terms will be the positive phase of the forcing cycle, the zero phase of the forcing cycle, the start of the forcing cycle and the end of the forcing cycle. The use of 'days' will likewise be replaced by forcing cycles. Also, note that for brevity that a simulation with a forcing cycle where $\tau = 3$ *hr* will be called a '3 *hr* simulation', although it is run for longer than 3 *hr*.

4.4.1 Timeseries characteristics for other forcing timescales

Figure 4.7 shows timeseries of cloud base mass flux for different values of forcing timescale (τ). At the longest forcing timescale, $\tau = 36$ *hr*, the response is reminiscent of the response with $\tau = 24$ *hr*. There is a strong convective response when the forcing is positive and no response when the surface forcing is switched off. Similarly to the $\tau = 24$ *hr* timeseries there is also a strong 'spike' when convection is triggered. Intriguingly, it can be seen that at the start of some forcing cycles, for example, just after 72 *hr* and 144 *hr*, the convection leads the start of the forcing. This probably relates to the comparatively long period for which the surface forcing is switched off, causing instabilities to build up. This is discussed further in Section 4.4.3. The response at these long forcing timescales resembles the convective response seen in the analytic model when the memory timescale was short. This in characterised by regime E in Section 2.6.

As the forcing timescale decreases convection triggers less rapidly and a 'spike' is not observed. At $\tau = 12$ *hr* triggering occurs relatively later in the forcing cycle compared to at longer timescales. The relationship between τ and the time to triggering will be discussed in Section 4.4.4. It can also be seen that triggering only occurs after the start of the surface forcing. With the shorter forcing timescale the surface forcing is switched off for a shorter period of time and the build-up of instability, seen when $\tau = 36$ *hr*, does not occur.

When the forcing timescale decreases the lag between the start of convection and the start of forcing increases relative to τ such that when $\tau = 3$ *hr* the maximum of the convective response actually occurs as the surface forcing switches off. The reason for this response will be discussed in Section 4.4.4. At this forcing timescale the maximum value of cloud base mass flux can be seen to vary significantly for different cycles. As, by design, each forcing cycle experiences the same forcing it is then possible to investigate the cause of the variability between successive forcing cycles. The

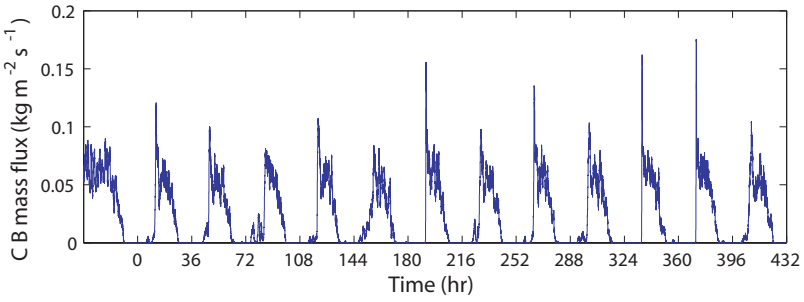

(a) $\tau = 36$ *hr*

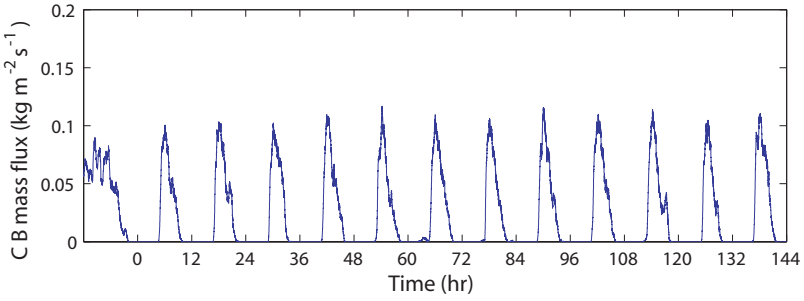

(b) $\tau = 12$ *hr*

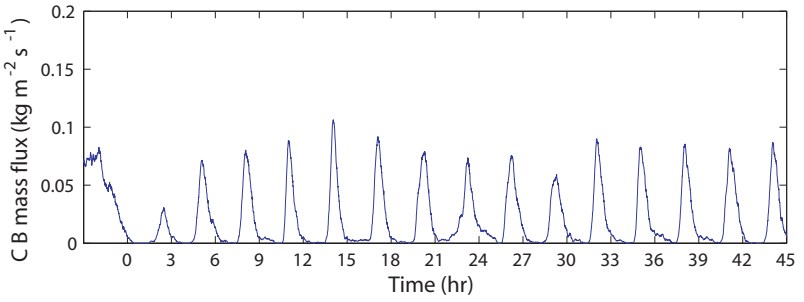

(c) $\tau = 3$ *hr*

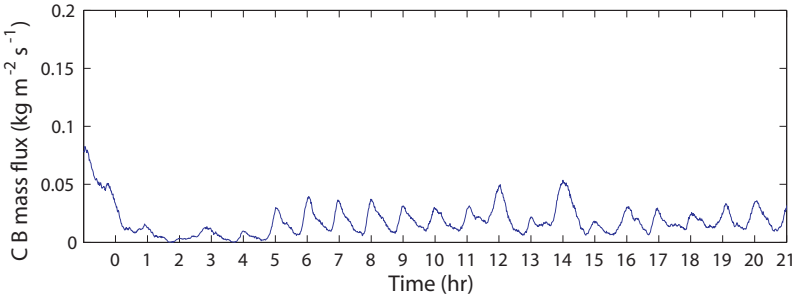

(d) $\tau = 1$ *hr*

Figure 4.7: *Timeseries of cloud base mass flux for various values of* τ*. a)* $\tau = 36$ *hr, b)* $\tau = 12$ *hr, c)* $\tau = 3$ *hr and d)* $\tau = 1$ *hr. Values of time* < 0 *represent the end of the control simulation. Figure 4.1 shows the forcing timeseries for reference.*

variability will be quantified in Section 4.6 and reasons for the variability will be the focus of the work in Chapter 5. A response with differing levels of convection, despite a forcing which is the same cycle-to-cycle, is similar to the response with 'moderate' memory characterised by regime C in Section 2.6. Note that the greatest variability occurs in Figure 4.7(c) in the first few cycles, just after $time = 0$. This point will be discussed in Section 4.4.2.

At very short values of forcing timescale the convection never switches off and is highly variable. The characteristic shape of the forcing is less visible. This convective response is like the response seen in the analytic model when the memory timescale was long compared to the forcing timescale. In regime B in Section 2.6 the response did not switch off but maintained a mean response with fluctuations about this mean. There is also a noticeable suppression of convection when $time \leq 6$ *hr* and this will be discussed in Section 4.4.2.

Composites of cloud base mass flux and surface precipitation for two extreme values of τ are shown in Figure 4.8. These should also be contrasted with Figure 4.3 which showed similar composites for $\tau = 24$ *hr*. Firstly, it should be noted that there is a phase shift between the triggering in the cloud base mass flux and the surface precipitation for all τ. The time of triggering is less clear for $\tau = 36$ *hr*, where the response is complicated by the convection starting before the forcing. However, for $\tau = 3$ *hr* the convection triggers 1 *hr* after the start of the forcing and precipitation 30 *min* later. For all τ precipitation occurs 30 *min* after the start of convection and its formation is therefore independant of τ. This is due to the time microphysical processes take to develop rain. Rogers and Yau (1989) suggested, based on observations, that precipitation took 20 *min* to develop.

When $\tau = 36$ *hr*, excluding the strong initial response, the cloud base mass flux follows the forcing closely, reinforcing the similarities with regime E (Section 2.6).

It has been shown that timeseries of cloud base mass flux and precipitation, in response to a periodic forcing, are sensitive to the timescale of that forcing. There are three notable characteristics that will be discussed further in the following sections. Firstly, the supression of convection after the switch from the control simulation to time-varying forcings, which is particularly seen at short forcing timescales. Secondly, the development of convection before the start of the forcing when $\tau = 36$ *hr*. And finally the increased relative delay to triggering seen as the forcing timescale shortens.

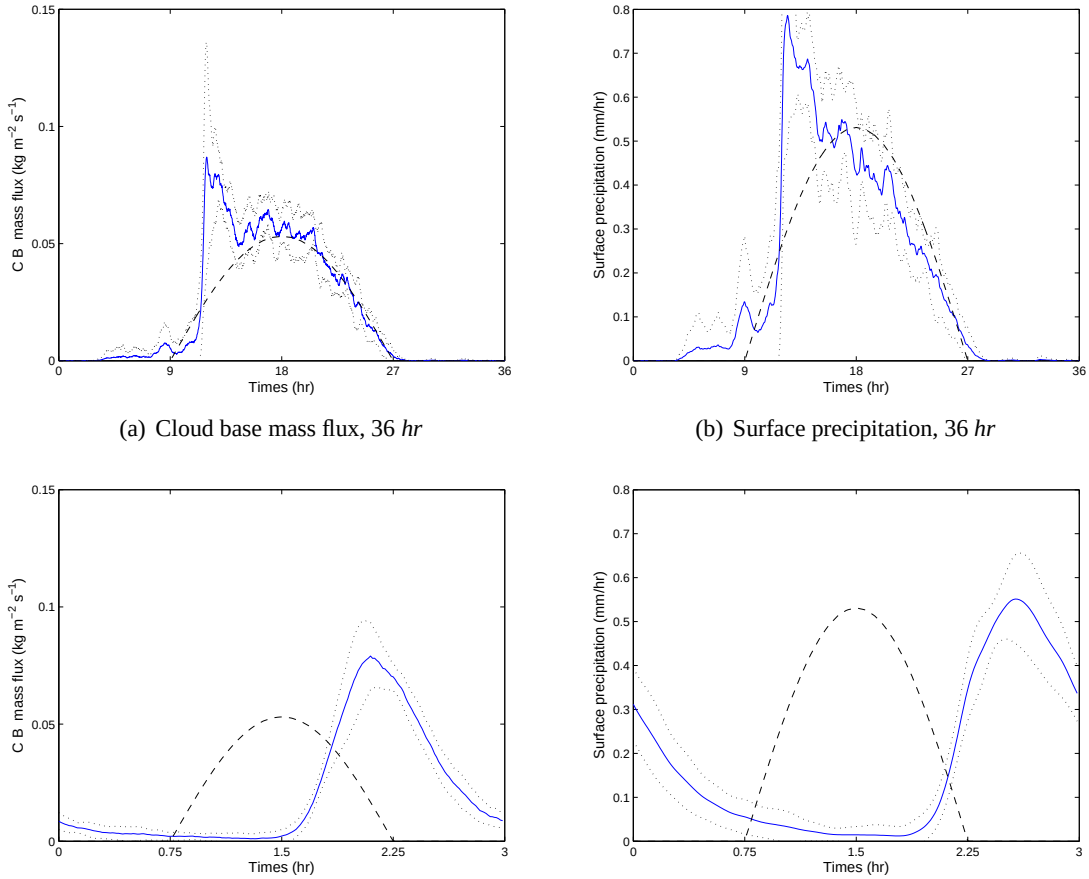

(a) Cloud base mass flux, 36 *hr*

(b) Surface precipitation, 36 *hr*

(c) Cloud base mass flux, 3 *hr*

(d) Surface precipitation, 3 *hr*

Figure 4.8: *Composite timeseries for* 36 *hr and* 3 *hr. Mean (blue line) with standard deviation (black, dotted line) for a) cloud base mass flux and b) surface precipitation. Composite over 11 forcing cycles. Timeseries of surface forcing (sensible + latent heat flux) shown for reference. Maximum reference surface forcing is* 530 $W\ m^{-2}$.

4.4.2 Initial adjustment to change in forcing

When the shape of the forcing of a convective system is changed (e.g. changing from a constant forcing in the control simulation to a periodic forcing in the time-varying simulation) the response does not instantly exhibit its usual settled response to the new forcing. There are transients following the change. Note, for example, the convection during the first few cycles in Figures 4.7(c) and 4.7(d). In this section the effect of this initial adjustment is discussed.

In Chapter 2 the convective response of the analytic model was characterised by the mean and standard deviation of the total time-integrated Q_1, $\overline{(\Delta T_{conv})}$ and $\sigma(\Delta T_{conv})$ respectively. In a similar manner the response of convection in the CRM will be characterised. The total integrated cloud base mass flux in each forcing cycle is defined in equation 4.1, normalised by the length of the

forcing cycle τ.

$$I_{M_b} = \frac{1}{\tau}\int_0^{\tau} M_b \, dt \tag{4.1}$$

where M_b is the cloud base mass flux.

From this the mean and standard deviation of I_{M_b}, i.e $\overline{I_{M_b}}$ and $\sigma(I_{M_b})$, can be calculated over successive cycles. As discussed in Section 2.2, Emanuel (1994) showed that there is a direct relationship between Q_1, convective heating due to convection, and mass flux. Therefore, $\overline{I_{M_b}}$ and $\sigma(I_{M_b})$ are assumed to be directly comparable to $\overline{(\Delta T_{conv})}$ and $\sigma(\Delta T_{conv})$ (Section 2.4.3).

This Section will focus on 3 *hr* and 1 *hr* simulations as these adjustment periods are most pronounced in Figures 4.7(c) and 4.7(d). Figure 4.9(a) shows that both the 3 *hr* and 1 *hr* simulation tend to the same $\overline{I_{M_b}}$, 0.02 $kg\ m^{-2}$. This mean value of mass flux represents the level of convection required to balance the forcing. The same $\overline{I_{M_b}}$, independent of τ may be anticipated as the system is forced at the same average rate, regardless of forcing timescale.

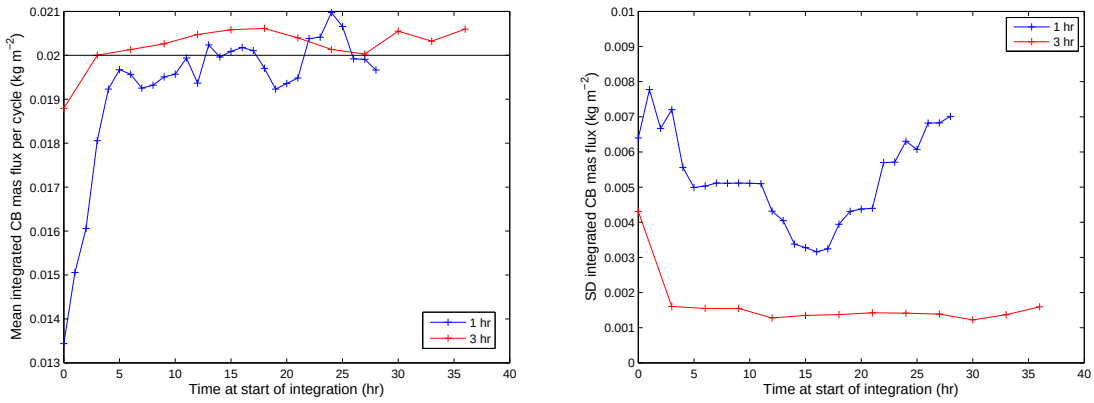

(a) $\overline{I_{M_b}}$ (b) $\sigma(I_{M_b})$

Figure 4.9: *Effect of the time window for which $\overline{I_{M_b}}$ and $\sigma(I_{M_b})$ are calculated when $\tau = 1$ hr (blue line) and $\tau = 3$ hr (red line). $\overline{I_{M_b}}$ and $\sigma(I_{M_b})$ are each calculated over a time window of 11 successive cycles. The time at the start of the time window in given on the x-axis. Time = 0 corresponds to zero time on Figure 4.1.*

Both $\overline{I_{M_b}}$ and $\sigma(I_{M_b})$ are dependent on the time window over which statistics are computed. It is only when the start of the time window is sufficiently long after the change in the shape of the forcing that $\overline{I_{M_b}}$ tends to a constant value. If the time window is close to the change in the shape of the forcing then the computed $\overline{I_{M_b}}$ is less than its steady state value for both values of τ. The

reduced $\overline{I_{M_b}}$ may be anticipated from the suppressed convection seen in Figures 4.7(c) and 4.7(d) immediately after $time = 0$.

The control simulation has a strong mass flux response (see Figure 3.5(a)), to balance the strong forcing. When the forcing becomes time-varying the total time integrated surface forcing is reduced. This can be seen by comparing the two shaded areas in Figure 4.10. If area A is greater than area B it shows there is less energy supplied when the forcing varies in time. In fact, $area\ A = \pi \times area\ B$. Hence there is less convection required to balance the time-varying forcing compared to the control simulation. When the forcing is reduced at $time = 0$ the convection does not respond instantaneously to the change; it takes time to be suppressed. Figure 4.9(a) shows that the time needed to adjust to the time-varying forcing is $\sim 5-7$ *hr* and is independent of τ.

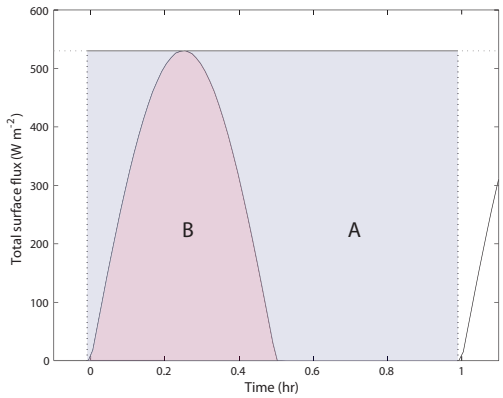

Figure 4.10: *Comparison of total energy supplied from both sensible and latent heat fluxes with the forcing constant in time ('blue' area, A) and with a time-varying forcing ('red' area, B) of $\tau = 1$ hr.*

Figure 4.9(b) shows that a similar time is required for the diagnostic $\sigma(I_{M_b})$ to settle following adjustment to the change in forcing in the 3 *hr* simulation. After ~ 5 *hr*, $\sigma(I_{M_b})$ is independent of the time window chosen, reaching a steady value. However, for the 1 *hr* simulation there is always strong variability in the mass flux and $\sigma(I_{M_b})$ has not settled even after 27 *hr*.

For other values of τ (shown in Figure 4.7) it is assumed that the same adjustment period applies even though it is not directly extractable from the mass flux timeseries when the adjustment time is less than τ. Due to this adjustment process an initial period, after the start of the time-varying surface forcing, is removed from the timeseries before further analysis is carried out. This period is chosen to be 10 *hr* in order to ensure all adjustment effects are removed but is rounded up to a whole number of forcing cycles. The number of forcing cycles removed in each case is shown in

Table 4.3. This is similar to the adjustment period discussed in Section 2.3.1, which was removed to ensure the system was in a well-adjusted state, independent of the initial conditions.

τ (*hr*)	36	24	18	12	6	3	1
Number of cycles	1	1	1	1	2	4	10

Table 4.3: *Number of forcing cycles removed prior to analysis in order to account for initial adjustment from control simulation to time-varying simulation. The system is assumed to be well-adjusted after these cycles are removed.*

The results presented in this section show that there is indeed an influence from previous convection on current levels of convection. In this case the influence is seen by a reduction in the convection (compared to that which would be expected given the instantaneous forcing). Moreover, it can also be seen (Figure 4.7(d)) that the adjustment occurs gradually. For example, in Figure 4.7(d) between $time = 0-4$ *hr* the level of convection is reduced compared to the level of convection before or after. The longwave cooling is constant, at the appropriate rate (see Section 4.2), during this period. Due to the strong convective response in the control simulation the initial convective response is 'more' suppressed. After a sufficient adjustment period of $\sim 5-7$ *hr* the system achieves a well-adjusted state.

4.4.3 Pre-forcing convective development

As highlighted in Section 4.4.1 for $\tau = 36$ *hr* the convective response was shown to lead the surface forcing. Figures 4.7(a) and 4.8(a) showed that convection could sometimes develop before the surface forcing started and that this convection was deep enough to produce precipitation (Figure 4.8(b)). The occurrence of this pre-forcing convection causes large variability in the timing of the strong convective response, the 'spike', seen in Figure 4.8(a). It was suggested that this convection occurs due to the longwave cooling, which can cause instability to develop even when the surface fluxes are zero. When τ is long there is a longer period when the surface forcing is zero, a period of length $0.5 \times \tau$, as seen in Figure 4.7. This may explain why such behaviour is not observed for shorter values of τ.

To investigate this a simulation is performed with a new, shorter forcing cycle. For 18 *hr* the surface fluxes are positive (a half-sine wave as in the $\tau = 36$ *hr* simulation) but this is followed by only 9 *hr* of zero surface forcing. The longwave cooling is also adjusted appropriately. Thus the forcing is identical to the 36 *hr* simulation in the positive phase of the cycle but has half the length of the zero

phase of the cycle. The composites of mass flux and surface precipitation for this new simulation are shown in Figure 4.11. The level of convection, and therefore also precipitation, occurring before the start of the surface forcing is greatly reduced. Indeed, this pre-forcing convection is now more comparable to that observed in the 24 *hr* simulation (Figure 4.3) which might be anticipated since the period of longwave cooling is 9 *hr* compared to 12 *hr* in the 24 *hr* simulation. As a result of the reduction in pre-forcing convection there is much less variation in the timing of the triggering, reducing the variability of the 'spike' seen in Figure 4.7(a).

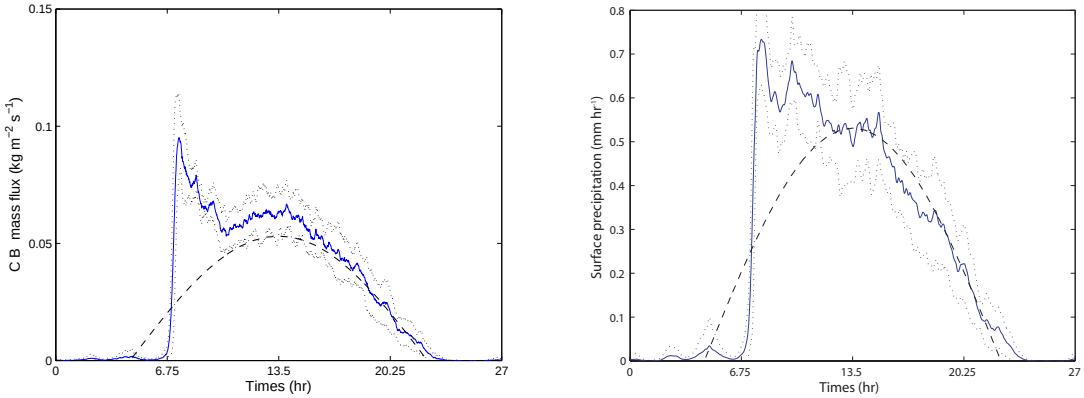

(a) Cloud base mass flux (b) Surface precipitation

Figure 4.11: *Composite timeseries for simulation where the forcing cycle is* 18 *hr long for the positive part of the cycle and* 9 *hr long when the forcing is zero. Mean (blue line) with standard deviation (black, dotted line) for a) cloud base mass flux and b) surface precipitation. Timeseries of surface forcing (sensible + latent heat flux) shown for reference. Maximum reference surface forcing is* 530 $W\ m^{-2}$.

These results show that the convection is a product of the three-way balance between the surface forcing, the atmospheric longwave cooling and the induced convection. This is different from to the more widely studied radiative-convective equilibrium where convection only balances one forcing mechanism - longwave cooling. In the case of a long τ, for example 36 *hr*, the influence of the longwave cooling is sufficient to destabilise the atmosphere and cause convection. Since the focus of this study is the convective response to a time-varying surface forcing this role of longwave cooling adds additional complexity to the problem. For example, in the case of Figure 4.7(a), the pre-forcing convection modifies the system such that the timing of triggering in response to the surface forcing is more variable. Indeed the re-stabilisation of the atmosphere by the pre-forcing convection may subtly alter the character and strength of the convection once triggered, although this may to some extent be masked by resolution issues (Section 4.3.2). Therefore, in this study there will not be great emphasis placed on the results from the 36 *hr* simulation. However, they will be useful in order to provide a forcing timescale longer than 24 *hr* in order that the case of the

diurnal cycle can be put into context.

4.4.4 The role of the boundary layer on the time of triggering

It was noted in Section 4.4.1 that there is a phase shift between the start of the forcing and when convection triggers. The length of this phase shift increases relatively with shortening forcing timescale. The aim of this section is to determine the relationship between the timing of triggering and the forcing timescale.

A basic understanding of boundary layer (BL) evolution can be achieved by considering a normal, 24 *hr*, diurnal cycle over land. At night a stable layer develops near the surface in the BL due to longwave cooling of the surface relative to the free troposphere above. In the surface inversion potential temperature increases with height whereas in the free BL above the air is well-mixed and the potential temperature is nearly constant with height. At dawn the positive surface heating gradually erodes this surface inversion, reducing the potential temperature gradient. Given sufficient time, surface heating will increase the surface layer temperature and dry convective instability will develop between the surface layer and the BL above. At this point warm thermals can rise from the surface layer, through the well-mixed layer above and, given the right atmospheric conditions in the free troposphere may initiate deeper moist convection.

The theory discussed above relates the surface heating to the erosion of the surface layer and therefore relates the surface heating to the deepening of the BL. The principles can be used analogously to relate the time of convective triggering to the surface heating in the simulations studied here. It is hypothesised that the surface heating in the sub-cloud layer controls the time, after the start of the forcing, for the system to start to convect. Below the cloud base, and before convection breaks out, all processes may reasonably be assumed to be dry and hence all heating during this time comes from sensible heat fluxes (F_s). In this situation the energy balance is given thus:

$$\text{Change in total BL } \theta = \text{Dry surface heating} + \text{Longwave cooling}$$

$$\Delta\theta = \int_{t_1}^{t_2} F_S dt + \int_{t_1}^{t_2} F_{rad} dt \tag{4.2}$$

where

$$\Delta\theta = \int_0^{z_b} \rho c_p \theta dz \Big|_{t_2} - \int_0^{z_b} \rho c_p \theta dz \Big|_{t_1} \tag{4.3}$$

Equation 4.2 may be re-written for convenience as

$$\int_{t_1}^{t_2} F_s dt = \Delta\theta - \int_{t_1}^{t_2} F_{rad} dt \tag{4.4}$$

where all symbols have either their usual meteorological meaning or else are shown on Figure 4.12. z_b is the height of the cloud base, assumed to be the top of the BL, and has been computed from simulation data as the height of the lowest moist point in the domain, where $q_l > 1 \times 10^{-5} kg/kg$. $\dot{T}$ is the longwave cooling rate which is discussed in Section 3.3.1. This relationship is similar to the model of boundary layer deepening proposed by Carson (1973) which related the depth of the BL to the surface heat supplied. The BL was modelled as a well-mixed layer represented by a potential temperature profile which was constant with height.

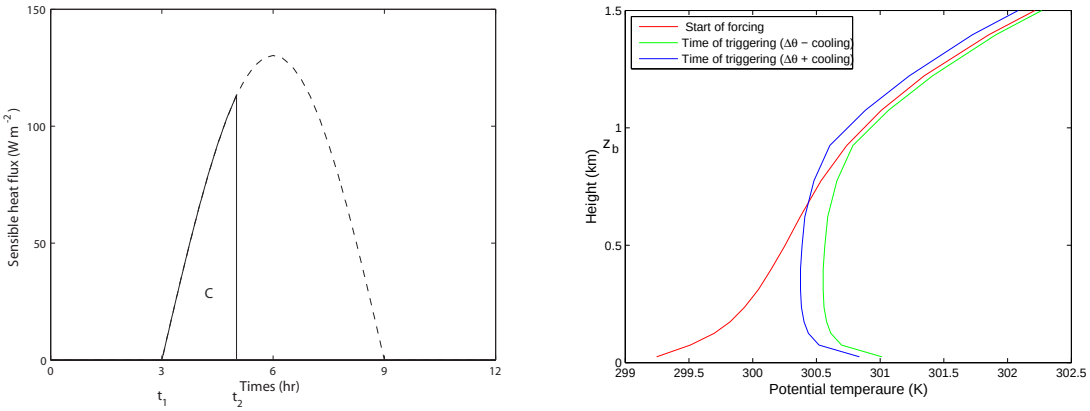

(a) Time evolution of sensible heat flux

(b) Vertical profiles boundary layer θ

Figure 4.12: *Diagrammatic representation of the energy balance which controls the timing of convective triggering (taken from one cycle when $\tau = 12$ hr). a) The area C is the energy supplied to the system by sensible heat flux (F_s) from the time of the start of the forcing (t_1) to the time of convective triggering (t_2). t_2 is defined as in Section 4.3.1. b) The profiles of boundary layer potential temperature at t_1 (red line) and t_2 (green and blue lines). The vertical profiles of potential temperature are those used in the height integrals in equations 4.2 and 4.3. The difference between the green and blue lines show the role of longwave cooling ($\dot{T}$) on boundary layer θ. The green line is the right-hand side of equation 4.4 whereas the blue line is the left-hand side of equation 4.2 showing the addition role of longwave cooling in triggering.*

This energy balance has been calculated for each τ for 11 forcing cycles. Figure 4.13 shows that

there is a direct relationship between the total F_s supplied and the erosion of the surface inversion. This relationship is less obvious when $\tau = 36$ *hr* although, as discussed in Section 4.4.3, for this forcing timescale the triggering of convection has different behaviour to other forcing timescales. The sensitivity to z_b when $\tau = 36$ *hr* is tested by increasing z_b by its standard deviation (open symbols on Figure 4.13). (The standard deviation of z_b was found by evaluating z_b for every point in the domain, at the time of triggering, using the definition given above.) Within this wider range of z_b it is shown that, for $\tau = 36$ *hr*, it is now possible to span the 1:1 line and therefore the correct solution for $\tau = 36$ *hr*, may lie on the 1:1 line, as the other forcing cycles do.

As stated in Section 4.4.3 there is a three-way balance between the forcing mechanisms. In the 36 *hr* simulation the atmosphere experiences cooling for a longer period of time. Increased cooling may modify the atmosphere such that the response when convection triggers is different and the time to triggering may not simply be explained by the energy supplied to the boundary layer. Other mechanisms that may contributed to the time and character of triggering will be discussed further in Chapter 5.

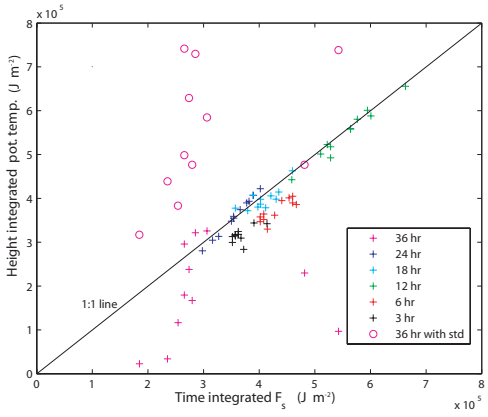

Figure 4.13: *Energy balance in the boundary layer for all τ. x-axis is the time integrated sensible heat flux (F_s) between the start of forcing and the time of triggering, i.e the left-hand side of equation 4.4. y-axis is the difference in the height integrated potential temperature (θ) in the boundary layer between the start of the forcing and the time of triggering, adjusted for the longwave cooling ($\dot{T}$) during this period, i.e the right-hand side of equation 4.4. The open symbols show results for $\tau = 36$ hr when z_b is redefined as $z_b + \sigma_{z_b}$.*

These results suggest that the timing of triggering is only dependent on the supply of sensible heat to the boundary layer. When τ is short a relatively longer time must elapse to provide this energy compared to a longer τ. As discussed in Section 4.3.3 the potential temperature profile is close to a moist adiabat throughout the depth of the free troposphere. This potential temperature

profile explained (Section 4.4.1) that the strong 'spike' response seen in the cloud base mass flux timeseries was due to rapid deepening of the convection once triggered. Coupled with the results here it is suggested that the timing of the convection is controlled by supplying sufficient heat to the boundary layer and, having brought the boundary layer to the point of convection, the convection rapidly deepens due to the moist, near neutral, temperature profile in the atmosphere.

4.5 Cloud statistics over complete forcing cycle

In Section 3.7 the characteristics of the cloud ensemble from the control simulation at radiative-convective equilibrium (RCE) were presented. In this section the cloud characteristics over a time-varying forcing cycle will be presented for $\tau = 24\ hr$ and for $\tau = 3\ hr$. These will be presented at key heights in the atmosphere. These are near the transition region from the shallow to deep convective region (1.2 *km*), in the deep convection (3 *km*) and towards the top of the deep convection, both above and below the transition to ice cloud (4.9 *km* and 6.1 *km*).

Figure 4.14 shows the cloud statistics for $\tau = 24\ hr$. The timeseries of the characteristics shows coherent structures with height. At the time of triggering a large number of clouds are produced rapidly (see Section 4.3.2) and are more numerous than at RCE. As the forcing cycle progresses the number of clouds decreases and all cloud statistics settle to values which are similar to those at RCE from the control simulation. Similar to RCE there is an increase in mean mass flux per cloud with height and the mean cloud size increases with height, but has similar values at 4.9 *km* and 6.1 *km*. Mean mass flux per cloud and mean cloud size do not vary substantially with time, away from triggering, suggesting that the time-evolution of the cloud base mass flux seen in Figure 4.3(a) is mainly caused by variations in the number of clouds, rather than changes in the characteristics of the clouds.

Figure 4.15 shows the time-evolution of cloud statistics for $\tau = 3\ hr$. As with the timeseries of cloud base mass flux (Figure 4.8(c)) there is not a strong 'spike' in the start of the convective response. The number of clouds can clearly be seen to evolve gradually, with the number of clouds increasing somewhat later at higher levels. There are similar numbers of clouds at both $\tau = 24\ hr$ and $\tau = 3\ hr$. There is limited time-evolution during the entire forcing cycle of both mean area of cloud and mean mass flux per cloud when $\tau = 3\ hr$. This confirms that evolution of the cloud field is again dominated by variability in the number of clouds rather than changes to the in-cloud

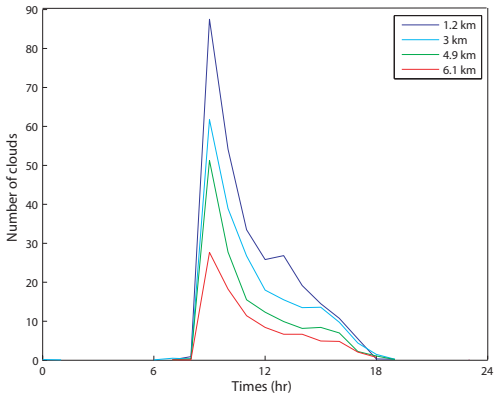

(a) Number of clouds

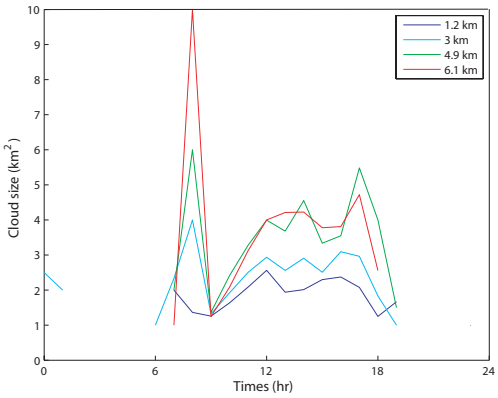

(b) Mean cloud area

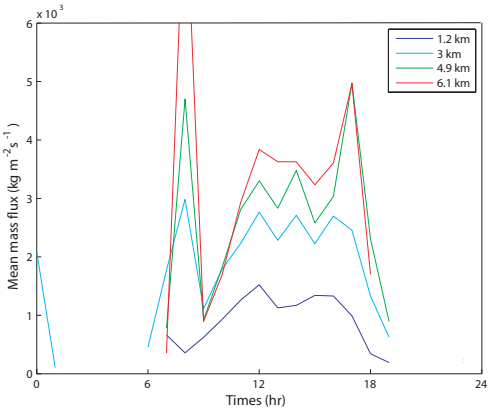

(c) Mean mass flux per cloud

Figure 4.14: *Cloud statistics at different heights for* $\tau = 24$ *hr using a buoyancy definition of a cloud. a) Number of clouds in domain, b) mean area of cloud and c) mean mass flux per cloud at heights of* 1.2 *km (blue line),* 3 *km (cyan line),* 4.9 *km (green line) and* 6.1 *km (red line).*

statistics. The mean area of cloud and mean mass flux per cloud have qualitatively similar vertical variations to those found for $\tau = 24$ *hr* and at RCE. However, the magnitude of these variations are smaller than those previously reported.

Despite the large differences between forcing at $\tau = 24$ *hr* and $\tau = 3$ *hr* there are similarities in the time-evolution of the cloud statistics. Primarily there is strong evidence that, independent of forcing timescale, the time-evolution of cloud base mass flux is mainly controlled by changes in cloud numbers rather than the in-cloud variables. This result was also noted by Plant and Craig (2008) who found that increasing the level of forcing at RCE did not modify the mean mass flux per cloud but rather the fractional area of updrafts. The results here are consistent with findings of Cohen (2001), who suggested that changes in the fractional area (at different forcing rates at RCE)

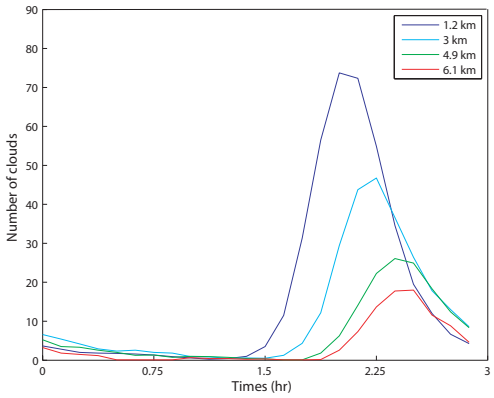

(a) Number of clouds

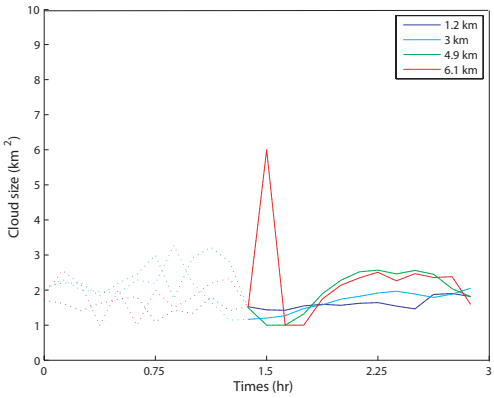

(b) Mean cloud area

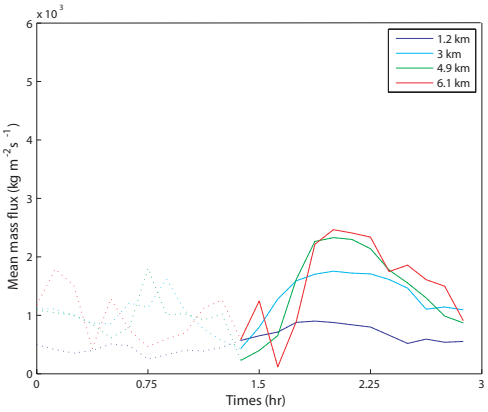

(c) Mean mass flux per cloud

Figure 4.15: *Cloud statistics at different heights for $\tau = 3$ hr using a buoyancy definition of a cloud. a) Number of clouds in domain, b) mean area of cloud and c) mean mass flux per cloud at heights of* 1.2 *km (blue line),* 3 *km (cyan line),* 4.9 *km (green line) and* 6.1 *km (red line). The dotted lines in a) and b) show the same variables as the solid lines but for times when there are fewer than 5 clouds in the domain and the statistics are less reliable.*

are mainly attributed to changes in the number of updrafts with changes in the size of the updrafts being less important. Also, the cloud statistics have similar vertical structures and magnitudes between the different time-varying simulations and RCE, particularly when away from the effects of triggering. These statistics will form the basis of further analysis in Section 5.3.2.

4.6 Variation in total convection per forcing cycle

It was noted in Section 4.4.1 that characteristics of the time evolution of convection are dependent on the forcing timescale. Some of these characteristics have been discussed in more detail in Sections

4.4.2, 4.4.3 and 4.4.4. As a result of some of these issues (for example, the timing of convection) it is not straightforward to define exactly how well the convective response 'matches' the imposed forcing. Two variables are introduced in Section 4.4.2, $\overline{I_{M_b}}$ and $\sigma(I_{M_b})$, based on equation 4.1. These are similar to the variables $\overline{(\Delta T_{conv})}$ and $\sigma(\Delta T_{conv})$ introduced in Chapter 2 which, together with the timeseries of the convective heating, were used to characterise the convective response. It was shown that $\sigma(\Delta T_{conv})$ was dependent on the relationship between the memory timescale and the forcing timescale. Similar variables are introduced here related to surface precipitation, $\overline{I_{ppt}}$ and $\sigma(I_{ppt})$. In Section 4.4.2 it was shown that when averaged over sufficient time $\overline{I_{M_b}}$ approached the same value when $\tau = 3$ *hr* and when $\tau = 1$ *hr*. In this section $\overline{I_{M_b}}$ and $\sigma(I_{M_b})$ will be further investigated for each forcing timescale.

Figure 4.16(a) shows $\overline{I_{M_b}}$ and $\sigma(I_{M_b})$ and Figure 4.16(b) similarly shows $\overline{I_{ppt}}$ and $\sigma(I_{ppt})$. It can be seen that for all τ the response averaged over 11 successive forcing cycles produces very similar values of $\overline{I_{M_b}}$ and $\overline{I_{ppt}}$ (see also the discussion in Section 4.4.2 and Figure 4.9). Both $\sigma(I_{M_b})$ and $\sigma(I_{ppt})$ have increased variability at shorter values of forcing timescale. The sensitivity of $\sigma(I_{M_b})$ and $\sigma(I_{ppt})$ at these short forcing timescales to the number of forcing cycles composited is tested by increasing the number of cycles used for $\tau = 3$ *hr* and $\tau = 1$ *hr*. Figure 4.16 shows that large values of $\sigma(I_{M_b})$ and $\sigma(I_{ppt})$ are characteristic of short forcing timescales, regardless of the number of forcing cycles used, but these variables are sensitive to exactly which forcing cycles are examined, particularly for $\tau = 1$ *hr*. The same result is also seen in Figure 4.9(b).

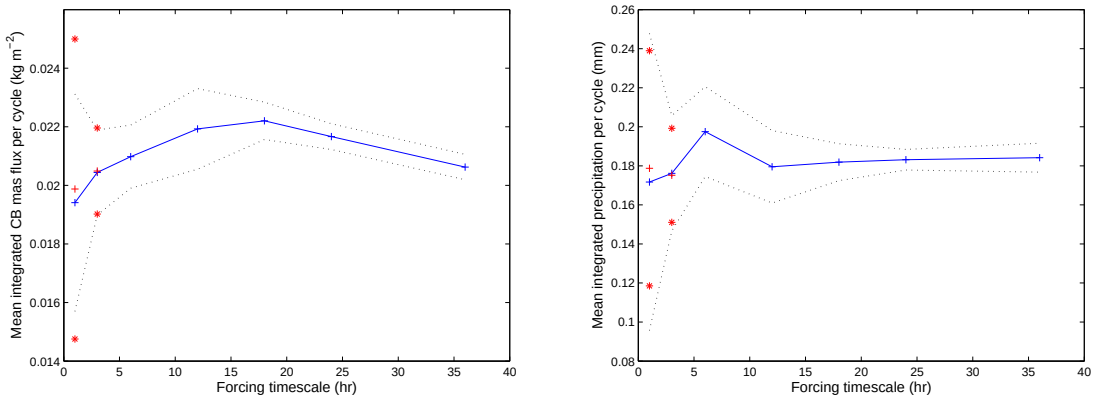

(a) Cloud base mass flux (b) Surface precipitation

Figure 4.16: *Composite integrated responses over 11 cycles with adjustment period removed, normalised by the length of the forcing cycle. a)* $\overline{I_{M_b}}$ *(blue line) and* $\sigma(I_{M_b})$ *(black, dotted line) and b)* $\overline{I_{ppt}}$ *(blue line) and* $\sigma(I_{ppt})$ *(black, dotted line). Red pluses and stars show composite means and standard deviations for* $\tau = 3$ *hr and* $\tau = 1$ *hr over 16 and 29 cycles respectively with adjustment period removed.*

This increase in $\sigma(I_{M_b})$ and $\sigma(I_{ppt})$ at short forcing timescales is similar to the increase in $\sigma(\Delta T_{conv})$ seen in the analytic model (Chapter 2) when there is a 'moderate' memory timescale such that τ is larger than the memory timescale but not significantly larger. This confirms discussion in Section 4.4.1 that there are similarities between the regimes seen in the analytic model and those observed in the CRM. Hence the characteristics of the CRM simulations may be summarised as follows:

• For short forcing timescales ($\tau < 10$ *hr*) the timeseries of the convective response was found to be non-repetitive and reminiscent of regime C from the simple model (Section 2.6). Here there is feedback within the system causing variability in the total integrated convection cycle-to-cycle.

• For longer forcing timescales the response is repetitive and the total integrated convection is the same for each forcing cycle. There are similarities with regime E in Section 2.6. The lack of memory in the system causes the response to be characterised by the time evolution of the forcing.

The results in Chapter 2 suggest that the presence of memory in a convective system causes feedback which results in the convection during one forcing cycle affecting the convection on subsequent cycles. It would be useful to assess whether the large values of $\sigma(I_{M_b})$ and $\sigma(I_{ppt})$ seen in Figure 4.16 are also due to the influence of convection on subsequent cycles. This can be determined by examining the relationship between the total convection in one forcing cycle and the total convection occurring in subsequent forcing cycles. Figure 4.17 shows the integrated cloud base mass flux (I_{M_b}) for one forcing cycle plotted against I_{M_b} on the subsequent forcing cycle. For $\tau = 3$ *hr* and $\tau = 1$ *hr* there is large scatter in the relationship between the integrated cloud base mass flux on one forcing cycle and the subsequent forcing cycle. This is consistent with the large variability in I_{M_b}, in agreement with Figure 4.16.

In Figure 4.18 lines of least-squares linear regression have been added to Figure 4.17 to show the regression of integrated cloud base mass flux for one cycle on that occuring in the previous cycle. Regression shows if there is dependence of one variable on another. In this case the aim is to test if there is inter-dependence of convection between forcing cycles. The data in Figure 4.18 has been split to show long forcing timescales and short forcing timescales separately. These represent the different regimes that have been identified from $\sigma(I_{M_b})$.

Figure 4.18 shows that for large τ (i.e. $\tau = 36,\ 24$ and 18 *hr*) there is almost no relationship between the integrated cloud base mass flux on one cycle and the integrated cloud base mass flux on the previous cycle. Here the regression lines are almost horizontal and in Table 4.4 the corresponding

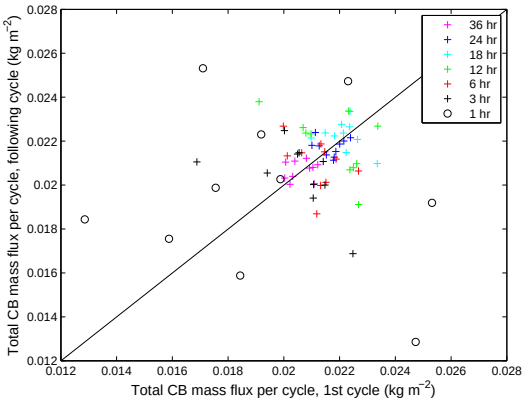

Figure 4.17: *Comparison of integrated cloud base mass flux during one forcing cycle compared to the following forcing cycle for all τ, normalised by the length of the forcing cycle. A 1:1 line shown for reference.*

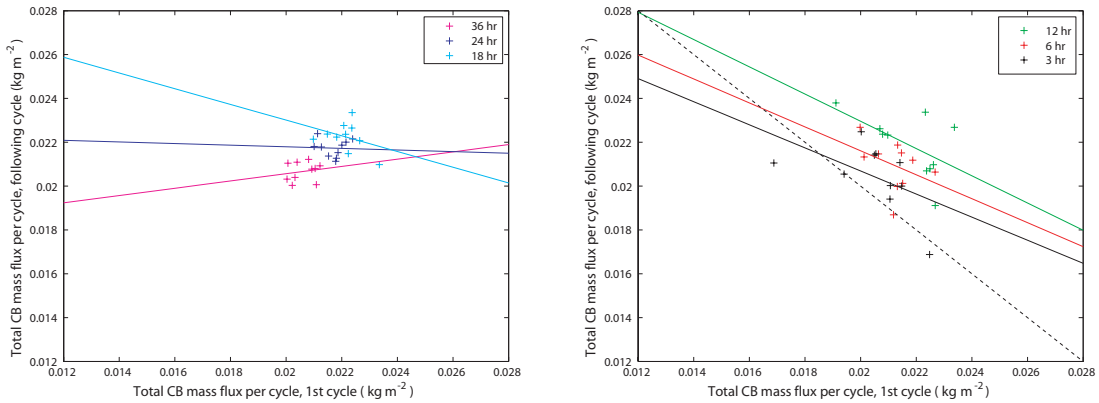

(a) Long forcing timescales (b) Short forcing timescales

Figure 4.18: *Comparison of integrated cloud base mass flux during one forcing cycle compared to the following forcing cycle for all τ, normalised by the length of the forcing cycle. Least-squares regressions of the integrated cloud base mass flux during one forcing cycle on the integrated cloud base mass flux during the previous cycle are also shown for a) 'long' forcing timescales of $\tau = 36,\ 24$ and 18 hr and b) 'short' forcing timescales of $\tau = 12,\ 6$ and 3 hr. In b) a 1:-1 dotted line is shown for reference..*

values of correlation coefficient (r) are small. As the length of the forcing timescale decreases the relationship between the two is stronger, and is negative (Figure 4.18(b)). The values of r also become more strongly negative. At very short forcing timescales, $\tau = 1$ *hr*, the relationship is not clear as seen by the increase in correlation. At these very short timescales, however, it may be that feedbacks within the system occur on timescales longer than 1 *hr* and, therefore, may not be seen in this diagnostic.

This section has shown that in a realistic convective ensemble characteristics can be observed that

τ (*hr*)	36	24	18	12	6	3	1
r	0.170	-0.042	0.035	-0.510	-0.390	-0.52	-0.140

Table 4.4: *Table of r correlation coefficients as used in the regression of integrated cloud base mass flux for one day on integrated cloud base mass flux for the previous day. Lines of least-squares regression are seen on Figure 4.18.*

are similar to those found in the simple model with memory (Chapter 2). It has been found that for short forcing timescales there is feedback where convection on one forcing cycle modifies the convection on the subsequent cycle. It was suggested this is due to memory in the system modifying the convective response. At longer forcing timescales, there is not a strong relationship between the convection on successive cycles as there is not feedback within the system.

4.7 Role of the mean state

One of the aims of this study is to identify physical mechanisms that may modify the convection in one cycle dependent on the level of convection during the previous cycle. Hence the aim is to suggest mechanisms that might cause memory within the system. In the first instance it is reasonable to look at the domain-mean initial profiles at the start of the forcing cycle. For example Derbyshire *et al.* (2004) showed that the intensity of convection, as seen in vertical profiles of updraft mass flux, was sensitive to mid-tropospheric relative humidity. Here, it may be that convection on previous cycles modifies the environment so as to promote more (or less) intense convection in the following cycle. It is useful to consider the "initial state" of the atmosphere, when the forcing starts, for the different forcing timescales. Two example forcing timescales are chosen. Firstly, $\tau = 24$ *hr* is chosen to represent long forcing timescales and 3 *hr* represents short forcing timescales.

Furthermore, in the case of the 3 *hr* simulation it is useful to determine any differences in the mean state at the start of the forcing cycle for different cycles. In particular, are there substantial differences between the initial states of those cycles that have larger total integrated convection and those with smaller total integrated convection?

4.7.1 Initial mean state for $\tau = 24$ *hr* and $\tau = 3$ *hr*

Figure 4.19 shows the initial profiles, at the start of the forcing cycle, composited over the 11 cycles of the well-adjusted state for both $\tau = 24$ *hr* and $\tau = 3$ *hr*. For potential temperature, static stability and water vapour mixing ratio, profiles are shown in the boundary layer as the greatest differences are found at lower levels. Relative humidity is very similar in the boundary layer and therefore is shown through the depth of the troposphere. Figure 4.19(a) shows that the potential temperature structure is very similar for both forcing timescales, although warmer and slightly more variable when $\tau = 3$ *hr*. The largest difference is seen near the surface which is more stably stratified when $\tau = 3$ *hr* (Figure 4.19(b)). Figure 4.19(c) shows differences in the vertical profile of water vapour. For $\tau = 3$ *hr* the water vapour field is more well-mixed in the vertical and more variable cycle-to-cycle than for $\tau = 24$ *hr*. This reflects the fact that there is still convection in the domain (Figures 4.7(c) and 4.15) when there is no surface forcing and that this convection has variable intensity. The relative humidity (Figure 4.19(d)) is very similar throughout the depth of the convection although it is slightly drier and more variable for $\tau = 3$ *hr*.

It is interesting to note that despite the differing lengths of time for which the 24 *hr* and 3 *hr* simulations are run, the initial profiles are very similar cycle-to-cycle for both of these forcing timescales (Figure 4.19). This may be anticipated as the methodology for the imposed forcing defines the system to be in moist-static-energy balance over a complete forcing cycle (Section 3.3.1). However, it is also noted that the 3 *hr* simulation has greater variability about the domain-mean initial profiles in Figure 4.19 than when $\tau = 24$ *hr*. The following section will identify, for $\tau = 3$ *hr*, if there is a direct relationship between the variations in this initial mean state and the total convection in the following forcing cycle.

4.7.2 Variability of initial mean state for $\tau = 3$ *hr* between forcing cycles

To investigate the role of the initial mean state in controlling the total convection in the following cycle these data are split depending on the strength of the total integrated cloud base mass flux (I_{M_b}). A total of six forcing cycles are used, 11 which formed the composites and one additional cycle. Six cycles for which there is the most I_{M_b} are classified as 'strong' and six cycles for which there is least I_{M_b} are classified as 'weak'. The initial profiles, at the start of the forcing, are composited over the six cycles for these two different categories.

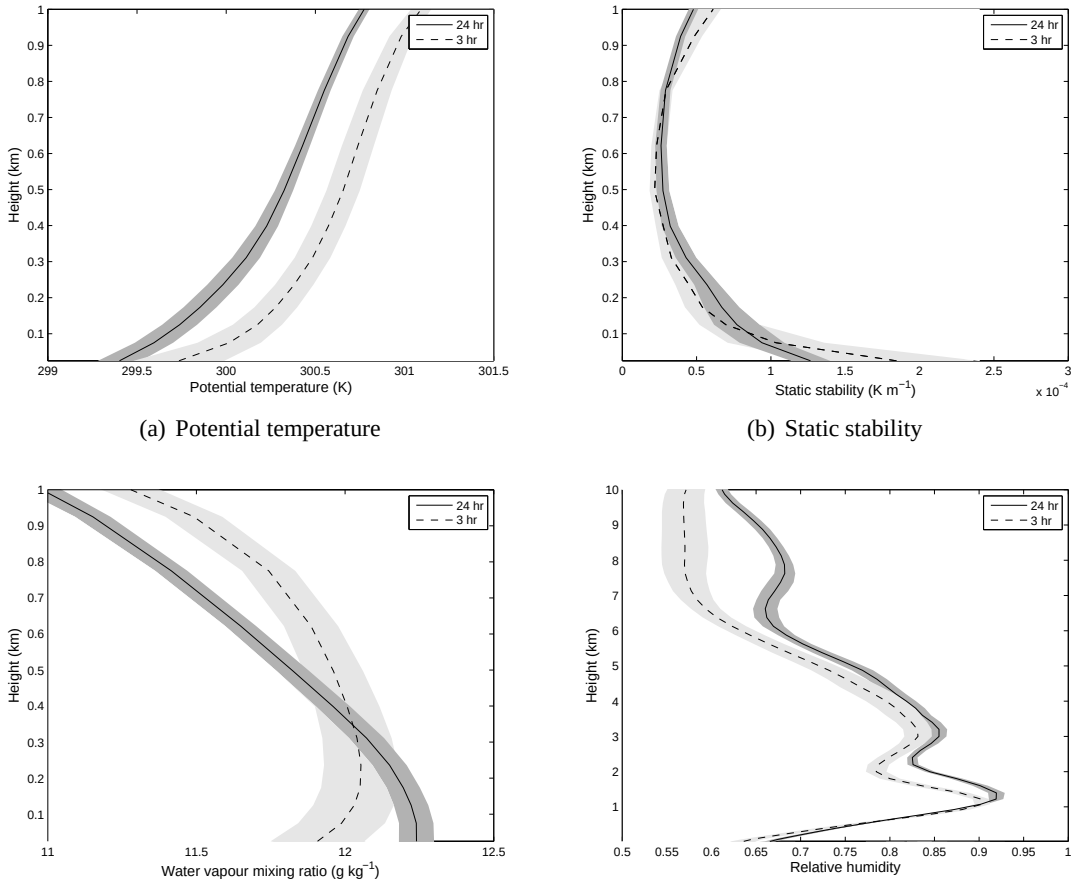

(a) Potential temperature

(b) Static stability

(c) Water vapour mixing ratio

(d) Relative humidity

Figure 4.19: *Composite mean vertical profiles with standard deviation, at the start of the forcing over 11 cycles with the adjustment period removed. a) Potential temperature, b) static stability, c) water vapour mixing ratio and d) relative humidity. Two forcing timescales are shown, for* $\tau = 24$ *hr (solid line) and* $\tau = 3$ *hr (dashed line) with standard deviations shaded. Note the different vertical axis between a), b) and c) and d). This is to reflect the heights where there is greatest difference between the vertical profiles.*

Figure 4.20 shows the initial profiles of potential temperature and water vapour mixing ratio for the 3 *hr* simulation partitioned by the strength of the subsequent convection. These are only shown for the boundary layer as there is the greatest difference at low levels. There is very little difference in the free troposphere. There is little difference in the initial profiles for both potential temperature and water vapour, such that the profiles preceding both 'strong' and 'weak' cycles lie within one standard deviation of the other. There is greater variability in both potential temperature and water vapour at the start of the 'strong' cycles. This suggests that the mechanisms which cause one forcing cycle to have more or less convection than another are not seen in the domain-mean initial state.

It has been shown that the initial mean state, at the start of the forcing cycle, is similar cycle-to-cycle

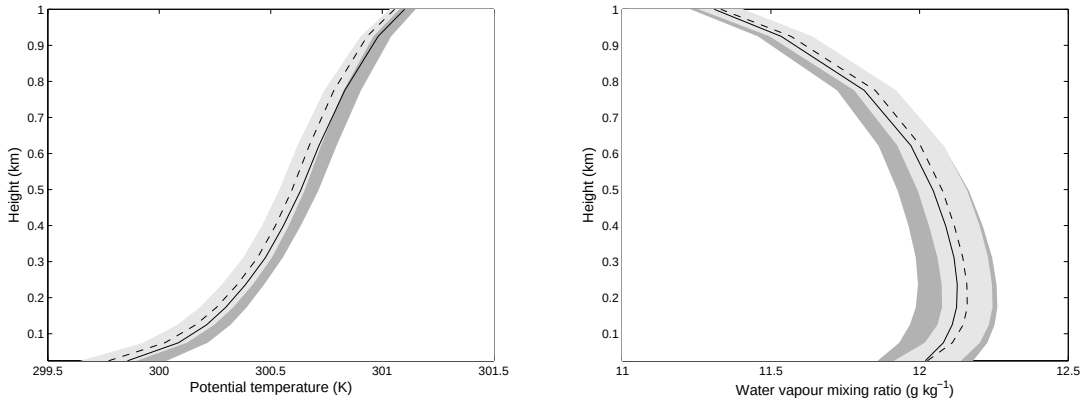

(a) Potential temperature (b) Water vapour mixing ratio

Figure 4.20: *Composite domain-mean vertical profiles, with standard deviation, at the start of the forcing over six cycles partitioned by the total integrated cloud base mass flux for $\tau = 3$ hr. a) Potential temperature and b) water vapour mixing ratio. Initial vertical profiles when there is 'strong' convection are shown as a solid line with dark shading and when there is 'weak' convection by a dashed line with light shading.*

for both long and short forcing timescales. There is small variability in the mean profiles (Figure 4.19). Also it can be seen that despite the differing lengths of the forcing cycles, the profiles have similar vertical structure. In addition, at short forcing timescales where there is variability in the total convection cycle-to-cycle the vertical profiles of the initial conditions are similar on cycles where there is 'strong' convection and those when there is 'weak' convection. It is, therefore, suggested that the memory in the system is not present in the mean state.

4.8 Summary and discussion

This chapter has described and discussed the response of a convective ensemble to a time-varying surface forcing. The simulations presented here are a continuation of the flux-forced control simulation but with time-varying surface sensible and latent heat fluxes based on those used in the EUROCS case study. The forcing timescale has been altered to investigate the effect of the rate at which the system is forced on the convective response. The switch to time-varying forcing requires a reduction of the longwave cooling, although the cooling rate is the same for all forcing timescales. After the switch between the control forcing and the time-varying forcing it was seen (particularly clearly at the very short forcing timescales) that the system took $5-7$ *hr* to exhibit the characteristics of the settled, well-adjusted response. Hence, the time-varying simulations were examined from 10 *hr* after the transition in the forcing.

For all forcing timescales the convective response has been quantified for both cloud base mass flux and surface precipitation. It is shown that the convective response is delayed relative to the start of the forcing and that this delay is directly controlled by the time it takes for sufficient sensible heat to be supplied to erode the stable boundary layer. After triggering the time-evolution of the convective response is dependent on the timescale at which it is forced. A metric is introduced which measures the standard deviation of the total time-integrated cloud base mass flux, $\sigma(I_{M_b})$, between the forcing cycles. The methodology (Section 3.3.1) states that the total moist static energy is balanced over a complete forcing cycle and, therefore, if the convective response is completely adjusted to the forcing over a cycle $\sigma(I_{M_b})$ will be small.

At long forcing timescales ($\tau \gtrsim 10$ *hr*) the convection is seen to 'spike' at the time of triggering. This is partly attributed to the horizontal resolution which, being relatively coarse, results in the convective response being overly reliant on the sub-grid scheme during the development of convection. However, even at higher resolution a strong initial response is still observed at triggering, due to the environment maintaining a moist adiabatic potential temperature profile in the troposphere. After triggering there is a strong convective response throughout the positive phase of the forcing cycle with very little convection observed after the forcing becomes zero. After the triggering phase the clouds have similar sizes and mass flux distributions in the vertical to those in the control simulation, suggesting that at these times the convection is similar to RCE. At these forcing timescales $\sigma(I_{M_b})$ is found to be small indicating that the convection is similar on subsequent cycles. Hence, it is suggested that the response is similar to that in the analytic model when the memory timescale is much shorter than the forcing timescale; i.e memory is not important for the evolution of the convection. Here the convective response may be directly related to the total forcing in that cycle.

At short forcing timescales ($\tau \lesssim 10$ *hr*) the convective response evolves more gradually over time and convection never completely switches off. As convection triggers in the domain the number of clouds increase although the size of the clouds and the mean mass flux per cloud remain similar. Hence, convection develops mainly through changes in the number of clouds rather than altering the in-cloud characteristics. Here $\sigma(I_{M_b})$ is found to be larger, indicating that the total convection is different cycle-to-cycle. The response is reminiscent of the response in the analytic model when there is a moderate memory timescale compared to the forcing timescale. This suggests feedback between the convection on subsequent cycles, which modifies the convective response. The presence of memory within the system suggests that convection is not simply related to the current forcing but is dependent on the time-history of the convective system.

Fundamentally there are different initial responses, at the time of triggering, when the forcing timescale is long compared to when it is short. This is in addition to the differences in the main convective response during the positive phase of the forcing cycle. It is suggested that the total convective response is characterised by two timescales, the length of time for which there is positive surface forcing and the length of time for which there is just longwave cooling. Mechanisms for the different responses will be discussed further in Chapter 5.

Analysis of the initial profiles (i.e. at the start of forcing) from the 3 *hr* simulation when there was 'strong' and 'weak' total time-integrated convection in the domain showed that there was little difference in the mean state between these two cases. Hence, the feedback of the convective response from cycle-to-cycle is not discernible from the mean state. Considered from a parameterisation perspective there would be insufficient information in the mean state alone to determine the total convective response on the following cycle. A parameterisation would produce similar convection on both the 'strong' and 'weak' cycles as the mean states are comparable. Chapter 5 develops the study of the simulation with a short forcing timescale, 3 *hr*, in order to identify mechanisms which may provide memory in the 3 *hr* simulation.

CHAPTER 5

Evolution and role of spatial structures in dis-equilibrium

5.1 Introduction

Chapter 4 investigated a convective ensemble forced at a range of forcing timescales. It was found that the characteristics of the convective response depended on the timescale of the forcing. At forcing timescales $\gtrsim 10$ *hr* the convective response was similar cycle-to-cycle; when the forcing timescale was $\lesssim 10$ *hr* the convective response was highly variable. The strong cycle-to-cycle variability was attributed to feedback in the system due to memory. The mechanism whereby memory is carried was not found in the domain-mean initial state, as this was similar for each forcing cycle. This chapter will directly contrast the spatial fields from two example forcing timescales with and without memory effects (3 *hr* and 24 *hr*, respectively) to determine if variations about the mean may provide memory.

A theory developed to explain fluctuations in the convective response at radiative-convective equilibrium (RCE) will be introduced and its validity will be tested at RCE for the specific model setup used here. The theory will then be applied to the temporally-evolving convective ensemble at both forcing timescales, and physical mechanisms for deviations from theory will be discussed. The spatial scales of the complete cloud lifecycle will be investigated using two techniques: the first is applied when clouds are present; the second is used at all times. The time-evolution of the clouds and their role in pre-conditioning the atmosphere will be discussed in the context of a mechanism for memory.

5.2 Horizontal inhomogeneities of the cloud domain

Chapters 3 and 4, respectively, discussed the characteristics of a convective ensemble in radiative-convective equilibrium (RCE) and when subject to a time-varying forcing. The system was characterised in terms of the large-scale time-evolution of the convective response and the statistics of the

clouds within the convective ensemble.

In Chapter 3 it was shown that at RCE cloud base mass flux reached a mean value that was constant in time but with variability about that mean. It was also shown that other characteristics of the convective ensemble had variations about their mean values. The fluctuations in the convective ensemble were shown to be due to under-representing the complete spectrum of clouds required for equilibrium (Section 3.8.2). Using a larger domain with a larger sample of clouds reduced the variability in cloud base mass flux (Figure 3.15).

With a time-varying forcing (Chapter 4), the time-evolution of cloud base mass flux has been shown to be dependent on the timescale at which the convection is forced. With shorter forcing timescales ($\lesssim 10$ *hr*) the standard deviation of the integrated mass flux, $\sigma(I_{M_b})$, was found to be large compared to longer forcing timescales ($\gtrsim 10$ *hr*). Other characteristics of the convective ensemble were also found to evolve in time, although the magnitudes of the cloud statistics were very similar to those found at RCE, particularly in the convective response away from triggering.

When $\tau \leq 10$ *hr* the variation in the total integrated mass flux, cycle-to-cycle, could not be attributed directly to any features in the domain-mean state (Section 4.7). Specifically, knowledge at the start of a forcing cycle of the domain-mean vertical thermodynamic structure does not indicate the total integrated mass flux that will occur in the following forcing cycle. As the domain-mean profile does not carry sufficient information it is hypothesised that spatial variations about this mean profile may be important.

Figure 5.1 shows example snapshots of the spatial variability of the cloud field and the moisture field at a height of 3 *km*. The clouds are found using a buoyant cloud definition and the moisture field is anomalies of water vapour mixing ratio from the domain-mean. Figure 5.1 shows that the structure of the water vapour field depends both on the timescale of the forcing and the phase within the forcing cycle. Characteristics of the cloud field are also variable, dependent on the phase and the forcing timescale.

This chapter will discuss a theory developed to explain the mass flux variance at RCE in terms of the variability of the cloud field (Section 5.3.1) and will test if the theory is also valid when the forcing varies in time (Section 5.3.2). Discussion will also explain the different characteristics in Figure 5.1 and determine the interactions between the clouds and spatial variations in the thermodynamic structure (Section 5.4). For example, horizontal variability of thermodynamic fields is likely to

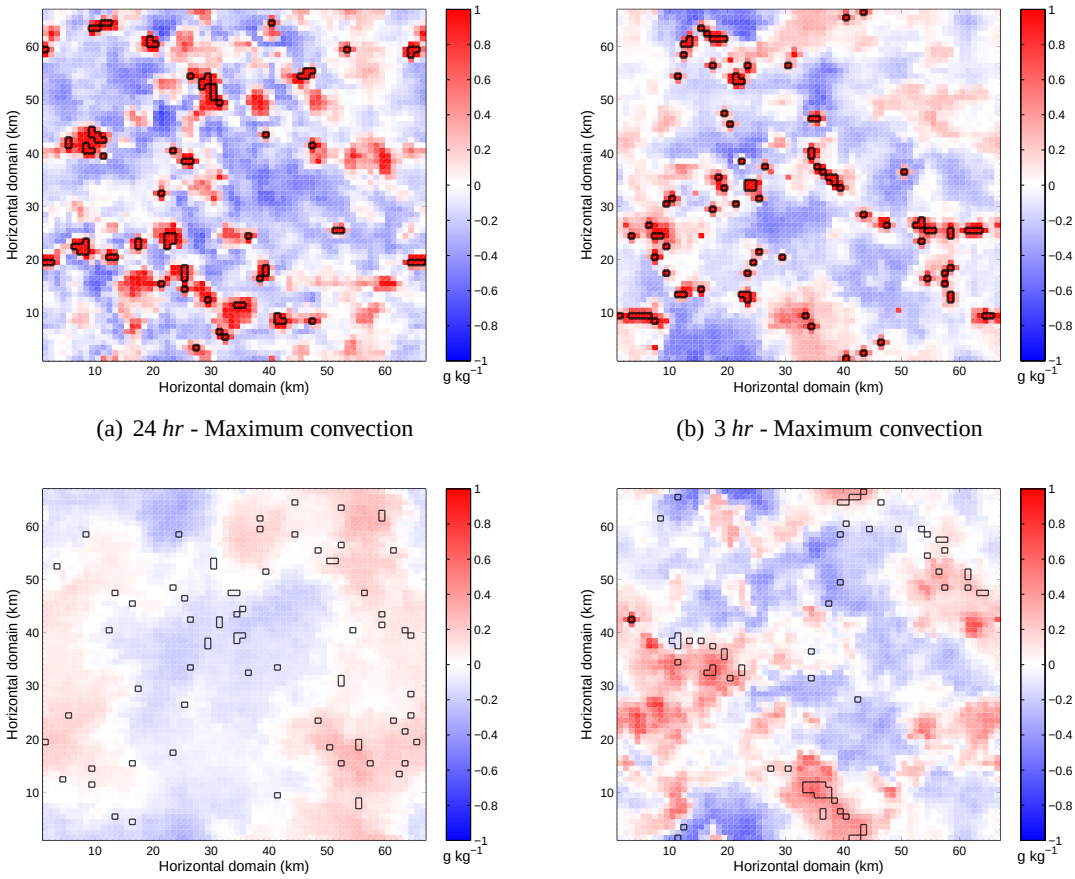

(a) 24 *hr* - Maximum convection

(b) 3 *hr* - Maximum convection

(c) 24 *hr* - Minimum convection

(d) 3 *hr* - Minimum convection

Figure 5.1: *Example snapshots of water vapour mixing ratio anomalies at two times during the forcing cycle for time-varying simulations, a, c)* $\tau = 24$ *hr and b, d)* $\tau = 3$ *hr at a height of* 3 *km. The times are chosen to represent times of a, b) maximum and c, d) minimum convection in the domain. Maximum convection is the time in the forcing cycle when there is strongest convective activity (excluding the 'spike' at* $\tau = 24$ *hr). The minimum convection occurs at a time which follows at the end of the same forcing cycle from which the maximum convection is shown, and is the time when there is least convective activity (*3 *hr) or at the start of the next forcing cycle (*24 *hr). The cloud field at the same time as the snapshot is shown (heavy black line). At the time of minimum convection the cloud field at the time of subsequent triggering is also shown (light black line). Clouds are defined using a buoyancy definition. At times of maximum convection water vapour mixing ratio anomalies may exceed the upper range of the plots (*$1g\ kg^{-1}$*) by* $2g\ kg^{-1}$.

influence the location of triggering subsequent clouds. Similarly the role of clouds in warming and moistening the atmosphere will create inhomogeneities in the thermodynamic field.

5.3 Theory for total mass flux variance

This section will introduce a theory that explains the variance in the large-scale convective response in terms of the natural variability inherent in a random cloud ensemble. This theory will be applied to convection at RCE and also when forced with a time-varying forcing. It will then be possible to discuss the variance in the large-scale cloud base mass flux in terms of the statistical characteristics of the clouds.

Craig and Cohen (2006); Cohen and Craig (2006) introduced a theory to explain the fluctuations seen in the large scale in the convective ensemble, about the mean state, in terms of the sub-domain cloud field. The authors based this theory on the principles of statistical mechanics, which can be used to explain the macroscale behaviour of a many-body gas system. At a microscopic level within the gas, individual molecules each have seemingly random behaviour. It has been widely shown through laboratory experiments, however, that these small-scale fluctuations do not need to be explicitly accounted for to understand the mean, large-scale characteristics of the gas. There is a spatial scale of separation of several orders of magnitude between the microscale fluctuations of the molecules and the large-scale variability of the system at a macroscopic level. This is analogous to the separation scale that is assumed in order to facilitate parameterisation of convective systems in numerical models. Where a scale separation exists between the convection and the large-scale forcing, convection can be parameterised in terms of the large scale. If such a scale separation exists in the convective ensemble, parameterisations can be made and the principles from statistical mechanics can be applied. Craig and Cohen (2006); Cohen and Craig (2006) formalised this analogy to derive a theory to explain the fluctuations of a convective ensemble about its mean state. As with the theory from statistical mechanics, this theory explains the 'natural fluctuations' in the convective ensemble about the mean state.

Key results from this theory are summarised here; a full derivation can be found in Craig and Cohen (2006). For a arbitrary n-cloud system the total mass flux at a given level is:

$$M(n) = \sum_{i=1}^{n} m_i \tag{5.1}$$

where m_i is the the mass flux of an individual cloud. If the clouds are randomly distributed in space

and non-interacting, a Possion distribution for the number of clouds (N) in a given area can be assumed, and the ensemble mean and variance of $M(n)$, $\langle M \rangle$ and $\langle (\delta M)^2 \rangle$, may be predicted.

$$\langle M \rangle = \langle N \rangle \langle m \rangle \quad \text{and} \quad \langle (\delta M)^2 \rangle = 2 \langle N \rangle \langle M \rangle^2 \tag{5.2}$$

where the angled brackets indicate an ensemble average and $\delta M = M - \langle M \rangle$.

From equation 5.2 the ensemble-mean mass flux variance can be found:

$$\frac{\langle (\delta M)^2 \rangle}{\langle M \rangle^2} = \frac{2}{\langle N \rangle} \tag{5.3}$$

Equation 5.3 may be re-written as $\mathscr{V}$ the normalised mass flux variance, which if the theory is valid will produce the value 2:

$$\text{Normalised mass flux variance, } \mathscr{V} = \frac{\langle (\delta M)^2 \rangle}{\langle M \rangle^2} \times \langle N \rangle = 2 \tag{5.4}$$

Hence, this theory explains the natural fluctuations (variations) in the mass flux in terms of the number and the mean mass flux of the clouds. This theory requires two key assumptions. Firstly, it requires that at the domain scale the clouds are in equilibrium with the forcing, such that variability is caused only by the natural fluctuations *within* the convective system rather than the adjustment of the system to changes in the large-scale forcing. For this assumption to be valid, the forcing must be sufficiently slowly varying in time and applied over a sufficiently large region such that the convection has time to adjust. Secondly, the theory requires that the clouds are point-like and do not interact with each other except through their effect on the mean flow (Craig and Cohen, 2006). As the clouds do not interact, the convective ensemble will not be organised and clouds will be randomly distributed in space.

Cohen and Craig (2006) developed and tested this theory for a RCE simulation that was surface-temperature-forced. It was found that theory explained the the normalised mass flux variance to

within 10 %. Both the strength of the forcing and the imposition of wind shear modified the results. Weaker forcings and greater wind shear (summarised in Table 5.1) were found to increase $\mathscr{V}$ by increasing organisation. In fact increased wind shear can compensate for deviations from theory at stronger forcings. However, the size of the domain did have a strong effect on the normalised mass flux variability with larger domains having reduced errors compared to smaller domains (their Figure A1a). Their results hinted that larger domains have increased organisation compared to smaller domains. However, undersampling the convective ensemble was to distort this result with undersampled statistics having values of $\mathscr{V}$ closer to theory than statistics taken from the whole domain. Undersampling the convective ensemble was shown to reduce deviations from theory as sub-sampling an organised ensemble makes the statistics appear 'more' random. Even with large domains it was found that results approached theory with a bias of ~ 10 %.

Model setup	Value of $\mathscr{V}$	Percentage error in $\frac{\langle(\delta M)^2\rangle}{\langle M\rangle^2}$
No shear	1.56	10 %
Low shear	1.83	4 %
High shear	1.93	1 %

Table 5.1: *Summary of findings from Cohen and Craig (2006) for simulations of RCE which are temperature-forced with a longwave cooling rate of* $-2\ K\ day^{-1}$. *The fluctuation statistics were computed at a height of* 2.4 *km.*

This theory will be used to test whether the variability seen in the cycle-to-cycle mass flux with a time-varying forcing is likely to be due to the natural fluctuations within the convective ensemble. However, the validity of this theory needs first to be tested when the system is flux-forced. The results are compared to when a system that is temperature-forced.

5.3.1 Distribution of clouds at radiative-convective equilibrium

Figure 5.2 shows the profiles, with height, of normalised mass flux variance ($\mathscr{V}$) from equation 5.4 at RCE for the two different definitions of a cloud (Section 3.7), using different forcing mechanisms and two different domain sizes. When the convective system is flux-forced compared to temperature-forced the mass flux variability is seen to increase and $\mathscr{V}$ approaches 2 (Figure 5.2(a)). With a vertical-velocity definition of a cloud, $\mathscr{V}$ is also consistently larger than with a buoyancy definition. This suggests either that the theory holds better for a vertical-velocity definition in a flux-forced simulation, or else that there are other physical mechanisms controlling the mass flux

variance that are not accounted for in the 'natural variability' explained by the theory. The assumptions made in developing the theory will therefore be examined to determine if they are justified in these simulations.

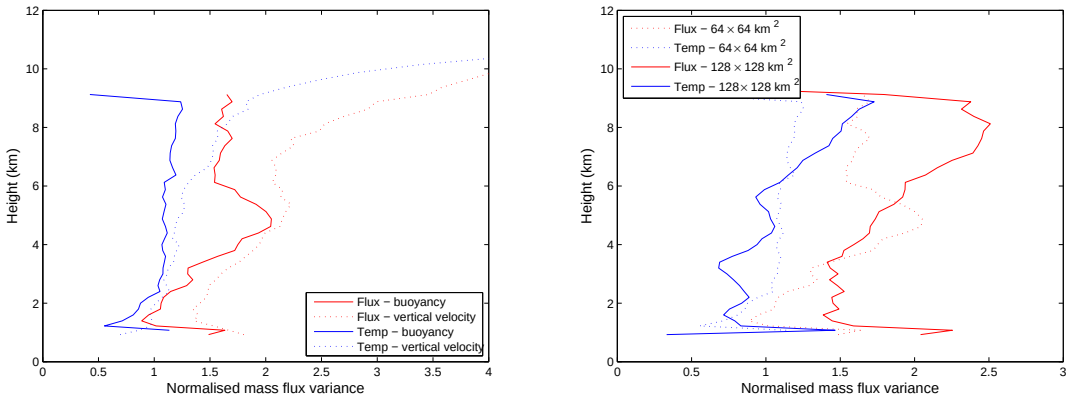

(a) Effect of forcing mechanism (b) Effect of domain size

Figure 5.2: *Normalised mass flux variance* $\left(\mathscr{V} = \frac{\langle(\delta M)^2\rangle}{\langle M\rangle^2} \times \langle N\rangle\right)$ *as a function of height for RCE, computed over a period of* 240 *hr, sampled every* 5 *hr, using two cloud definitions, for two forcing mechanisms at two domain sizes. a)* $\mathscr{V}$ *for a buoyancy definition (solid lines) and a vertical-velocity definition (dotted lines) for flux-forced RCE (red lines) and temperature-forced RCE (blue lines). b)* $\mathscr{V}$ *for a domain* 128×128 *km*^{2} *(solid lines) and* 64×64 *km*^{2} *(dotted lines) for flux-forced RCE (red lines) and temperature-forced RCE (blue lines) with a buoyancy definition of a cloud. These are based on the cloud statistics from Figures a) 3.14 and b) 3.16.*

The first assumption is valid here: by construction the convective system is well adjusted to the large-scale forcing. At RCE the convective system has adjusted to the constant forcing and the time-averaged domain-mean cloud base mass flux and cloud statistics do not change with time. Secondly, it was assumed that the clouds do not interact with each other and that there is no organisation in the domain. This assumption is explicitly examined by calculating the spatial distribution of the clouds in terms of the spacing of the clouds.

The location of each cloud is defined by the mid-point of the cloud, calculated from the maximum width of the cloud in the x and y directions. An example of such a location is shown by point A on Figure 5.3. This is a rather arbitrary definition that works best when the cloud has a simple shape with a similar extent in the x and y directions. Large, organised clouds as seen in Figure 3.9(a) are not common in these simulations and therefore using this basic definition is expected to be reasonable. Khairoutdinov and Randall (2006) used a similar method for defining the size of a cloud by calculating its mean diameter over four directions: x, y and two diagonals.

The spatial distribution of the clouds shows the frequency of occurrence of cloud spacings within the domain. It is calculated in two phases: 1- cumulative probability distribution of cloud spacing is calculated for the spacings of each cloud to all other clouds (Figure 5.3), 2- a similar cumulative distribution is calculated based on the distance between each point in the domain to all other points in the domain and normalised by the total number of cloud spacings found in phase 1. This gives the cumulative probability distribution that the same number of clouds would have if they were randomly distributed. Finally, the distribution from 1 is normalised by that from 2 in order to produce the final *normalised* cumulative probability distribution. This function shows the deviations of the convective ensemble from a random distribution. If the clouds were completely un-organised and had a random distribution, the normalised probability distribution would be 1 for all cloud spacings. Deviations from 1 suggest organisation on a particular scale.

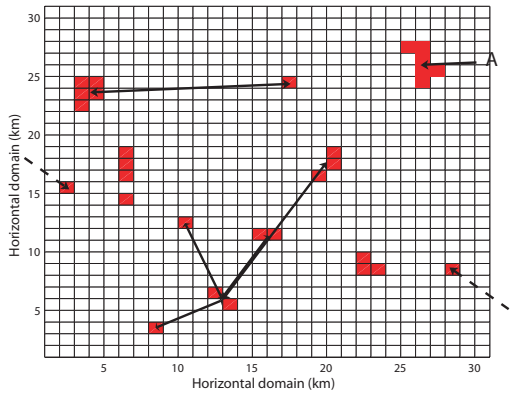

Figure 5.3: *Schematic of the calculation of the probability distribution of cloud spacings. The cloud spacing is defined as the shortest distance (arrows) of each cloud (red squares) from all other clouds. The location of a cloud is given by the mid-point of the cloud calculated from the maximum extent of the cloud in the x and y directions. Due to the bi-periodic domain some clouds may be closer if wrapped around the domain (dashed arrow). The cloud spacing represented (dashed arrow) is computed around the edge of the domain rather than across the the centre of the domain. Point A shows a representative location of the mid-point of a cloud.*

Figure 5.4(a) shows the distribution of the clouds in Figure 5.2(a). This distribution shape is similar to that found by Cohen and Craig (2006), who noted organisation of convection on scales of 10 – 20 *km* at RCE when forced with cooling rates 2 $K\ day^{-1}$ and 4 $K\ day^{-1}$. The distribution shows similar characteristics for different forcing mechanisms and cloud definitions. Note first that there are no clouds that are 1 *km* apart as the corresponding cloudy grid points would have been classified as part of the same cloud. There are very few, or no, clouds at 2 *km* spacing, suggesting that downdrafts in the immediate vicinity of a cloud prevent other clouds forming closeby. There are

significant deviations from a random distribution, for cloud spacings of $\approx 5-10$ *km* for all forcing mechanisms and cloud definitions, suggesting some organisation within the convective ensemble.

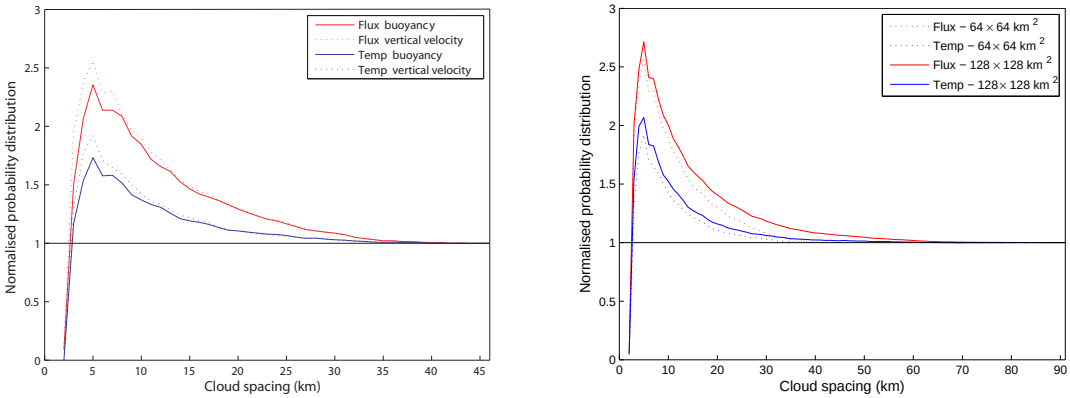

(a) Effect of forcing mechanism (b) Effect of domain size

Figure 5.4: *Cloud distribution at a height of* 3 *km for RCE computed over a period of* 240 *hr, sampled every* 5 *hr, using two cloud definitions, for two forcing mechanisms at domain sizes. a) Cloud distribution for a buoyancy definition (solid lines) and a vertical-velocity definition (dotted lines) for flux-forced RCE (red lines) and temperature-forced RCE (blue lines). b) Cloud distribution in domains of size* 128×128 *km*^{2} *(solid lines) and* 64×64 *km*^{2} *(dotted lines) for flux-forced RCE (red lines) and temperature-forced RCE (blue lines) using a buoyancy definition of a cloud. The cloud distribution is defined as the cumulative probability distribution of cloud spacings between all clouds normalised by a random cumulative distribution. A completely random cloud distribution would be indicated by a value of 1.*

The mechanism through which clouds have organised at $\approx 5-10$ *km* is not clear. Basic principles of convection from theory and laboratory experiments suggest that simple Rayleigh-Benard convection develops cells that have a spacing given by the convective layer depth (Section 1.2). Hence it is suggested that the convection here may also develop with a prefered length scale set by the tropospheric depth. This idea cannot be tested with these results, however, as the tropopause remains at the same height in all simulations. Another suggestion is that convective organisation develops on the edge of cold pools, as illustrated in Figure 5.5, but the direct attribution of convection to cold pools has not been tested here. It is clear, however, that the convection experiences *greater* organisation when flux-forced than temperature-forced, regardless of how the convection organised in the first instance.

This greater organisation may be due to differences in the role of cold pools with the different forcing mechanisms (Figure 5.5). When flux-forced, the surface sensible heat fluxes are held fixed to their pre-defined values. When the surface temperature is held fixed (temperature-forced), however, the surface fluxes are free to evolve (Figure 3.13(a)) based on the temperature difference between

the surface and the lowest model level. On average, the same surface fluxes are attained independent of the forcing mechanism. However, the spatial variability of the surface fluxes when temperature-forced could to have a role in suppressing the organisation of the convection. Around a cloud, downdrafts spread into cold pools, locally reducing the temperature near the surface. These downdrafts suppress convection in the immediate vicinity of the cloud, as illustrated by the X in Figure 5.5. By fixing the surface temperatures (temperature-forced), stronger surface heat fluxes develop in the outflow region, which erode the horizontal temperature gradient created at the edge of the spreading cold pool. Surface fluxes are, therefore, slightly weaker outside the cold pool. The fixed surface fluxes (flux-forced) are the same inside and outside the cold pool. As more energy is supplied to the cold pools when temperature-forced, in order to remove the temperature anomaly due to the cold pool, less energy is available to convection outside the cold pool. Regardless of whether convection organises on scales of $\approx 5-10$ *km* due to cold pool dynamics or whether the scale of organisation is set by the depth of the tropopause, there is relatively more energy supplied to the active convection in the domain when flux-forced. The organisation of the convection is therefore amplified when flux-forced.

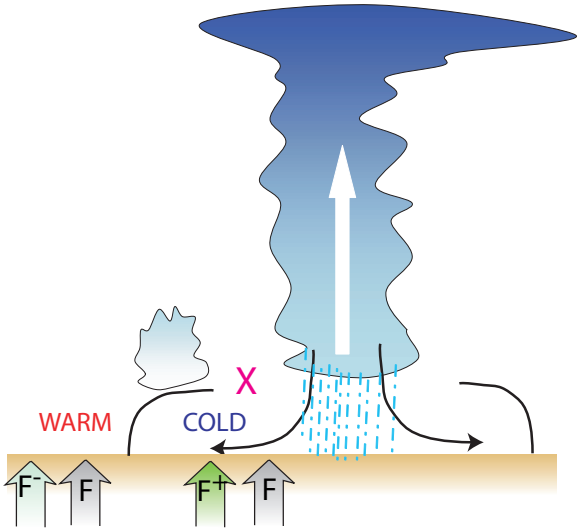

Figure 5.5: *Schematic showing the differing roles of cold pools with different forcing mechanisms. The convective cloud produces downdrafts that spread out at the surface. Close to the cloud there is a region (X) in which the downdraft suppresses convection. Further from the original cloud, uplift at the leading edge of the outflow promotes secondary convection. The air is characterised relative to the domain-mean temperature as COLD in the downdraft and WARM outside. The surface fluxes (F) are shown when flux-forced (grey arrows) and temperature-forced (green arrows). Both forcing mechanisms provide the same mean F, but whilst F is the same inside and outside the outflow when flux-forced, it is relatively larger inside the cold pool when temperature-forced.*

There is greater organisation diagnosed with a vertical-velocity definition than with a buoyancy definition (Figure 5.4(a)). It was shown in Figure 3.12(a) that there were more clouds diagnosed in the domain when a vertical-velocity definition is used. It is suggested therefore that these additional clouds identified with the vertical-velocity definition are also more organised than a random distribution.

The effect of domain size on the mass flux variance is shown in Figure 5.2(b). There is an increase in mass flux variance when flux-forced with the larger domain compared to the smaller domain. This effect is not observed when temperature-forced. This increase in mass flux variance may be explained by the increase in organisation on the larger domain as seen in Figure 5.4(b). This result is consistent with findings of Cohen and Craig (2006), who noted sensitivities to domain size. However, the results presented here also suggest that the level of organisation depends on the forcing mechanism used (Figure 5.4(a) and 5.4(b)) and the definition of a cloud (Figure 5.4(a)).

At both domain sizes the mass flux variance increases above 5 *km*. The freezing level is at approximately 4 *km* and above this height ice cloud begins to form. This reduces the total number of clouds but also increases the organisation (not shown). The peak in the normalised probability distribution is still found at $\approx 5-10$ *km*.

This section has shown that the theory for the mass flux variance from Craig and Cohen (2006); Cohen and Craig (2006) can explain the variance in flux-forced RCE simulations. These results for $\mathscr{V}$ are smaller than those from both theory and Cohen and Craig (2006), who found that $\mathscr{V}$ was 1.56 at a height of 2.4 *km* (Table 5.1). This discrepancy is explained by increased organisation in the domain. The level of organisation was found to depend slightly on domain size and the cloud definition used. The majority of the organisation, however, was found to depend on the forcing mechanism used. Flux-forced RCE has greater organisation than a temperature-forced simulation and this increases the normalised mass flux variance. Hence, the results for flux-forced RCE will be used to provide a benchmark for the normalised mass flux variance to account for the effects of organisation, rather than the theoretically predicted $\mathscr{V} = 2$. The normalised mass flux variance that occurs when forced with a time-varying forcing will be compared to the value of $\mathscr{V}$ from RCE at the same vertical level.

5.3.2 Distribution of clouds in response to a time varying forcing

The time evolution of the normalised mass flux variance ($\mathscr{V}$) is examined for forcing timescales of 24 *hr* and 3 *hr*. In Figure 5.6 the evolution of $\mathscr{V}$ is shown at different heights: near the transition region from shallow to deep convection (1.2 *km*), in the deep convection (3 *km*) and towards the top of the deep convection, both above and below the transition to ice cloud (4.9 *km* and 6.1 *km*). With a 24 *hr* forcing timescale, results are reasonably insensitive to the height chosen as the convective variance evolves similarly at different heights at this forcing timescale (see Figure 4.14). As seen in Figure 4.15 with $\tau = 3$ *hr*, $\mathscr{V}$ shows a shift in response with height: lower levels (1.2 *km*) respond rapidly and strongly; upper levels (6.1 *km*) have a delayed and weaker response.

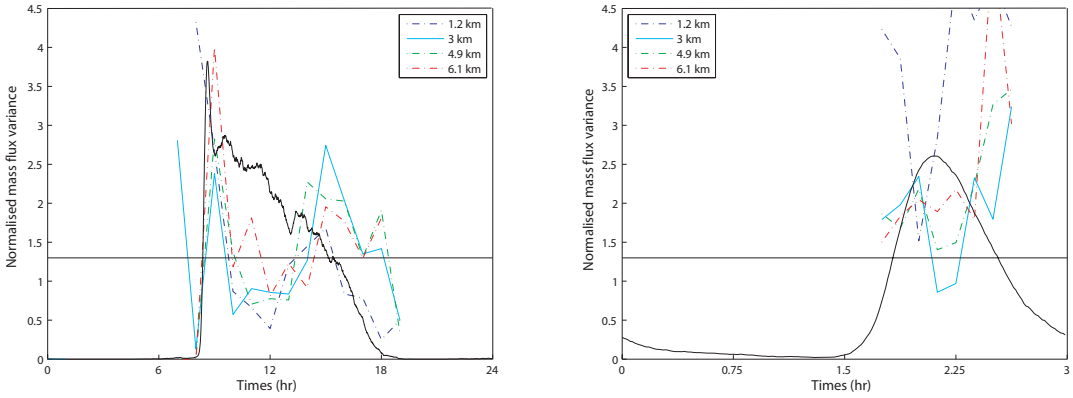

(a) $\tau = 24$ *hr* (b) $\tau = 3$ *hr*

Figure 5.6: *Normalised mass flux variance* $\left(\mathscr{V} = \frac{\langle(\delta M)^2\rangle}{\langle M\rangle^2} \times \langle N\rangle\right)$ *at different heights for time-varying simulations using a buoyancy definition of a cloud.* $\mathscr{V}$ *is plotted for a)* $\tau = 24$ *hr and b)* $\tau = 3$ *hr at heights of* 1.2 *km (blue line),* 3 *km (cyan line),* 4.9 *km (green line) and* 6.1 *km (red line). The horizontal line is the value of* $\mathscr{V}$ *obtained from the equivalent flux-forced RCE (see Figure 5.2(a)) at* 3 *km. These are based on the cloud statistics from Figures a) 4.14 and b) 4.15. In both a) and b)* $\mathscr{V}$ *is not shown where there are fewer than 5 clouds on average as the results are not reliable. The black line is the mean composite cloud base mass flux, shown for reference (as in Figure 4.3(a) and Figure 4.8(c)).*

From the results of the RCE simulations it is proposed that the organisation of the convection has a role in modifying the normalised mass flux variance. The time-evolution of $\mathscr{V}$ when the forcing varies in time suggests, therefore, that the organisation of convection may also be time-dependent. The evolution of the organisation of the convection through the forcing cycle is discussed by considering the distribution of the clouds at key times. The distribution will specifically be discussed at a height of 3 *km* for both forcing timescales, as the shape of the distribution is very similar at other heights, but with a tendency for increased organisation at higher levels. The times chosen for 24 *hr*

and 3 *hr* are shown in Figure 5.7. The distribution of clouds at these key times for both forcing timescales is shown in Figure 5.8.

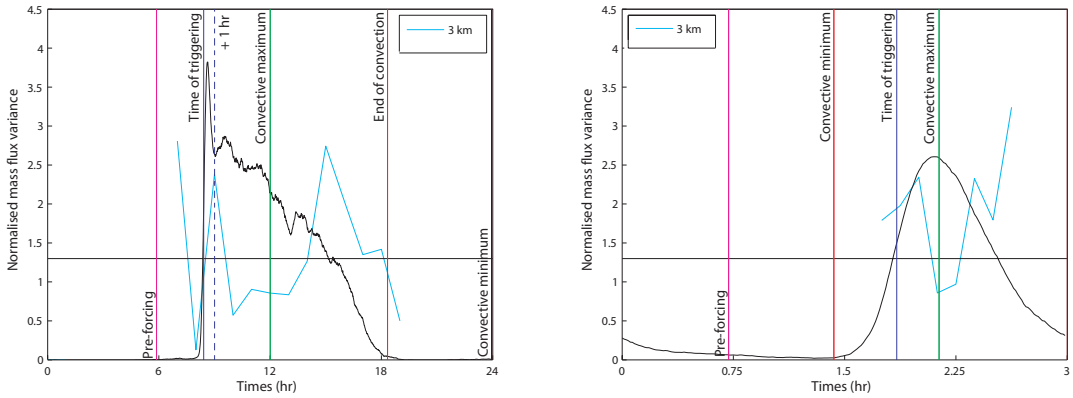

(a) $\tau = 24$ *hr* (b) $\tau = 3$ *hr*

Figure 5.7: *Normalised mass flux variance* $\left(\mathscr{V} = \frac{\langle(\delta M)^2\rangle}{\langle M\rangle^2} \times \langle N\rangle\right)$ *at a height of* 3 *km for time-varying simulations, with a)* $\tau = 24$ *hr and b)* $\tau = 3$ *hr, using a buoyancy definition of a cloud. The horizontal line is the value of* $\mathscr{V}$ *obtained from the equivalent flux-forced RCE (see Figure 5.2(a)) at* 3 *km. Shown in cyan are the values of* $\mathscr{V}$ *from Figure 5.6. The times highlighted by coloured vertical lines are key times for which the cloud ensemble and its spatial distribution are discussed in the text. Times which are represented by the same colour in the two panels are considered to be similar points in time* between *the forcing cycles. These timings are discussed in Table 5.2.*

Time	24 *hr*	3 *hr*
Pre-forcing	1 *hr* before forcing begins at both forcing timescales	
Triggering	Time at which the cloud base mass flux reaches 50 % of the maximum cloud base mass flux	
Convective maximum	Times of maximum cloud base mass flux (excluding 'spike' for 24 *hr*)	
End of convection	End of positive phase of forcing cycle	-
Convective minimum	Time mid-way between end of positive phase forcing cycle and start of subsequent forcing cycle	Time of minimum cloud base mass flux

Table 5.2: *Table summarising key times in* 24 *hr and* 3 *hr forcing cycles, shown in Figure 5.7.*

At the time of triggering the normalised mass flux variance increases for both forcing timescales (Figure 5.7). The convection is strongly organised at this time, although it is organised over a larger range of cloud spacings when $\tau = 24$ *hr* (Figure 5.8). With $\tau = 3$ *hr* there is organisation with preferred cloud spacings of $\approx 5 - 10$ *km*, which is similar to the organisation at RCE (Figure 5.4).

The strong organisation at triggering seen when $\tau = 24$ *hr* is possibly due to the interactions between clouds as they rapidly deepen. It has been shown that the vertical profiles are close to neutral for moist convective ascent (Figure 4.6(a)) and that deep convection is triggered when the boundary layer inversion is eroded (Figure 4.13). Although convection triggers at similar times across the domain, it must trigger initially in one, or a limited number, of locations. It is possible that the triggering of the first convective cell rapidly modifies the neighbouring environment, for example by producing gravity waves and making further convection occur preferentially in nearby locations. For example, Marsham and Parker (2006) showed that secondary convection could be initiated by gravity waves, not just cold pool dymanics, although they were considering the development of convection over longer spatial scales. The cloud spacing at triggering would therefore not be random, but set by the distance at which subsequent convection was initiated. With $\tau = 24$ *hr* the convective rapidly 'dis-organises'; in fact 1 *hr* later the cloud distribution is close to random (Figure 5.8(a)).

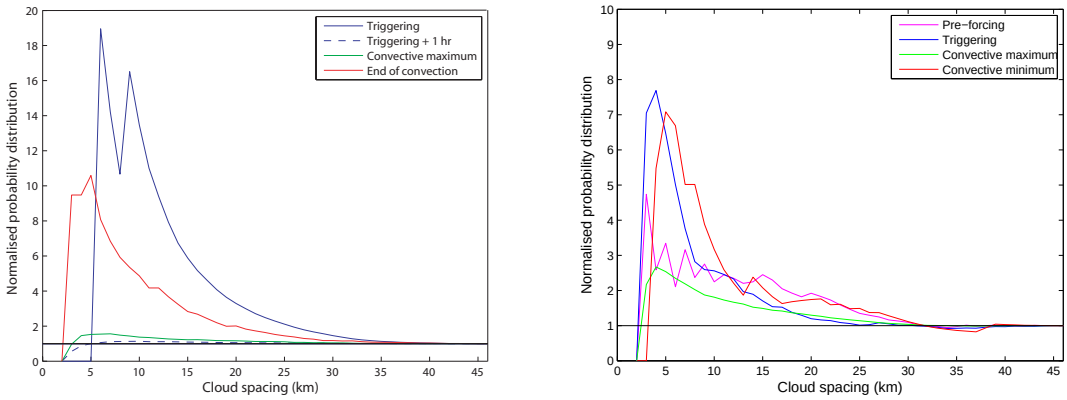

(a) $\tau = 24$ *hr* (b) $\tau = 3$ *hr*

Figure 5.8: *Cloud distributions at a height of* 3 *km at key times during the forcing cycle for time-varying simulations, with a)* $\tau = 24$ *hr and b)* $\tau = 3$ *hr using a buoyancy definition of a cloud. The key times shown for* 24 *hr are triggering (blue line), convective maximum (green line) and the end of convection (red line). For* 3 *hr the key times are pre-forcing (magenta line), triggering (blue line), convective maximum (green line) and the end of convection (red line). These timings are discussed in Table 5.2. The cloud distribution is defined as the cumulative probability distribution of cloud spacing between all clouds normalised by a random distribution. A completely random distribution would be indicated by a value of 1. Note different y-axis between panels.*

The increase in normalised mass flux variance when convection triggers gives way to a large reduction in $\mathscr{V}$ when the convection reaches a maximum at both forcing timescales. In fact it reduces below the level seen at RCE. At this time the organisation is also found to reduce, with the dis-

tribution when $\tau = 24$ *hr* being very close to random although there is some hint that whatever organisation does exist remains at cloud spacings of $\approx 5-10$ *km*. For $\tau = 3$ *hr* the convection is more definitely organised, to a similar extent as at RCE, with preferred cloud spacings $\approx 5-15$ *km*. In view of the organisation having a similar magnitude to RCE, but a lower value of mass flux variance, the instantaneous level of organisation cannot be the sole explanation for the evolution of $\mathscr{V}$.

As the convection begins to decay both forcing timescales show an increase in organisation at the $\approx 5-10$ *km* cloud spacing, associated with an increase of normalised mass flux variance. For $\tau = 24$ *hr* there are no clouds diagnosed in the domain from which to determine the evolution of the cloud field after the forcing switches off and the convection decays. (Another method of tracking the changes in the complete lifecycle of the clouds will be discussed in Section 5.4). However, for $\tau = 3$ *hr* there remain sufficient clouds in the domain to determine the level of organisation even after the strongest convection has died down. With a 3 *hr* forcing timescale the convection becomes increasingly organised at the $\approx 5-10$ *km* as it decays. When the convection triggers at 3 *km* it initially forms at cloud spacings of $\approx 5-10$ *km*, i.e. in line with the pre-existing scale of organisation in the domain.

It has therefore been found that the theory of normalised mass flux variance, previously used at RCE, can also be applied to simulations with a time-varying forcing with different forcing timescales. Similarly to RCE the organisation of the convection can be used to explain the difference from the values predicted by theory. The levels of organisation can be put in to context from the physical interactions between the clouds as they evolve through their lifecycle. It was shown that with $\tau = 3$ *hr* the convection remained organised throughout the forcing cycle. In contrast, for $\tau = 24$ *hr* it was seen that the organisation did not persist from one cycle to the next. It is suggested that two timescales are important. Firstly, the time that convection takes to become organised and secondly, the time convection takes to decay fully (become dis-organised). In the 24 *hr* simulation these times are distinguishable, whereas when $\tau = 3$ *hr* the timescales cannot be separated.

The cloud distribution shows the organisation of clouds and does not show how convection organises during periods when clouds are not diagnosed. The following section will discuss the time-evolution of the spatial fields at the different forcing timescales to account for the complete cloud lifecycle and the role the spatial fields have in the development of convection.

5.4 Spatial scales in the cloud ensemble

Analysis in the previous section focussed on the evolution in time of the cloud field at two forcing timescales. This type of analysis can only be carried out when the domain has identifiable clouds. Convective clouds have a complete lifecycle which incorporates not only the development and active stages, but also the decay phase as a cloud ceases to be active and the cloudy air is dissipated, being entrained and mixed with the surrounding environment.

In this section the spatial structures within the domain are characterised. Fourier analysis is used to identify the dominant scales within the domain. The time evolution of these structures and their dependence on forcing timescale is also discussed. The horizontal spatial structures have been examined at different heights in the vertical, but no attempt has been made to analyse vertical spatial structures.

Firstly, the method of Fourier decomposition is outlined. A Fourier series can be used to describe an infinite, periodic function, $f(x)$, as a series of sines and cosines, thus:

$$f(x) = \frac{1}{2}a_0 + \sum_{n=1}^{\infty} a_n cos(nx) + \sum_{n=1}^{\infty} b_n sin(nx) \tag{5.5}$$

Euler's formula describes the of sine and cosine functions in terms of complex exponentials. The Fourier series can be re-written in terms of these complex exponentials where the co-efficients A_n are complex, having both real and imaginary parts given by $A_n = \Re(A_n) + \Im(A_n)$:

$$f(x) = \sum_{n=0}^{\infty} A_n e^{inx} \tag{5.6}$$

If $f(x)$ is not a continuous function but has N discrete points then a similar discrete function can be used to represent the series:

$$f(x) = \sum_{k=0}^{N-1} A_k e^{\frac{2\pi ikx}{N}} \tag{5.7}$$

where k is the wavenumber and the complex co-efficients A_k may be obtained from a Fourier Transform,

$$A_k = \frac{1}{N}\sum_{x=0}^{N-1} f(x)e^{\frac{-2\pi ikx}{N}} \tag{5.8}$$

Fourier transforms may be found computationally by the fast Fourier transform method (FFT). As Fourier analysis inherently assumes periodic functions, data may need to be modified in some situations (for example in the location of strong gradients or near boundaries), perhaps by tapering it to zero near the boundaries or detrending the data, to prevent misleading results. Due to the bi-periodic nature of the domain used here the spatial fields of variables are periodic, and therefore strong gradients should not be encountered. In fact the bi-periodic, homogeneous nature of the domain is exploited in the analysis of the spatial fields. At any given time the FFTs are performed at a particular level in the x and y directions separately and then all the individual FFTs are composited together. Tests have confirmed that the domain is indeed homogeneous and that there is no significant difference between when the FFTs are taken separately in the x and y directions and when they are composited.

The power at each wave number (a_k), below the Nyquist wavenumber (here $k_{Nyquist} = 32$) is given by $A_k A_k^*$ where A_k^* is the complex conjugate of A_k.

$$a_k = 2(\Re(A_k)^2 + \Im(A_k)^2) \tag{5.9}$$

Discussion will focus on the normalised power of the spatial structures of a particular field (see the discussion around Figure 5.10 for more details). Using normalised power enables the comparison of the *relative* power of spatial scales at different times in the forcing cycle, as well as inter-comparison of the spatial structures seen using different forcing timescales. The normalised power $a_{k_{norm}}$ is given by:

$$a_{k_{norm}} = a_k \times \frac{1}{\sum_k a_k} \tag{5.10}$$

Scales will be discussed in terms of wavelength rather than wavenumber, where the wavelength λ_k for a domain of length L is given by:

$$\lambda_k = \frac{L}{k} \tag{5.11}$$

λ_k gives the wavelength of the structures observed in these simulations and is dependent on domain size. Hence when $k = 0$ the wavelength is infinite, implying the constant term of the field, a_0 in equation 5.5, or the mean of the field. The FFT when $k = 0$ will not discussed here as the domain-mean fields have been discussed in Chapter 4. When $k = 1$, $\lambda_k = 64\ km$ and represents wave number one for these simulations.

Similar to the discussion of the cloud distribution, in the first instance spatial scales will be discussed at RCE (Section 5.4.1) as this will provide a useful reference point for understanding of the spatial scales present in a convective ensemble. The time-evolution of the structures in the spatial field when the forcing varies in time can then be discussed (Section 5.4.2).

5.4.1 Spatial scales of a cloud ensemble at radiative-convective equilibrium

Figure 5.9 shows the spatial scales existing at RCE for a flux-forced simulation. The vertical velocity field (Figure 5.9(a)) exists at a wide range of scales. Very near the surface where there are dry, boundary layer plumes, vertical velocity structures exist at all scales, with many small-scale structures. As height increases, the relative power at the small scale decreases and a larger portion of the power is found on the large scales. This is consistent with there being fewer clouds with increasing height, as seen in Figure 3.12.

The potential temperature, water vapour mixing ratio and relative humidity have similar characteristics, exhibiting the same spatial structures almost independent of height. All these thermodynamic variables show increasing relative power at longer wavelengths. Furthermore, the magnitudes of the

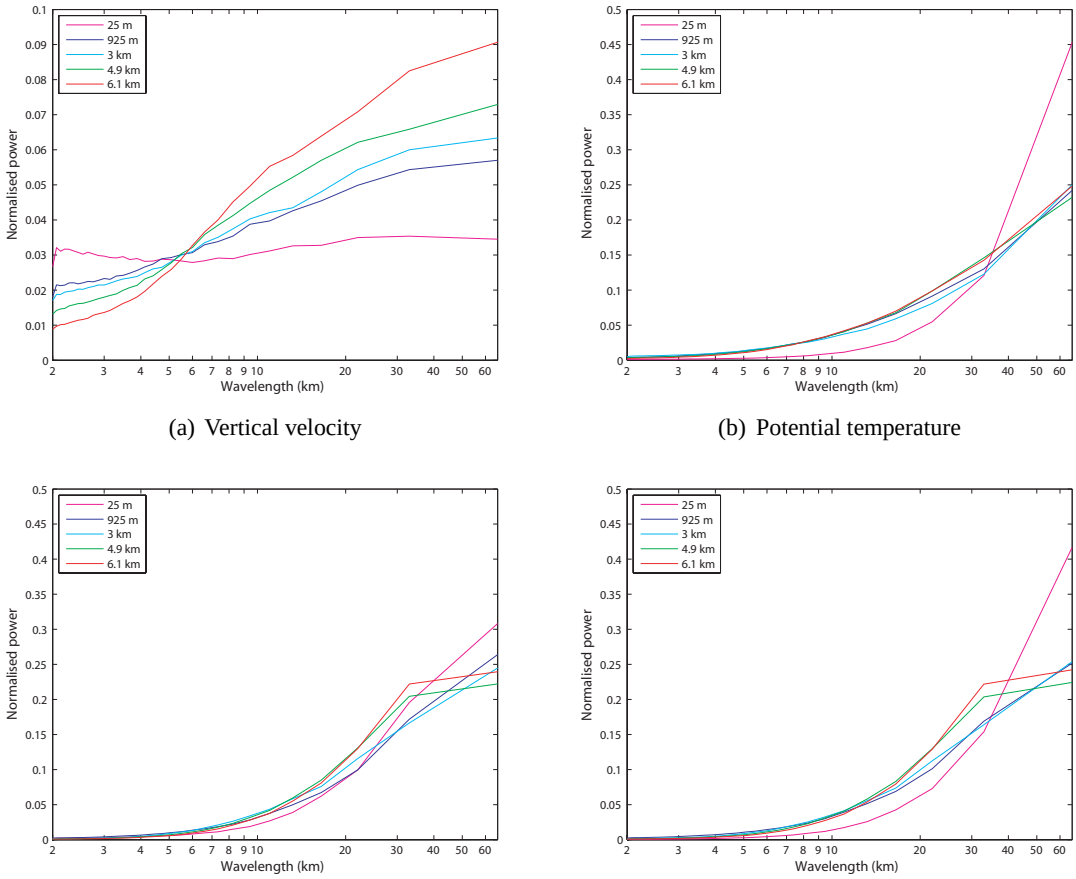

(a) Vertical velocity

(b) Potential temperature

(c) Water vapour mixing ratio

(d) Relative humidity

Figure 5.9: *Normalised power of spatial fields of a) vertical velocity, b) potential temperature, c) water vapour mixing ratio and d) relative humidity at different heights for flux-forced RCE taken from a period of* 240 *hr, sampled every* 5 *hr. All fields are shown at heights of* 25 *m (magenta line),* 925 *m (blue line),* 3 *km (cyan line),* 4.9 *km (green line) and* 6.1 *km (red line). These heights are chosen to be the same as those in Figure 5.6, but also include some lower levels. Note the different vertical axis in a).*

normalised power are similar; Figures 5.9(b), 5.9(c) and 5.9(d) are on the same scale. The main differences in the thermodynamic structures are in the potential temperature near to the surface and the water vapour mixing ratio structures above 4.9 *km*.

Potential temperature shows increased power at long wavelengths near the surface, suggesting that the power is predominantly at the domain mean. A reason for this may be due to the boundary layer structure below the clouds. The temperature structure is constrained, with sensible heat fluxes decreasing with height through the majority of the boundary layer, although at the top of the boundary layer there is a downwards heat flux due to the entrainment of higher potential temperature air from above. As the system is in RCE, this heat-flux profile mediates the fluxes between the surface and

the cloud base. The surface sensible heat fluxes are uniform, so near the surface the temperature field can exist only on large scales. It is likely that the water vapour mixing ratio field in the sub-cloud layer is found on a greater range of scales, as this field is influenced by moisture structures in the clouds. Larger variations in moisture fluxes compared to sensible heat fluxes are shown in Stull (1988), their Figures 3.1 and 3.2.

Above 4.9 *km* there is relatively less power in the water vapour structures at large scales. The freezing level is 4 *km* (Figure 3.6(b)), so above this height there is relatively little water vapour and the water vapour that does exist is found on smaller scales.

The focus of this study is the time-evolution of deep convection well above the boundary layer, within the deep convective cloud layer. At these levels the spatial fields of the thermodynamic variables are shown in Figure 5.9 to be insensitive to the exact height chosen. They will be discussed at 3 *km*.

5.4.2 The evolution of spatial scales with time-varying forcing

The spatial scales of the thermodynamic variables will be discussed at a height of 3 *km* for $\tau = 24$ *hr* and $\tau = 3$ *hr*. The spatial scales of vertical velocity will not be discussed in detail as the time evolution of this field is closely coupled with the forcing, and is therefore qualitatively similar for different forcing timescales. However, the vertical velocity field will be used here to illustrate the characteristics of a spatial field as represented by both the absolute and normalised power.

Figure 5.10 compares of the spectral power of vertical velocity at different times in the forcing cycle when $\tau = 24$ *hr*. It shows that when there is no convection in the domain (i.e. pre-forcing) and also at the convective minimum, there is low power in absolute terms at all wavelengths. *Relatively* speaking, however, there is more power at longer wavelengths (Figure 5.10(b)), suggesting a dominance by the mean state. When convection triggers, power increases at all scales, with more relative power at the small scales associated with the scattered clouds seen in Figure 4.4. At the maximum of convection, as the clouds become organised, the power in both absolute and relative terms decreases (increases) at the smaller (longer) wavelengths. As the convection begins to decay the power reduces at all scales, although relatively it decays more rapidly at the smaller wavelengths.

This example serves to show that there is useful information in both the absolute and the normalised power field. The absolute field will show how the time evolution of the convection modifies the

spatial structures, but it cannot be used straightforwardly to compare the power at different times in the forcing cycle. The normalised power shows clearly the dominant scales. For this reason, normalised power will be used in the remainder of this section to discuss the thermodynamic fields at different times in the forcing cycles of differing length.

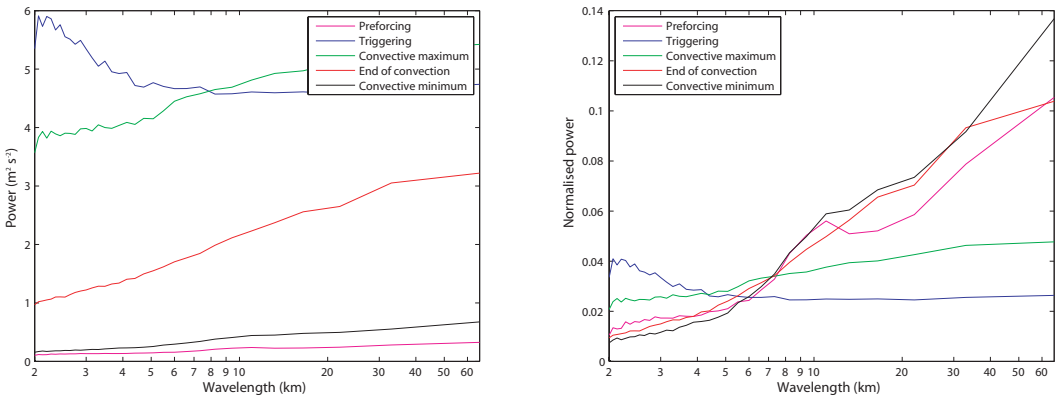

(a) Vertical velocity spectrum (b) Normalised vertical velocity spectrum

Figure 5.10: *A comparison of a) the power and b) the normalised power of the spatial field of vertical velocity at a height of* 3 *km for key times during the forcing cycle for a time-varying simulation where* $\tau = 24$ *hr. These times are chosen to be the same as those in Figure 5.8: i.e. time of triggering (blue lines), convective maximum (green lines) and end of convection (red lines), but also include times when there are no clouds in the domain, notably pre-forcing (magenta lines) and convective minimum (black lines). These times are illustrated in Figure 5.7 and discussed in Table 5.2.*

Dependent on the forcing timescale there are significant differences in the time evolution of the spatial fields of potential temperature and water vapour mixing ratio (Figure 5.11), although the spatial characteristics of each thermodynamic variable are similar. Therefore, the temperature and water vapour spatial structures will be discussed as one thermodynamic field. With a long forcing timescale ($\tau = 24$ *hr*), before the convection triggers the thermodynamic field exists at longer wavelengths, although these structures are weak, as seen in Figure 5.1(c). When convection triggers, power increases at the smaller wavelengths. At convective maximum the relative power shifts to slightly larger scales and moderate wavelengths ($\approx 8-20$ *km*). As the convection starts to decay, similar to the results for the vertical velocity field, the relative power is reduced at the smaller wavelengths and remains on the longer wavelengths. After the surface forcing is switched off, power is removed at all wavelengths, with a weak relative shift to longer wavelengths.

The spatial structures undergo very limited temporal evolution at 3 *km* when forced at $\tau = 3$ *hr*. At all times the thermodynamic field has significant power for wavelengths > 7 *km*. When convection

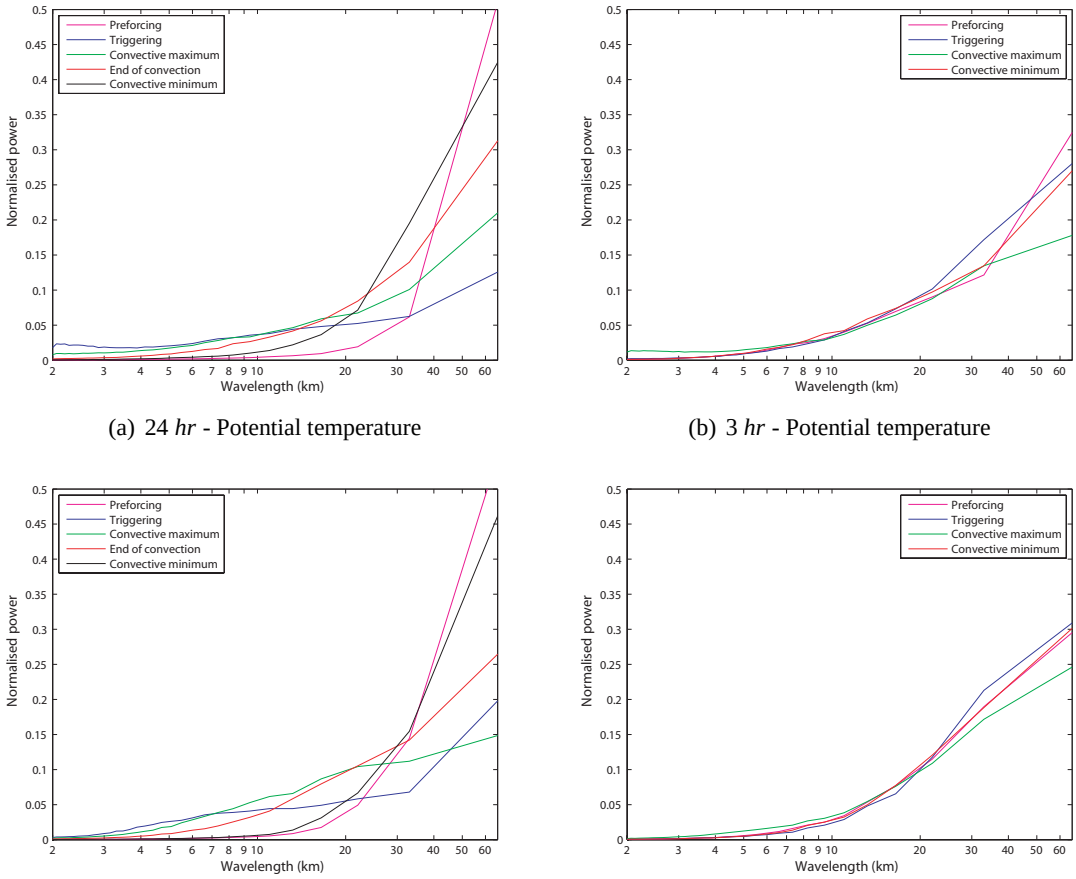

(a) 24 *hr* - Potential temperature

(b) 3 *hr* - Potential temperature

(c) 24 *hr* - Water vapour mixing ratio

(d) 3 *hr* - Water vapour mixing ratio

Figure 5.11: *Normalised power of thermodynamic spatial fields at a height of* 3 *km for key times during the forcing cycle of time-varying simulations. a, c)* $\tau = 24$ *hr and b, d)* $\tau = 3$ *hr. For a, b) potential temperature and c, d) for water vapour mixing ratio. The times are pre-forcing (magenta lines), the time of triggering (blue lines), convective maximum (green lines), the end of convection (red lines) and convective minimum (black lines). These times are illustrated in Figure 5.7 and discussed in Table 5.2.*

is at a maximum, it is possible to detect the clouds producing small-scale structure in the potential temperature, but otherwise the structures are fairly consistent with time.

Figure 5.12 summarises the findings in Figure 5.11 using relative humidity, which (as shown in Figure 5.9(d)) has the characteristics of both potential temperature and water vapour. The normalised power is shown at two important times in the forcing cycle. These are convective maximum and pre-forcing for $\tau = 24$ *hr* and convective maximum and convective minimum for $\tau = 3$ *hr*. The timings for each forcing timescale are taken to be comparable as illustrated in Figure 5.7.

With $\tau = 24$ *hr*, at maximum convection there is power at all wavelengths, although as the convection decays the power reduces relatively at the moderate scales of $\approx 5 - 20$ *km* and shifts to the

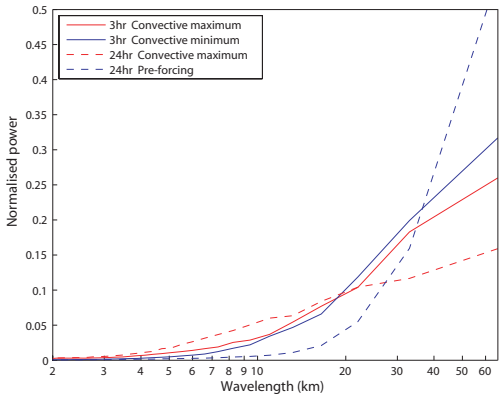

Figure 5.12: *Normalised power of relative humidity field at a height of* 3 *km and at two times during the forcing cycle of time-varying simulations* $\tau = 24$ *hr (dashed line) and* $\tau = 3$ *hr (solid line). The times of convective maximum are shown by red lines and the pre-forcing and convective minimum are shown as blue lines. These times are illustrated in more detail in Figure 5.7 and discussed in Table 5.2.*

longer wavelengths. Interestingly, there is more power at convective maximum on moderate scales when $\tau = 24$ *hr* than when $\tau = 3$ *hr*. For $\tau = 3$ *hr*, there is power at the same scales at both times of maximum and minimum convection. At convective minimum, for $\tau = 3$ *hr* there is relatively more power in the scales of $\approx 5-30$ *km* than for $\tau = 24$ *hr*, despite the longer forcing timescale having more power on moderate scales at convective maximum.

These characteristics of the spatial variability are well illustrated by Figure 5.1. At the longer forcing timescale, $\tau = 24$ *hr*, the water vapour anomaly field evolves from a large range of strong spatial structures at the time of maximum convection to a very weak, large-scale field just before convection triggers. When the convection does trigger it produces small clouds all over the domain. At a short forcing timescale, $\tau = 3$ *hr*, the large variability in the water vapour field is still present when convection triggers. When convection triggers, clouds occur predominantly in the more moist regions of the domain.

5.5 Summary and discussion

This chapter has discussed the spatial structure of the thermodynamic fields within a convective ensemble forced by time-varying surface fluxes. Investigations have focussed on two forcing timescales (24 *hr* and 3 *hr*), as in Chapter 4 the convective response was found to have different

characteristics at these timescales. It was found that with a forcing timescale of 3 *hr* the convective response was indicative of a system with memory. In contrast, when the forcing timescale was 24 *hr* any effects of memory were not readily apparent. As the domain-mean, initial state potential temperature and moisture were found not to provide any indication of the total convective response to a forcing cycle, it was hypothesised that spatial variations about this mean may be important.

A theory for the normalised mass flux variance ($\mathscr{V}$) was introduced. This had been previously used to explain fluctuations about radiative-convective equilibrium (RCE) when temperature-forced. Cohen and Craig (2006) showed that the validity of the theory was senstive to the domain size used. It was shown here that the theory was also sensitive (weakly) to the cloud definition used and (more strongly) to the method by which the convection was forced. Deviations from theory, however, were of a similar magnitude to Cohen and Craig (2006). The assumption of a random distribution of clouds, made in formulating the theory, was examined and it was suggested that deviations from the theory may be explained by organisation of the convective clouds. The organisation of clouds was measured by the cumulative probability distribution of cloud spacings, normalised by a completely random probability distribution. At RCE clouds were found to organise at scales of $5-10$ *km*.

The theory was tested for simulations with a time-varying forcing. $\mathscr{V}$ was found to vary in time with deviations from theory attributable to the time-evolution of convective organisation. In the 24 *hr* simulation convection triggered on a range of scales, with $\mathscr{V}$ being relatively large. Shortly after triggering the clouds are distributed increasingly randomly and $\mathscr{V}$ reduces. During the remainder of the convective response, $\mathscr{V}$ increases and convection organises on scales of $5-10$ *km*. For $\tau = 3$ *hr*, $\mathscr{V}$ experienced less time evolution. Convection triggers on scales of $5-10$ *km* and remains on these scales throughout the forcing cycle. When the convective response is strongest, the organisation is slightly more random and $\mathscr{V}$ decreases accordingly.

The evolution of the complete convective lifecycle cannot be determined from the cloud distribution when clouds are not present. Therefore, in conjuction with the cloud distribution, power spectra of the horizontal spatial fields were examined. Normalised power spectra were used to compare the relative power of the spatial structures at different times and with different forcing timescales. (Absolute power was strongly affected by the phase of the cycle.) It was shown that dynamic variables such as vertical velocity were dependent on the current level of forcing, but that thermodynamic variables were not directly linked to the forcing. Potential temperature and water vapour mixing ratio (and hence also relative humidity) had similar time evolutions, but it was shown that these

thermodynamic structures evolved differently for $\tau = 24$ *hr* and $\tau = 3$ *hr*.

In particular, it was shown that the thermodynamic spatial structures in the 3 *hr* simulation underwent limited time evolution. Structures were observed at scales of $5-20$ *km* at convective maximum, and these structures were still present at convective minimum, when the majority of the convective clouds had decayed. For $\tau = 24$ *hr*, the spatial structures experienced greater time evolution. Notably, when convection was at a maximum spatial structures were observed on scales similar to those for $\tau = 3$ *hr*. However, when convection reached a minimum there was limited relative power on scales of $5-20$ *km* and greater power at longer wavelengths.

These findings are summarised in Figure 5.13, which shows the time-evolution of the cloud field and the spatial structures of water vapour at 3 *km* for both 24 *hr* and 3 *hr* forcing timescales. It may be noted that the horizontal water vapour anomalies and cloud fields are most similar at convective maximum. At this time the convection has become organised on scales of $5-10$ *km* and the spatial structures are present on scales of $5-20$ *km*. As the convection decays to its minimum level, differences occur between the forcing timescales. At $\tau = 3$ *hr* convection may still be present at scales of $5-10$ *km*, and there is still power in the water vapour field on scales of $5-20$ *km*. However, at $\tau = 24$ *hr* there is no convection and there is no significant power in the spatial structures on scales of $5-20$ *km*. When convection triggers on a forcing timescale of 3 *hr* the convection is organised on scales of $5-10$ *km* in locations that are more moist, but for $\tau = 24$ *hr* convection triggers almost randomly on a range of scales. It is suggested the organisation at triggering when $\tau = 3$ *hr* is due to the presence of spatial structures on scales of $5-20$ *km*. Futhermore, it is suggested that these spatial structures, which persist when $\tau = 3$ *hr* and not when $\tau = 24$ *hr*, provide the mechanism for memory in the convective system.

Figure 5.13 suggests that two timescales are important. The first is the timescale at which convection organises. As seen when $\tau = 24$ *hr*, convection takes a finite period to adjust to a preferred spatial scale. The second key timescale is the time needed for convection to decay fully. By contrasting the spatial fields for the 24 *hr* and 3 *hr* forcing timescales, given sufficient time it can be seen that the dissiption of cloudy air will remove any spatial structures. Hence, if there is sufficient time to remove spatial structures, the convective system has no memory of previous convection. However if convection has insufficent time to organise in the first instance, then strong spatial structures may not be formed.

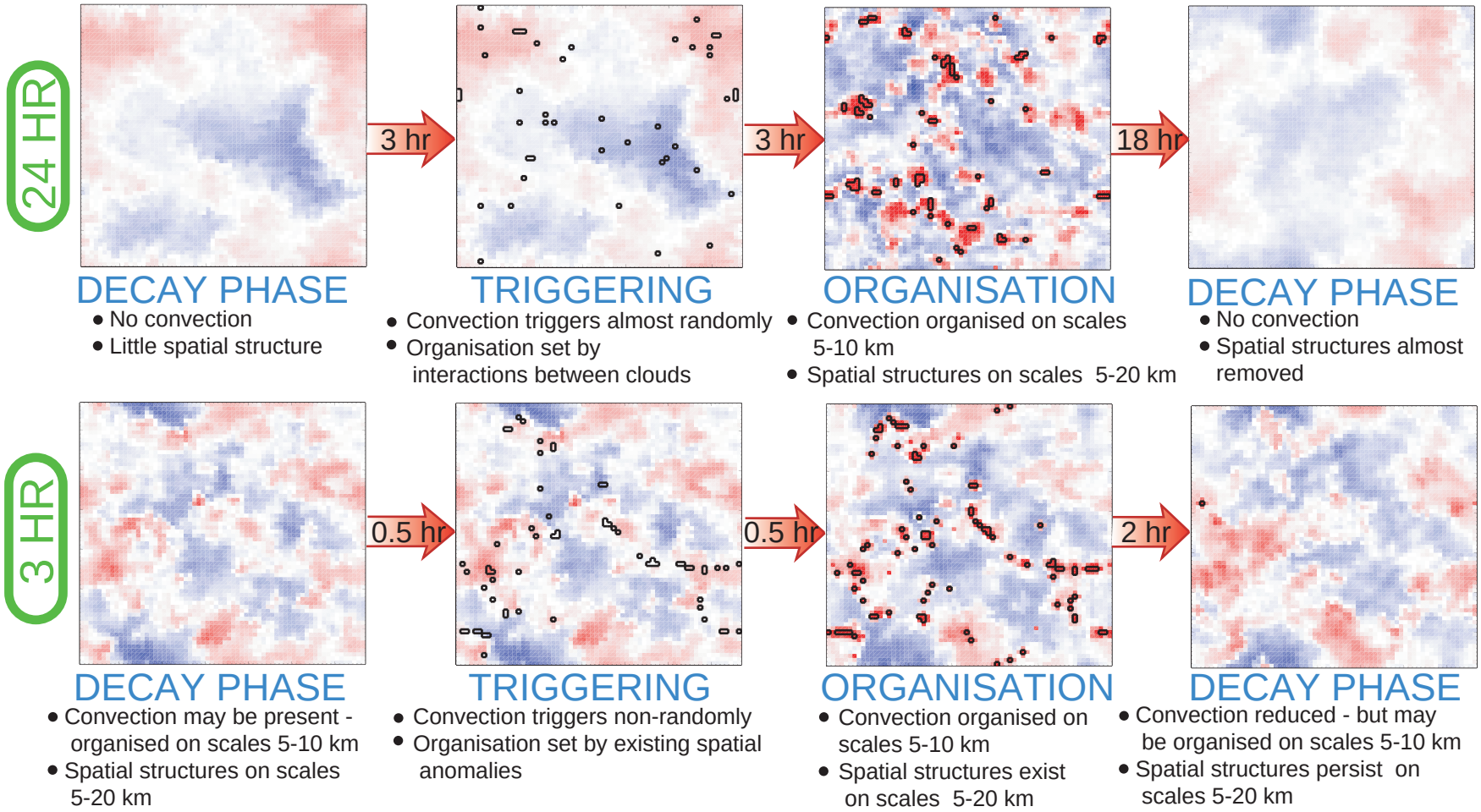

Figure 5.13: *Schematic to show the time evolution of a convective ensemble at a height of* 3 *km when forced at timescales of* 24 *hr and* 3 *hr. The 'decay phase' is pre-forcing for* $\tau = 24$ *hr and at convective minimum for* $\tau = 3$ *hr. The organisation phase occurs at convective maximum for both forcing timescales. The coloured contours are water vapour anomalies in the range* $\pm 1g\ kg^{-1}$*. Red colours are moist and blue contours are dry. The black lines show the clouds concurrent with the moisture anomalies, diagnosed by a buoyancy definition.*

It is speculated that the lack of spatial structures due to an absence of memory may contribute to the 'spike' observed when $\tau = 24$ *hr*. As there are no pre-existing spatial strutures in the domain, convection triggers strongly, with each cloud triggered acting independently. As the convection organises the clouds within the ensemble interact begin to interact.

It has been shown that convective clouds within an ensemble organise even when homogeneously forced. In this study clouds organised with preferred cloud spacings of $5-10$ *km*. These clouds preferentially warm and moisten their surrounding environments creating spatial structures on scales of $5-20$ *km*. The presence of these structures modifies the subsequent convective response and provides memory. If a convective ensemble is given sufficient time to decay these structures will be removed. In these situations there will be no feedback within the system and the convective ensemble will be predominantly affected by the current forcing.

CHAPTER 6

Conclusions

Convection and convective processes play an important role in the atmosphere. The vertical motions resulting from convection transport large amounts of heat and moisture from the surface into the free troposphere where complex interactions occur with weather and climate systems. As convective processes have a fundamental role in the atmosphere, realistic numerical atmospheric models require some form of representation of convection. In low horizontal resolution numerical weather prediction and climate models the effects of convection, which occur on scales smaller than the grid length, are represented by means of a *parameterisation*. A convective parameterisation represents the mean effect of the sub-grid convection on the large scale flow: i.e. the scheme approximates the un-resolved convection forced by the resolved large-scale flow, and modifies the large-scale environment to account for the effect of the convection.

The development of convective parameterisations has relied on assumptions about the sub-grid convection and its relationship to the large-scale. In particular, a scale separation is assumed to exist in space and time between the cloud scale and the large-scale flow, with the sub-grid convection having much smaller temporal and spatial scales than the large scale forcing. If this assumption is valid then the sub-grid convection can (at least in principle) be approximated in terms of the current large-scale forcing. In these situations the convection is defined to be in *equilibrium* with the large-scale forcing. One key aspect underlying this equilibrium assumption is very important for a time-varying forcing mechanism. Specifically, it is assumed that the timescale on which convection adjusts to the forcing (τ_{adj}) is much smaller than the timescale of the evolution of the forcing (τ_{ls}). The convection will then adjust to the forcing through a series of quasi-equilibrium states. Inherent is the idea that it is possible to separate the forcing and the convective response. In the real atmosphere convection directly affects the forcing and, therefore, the forcing cannot be truly time-invariant. These complex interactions are not directly considered in this thesis. However, this issue highlights the need to investigate convection in response to a time-varying forcing.

The validity of the assumption of scale separation between the convective timescales and the timescale of the forcing was the specific focus of this study. The overall aim has been to understand

how convection responds to a time-varying forcing when forced at different timescales. Hence the forcing timescale (τ_{ls}) has been prescribed and the simulated convection has been allowed to respond freely to the forcing. The validity of an equilibrium, or quasi-equilibrium, assumption was examined by investigation of the convective response for a range of near-diurnal and sub-diurnal forcing timescales.

This study was directed in two, parallel directions. The first strand was an analytic model of convection with an explicit memory timescale, forced at different timescales. With the analytic model it was shown that the presence of memory modified the convective response, and the response was characterised for different combinations of memory and forcing timescales. The second strand involved investigating a cloud-resolving model (CRM), which explicitly resolves the ensemble of convection that a parameterisation attempts to represent in a numerical model. The response of the CRM was investigated when forced at different timescales. The CRM was used to test the quasi-equilibrium assumption for a realistic convective ensemble and the results were compared to those found from the analytic model to determine the effect of memory in the convective system. In a CRM the memory timescale is inherently set by the physical convective processes, and therefore the effects of memory can only be determined by comparing the characteristics of the response from the CRM with those from the analytic model.

For forcing timescales where memory may be modifying the convective response ($\lesssim 10$ *hr*), the cloud field in the CRM was studied in order to elucidate the physical mechanisms that control memory. This method, whereby insightful analysis of CRM simulations is used to generate 'better ideas' for parameterisations, is called the "Aha" mechanism (Randall *et al.*, 2003). By artificially controlling the prescribed forcing timescale the physical processes that control memory could be investigated in a manner not possible in the real atmosphere.

6.1 Summary and discussion

The main part of this thesis is a study investigating the response of a convective ensemble in a CRM to a time-varying surface forcing. From this it was determined that for some forcing timescales the convection experienced feedback from previous convection and that the response resembled a system with memory. This implies that the convective response was not simply related to the current forcing but depended on the time-history of the convective system.

To prescribe a time-varying forcing in a physically meaningful, energetically-controlled manner the forcing was specified as time-varying surface sensible and latent heat fluxes and constant longwave cooling. In the case of a forcing timescale of 24 *hr* the convective ensemble was shown to resemble a convective ensemble experiencing a diurnal cycle. However, other values of forcing timescale were also investigated. The model setup was a departure from previous studies that have used a CRM forced to radiative-convective equilibrium (RCE), by specifying a constant longwave cooling and a constant sea surface temperature. It was found that the bulk RCE properties of the convective ensemble were very similar regardless of whether surface temperature or surface fluxes were specified. Similarly the cloud statistics at RCE had little sensitivity to the domain size chosen. Convective organisation was found to occur using both forcing mechanisms although increased organisation was found when surface fluxes were specified. This was attributed to differences in the cold pool dynamics.

The surface-flux-forced convective ensemble, in conjunction with the analytic model, were used to answer the following thesis questions:

Q1. How can a state of equilibrium usefully be defined when the forcing is time-varying? Quasi-equilibrium thinking suggests that convection at each point in time is related to the current forcing. Can this idea be applied for a given time-varying convective response? And if not, how might the ideas from theory be adapted?

A quasi-equilibrium assumption which directly relates the timeseries of the convective response to the forcing cannot be applied when the forcing varies in time. Transition periods, for example the development of convection when first triggered, are associated with a convective response which is delayed in comparison with the forcing timeseries. Furthermore, in the time-varying simulation studies presented here the moist static energy is designed to be in balance only over a *complete forcing cycle*. At any point in time the convective heating may not be in direct balance with the forcing. It may, however, be argued that for a time-varying forcing the total convection should balance the total forcing the over the complete forcing cycle.

The budget over a forcing cycle provided a useful measure of the ability of the system to achieve equilibrium. The total prescribed forcing was identical cycle-to-cycle and therefore (if the system can be meaningfully said to be in equilibrium with the forcing) the total convective response should be identical cycle-to-cycle. A measure of the consistency of the response cycle-to-cycle was the standard deviation of the total convection over several successive cycles. Small standard

deviations denote systems where this 'new' definition of an equilibrium was achieved. Large standard deviations suggested that equilibrium was not achieved. In situations where an equilibrium was not achieved, it was suggested that memory of previous convection was modifying the current convective response.

The 'new' definition of equilibrium used in this thesis is useful in a theoretical context, as the forcing is explicitly known and each individual forcing cycle can be separated from the previous and subsequent forcing cycles. The convection associated with *each* forcing cycle can also be isolated and attributed to a forcing cycle. The definition of equilibrium exploits the periodic and repetitive nature of the forcing and this is used to imply a regular, repetitive convective response. However, this definition would be more difficult to apply in the real atmosphere where the timeseries for the convective forcing may be difficult to define. Furthermore, as the forcing is unlikely to be repetitive, a standard deviation of the total convective response is not meaningful in terms of an equilibrium. Whilst this definition of an equilibrium may only be useful in idealised CRM studies, it represents a first attempt to quantify the equilibrium when the convective forcing varies in time.

By defining equilibrium in relation to the total convective response over a complete forcing cycle, the convection is linked in the 'weakest' possible terms to the forcing. The moist static energy in the system is only balanced over a complete forcing cycle so at the very *least* equilibrium convection should balance the forcing over a complete forcing cycle. This definition of equilibrium is proposed as a necessary condition for the system to be in a meaningful equilibrium. Other, stronger definitions (for example a strict condition relating the convective response at any time to the forcing at that time) could be envisaged. However, such definitions of equilibrium can only be satisfied if the definition of equilibrium introduced in this thesis is also satisfied.

As this 'new' definition of equilibrium considers convection integrated over a period of time, the lifecycle of convective development and decay is encoded into the definition. If a convective cloud is triggered in response to a change in forcing, then the resulting cloud forms a part of the energy balance through which the instability is removed. The cloud must complete its lifecycle in order to complete the adjustment required to balance the forcing. Whenever the 'new' definition of equilibrium holds then all convective clouds triggered during a forcing cycle complete their lifecycle within that forcing cycle, and therefore fully adjust the system in response to the imposed forcing. If the definition of equilibrium does not hold then the clouds produced will not have completed their entire lifecycles and the convection has not fully adjusted to the forcing within that forcing cycle. This implies that the system will experience memory.

Q2. Given a useful definition of an equilibrium from Q1, for what values of forcing timescale is the equilibrium assumption valid? Do situations, where the assumption is not valid, resemble situations where a system has memory?

The 'new' definition of equilibrium was used to investigate the response of a convective ensemble in a CRM when forced on a range of timescales. It was found that when convection was forced at long timescales ($\gtrsim 10$ *hr*), the standard deviation of the total convection was small. In these situations the convection was the same cycle-to-cycle and therefore the convection is adjusting to the forcing for each forcing cycle within the forcing cycle. In these situations the convection can be considered to be in an equilibrium with the forcing. When the forcing timescale was short ($\lesssim 10$ *hr*), the values of standard deviation were larger, indicating variations in the total convection between the cycles. For these values of forcing timescale the convection was not completing the adjustment to the forcing within the forcing cycle; some convective clouds had not completed their lifecycle during the forcing cycle. These clouds provide a mechanism whereby the convection can modify the convection on the subsequent forcing cycle.

An analytic model was used to investigate the convective response in a system that had memory. The model had three timescales associated with it - a forcing timescale, which defined the period of the forcing; the closure timescale, which defined the rate at which convection developed in response to a forcing; and the memory timescale, which defined how rapidly the convection adjusted to a change in forcing. The characteristics of the convective response were set by the relationship of the forcing timescale to the memory timescale. Many convective parameterisations include a closure timescale, but have no analogue of the memory timescale.

It was found that when the memory timescale and the forcing timescale were very different the response was simple and predictable. For $\tau \gg t_{mem}$ there was sufficient time for the convection to adjust to the forcing and the response was repetitive, similar in shape to the forcing function. The convective response was the same cycle-to-cycle and, therefore, based on the 'new' definition of equilibrium, the convection was in an equilibrium with the forcing. When there was a 'moderate' memory (i.e. there is a smaller difference between the memory and the forcing timescale) there is less similarity between the convection and the forcing. There was insufficient time in a single cycle for the convection to respond to the forcing in that cycle and hence there was feedback of convection onto subsequent cycles. This results in different amounts of total convection cycle-to-cycle. From the 'new' definition of equilibrium, the convection was found not be in an equilibrium with the forcing. Hence, when memory effects become more pronounced the convection shows increasing

levels of dis-equilibrium with the forcing.

From a comparison of the results from the CRM and the analytic model it can be concluded that:

• A convective ensemble is in an equilibrium with its forcing when forcing timescales are long ($\gtrsim 10$ *hr*). The convection fully adjusts to the forcing at these timescales.

• At short forcing timescales ($\lesssim 10$ *hr*) convection does not achieve an equilibrium with the forcing. Here the convective clouds produced within a forcing cycle do not complete the adjustment to the forcing and so there is memory in the system.

Q3. In situations where an equilibrium assumption is not valid, what physical mechanisms may be causing the convective response to differ from that expected for the current forcing?

The convective response was found to be in an equilibrium with the forcing for $\tau \gtrsim 10$ *hr* and not to be in equilibrium for $\tau \lesssim 10$ *hr*. Two particular forcing timescales were chosen to represent an equilibrium situation and a non-equilibrium situation, 24 *hr* and 3 *hr* respectively. Detailed analysis was performed on the time-evolution of the convective ensemble at these forcing timescales to determine physical mechanisms for departures from equilibrium. Contrasts between the characteristics of the convective response at the two forcing timescales enabled investigation of the mechanisms which caused memory.

In the 3 *hr* simulation, non-equilibrium was characterised by total convection which was different cycle-to-cycle. It was suggested that this was due to the system retaining memory of the previous convection. If there was memory in the system, sufficient to modify the response, then some signature of the convection in the previous cycle should be present in the initial conditions at the start of the forcing cycle. Comparison of the initial conditions of the 3 *hr* simulation to an equilibrium case (24 *hr*) showed that at both forcing timescales the mean and standard deviations of the domain-mean initial profiles of potential temperature, moisture and stability were similar.

Further analysis was performed for the 3 *hr* simulation by partitioning the cycles with the strongest convection and the weakest convection, and conditionally compositing the domain-mean initial profiles. It was found that there was little difference in the composited initial profiles, and in particular that the strongest and weakest convective cycles were within one standard deviation. Hence, from a diagnostic parameterisation perspective the convection would be the same in both cases. Memory was not communicated through the mean profile.

Further investigations utilised two methods of defining spatial distributions in the domain. The first, which could only be used when clouds were present, focussed on determining cloud spacings. The clouds were found to organise, during the positive phases of the response cycles, with preferred spacings of $5-10$ *km*. In the 24 *hr* simulation the convection decayed while the surface forcing was switched off. However, for the 3 *hr* simulation some convection remained throughout the complete forcing cycle. The second measure of spatial distribution involved computing horizontal Fourier transforms of the thermodynamic spatial structures in the domain. These could be found even when no clouds were present. For $\tau = 3$ *hr*, spatial structures were found to persist on scales of $5-7$ *km* throughout the forcing cycle. For $\tau = 24$ *hr*, these structures decayed while convection was inactive, and there was very little indication of the earlier structures at the start of the next forcing cycle. At the start of each forcing cycle, the spatial structure of the thermodynamic variables in the domain was dominated by the domain mean.

It is hypothesised that these thermodynamic spatial structures, which are the remnants of previous convective events, modify the atmosphere in such a manner that they provide memory. The spatial structures represent part of the lifecycle of convection - the decay phase of strong convective clouds. Hence if there is insufficient time for these structures to be removed then the convective clouds have not completed their lifecycle. The persistence of such structures relating to previous convection prevents the convection achieving equilibrium.

Two relevant timescales can be identified for this mechanism - the time taken for convection to organise and the time taken for convection to decay. By allowing the ensemble to adjust to a state in which convection organises, regions close to the most active convection are modified compared to their surroundings. These areas are preferentially more warm and moist. As the convection decays over its complete lifecycle such regions are gradually eroded. In both simulations (3 *hr* and 24 *hr*) convection organises, although organisation occurs more rapidly when $\tau = 3$ *hr*. For the 24 *hr* simulation convection decays almost completely whereas when $\tau = 3$ *hr* convection does not completely decay, hence allowing memory and more rapid organisation in subsequent cycles.

6.2 Limitations and future work

This study has raised further questions that have not been answered as part of this thesis. The limitations of this study will be put in context of further work that is recommended.

• It has been shown that the statistics of the convective ensemble are sensitive to the model resolution used. The convective clouds here have been shown to have a range of sizes, although predominantly they are small, close to the grid scale. These clouds therefore have strong local effects, intensely modifying the atmosphere over a small area. At higher resolution the clouds may have more structure and may develop different organisations.

• In this study and previous studies it has been shown that convective organisation is stronger on larger domains, or rather that small domain sizes may artificially dampen the effects of organisation. If a parameterisation is representing the convection in a climate model grid box of length Δx then it may be that the parameterisation should be representing organisation. However, the effects of organisation are likely to be dependent on Δx.

• The simulations presented do not include large-scale advection (for example) as an external forcing. In these simulations, it was shown that the potential temperature maintains a moist adiabatic profile when the surface forcing is switched off and that spatial structures are able to persist during this time, remaining coherent in the vertical. If there were additional external forcings acting then these structures may be modified and the mechanism for memory might be less apparent. On the other hand, large-scale imposed vertical wind shear has been shown to organise convection and may provide another mechanism for memory effects.

• In dry, Rayleigh-Benard convection (i.e. without complex non-linear interactions due to moisture) there is organisation on the scale of the depth of the convective layer. In the atmosphere convection is known to organise due to various mechanisms, such as secondary convection occurring at the leading edge of cold pools. However, it has not yet been shown whether convection in the atmosphere also has a similar intrinsic scale of organisation, set by the depth of the convective layer. In these idealised simulations, many of the mechanisms leading to organisation in the atmosphere have been disabled (e.g. wind shear, rotation, interactive radiation). It would therefore be of interest to perform sensitivity studies modifying the depth of the convection (i.e. the depth of the troposphere) in order to test what sets the scale on which the convection organises. Tests modifying the evaporative downdrafts could be used in parallel to determine the role of cold pools on the organisation.

• Cohen and Craig (2006) investigated the response of a convective ensemble to different strengths of longwave cooling. The authors showed that when it is more strongly forced the convective ensemble exhibits less organisation. With a strong forcing an increased number of clouds per unit

area are required, and additional interactions reduced the level of organisation. It would be useful to understand how the reduced organisation in such simulations effects the spatial structures of thermodynamic variables and hence the memory in the system. It must be noted that the forcing used in this thesis represents a relatively strong diurnal cycle. If weaker forcings tend to organise more strongly then the effects of memory may also be stronger in such cases.

• This study has shown that for a convective system with memory, this memory is carried in the thermodynamic spatial structures. It is yet to be determined how to quantify the impact of these structures on the subsequent convection. Figure 6.1 shows the mean normalised power of the relative humidity field, with standard deviation, for composite cycles with 'strong' and 'weak' convection, and $\tau = 3$ *hr* (as introduced in Section 4.7.2). The strong cycles are six cycles with the largest total integrated cloud base mass flux, and the weak cycles are six cycles with the smallest total integrated cloud base mass flux. Figure 6.1 shows that there is no difference in the power in the spatial structures on scales of $5-20$ *km* between the strong and weak convective cycles. There is also very little difference in the standard deviations. Thus, the convective activity in the subsequent forcing cycle cannot be simply related to the strength of the spatial structures. Future work would be necessary to determine what aspects of the spatial structures do modify the intensity of subsequent convection.

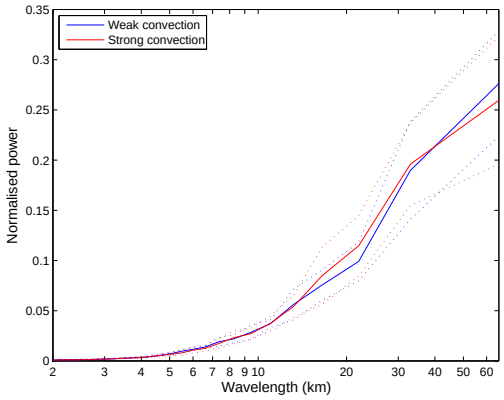

Figure 6.1: *Normalised power of relative humidity field for $\tau = 3$ hr at a height of 3 km. The relative humidity field at the start of the forcing for 12 successive cycles has been partitioned by the total integrated cloud base mass flux. The mean FFT is given by solid lines and standard deviation by dashed lines. When there is 'strong' convection lines are red and 'weak' convection lines are blue. (See Section 4.7.2 for further discussion of the partioning.)*

• The study has investigated convection forced by a timeseries that has equal lengths of positive

forcing and zero forcing. Hence the convection has the same time in the organisation phase as in the decay phase (Figure 5.13). Results showed that for a 3 *hr* forcing timescale convection was organised on scales $5-10$ *km* and that the signature of this organisation persisted through successive forcing cycles. For $\tau = 24$ *hr* the convection became organised during the positive phase of the forcing cycle but the long period without surface forcing allowed the convective spatial structures to decay. It was shown in Section 4.4.3 that modifying the length of time for which there was zero surface forcing altered the characteristics of the convective response when convection triggered. In a similar manner, it might be anticipated that increasing the length of the time with zero forcing in the 3 *hr* simulation would allow the spatial structures to decay further, reducing the memory in the system. Reducing the period of zero forcing in the 24 *hr* simulation may allow spatial structures to persist, therefore adding memory to the response. To understand the complete lifecycle of the convective system it would also be necessary to determine the timescale on which convection organises. The organisation and decay timescales may not be the same but this cannot be determined from these simulations.

6.3 Implications

Through this study it has been possible to show that convection does *self-organise*. The convective ensemble investigated in a CRM was homogeneously forced and mechanisms that promoted organisation, such as rotation, wind shear and interactive radiation, were excluded. However, it was found that convection organised on scales of $5-10$ *km*. The extent of the organisation was sensitive to the method of forcing (specified SST or fluxes) but was present in both cases.

This is contrary to most current convective parameterisations which are based on the assumption of a random distribution of clouds, which was introduced by Arakawa and Schubert (1974). For example, a recent parameterisation by Plant and Craig (2008) bases a stochastic parameterisation on the theory of mass flux variance introduced by Craig and Cohen (2006), which explicity assumes a completely random distribution of clouds. If, through convective self-organisation the distribution is not random, then this is a defect of current parameterisations. Recent thinking has included consideration of the representation of mesoscale organisation, for example (Gray and Shutts, 2002).

The self-organisation of convection within the ensemble can cause memory within the convective system. Memory prevents the convective response being directly related to the current forcing. The

explicit inclusion of memory in a parameterisation may be achieved by using a prognostic convective parameterisation to directly feedback previous convection (Pan and Randall, 1998; Piriou *et al.*, 2007). However, it is not yet clear how that would be achieved. Stochastic parameterisations introduce variability to the convection parameterised by traditional parameterisations, hence providing deviations from equilibrium (Arribas, 2004). It may be that the effects of memory are similar to those implied in a stochastic scheme (Neelin *et al.*, 2008). However, through a parameterisation scheme including memory, it may be possible to include variability in a more physically meaningful manner.

The results of this study, by showing that convection has memory, provide further evidence of the limitations of diagnostic parameterisation schemes. For example, a parameterisation may diagnose that some depth of the atmosphere will support convection and attempt to modify the large scale accordingly. However, if the effects of any previous convection are not simply encoded in the large scale state then the depth of the atmosphere that supports convection could also be dependent on the depth of previous convection. It may be that memory could be introduced into a parameterisation by carrying forwards some measures of the depth and intensity of previous convection.

To account for the effects of departures from strict equilibrium, closure timescales have been introduced to the current generation of parameterisations. The closure timescale has become 'a tunable parameter' in that there are no direct measurements of this timescale, and its value is set through a combination of experimentation and our existing understanding of the rate at which convection adjusts to the forcing. Because of its importance and uncertainty it has been used as a parameter for testing climate sensitivities (Murphy *et al.*, 2004) and in ensemble climate prediction (Collins *et al.*, 2006). The closure timescale has also been directly modified when increasing model resolution in numerical weather prediction (N. Roberts, *pers. comm.*). This study is partly an attempt to understand at what timescales convection does adjust to the forcing, with the hope that uncertainties in the closure time can be removed. With further effort to understand more fully the physical mechanisms whereby convection self-organises, and the role of memory, it is hoped that further developments to parameterisations can be achieved for the benefit of the atmospheric modelling community.

APPENDIX A

Notation conventions

M_c or M	Total mass flux in convective ensemble $\left[kg\ s^{-1}\right]$ or $\left[kg\ m^{-2}\ s^{-1}\right]$ when normalised by domain size (preferred)
M_b	Cloud base mass flux $\left[kg\ m^{-2}\ s^{-1}\right]$
T	Atmospheric temperature $[K]$
T_s	Surface temperature $[K]$
$COOL$	Atmospheric cooling rate $\left[K\ s^{-1}\right]$
Q_1	Convective heating rate $\left[K\ s^{-1}\right]$
R	Equilibrium convective heating rate $\left[K\ s^{-1}\right]$
t_{mem}	Memory timescale $\left[s^{-1}\right]$
t_{close}	Closure timescale $\left[s^{-1}\right]$
Δt	Time step $[hr]$ in analytic model or $[s]$ in CRM
τ	Forcing timescale $[hr]$
ΔT_{conv}	Total convective heating over a forcing cycle
$\overline{(\Delta T_{conv})}$	Mean total convective heating averaged over successive forcing cycles
$\sigma(\Delta T_{conv})$	Standard deviation in the total convective heating over successive forcing cycles
τ_{damp}	Damping timescale $\left[s^{-1}\right]$
z_D	Base of damping layer $[m]$
H_D	Depth of damping layer $[m]$
F_S	Sensible heat flux $\left[W\ m^{-2}\right]$
F_L	Latent heat flux $\left[W\ m^{-2}\right]$
F_{rad}	Radiative cooling $\left[W\ m^{-2}\right]$
$\dot{T}$	Longwave cooling rate $\left[K\ s^{-1}\right]$
I_{M_b}	Total integrated cloud base mass flux over a forcing cycle $\left[kg\ m^{-2}\right]$
$\overline{I_{M_b}}$	Mean total integrated cloud base mass flux over a forcing cycle $\left[kg\ m^{-2}\right]$
$\sigma(I_{M_b})$	Standard deviation total integrated cloud base mass flux over a forcing cycle $\left[kg\ m^{-2}\right]$
$\overline{I_{ppt}}$	Mean total integrated surface precipitation over a forcing cycle $[mm]$
$\sigma(I_{ppt})$	Standard deviation total integrated precipitation over a forcing cycle $[mm]$
$\langle N \rangle$	Number of clouds
$\langle m \rangle$	Mean mass flux per cloud $\left[kg\ m^{-2}\right]$
$\langle A \rangle$	Mean cloud area $\left[km^2\right]$
$\mathscr{V}$	$\mathscr{V} = \frac{\langle (\delta M)^2 \rangle}{\langle M \rangle^2} \times \langle N \rangle$ Normalised mass flux variance

Bibliography

Anthes, R. A. (1977). A cumulus parameterization scheme utilising a one-dimensional cloud model. *Mon. Wea. Rev.*, **105**, 270–286.

Arakawa, A. (2004). The cumulus parameterisation problem: past, present and future. *J. Atmos. Sci.*, **17**(13), 2493–2525.

Arakawa, A. and Lamb, V. R. (1977). Computational design of the basic dynamical processes of the UCLA general circulation model. *Methods in computational physics, Academic Press*, **17**, 173–265.

Arakawa, A. and Schubert, W. (1974). Interaction of a cumulus cloud ensemble with the large-scale environment, Part1. *J. Atmos. Sci.*, **31**, 674–701.

Arribas, A. (2004). Results of an inital stochastic physics scheme for the Met Office Unified Model. *Forecasting technical report.*, **No. 452**.

Beare, R. J., Edwards, J. M., and Lapworth, A. J. (2006). Simulation of the observed evening transition and nocturnal boundary layers: Large-eddy simulation. *Quart. J. Roy. Meteor. Soc.*, **132**, 81–99.

Bechtold, P., Chaboureau, J. P., Beljaars, A., Betts, A. K., Khler, M., Miller, M., and Redelsperger, J. L. (2004). The simulation of the diurnal cycle of convective precipitation over land in a global model. *Quart. J. Roy. Meteor. Soc.*, **130**, 3119–3137.

Betts, A. K. (1973). Non-precipitating cumulus convection and its parameterisation. *Quart. J. Roy. Meteor. Soc.*, **99**, 674–701.

Betts, A. K. and Miller, M. J. (1986). A new convective adjustment scheme. Part II: Single column tests using GATE wave, BOMEX, ATEX and arctic air-mass data sets. *Quart. J. Roy. Meteor. Soc.*, **112**, 693–709.

Bretherton, C. and Smolarkiewicz, P. (1997). Gravity waves, compensating subsidence and detrainment around cumulus clouds. *J. Atmos. Sci.*, **46**, 740–759.

Bretherton, C. S., Blossey, P. N., and Khairoutdinov, M. (2005). An energy-balance analysis of deep convective self-aggregation above uniform SST. *J. Atmos. Sci.*, **62**, 4273–4292.

Brown, P. R. and Swann, H. A. (1997). Evaluation of key microphysical parameters in three-dimensional cloud-model simulations using aircraft and multiparameter radar data. *Quart. J. Roy. Meteor. Soc.*, **123**, 2245–2275.

Brown, R. G. and Bretherton, C. (1997). A test of the strict quasi-equilibrium theory on long time and space scales. *J. Atmos. Sci.*, **54**, 624–638.

Bryan, G. H., Wyngaard, J., and Fritsch, J. (2003). Resolution requirements for the simulation of deep moist convection. *Mon. Wea. Rev.*, **131**, 2394–2416.

Carson, D. J. (1973). The development of a dry inversion-capped convectively unstable boundary layer. *Quart. J. Roy. Meteor. Soc.*, **99**, 450–467.

Chaboureau, J. P., Guichard, F., Redelsperger, J. L., and Lafore, J. P. (2004). The role of stability and moisture in the diurnal cycle of convection over landPolar low le Cygne: Satellite observations and numerical simulations. *Quart. J. Roy. Meteor. Soc.*, **130**, 3105–3117.

Cohen, B. (2001). *Fluctuations in an Ensemble of Cumulus Clouds*. Phd thesis, The University of Reading, Department of Meteorology, The University of Reading, Reading, UK, RG6 6BB.

Cohen, B. and Craig, G. (2004). The time response of a convective cloud ensemble to a change in forcing. *Quart. J. Roy. Meteor. Soc.*, **130**, 933–944.

Cohen, B. and Craig, G. (2006). Fluctuations in an equilibrium convective ensemble. Part II: Numerical experiments. *J. Atmos. Sci.*, **63**, 2005–2015.

Collins, M., Booth, B. B., Harris, G. R., Murphy, J. M., Sexton, D. M., and Webb, M. J. (2006). Towards quantifying uncertainty in transient climate change. *Climate Dynam.*, **27**, 127–147.

Craig, G. and Cohen, B. (2006). Fluctuations in an equilibrium convective ensemble. Part I: Theortetical formulation. *J. Atmos. Sci.*, **63**, 1996–2004.

Derbyshire, S. H., Brown, A. R., and Lock, A. P. (1994). The Meteorological Office Large-Eddy Simulation model. *Met Office (APR) Turbulence and diffusion note*, **No. 123**.

Derbyshire, S. H., Beau, I., Bechtold, P., Grandpeix, J. Y., Piriou, J. M., Redelsperger, J. L., and Soares, P. M. (2004). Sensitivity of moist convection to environmental humidity. *Quart. J. Roy. Meteor. Soc.*, **130**, 3055–3079.

Donner, L. J. and Phillips, V. T. (2003). Boundary layer control on convective available potential energy: Implications for cumulus parameterization. *J. Geophys. Res.*, **108**, (7)1–(7)12.

Donner, L. J., Kuo, H. L., and Pitcher, E. J. (1982). The significance of thermodynamic forcing by cumulus convection in a general circulation model. *J. Atmos. Sci.*, **39**, 2159–2181.

Emanuel, K. A. (1994). *Atmospheric Convection*. Oxford University Press, first edition.

Emanuel, K. A. (1995). The behavior of a simple hurricane model using a convective scheme based on subcloud-layer entropy equilibrium. *J. Atmos. Sci.*, **52**(22), 3960–3968.

Emanuel, K. A., Neelin, J. D., and Bretherton, C. S. (1994). On Large-Scale Circulations in Convecting Atmospheres. *Quart. J. Roy. Meteor. Soc.*, **120**, 1111–1143.

Ferrier, B. S. (1994). A double-moment multiple-phase four-class bulk ice scheme. Part I: Description. *J. Atmos. Sci.*, **51**, 249–280.

Ferrier, B. S., Tao, W. K., and Simpson, J. (1995). A double-moment multiple-phase four-class bulk ice scheme. Part II: Simulations of convective storms in different large-scale environments and comparisons with other bulk parameterizations. *J. Atmos. Sci.*, **52**, 1001–1033.

Fritsch, J. M. and Chappell, C. F. (1980). Numerical prediction of convectively driven mesoscale pressure systems. Part I: Convective parameterisation. *J. Atmos. Sci.*, **37**, 1722–1733.

Futyan, J. M. and Genio, A. D. D. (2007). Deep convective system evolution over Africa and the tropical Atlantic. *J. Climate*, **20**, 5041–5060.

Grabowski, W. W., Wu, X., Moncrieff, M. W., and Hall, W. (1998). Cloud-resolving modeling of cloud systems during Phase II of GATE. Part II: Effects of resolution and the third spatial dimension. *J. Atmos. Sci.*, **55**, 3264–3282.

Grant, A. L. and Lock, A. P. (2004). The turbulent kinetic energy budget for shallow cumulus convection. *Quart. J. Roy. Meteor. Soc.*, **130**, 401–422.

Gray, M., Petch., J., Derbyshire, S., Brown, A., Lock, A., Swann, H., and Brown, P. (2001). Version 2.3 The Met Office Large Eddy Model: Part II Scientific documentation. *User documentation*.

Gray, M. E. (2000). Characteristics of numerically simulated mesoscale convective systems and their application to parameterization. *J. Atmos. Sci.*, **57**, 3953–3970.

Gray, M. E. and Shutts, G. J. (2002). A stochastic scheme for representing convectively generated vorticity in general circulation models. *Met Office (APR) Turbulence and diffusion note*, **No. 285**.

Gregory, D. and Rowntree, P. R. (1990). A mass flux convection scheme with representation of cloud ensmble characteristics and stability dependant closure. *Mon. Weather. Rev.*, **118**, 1483–1506.

Gregory, D., Morcrette, J. J., Jakob, C., Beljaars, A. C. M., and Stockdale, T. (2000). Revision of convection, radiation and cloud schemes in the ECMWF Integrated Forecast Model. *Quart. J. Roy. Meteor. Soc.*, **126**, 1685–1710.

Guichard, F., Petch, J. C., Redelsperger, J. L., Bechtold, P., Chaboureau, J. P., Cheinet, S., Grabowski, W., Grenier, H., Jones, C. G., Khler, M., Piriou, J. M., Tailleux, R., and Tomasini, M. (2004). Modelling the diurnal cycle of deep precipitating convection over land with cloud-resolving models and single-column models. *Quart. J. Roy. Meteor. Soc.*, **130**, 3139–3171.

Held, I. M. (1999). The macroturbulence of the troposphere. *Tellus Series A*, **51**, 59–70.

Held, I. M., Hemler, R. S., and Ramasway, V. (1993). Radiative-convective equilibrium with explicit two-dimensional moist convection. *J. Atmos. Sci.*, **50**, 3909–3927.

Holloway, C. E. and Neelin, J. D. (2007). The Convective Cold Top and Quasi Equilibrium. *J. Atmos. Sci.*, **64**(5), 1467–1487.

Jakob, C. and Siebesma, A. P. (2003). The step-mountain coordinate model: Further developments of the convection, viscous sublayer, and turbulence closure schemes. *Mon. Wea. Rev.*, **131**, 2765–2778.

Janjic, Z. I. (1994). The step-mountain coordinate model: Further developments of the convection, viscous sublayer, and turbulence closure schemes. *Mon. Wea. Rev.*, **122**, 927–945.

Khairoutdinov, M. and Randall, D. (2006). High-resolution simulation of shallow-to-deep convection transition over land. *J. Atmos. Sci.*, **63**, 3421–3436.

Krishnamurti, T. N., S, L. N., and Pasch, R. (1983). Cumulus parametrization and rainfall rates II. *Mon. Wea. Rev.*, **111**, 815–828.

Kuang, Z. (2008). Modeling the interaction between cumulus convection and linear gravity waves using a limited-domain cloud system-resolving model. *J. Atmos. Sci.*, **65**, 576–591.

Kuo, H. L. (1974). Further studies of the parameterization of the influence of cumulus clouds on the large-scale flow. *J. Atmos. Sci.*, **31**, 1232–1240.

Kuo, K. S., Welch, R., Weger, R., Engelstad, M., and Sengupta, S. (1993). The three-dimensional structure of cumulus clouds over the ocean 1. Structural analysis. *J. Geophys. Res.*, **98**, 1232–1240.

Lean, H. W. and Clark, P. A. (2003). The effects of changing resolution on mesocale modelling of line convection and slantwise circulations in FASTEX IOP16. *Quart. J. Roy. Meteor. Soc.*, **129**, 2255–2278.

LeMone, M. A. and Zipser, E. J. (1980). Cumulonimbus vertical velocity events in GATE. Part I: Diameter, intensity and mass flux. *J. Atmos. Sci.*, **37**, 2444–2457.

LeMone, M. A., Zipser, E. J., and Trier, S. B. (1998). The role of environmental shear and thermodynamic conditions in determining the structure and evolution of mesoscale convective systems during TOGA COARE. *J. Atmos. Sci.*, **55**, 3493–3519.

Lin, X., Randall, D. A., and Fowler, L. D. (2000). Diurnal variability of the hydrologic cycle and radiative fluxes: Comparisons between observations and a GCM. *J. Climate*, **13**, 4159–4179.

Lin, Y. L., Farley, R. D., and Orville, H. D. (1983). Bulk Parameterization of the Snow Field in a Cloud Model. *J. Climate. Appl. Met.*, **22**, 1065–1092.

Liu, W. T., Tang, W., and Niiler, P. P. (2000). Humidity Profiles over the Ocean. *J. Climate*, **4**, 1023–1034.

Lock, A. P. (2006). The parametrization of entrainment in cloudy boundary layers. *Quart. J. Roy. Meteor. Soc.*, **124**, 2729–2753.

Madden, R. A. and Julian, P. R. (1971). Detection of a 40-50 day oscillation in the zonal wind in the tropical pacific. *J. Atmos. Sci.*, **28**, 702–708.

Manabe, S. and Strickler, R. (1964). On the thermal equilibrium of the atmosphere with a convective adjustment. *J. Atmos. Sci.*, **21**, 361–385.

Manabe, S., Smagorinsky, J., and Strickler, R. (1965). Simulated climatology of a general circulation model with a hydrologic cycle. *Mon. Wea. Rev.*, **93**, 769–798.

Mapes, B. E. and Wu, X. (2001). Convective eddy momentum tendencies in long cloud-resolving model simulations. *J. Atmos. Sci.*, **58**, 517–526.

Marsham, J. H. and Parker, D. J. (2006). Secondary initiation of multiple bands of cumulonimbus over southern Britain. II: Dynamics of secondary initiation. *Quart. J. Roy. Meteor. Soc.*, **132**, 1053–1072.

Mason, P. J. (1989). Large-Eddy Simulation of the convective atmospheric boundary layer. *J. Atmos. Sci.*, **46**, 1492–1516.

Murphy, J. M., Sexton, D. M., Barnett, D. N., Jones, G. S., Webb, M. J., and Collins, M. (2004). Quantification of modelling uncertainties in a large ensemble of climate change simulations. *Nature*, **430**(7001), 768–772.

Neelin, J. D., Peters, O., Lin, J. W., Hales, K., and Holloway, C. E. (2008). Rethinking convective quasi-equilibrium: observational constraints for stochastic convective schemes in climate models. *To appear in Phil. Trans. Royal Soc. London A*.

Nieuwstadt, F. T. and van Dop, H. (1982). *Atmospheric turbulence and air pollution modelling*. D. Reidel Publishing Company.

Pan, D. M. and Randall, D. A. (1998). A cumulus parameterisation with a prognostic closure. *Quart. J. Roy. Meteor. Soc.*, **124**, 949–981.

Petch, J. C. (2004). The predictability of deep convection in cloud-resolving simulations over land. *Quart. J. Roy. Meteor. Soc.*, **130**, 3173–3187.

Petch, J. C. (2006). Sensitivity studies of developing convection in a cloud-resolving model. *Quart. J. Roy. Meteor. Soc.*, **132**, 345–358.

Petch, J. C., Brown, A., and Gray, M. (2002). The impact of horizontal resolution on the simulations of convective development over land. *Quart. J. Roy. Meteor. Soc.*, **128**, 2031–2044.

Piriou, J. M., Redelsperger, J. L., amd J. P. Lafore, J. F. G., and Guichard, F. (2007). An approach for convective parameterization with memory: Separating microphysics and transport in grid-scale equations. *J. Atmos. Sci.*, **64**, 4127–4139.

Plank, V. G. (1969). The Size Distribution of Cumulus Clouds in Representative Florida Populations. *J. Appl. Meteorol.*, **8**, 46–67.

Plant, R. S. and Craig, G. C. (2008). A Stochastic Parameterization for Deep Convection Based on Equilibrium Statistics. *J. Atmos. Sci.*, **65**, 87–105.

Randall, D., Khairoutdinov, M., Arakawa, A., and Grabowskic, W. (2003). Breaking the cloud parameterization deadlock. *Bull. Amer. Meteor. Soc.*, **84**(11), 1547–1564.

Raymond, D. J. (1995). Regulation of moist convection over the West Pacific warm pool. *J. Atmos, Sci.*, **52**(22), 3945–3959.

Robe, F. R. and Emanuel, K. A. (2001). The effect of vertical wind shear on radiative-convective equilibrium states. *J. Atmos, Sci.*, **58**, 1427–1445.

Rogers, R. R. and Yau, M. K. (1989). *A short cource in cloud physics*. Butterworth-Heinemann, third edition.

Rotunno, R., Klemp, J. B., and Weisman, M. L. (1988). A Theory for Strong, Long-Lived Squall Lines. *J. Atmos, Sci.*, **45**(4), 463–485.

Rutledge, S. A. and Hobbs, P. V. (1984). The mesoscale and microscale structure and organization of clouds and precipitation in midlatitude cyclones. XII: A diagnostic modeling study of precipitation development in narrow cold-frontal rainbands. *J. Atmos. Sci.*, **41**, 2949–2972.

Shutts, G. J. and Gray, M. E. B. (1999). A numerical modelling study of the geostrophic adjustment process following deep convection. *Quart. J. Roy. Meteor. Soc.*, **120**, 1145–1178.

Siebesma, A. P. and Cuijpers, J. W. (1995). Evaluation of parametric assumptions for shallow cumulus convection. *J. Atmos. Sci.*, **52**, 650–666.

Smith, S. A. and Jonas, P. R. (1995). Observations of the turbulent fluxes in fields of cumulus clouds. *Quart. J. Roy. Meteor. Soc.*, **121**, 1185–1208).

Steiner, M., Houze, R., and Yuter, S. (1995). Climatological characterisation of three-dimensional storm structure from operational radar and rain gauge data. *J. Appl. Meteorol.*, **34**, 1978–2007.

Stirling, A. and Petch, J. (2004). The impacts of spatial variability on the development of convection. *Quart. J. Roy. Meteor. Soc.*, **130**, 3189–3206.

Stommel, H. and Arons, A. B. (1961). On the abyssal circulation of the world ocean- I. Stationary planetary flow patterns on a sphere. *Deep-Sea Research*, **6**, 140–154.

Stull, R. B. (1988). *An introduction to boundary layer meteorology*. Kluwer Academic Publishers, second edition.

Sui, C. H. and Lau, K. M. (1992). Multiscale phenomena in the tropical atmosphere over the western Pacific. *Mon. Wea. Rev.*, **120**, 408–430.

Sun, D. Z. and Lindzen, R. S. (1993). Distribution of tropical tropospheric water vapor. *J. Atmos. Sci.*, **50**, 1643–1660.

Tao, W. K., Simpson, J., and Soong, S. T. (1987). Statistical Properties of a Cloud Ensemble: A Numerical Study. *J. Atmos. Sci.*, **44**, 3175–3187.

Tao, W. K., Lang, S., Simpson, J., Sui, C. H., Ferrier, B., and Chou, M. D. (1996). Mechanisms of cloud-radiation interaction in the tropics and midlatitudes. *J. Atmos. Sci.*, **53**, 2624–2651.

Thompson, R. M., Payne, S. W., Reckel, E. E., and Reed, R. (1979). Structure and properties of synoptic-scale wave disturbances in the intertropical convergence zone of the eastern Atlantic. *J. Atmos. Sci.*, **36**, 53–72.

Tiedtke, M. (1989). A comprensive mass flux scheme for cumulus parameterisation in karge-scale models. *Mon. Wea. Rev.*, **117**, 1779–1800.

Tompkins, A. M. (2000). The impact of dimensionality on long-term cloud-resolving model simulations. *Mon. Wea. Rev.*, **128**, 1521–1535.

Tompkins, A. M. and Craig, G. (1998a). Radiative-convective equilibrium in a three dimensional cloud-ensemble model. *Quart. J. Roy. Meteor. Soc.*, **124**, 2073–2097.

Tompkins, A. M. and Craig, G. (1998b). Timescales of adjustment to radiative-convective equilibrium in the tropics. *Quart. J. Roy. Meteor. Soc.*, **124**, 2693–2713.

Tompkins, A. M. and Emanuel, K. A. (2000). The vertical resolution sensitivity of simulated equilibrium temperature and water-vapour profiles. *Quart. J. Roy. Meteor. Soc.*, **126**, 1219–1238.

Vallis, G. K., 2, G. J. S., and Gray, M. E. (1997). Balanced mesoscale motion and stratified turbulence forced by convection. *Quart. J. Roy. Meteor. Soc.*, **123**, 1621–1652.

Wu, X., Liang, X. Z., and Park, S. (2007). Cloud-Resolving model simulations over the ARM SGP. *Mon. Wea. Rev.*, **135**, 2841–2853.

Xie, S., Xu, K. M., Cederwall, R. T., Bechtold, P., Genio, A. D. D., Klein, S. A., Cripe, D. G., Ghan, S. J., Gregory, D., Iacobellis, S. F., Krueger, S. K., Lohmann, U., Petch, J. C., Randall, D. A., Rotstayn, L. D., Somerville, R. C., Sud, Y. C., Salzen, K. V., Walker, G. K., Wolf, A., Yio, J. J., Zhang, G. J., and Zhang, M. (2002). Intercomparison and evaluation of cumulus parametrizations under summertime midlatitude continental conditions. *Quart. J. Roy. Meteor. Soc.*, **128**, 1095–1136.

Xu, K. M. and Randall, D. A. (1995). Impact of interactive radiative transfer on the macroscopic behavior of cumulus ensembles. Part II: Mechanisms for cloud-radiation interactions. *J. Atmos. Sci.*, **52**, 800–817.

Xu, K. M., Cederwall, R. T., Donner, L. J., Grabowski, W. W., Guichard, F., Johnson, D. E., Khairoutdinov, M., Krueger, S. K., Petch, J. C., Randall, D. A., Seman, C. J., Tao, W. K., Wang, D., Xie, S. C., Yio, J. J., and Zhang, M. H. (2002). An intercomparison of cloud-resolving models with the atmospheric radiation measurement summer 1997 intensive observation period data. *Quart. J. Roy. Meteor. Soc.*, **580**, 593–624.

Yanai, M. S., Esbensen, J. H., and Chu, J. H. (1973). Determination of bulk properties of tropical cloud structures from large-scale heat and moisture budgets. *J. Atmos. Sci.*, **30**, 611–627.

Yang, G. Y. and Slingo, J. (2001). The diurnal cycle in the tropics. *Mon. Wea. Rev.*, **129**, 784–801.

Zhang, G. J. (2002). Convective quasi-equilibrium in midlatitude continental environment and its effect on convective parameterization. *J. Geophys. Res.*, **107**, (12)1–(12)16.

Zhang, G. J. (2003). Convective quasi-equilibrium in the tropical western Pacific: Comparison with midlatitude continental environment. *J. Geophys. Res.*, **108**, (1)1–(1)9.